REFERENCE ONLY

UNIVERSITY OF LONDON THESIS

Degree PhD Year 2000 Name of Author CINELLI J M.

This thesis comes within category D.

☑ This copy has been deposited in the Library of UCL

☐ This copy has been deposited in the Senate House Library, Senate House, Malet Street, London WC1E 7HU.

Global Instability in Strongly Nonhomogeneous Systems

Jonathan Matthew Linkins
University College London
University of London

A thesis submitted for the degree of
Doctor of Philosophy
Supervisor: Dr S. N. Timoshin
December 2005

ProQuest LLC
789 East Eisenhower Parkway
P.O. Box 1346
Ann Arbor, MI 48106-1346

Abstract

A number of fluid-dynamical systems are considered with regard to their global stability. First, a simple linearised Ginzburg-Landau-type system with periodic coefficients is shown to be absolutely unstable under certain conditions.

Some two-fluid channel-flow problems with application to stability of flow through pipes and ducts and to cavity tones are considered next. Firstly, flow through a channel with periodically-deformed walls is shown, using Floquet's theorem, to be absolutely unstable for any case other than that of homogeneous coefficients. This is due to a three-wave interaction. A finite-range variation in the channel shape is then considered. It is found that, for a contraction in the channel, global instability appears for an obstacle of any length. For an expanded channel section, a large length is required for global instability to be observed. As a simplification, a system with two fluids separated by a solid wall containing a finite-length aperture is considered. A finite number of unstable global modes are found and some analysis is done for the infinite-range limit.

Next, two systems are investigated of which, if infinite, all harmonic wave-like perturbations would be considered to be stable, but in which transient growth is observed in the temporal evolution of disturbances. It is found that the equivalent finite-range formulation shows global instability due to feedback between the ends. The first system exhibits such behaviour due to transient growth of a spatial nature, while the second exhibits purely temporal transients.

Finally, a system governed by a Benjamin-Ono equation is considered. It is shown that, for a homogeneous problem, the greatest contribution to the instability of the system can come from a branch point at the origin in the wavenumber plane. Some problems with numerical computation of stability for problems with a Cauchy-type integral are then discussed.

Acknowledgements

Firstly, I would like to thank my supervisor, Dr Sergei Timoshin, for his guidance, advice, insight and continuing interest. It has been a pleasure to work with him over the past few years.

My thanks must also go to the members of the UCL Mathematics Department: the academic and administrative staff, and especially to the postgraduate student community, for helping to make my time at the college as enjoyable as it has been.

I am also very grateful to my friends and family. My parents deserve special mention for their support, especially in times of financial hardship.

This work was undertaken with a research grant from the Engineering and Physical Sciences Research Council (EPSRC), to whom I am indebted for the opportunity that their funding has given me to carry out this project.

Finally, I would like to thank Lucy for all the love, support and encouragement she has given me.

Declaration

I hereby certify that this thesis is my own work, except where otherwise indicated. All external sources of information have been identified as such.

Signed ..... Date .....

Contents

List of Figures

Chapter 1

Introduction

1.1 Background

The study of hydrodynamic stability began over a hundred years ago, since which time it has become one of the central areas of research in fluid mechanics. It has long been known that the properties of a turbulent flow can be very different to those of a laminar flow and so understanding the breakdown of a laminar flow into a turbulent one is a very important concern. It is clear that a laminar flow which is stable, in the sense that any perturbation to the flow decays in space and time, cannot ever undergo a significant change in its flow pattern. Thus, a necessary condition for transition must be the flow being, or becoming, unstable.

Early theoretical work on the stability of fluid flows was carried out by Helmholtz [30], Kelvin [36] and Rayleigh [52], [53] amongst others, but it is Reynolds' experiment [55] which has become the most famous starting point for the subject. A streak of dye was injected into water flowing through a pipe. By varying the speed of the flow and the amount of disturbance at the inlet, Reynolds performed a systematic study of the breakdown of the laminar water flow and its transition to turbulence. He showed that the transition depended

on a ratio of parameters which is now named after him.

At the beginning of the Twentieth Century, Orr [46] and Sommerfeld [61] began considering wavelike perturbations of a steady base flow and derived the famous equation which now bears their names. However, early attempts to solve this did not match particularly well with experimental observations, in either Couette or the experimentally-easier Poiseuille flow. For example, experiments found instability for plane Couette flow, whereas the Orr-Sommerfeld equation predicts stability. In fact, Couette flow is stable, but only to infinitesimal perturbations.

More successful in matching theoretical predictions with experimental observations were Heisenberg [29], Tollmien [67] and Schlichting [58]. Their large Reynolds number asymptotics of the Orr-Sommerfeld equation predicted the existence of waves now known as Tollmien-Schlichting waves. These were subsequently verified by the experiments of Schubauer and Skramstad [60].

Two transition problems which are worthy of mention for the ideas they contributed to the study of fluid stability are the break-up of a jet of one fluid in another and the transition of a wake to turbulence, see e.g. Batchelor and Gill [2] and Lessen and Singh [39]. Analysis of such problems led to the method of normal modes and a distinction between absolute and convective instability. This was formalised by Sturrock [62], Briggs [11] and Bers [6] and received some experimental confirmation of its validity in Crighton and Gaster [21]. These ideas will be covered in more detail in subsequent sections.

The normal mode method has found application to many problems, such as instability in plasma physics [7] and waveguides [22], both analytically (see later) and computationally [37]. However, the majority of this thesis is concerned with more theoretical problems related to fluid dynamics and we now discuss how such problems may be approached.

1.2 Stability in general

The approach used to understand the linear stability of a particular fluid-dynamical system depends on the nature of the system. One obvious distinguishing factor between systems is whether their spatial extent is finite or infinite.

Examples of finite-range systems include Bénard convection in a box [23] or two-dimensional Couette flow (also [23]). If such systems have no explicit dependence on time t in their base state then we often assume that whichever flow variable we are solving for in the disturbed state (usually velocity, pressure or some combination of the two) can be separated into a time-dependent part and a space-dependent part. The time variation is taken to be of the form $e^{\lambda t}$ or $e^{-i\omega t}$. Applying boundary conditions, usually at the edges of our finite domain, leads to an eigenvalue problem for λ. As an example, consider

$$\begin{aligned} \tfrac{\partial u}{\partial t} &= \tfrac{\partial^2 u}{\partial x^2} - c\tfrac{\partial u}{\partial x} \quad \text{with,} \\ u(0,t) &= u(\pi,t) = 0. \end{aligned} \tag{1.1}$$

c is taken to be real. A substitution of the form

$$u(x,t) = u_0 e^{\lambda t} e^{cx/2} \sin(nx), \tag{1.2}$$

leads to

$$\lambda u = \left(-\frac{c^2}{4} - n^2\right) u \tag{1.3}$$

and so $\lambda_n = \lambda(n) = -\frac{c^2}{4} - n^2$. We do not prove here that every nontrivial solution is of the form (1.2), although this is the case; neither do we prove that the eigenfunctions $e^{cx/2}\sin(nx)$ form a complete set. However, this may be seen, using the result that a set of sine functions is complete, as follows: for any suitable function $v(x)$, consider the sine-series expansion for $v(x)e^{-cx/2}$, $\sum_n a_n \sin(nx)$, say. This can always be found as the sine functions form a complete set. It follows that any function can be written in the form $v(x) =$

$\sum_n a_n e^{cx/2} \sin(nx)$. Thus, we may write any solution to (1.1) as

$$u(x,t) = \sum_n a_n e^{\lambda_n t} e^{cx/2} \sin(nx). \tag{1.4}$$

By the completeness of the set of spatial eigenfunctions, we can choose the a_ns to approximate any initial condition with arbitrary accuracy.

It is worth noting here that it is often the case with such finite-range linear problems that we can find a complete set of eigenfunctions and thus solve problems in this fashion. We call such a system *stable* if all the eigenvalues have negative real part, so all solutions to the stability problem eventually decay to zero. It is *unstable* if at least one eigenvalue has positive real part.

The other major group of stability problems comprises those which are infinite in spatial extent. These may be further divided into spatially-homogeneous problems, i.e. those for which the geometry is homogeneous in the flow direction, and spatially-nonhomogeneous problems. The former includes, for example, Poiseuille flow [23] in an infinitely-long channel. The theory for homogeneous problems is quite well-understood, but is sufficiently subtle and sufficiently important to Chapters 2 and 3 to warrant a fuller explanation in the next section. In general, for a system homogeneous in x, we may make a substitution of the form $u(x,t) = u_0 e^{ikx - i\omega t}$ and find a relationship between k and ω known as the dispersion relation. We then have one or more ks for each ω (or vice versa), forming a continuous spectrum. This may be contrasted with the discrete, countable spectrum of λs we had in the finite-range case.

Lastly, we consider systems which are infinite, or semi-infinite, in extent but nonhomogeneous. This includes wake flow [26], for example. In general, these systems possess both discrete and continuous spectra, the former being due to the nonhomogeneity and the latter coming from an integral similar to those in the following section, albeit made more complex by the presence of the nonhomogeneity.

Before moving on to nonhomogeneous systems, however, we first summarise the theory for homogeneous ones.

1.3 Parallel flow stability concepts

Linear stability theory is concerned with the development in space and time of infinitesimal perturbations of a base flow. A thorough explanation of the concepts involved in the study of the linear stability of parallel flows may be found in Huerre and Monkewitz [35] and we follow their description here. We consider such infinitesimal perturbations to be modelled by a partial differential equation involving space (x) and time (t) of the form

$$\widetilde{D}\left(-i\frac{\partial}{\partial x},\ i\frac{\partial}{\partial t}\right)\psi\left(x,t\right)=\Psi\left(x,t\right), \tag{1.5}$$

for some operator $\widetilde{D}$, with possible dependence on other parameters, such as the Reynolds number, which we omit for simplicity. We note that, for parallel flow in which another spatial direction, y say, must be considered, the boundary conditions on y often enable us to arrive at an equation of this form. An example of this is 2D parallel flow past a flat surface with appropriate boundary conditions at $y=0$ and as $y\to\infty$. As suggested by the name, such equations are arrived at by considering only perturbations which are linear in the perturbation parameter.

Our approach to solving this system comes from the theory of Green's functions. If we define a Green's function, or impulse response, G, by

$$\widetilde{D}\left(-i\frac{\partial}{\partial x},\ i\frac{\partial}{\partial t}\right)G\left(x,t\right)=\delta\left(x\right)\delta\left(t\right), \tag{1.6}$$

where the δs are Dirac delta functions, then we may arrive at the more general solution $\psi\left(x,t\right)$, for forcing $\Psi\left(x,t\right)$, by convolution of Ψ and G (see [56]). Note that our equation must be linear for this to hold.

We are now in a position to define some terms relating to stability. Our system is *stable* with respect to this impulse if,

$$\text{along any ray } \frac{x}{t} = \text{const}, \lim_{t\to\infty} G(x,t) = 0.$$

A system is *unstable* if,

$$\text{there exists some ray } \frac{x}{t} = \text{const}, \text{ such that } \lim_{t\to\infty} G(x,t) = \infty.$$

We may further subdivide this into flows which are *convectively unstable*, i.e. the flow is unstable but,

$$\text{along the ray } \frac{x}{t} = 0, \lim_{t\to\infty} G(x,t) = 0, \tag{1.7}$$

and those unstable flows which are *absolutely unstable*, i.e.

$$\text{along the ray } \frac{x}{t} = 0, \lim_{t\to\infty} G(x,t) = \infty.$$

These ideas are illustrated in Figure 1.1. We note that although, strictly, these criteria apply to the response to an impulse, we anticipate that many realistic initial conditions will have a response which appears similar to these, for large x and t.

1.3.1 Fourier and Laplace transform spaces

We now turn our attention to the criteria for distinguishing the various kinds of (in)stability. These are easier to derive after carrying out a Laplace transform in time (with ω as our transform parameter) and a Fourier transform in space (with k as parameter). For simplicity, we consider this for our impulse system, (1.6), rather than the full system. We note also that, as we expect $G(x,t)$ to be causal, i.e. $G(x,t) = 0$ for $t < 0$, our Laplace transform in time may be seen as another Fourier transform, with the lower limit at $-\infty$ (see [1]). After the usual substitutions for derivatives under Fourier transformation, our operator $\widetilde{D}$ becomes a function $D(k,\omega)$.

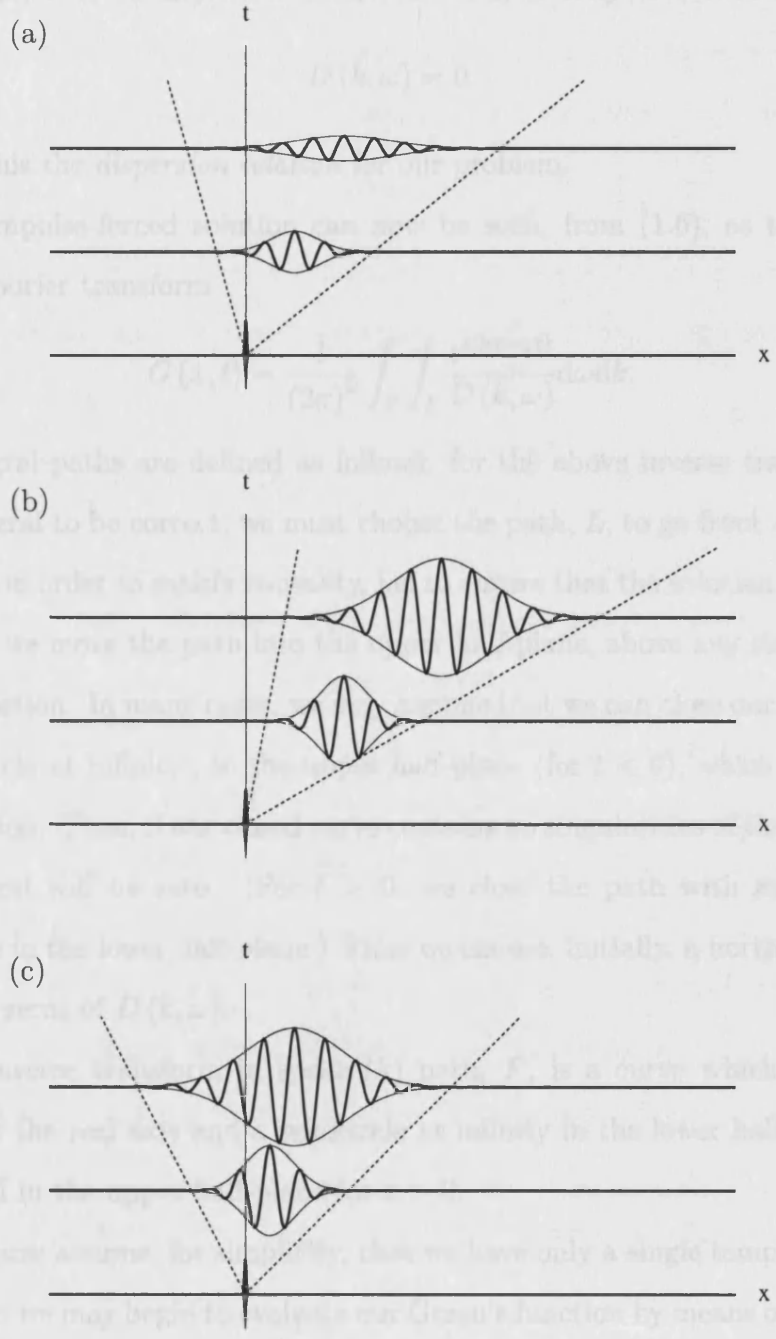

Figure 1.1: Representations of stability, convective instability and absolute instability. In (a) the wavepacket is stable, in (b) it is convectively unstable and in (c) it is absolutely unstable.

Temporarily returning to the full system (1.5), we note that in the unforced case $\Psi(x,t) = 0$, we may allow nontrivial solutions only when

$$D(k,\omega) = 0. \tag{1.8}$$

We call this the *dispersion relation* for our problem.

Our impulse-forced solution can now be seen, from (1.6), as the double inverse-Fourier transform

$$G(x,t) = \frac{1}{(2\pi)^2}\int_F\int_L \frac{e^{i(kx-\omega t)}}{D(k,\omega)}\mathrm{d}\omega\mathrm{d}k. \tag{1.9}$$

Our integral paths are defined as follows: for the above inverse transform in time integral to be correct, we must choose the path, L, to go from $-\infty$ to ∞. However, in order to satisfy causality, i.e. to ensure that the solution is zero for all $t < 0$, we move the path into the upper half-plane, above any singularities of the function. In many cases, we may assume that we can close our path with a 'semicircle at infinity', in the upper half-plane (for $t < 0$), which makes no contribution. Then, if our closed curve contains no singularities of the function, the integral will be zero. (For $t > 0$, we close the path with an 'infinite' semicircle in the lower half-plane.) Thus we choose, initially, a horizontal path above all zeros of $D(k,\omega)$.

The inverse transform in space (k) path, F, is a curve which, initially, comprises the real axis and a semicircle at infinity in the lower half-plane for $x < 0$ and in the upper half-plane for $x > 0$.

If we now assume, for simplicity, that we have only a single temporal mode $\omega(k)$, then we may begin to evaluate our Green's function by means of a residue calculation for the ω-integral, i.e.

$$G(x,t) = -\frac{i}{2\pi}H(t)\int_F \frac{e^{i(kx-\omega t)}}{\frac{\partial D}{\partial\omega}(k,\omega)}\mathrm{d}k, \tag{1.10}$$

where ω is now considered as a function of k. Here $H(t)$ is the Heaviside unit-step function, indicating that our system has no response before $t = 0$.

From our definitions of (in)stability, we are clearly interested in the behaviour of $G(x,t)$ for large t, with x/t fixed. To this end, we assume that we may choose a single value of k, k_c say, such that the group velocity at this value of k corresponds to any particular ray, i.e. any value of x/t, so

$$\frac{\partial \omega}{\partial k}(k_c) = x/t, \tag{1.11}$$

and also that we can deform our original F contour so that it passes through k_c. Then we may asymptotically evaluate $G(x,t)$ for large t by the method of steepest descents (see [35]),

$$G(x,t) \sim \frac{1}{\sqrt{2\pi}} \frac{e^{i(k_c x - \omega(k_c)t)}}{\frac{\partial D}{\partial \omega}(k_c, \omega(k_c)) \left(t \frac{d^2\omega}{dk^2}(k_c)\right)^{1/2}}. \tag{1.12}$$

Along each ray x/t the solution is dominated by the wavenumber (k-value) k_c defined above. Note that, although the formal ideas underlying this method are fairly recent, the general idea of asymptotically approximating the dominant contribution to the solution goes back a long way (see e.g. Havelock [28]).

It is important to distinguish at this stage between temporal and spatial (in)stability. In general, in temporal problems, we take the wavenumbers k to be real, and consider complex frequencies ω, with $\omega_i > 0$ indicating growth in time. In spatial problems, the frequencies are taken to be real and the wavenumbers complex, with $k_i < 0$ indicating growth for $x > 0$. We will use the subscripts r and i to indicate the real and imaginary parts of a quantity throughout.

For a temporal problem, we may define the maximum growth rate as

$$\omega_{i,max} = \omega(k_{max}), \tag{1.13}$$

where k_{max} is chosen such that

$$\frac{\partial \omega_i}{\partial k}(k_{max}) = 0, \tag{1.14}$$

at a maximum of $\omega_i(k)$. Equation (1.11) tells us that this is observed along the ray with $x/t = \frac{\partial \omega_r}{\partial k}(k_{max})$. From our discussion above, it is clear that if

$\omega_{i,max}$ is positive, then our flow is unstable and if it is negative, our flow is stable. We proceed to further classify unstable flows in accordance with (1.7). The *absolute frequency* is defined as

$$\omega_0 = \omega(k_0), \tag{1.15}$$

where k_0 is chosen such that

$$\frac{\partial \omega}{\partial k}(k_0) = 0. \tag{1.16}$$

It is clear that this corresponds to the solution along the ray $x/t = 0$. The absolute frequency is insufficient, on its own, to determine the nature of any instability in a flow: the pinch-point condition, described below, must first be considered. If, however, the pinch-point condition is met, then the absolute frequency may be used to classify flows as follows: if the imaginary part of the absolute frequency is positive, we have absolutely unstable flow, with negative imaginary part corresponding to convectively unstable flow. It is also worth noting that $\omega_{i,max}$ is an upper bound for any growth rate, so (see [35])

$$\omega_{i,0} < \omega_{i,max}. \tag{1.17}$$

1.3.2 The pinch-point condition

In order to fully describe the dominant contribution to the large-t asymptotics of our system, we find saddle points of $k(\omega)$ and use the method of steepest descents (see [44]). It is clear that simply finding points where the derivative is zero is insufficient: behaviour in the vicinity of such points is also important. To determine the location of the saddle points we use the method of Briggs and Bers ([11], [62], [7]) and the pinch-point condition described here will subsequently be referred to as the Briggs-Bers criterion.

We begin by noting that a saddle point in $k(\omega)$ will usually correspond to a branch cut in $\omega(k)$. We now consider the double inverse Fourier integral (1.9).

The contour L was chosen to be above all singularities in $\omega(k)$, including the branch point corresponding to such a branch cut. We define $k_L(\omega)$ to be $k(\omega)$ with ω constrained to lie on our contour L and similarly $\omega_F(k)$ to be $\omega(k)$ with k lying on the contour F. Note that these may each describe more than one line due to $D(k,\omega)$ possibly having multiple roots for k or ω.

Firstly, we can say that our curves $k_L(\omega)$ cannot cross the contour F, taken initially to be the real axis, in the k-plane. This is due to F being closed in a half-plane for the dynamics of $x > 0$ (upper) or $x < 0$ (lower). If the points on the contour L have large enough imaginary part, then the $k(\omega)$ curves in one half-plane affect dynamics of either $x > 0$ or $x < 0$, but not both, and they therefore cannot pass between half-planes.

From now on, for simplicity, we will assume that our system admits a single temporal mode and two spatial branches. We also assume that the system admits a single saddle point in k, i.e. k_0. We begin to displace our L contour downwards, keeping it above $\omega_F(k)$ and thus the branch-point singularity we are interested in. It is now possible that the $k_L(\omega)$ curves will begin to move into the other half-plane. We thus simultaneously deform our contour F, keeping it between the two $k_L(\omega)$ curves. The procedure is illustrated in Figure 1.2.

This process can be continued until our L contour meets the singularity in the ω-plane. At this point, the two $k_L(\omega)$ curves will meet and pinch the F contour. Now, $\omega_F(k)$ must meet our L contour precisely at the branch point ω_0 and the two $k_L(\omega)$ curves must pinch the F contour at the saddle point k_0. This enables us to locate the saddle point which determines the large-t evolution of our system. If ω_0 is located in the upper half-plane, the instability is absolute. If it is in the lower half-plane, the instability is convective. This follows from the fact that the absolute frequency ω_0 corresponds to the solution along the ray $x/t = 0$. If growth in time is observed along this ray, the sys-

tem is absolutely unstable; otherwise, an unstable system is only convectively unstable.

It is important to note that it is implicit in our simplified discussion that the pinching occurs between $k_L(\omega)$ curves which originate (when the ωs on L have large imaginary part) in opposite half-planes. This is necessary to ensure that we do indeed find a saddle point. This is not always the case, as may be seen in e.g. [7] and [50].

At this point we briefly mention the recent work of Fokas and Papageorgiou, who in [25] present two examples for which a modified version of the absolute/convective instability criterion, altered to be more geometrical in nature, is used. However, for the rest of this thesis we will use the more widely-recognised criterion described above.

1.3.3 Discrete and continuous spectra

For a system with no explicit time dependence, it is common to make a substitution of the form

$$u(x,t) = \bar{u}(x)e^{-i\omega t}. \tag{1.18}$$

We note that, due to the $\frac{\partial}{\partial t}$ terms which describe the temporal evolution of the system, this substitution leads to an eigenvalue problem for the eigenvalue ω. In higher-dimensional systems, x in this equation can be any position vector. For certain systems, for a fixed set of parameters, it is possible to find a set of discrete complex values of ω. An example of such a system is plane Poiseuille flow, see e.g. [40]. However, this is especially true of nonhomogeneous (in space) systems, such as those considered here. These eigenvalues form the discrete spectrum of our system.

If a discrete eigenvalue, ω, can be found with imaginary part $\omega_i > 0$, for some realistic boundary conditions, then the corresponding eigenfunction is often referred to as an *unstable global mode.*

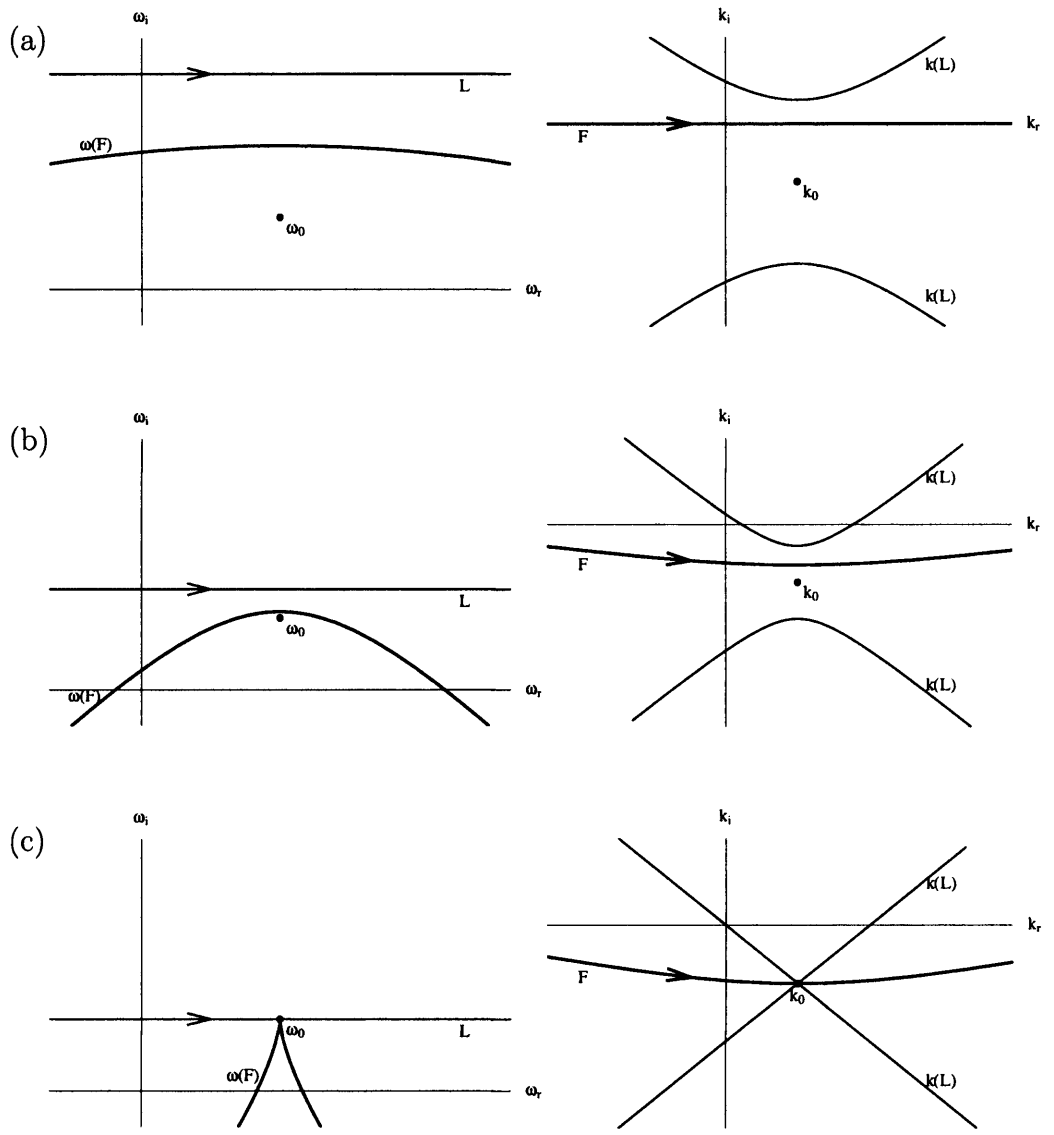

Figure 1.2: The pinching process. The diagrams on the left show the ω-plane, those on the right the k-plane. We begin, in (a), with the L contour above all singularities in the ω-plane and the F contour along the real axis in the k-plane. As the L contour is displaced downward in (b), it becomes necessary to curve the F contour. Eventually, in (c), the F contour becomes pinched between spatial branches and the L contour cannot be lowered any further. This happens at the branch point ω_0.

In many problems, however, the system also possesses a continuous spectrum. This is typically more difficult to find numerically and often manifests itself in calculations as a cluster of modes, along a line for example, the exact position of which is dependent on the discretisation in the numerical scheme. An example of this is boundary layer flow stability, see e.g. [59].

1.4 Global and local instability

Having defined and discussed the ideas of convective instability and absolute instability in the previous section, we now consider the concepts of global and local instability. A system is *globally unstable* if it supports an unstable global mode. This is a mode with a nontrivial eigenfunction whose frequency, ω, has positive imaginary part so that it grows everywhere in time. Unlike convective instability and absolute instability which, strictly, are only applicable to infinite-range systems, this is applicable to both finite-range and infinite-range systems.

Local stability refers to the stability of a flow-like system at a particular streamwise station. At such a station, we determine the parameters of the (full) system at that point. We then perform a stability analysis of a homogeneous system with the same parameters as those at the station. This then determines the *local stability* of the system at the station. Thus a flow, at a particular location, may be locally stable, locally convectively unstable, or locally absolutely unstable. The short-range nature of local stability makes it, too, relevant to both finite-range and infinite-range systems.

1.4.1 Recent work

As suggested previously, the study of absolute and convective instability and their relation to local and global instability has developed into a subject in

its own right. Huerre and Monkewitz [35] comprehensively reviewed the linear case for a number of physical scenarios. This work included the important result that a finite range of absolute instability can lead to self-sustained growth and hence global instability ([15], [34], [38], [42], [49]). Work in this area has been extended to include the nonlinear case, see for example [12], [19] and the recent review by Chomaz [13]. Tobias et al. [66] also extended the terminology to include disturbances in finite geometries.

Recently, some attention has been turned to analysis of the strongly non-parallel flow problem. This includes both the linear and nonlinear cases, see for example Edwards et al. [24], Tuckerman et al. [71], and the book by Schmid and Henningson [59].

1.5 Problems of recent interest

As mentioned in Section 1.2, there are many 'classical' linear stability problems in fluid mechanics which are quite well understood. However, there are also many problems which are less well understood, or where effects other than those found in the classical problems are important.

Non-self-adjoint systems are an example of such problems. A non-self-adjoint linear operator is one that is not equal to its adjoint. Given an inner product $\langle , \rangle$ on a space of functions, the adjoint of an operator $\widetilde{L}$ is the operator $\widetilde{L}^*$ such that, for all functions u and v, $\langle \widetilde{L}u, v\rangle = \langle u, \widetilde{L}^* v\rangle$. The formal definition of such an operator and proofs of existence, uniqueness etc. are quite involved and the reader is referred to a textbook on functional analysis, such as [17]. Instead, we concentrate on an example. Consider

$$\begin{gathered} \frac{\partial u}{\partial t} = \widetilde{L}u \quad \text{with} \quad \widetilde{L} = \frac{\partial^2}{\partial x^2} - c\frac{\partial}{\partial x} + \beta, \\ u(0,t) = u(\pi,t) = 0, \end{gathered} \tag{1.19}$$

for real constants c and β, representing a simple linearised Ginzburg-Landau

equation which includes an advection term. The adjoint of the operator $\widetilde{L}$ is

$$\widetilde{L}^* = \frac{\partial^2}{\partial x^2} + c\frac{\partial}{\partial x} + \beta \tag{1.20}$$

(see e.g. [56]) and therefore this problem is non-self-adjoint. To solve (1.19), we make our usual substitution $u(x,t) = e^{\lambda t}\bar{u}(x)$. The eigenfunctions of $\widetilde{L}$ are

$$\bar{u}(x) = e^{\frac{cx}{2}} \sin(nx) \tag{1.21}$$

and the eigenvalues are $\lambda_n = -c^2/4 - n^2 + \beta$, for integer $n \neq 0$. We note that, as a consequence of the non-self-adjointness of the linear operator, the eigenfunctions are not orthogonal:

$$\int_0^\pi e^{\frac{cx}{2}} \sin(n_1 x)\, e^{\frac{cx}{2}} \sin(n_2 x)\, \mathrm{d}x = \begin{cases} \frac{2c(e^{c\pi}-1)n_1 n_2}{\left(c^2+(n_1-n_2)^2\right)\left(c^2+(n_1+n_2)^2\right)}, & n_1+n_2 \text{ even} \\ \frac{-2c(e^{c\pi}+1)n_1 n_2}{\left(c^2+(n_1-n_2)^2\right)\left(c^2+(n_1+n_2)^2\right)}, & n_1+n_2 \text{ odd,} \end{cases} \tag{1.22}$$

for $n_1 \neq n_2$. These are not zero for $c \neq 0$. This can have important consequences for certain initial conditions.

We now turn our attention to non-self-adjoint matrices, i.e. matrices which are not equal to the complex conjugate of their transpose. There are a number of similarities between these and non-self adjoint differential operators. We will comment further on this later, but now give some examples which demonstrate properties of non-self-adjoint systems.

One important property of such systems we wish to demonstrate is that they may exhibit strong transients. Consider

$$\frac{\mathrm{d}\mathbf{u}}{\mathrm{d}t} = A\mathbf{u} \quad \text{with,} \tag{1.23}$$

$$A = \begin{pmatrix} -1 & \Lambda \\ 0 & -2 \end{pmatrix}. \tag{1.24}$$

Here, $\Lambda \in \mathbb{R}$ is large. This has solutions

$$\mathbf{u}(t) = a_1 e^{-2t} \begin{pmatrix} 1 \\ 0 \end{pmatrix} + a_2 e^{-t} \begin{pmatrix} \Lambda \\ -1 \end{pmatrix}, \tag{1.25}$$

for arbitrary constants a_1 and a_2. Therefore, for any initial condition, solutions eventually decay to 0. Note that, as Λ is large, the eigenvectors are nearly parallel. We put $a_1 = \Lambda$ and $a_2 = -1$ to satisfy the initial condition $\mathbf{u}(0) = (0\ 1)^T$, where the superscript T denotes the transpose. If we then measure the 'size' of $\mathbf{u}$, which we label $|\mathbf{u}|$, by the square root of the sum of the squares of its two components, it is straightforward to show that the maximum value of this is

$$|\mathbf{u}|_{max} = \sqrt{\frac{8\left(1+\Lambda^2\right)^3\left(\Lambda^2+\Lambda\sqrt{\Lambda^2-8}-2\right)}{\Lambda^2\left(3\Lambda+\sqrt{\Lambda^2-8}\right)^4}}, \tag{1.26}$$

which, for example, equals 5.025 when $\Lambda = 20$. A plot of $|\mathbf{u}|$ against t for this case is shown in Figure 1.3. It is also straightforward to show that, for Λ large, $|\mathbf{u}|_{max} \approx \Lambda/4$. Thus, by varying Λ, we have an initial condition of fixed size and an arbitrarily-large transient.

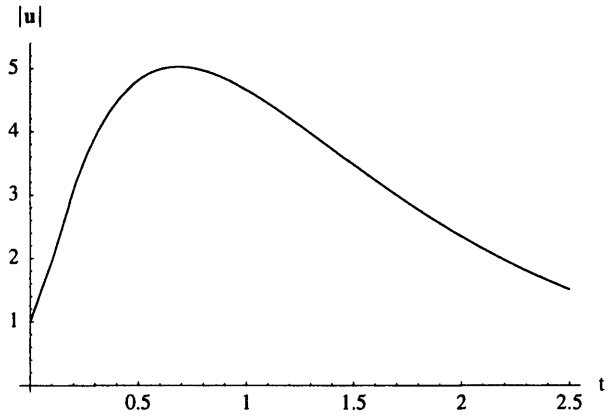

Figure 1.3: $|\mathbf{u}|$ against t for $\Lambda = 20$. Although the solution eventually decays, we see that it can become several times larger than the initial condition before it starts to do so.

We now demonstrate that it is the non-self-adjointness of A which leads to this transient. If we replace A by a general 2×2 self-adjoint matrix with

complex-valued elements

$$A = \begin{pmatrix} A_{(11)} & A_{(12)} \\ A^*_{(12)} & A_{(22)} \end{pmatrix}, \tag{1.27}$$

where the superscript asterisk denotes the complex conjugate. $A_{(11)}$ and $A_{(22)}$ are real. We assume that this matrix is nonsingular. The eigenvalues of the matrix are

$$\begin{aligned} \lambda_1 &= \tfrac{1}{2}\left(A_{(11)} + A_{(22)} - \sqrt{\left(A_{(11)} - A_{(22)}\right)^2 + 4A_{(12)}A^*_{(12)}}\right) \\ \lambda_2 &= \tfrac{1}{2}\left(A_{(11)} + A_{(22)} + \sqrt{\left(A_{(11)} - A_{(22)}\right)^2 + 4A_{(12)}A^*_{(12)}}\right), \end{aligned} \tag{1.28}$$

both of which are real. The corresponding eigenvectors are

$$\begin{aligned} \mathbf{q}_1 &= \begin{pmatrix} A_{(11)} - A_{(22)} - \sqrt{\left(A_{(11)} - A_{(22)}\right)^2 + 4A_{(12)}A^*_{(12)}} \\ 2A^*_{(12)} \end{pmatrix} \\ \mathbf{q}_2 &= \begin{pmatrix} A_{(11)} - A_{(22)} + \sqrt{\left(A_{(11)} - A_{(22)}\right)^2 + 4A_{(12)}A^*_{(12)}} \\ 2A^*_{(12)} \end{pmatrix}. \end{aligned} \tag{1.29}$$

Note that $\mathbf{q}_2^H\mathbf{q}_1 = 0$, where the superscript H indicates the conjugate transpose. Although we do not prove it here, this is true of any pair of distinct eigenvectors of a nonsingular self-adjoint complex matrix of any size. The solution to (1.23) with (1.27) is

$$\mathbf{u}(t) = a_1 e^{\lambda_1 t}\mathbf{q}_1 + a_2 e^{\lambda_2 t}\mathbf{q}_2, \tag{1.30}$$

for arbitrary a_1 and a_2. We assume that solutions eventually decay, so $\lambda_{1,2} < 0$. If $|\mathbf{u}| = \sqrt{\mathbf{u}^H\mathbf{u}}$, which coincides with the definition used previously, then

$$|\mathbf{u}(t)| = \sqrt{a_1^* a_1 e^{2\lambda_1 t}\mathbf{q}_1^H\mathbf{q}_1 + a_2^* a_2 e^{2\lambda_2 t}\mathbf{q}_2^H\mathbf{q}_2}, \tag{1.31}$$

as $\mathbf{q}_2^H\mathbf{q}_1 = 0$. The terms $a_1^*a_1$, $\mathbf{q}_1^H\mathbf{q}_1$, $a_2^*a_2$ and $\mathbf{q}_2^H\mathbf{q}_2$ are all real and positive, so $|\mathbf{u}(t)|$ decays monotonically; this may not be the case if $\mathbf{q}_2^H\mathbf{q}_1 \neq 0$ for a pair of eigenvectors, which could be true for a non-self-adjoint matrix. We

conclude that it is non-self-adjointness in such systems which can lead to the initial transient growth of solutions.

The transient growth experienced by some systems can be very important. For example, if the system described by (1.23) and (1.24) arose from linearising a more complex system then, for Λ large enough, the transient could take the solution completely out of the linear régime and although the prediction of the linear model is that all solutions decay, this may not be observed in practice. Thus transient growth has received considerable coverage in the literature (see e.g. [9], [32], [47]).

Another important consequence of non-self-adjoint systems is the sensitivity of their eigenvalues to small perturbations. In classical linear stability theory, it is the eigenvalues which determine the stability, or otherwise, of a system. Thus this sensitivity can be a very important consideration as a small perturbation of such a system can lead to a large change in the spectrum. We consider an example which is similar to the one considered in (1.23) and (1.24), i.e.

$$\frac{\mathrm{d}\mathbf{u}}{\mathrm{d}t} = A\mathbf{u} \quad \text{with} \quad A = \begin{pmatrix} -\frac{1}{2} & \Lambda \\ \epsilon & -2 \end{pmatrix}, \tag{1.32}$$

where Λ is real and large. This has -1/2 and -2 as eigenvalues for $\epsilon = 0$. For $\epsilon \neq 0$, the eigenvalues become $\lambda_{1,2} = \frac{1}{4}\left(-5 \pm \sqrt{9 + 16\epsilon\Lambda}\right)$. This means that a perturbation of size $|\epsilon| \approx 1/\Lambda$ can have a significant effect on the observed eigenvalues. If Λ is large, making the matrix strongly non-self-adjoint, then this can be quite a small perturbation. Figure 1.4 shows the size of this variation. The eigenvalues of an ϵ-perturbed matrix are referred to as the *ϵ-pseudospectrum* of the original matrix. We see that a perturbation of size $|\epsilon| > 1/\Lambda$ can be sufficient to push the decaying solution with eigenvalue -1/2 into the right half-plane, which corresponds to a growing solution. Rigorous definitions and examples of recent work on pseudospectra can be found in [54], [68], [69] and [70].

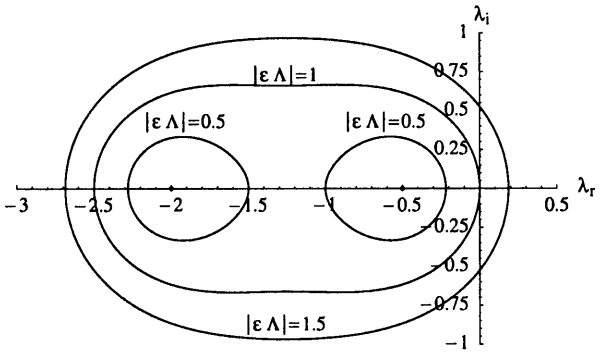

Figure 1.4: The ϵ-pseudospectra of the matrix A in (1.32). If ϵ is a complex-valued perturbation such that $|\epsilon\Lambda|$ is fixed, then the boundary of the region in which the eigenvalues can then be observed is shown by the corresponding line. The dots indicate the eigenvalues of the $\epsilon = 0$ system.

As an example of the connection between non-self-adjoint linear differential operators and non-self-adjoint matrices, we return to (1.19). One means of obtaining a solution to systems like this is to discretise the problem in space, replace the differential operators by small changes over a single step in space and time and arrive at an algebraic problem. It can then be shown that, for a good approximation scheme, in the limit of small steps in space and time, the algebraic system will have the same solution as the differential one.

We now discretise $\widetilde{L}u$ from (1.19) by means of a simple, symmetric in space, finite-difference system. Letting u_n^j be the value of our function at time-step j and position n and Δt and Δx be our step-lengths in time and space, we have

$$\begin{aligned} \frac{\partial u}{\partial t} &\approx \frac{u_n^{j+1} - u_n^j}{\Delta t} \\ \frac{\partial u}{\partial x} &\approx \frac{u_n^{j+1} - u_n^{j-1}}{2\Delta x} \\ \frac{\partial^2 u}{\partial x^2} &\approx \frac{u_n^{j+1} - 2u_n^j + u_n^{j-1}}{\Delta x^2}. \end{aligned} \tag{1.33}$$

Putting in these approximations and rearranging we get

$$\begin{bmatrix} \vdots \\ \vdots \\ u_n^{j+1} \\ \vdots \\ \vdots \end{bmatrix} = \begin{bmatrix} \ddots & \ddots & 0 & 0 & 0 \\ \ddots & m_0 & m_{-1} & 0 & 0 \\ 0 & m_1 & m_0 & m_{-1} & 0 \\ 0 & 0 & m_1 & m_0 & \ddots \\ 0 & 0 & 0 & \ddots & \ddots \end{bmatrix} \begin{bmatrix} \vdots \\ \vdots \\ u_n^{j} \\ \vdots \\ \vdots \end{bmatrix}, \tag{1.34}$$

where $m_{-1} = \frac{\Delta t}{\Delta x^2} - \frac{c\Delta t}{2\Delta x}$, $m_0 = 1 + \frac{-2\Delta t}{\Delta x^2} + \beta\Delta t$ and $m_1 = \frac{\Delta t}{\Delta x^2} + \frac{c\Delta t}{2\Delta x}$. We can see that the condition for $\widetilde{L}$ to be non-self-adjoint, i.e. that $c \neq 0$, is exactly the same condition as that which makes the matrix above non-self-adjoint. If we decide to study the system on the finite range $0 < x < L_0$, then as L_0 increases, the number of points required to accurately represent u increases and the matrix above becomes larger. The errors in eigenvalues found numerically are generally proportional to the Euclidean (Frobenius) norm of the matrix to which they correspond ([51]). This will typically grow as the matrix grows and thus the system becomes more difficult to solve. This is a fundamental aspect of the problem, not a numerical issue with the discretisation, although it does, of course, affect our ability to compute results.

Another important consequence of the non-self-adjointness is that the spectra of the infinite-range problem and that of any finite-range approximation may be very different. This can remain true even in the limit of the length of the finite-range problem tending to infinity. This phenomenon has been explored in [14] and [18].

A simple explanation of this property may be found by considering the evolution of a small pulse introduced in the middle of each system. For the infinite-range system, of course, this can be taken to be anywhere. If the infinite range system is convectively unstable and our non-self-adjointness is due to advection, then the pulse will grow as it advects away. The continuous spectrum therefore contains a range of wavenumbers for which the imaginary

part of the frequency is positive.

If the same pulse is introduced into a finite-range system, initially the behaviour will be similar to the case just described. The pulse will advect away and grow, until its influence reaches an end of the system. If this end then reflects some or all of the signal back in the opposite direction, as many reasonable end conditions will, the signal will be sent back and decay in space and time. Upon reaching the other end, it will return, possibly growing again. In many such systems, during this cycle some of the signal will be lost to the end conditions or to dissipation. Thus the pulse may be 'weaker' when it returns. Every frequency of the system thus decays over a cycle and hence decays as time tends to infinity, so all frequencies are stable. This remains true as the length of the system tends to infinity and can mean that the long-length-limit finite-range system has an entirely different spectrum to the infinite-range one.

Another important result, as discussed in [16] and [42] is that, in a slowly varying system satisfying the WKBJ approximation (see [5]), a global mode may be found by considering the properties of the local absolute frequency. As mentioned in Section 1.4.1, it is then found that a region of absolute instability is required for such a global mode to be unstable, i.e. to grow in time.

1.6 Overview

The main theme in this thesis is instability analysis of spatially-nonhomogeneous systems. The focus will be on several representative examples, which illustrate various aspects of the general problem, often with quite unexpected properties. It is worth emphasising from the outset that the method of analysis is strongly dependent on the nature of the nonhomogeneity. For example, in a flow through a periodically-deformed channel we are interested in criteria for absolute and convective instability and hence in continuous

spectra. In a channel flow with a localised expansion or contraction the focus will be on computing eigenvalues of discrete global modes, even though the continuous spectrum is present in the problem. In a problem formulated in a finite spatial domain, only discrete eigenfunctions are of relevance. Clearly, in practical applications, a wide range of nonhomogeneities is possible.

The work in this thesis will be fairly theoretical: although mention of practical applications of the examples presented will be made, we will make no specific engineering recommendations relating to, for example, the suppression of instability. Instead, it is hoped that the approaches developed in this thesis will contribute to the still lacking general theory of instability in nonhomogeneous systems.

The following subsection describes the content of subsequent chapters.

1.6.1 Chapter summary

The linearised Ginzburg-Landau equation is an important equation for a number of problems in fluid dynamics. For example, Huerre [33] used it as a simple illustration of convective and absolute instability. We begin, in Chapter 2, by considering this equation with a spatially-periodic linear growth rate term. Floquet theory is used to evaluate the spectra and investigate the question of absolute and convective instability in such strongly nonhomogeneous systems, using the so-called signalling problem.

A number of interesting results are obtained from this system. Firstly, the system may be made stable, convectively unstable or absolutely unstable by appropriate combinations of the parameters. The combinations required for such situations to occur are not straightforward. Secondly, although the sinusoidal variations of the linear growth rate term are chosen to have the same average, over a period, as the homogeneous case, adding the periodic variation makes the system more unstable. However, it is also found that the spatial

periodicity can cause regions of local absolute instability to appear while the system remains convectively unstable overall.

In Chapter 3 a problem of fluid-dynamical stability is investigated. We consider two fluids flowing through a channel whose width is small. A thin-layer approximation is made and, with one further simplifying assumption, an analytic solution is found to the governing equations. This is considered to be a base flow, of which we consider the evolution of perturbations.

The first nonhomogeneous case we consider is that of sinusoidally-varying wall shape, as shown in Figure 1.5(a). This, like the system investigated in Chapter 2, is a differential system with spatially-periodic coefficients and we again use the signalling problem to determine its spatial stability. Computation of the characteristic exponent (wavenumber) spectrum, using Floquet's theorem, shows that branch reconnections occur for frequencies with positive imaginary part for sinusoidal wall variations of any magnitude. This indicates that the flow is absolutely unstable in this case. It is then shown that the instability arises due to a three-wave resonance between branches, with one 'branch' being the variation in the channel wall.

In Chapter 4, a problem is discussed for which the physics is similar to that in Chapter 3. However, we take the nonhomogeneity in the channel shape to be confined to a finite x-range. The remainder of the channel is taken to be straight, with the upstream and downstream sections having equal dimensions, as shown in Figure 1.5(b). This is an example of a infinite-range nonhomogeneous problem and, as discussed previously, we search for a discrete spectrum of modes. It is important to note that the finite-range nature of the problem means that the distinction between absolute and convective instability is now less relevant: a system either supports unstable global modes or it does not.

Firstly, we consider the case where the wall-shape nonhomogeneity is si-

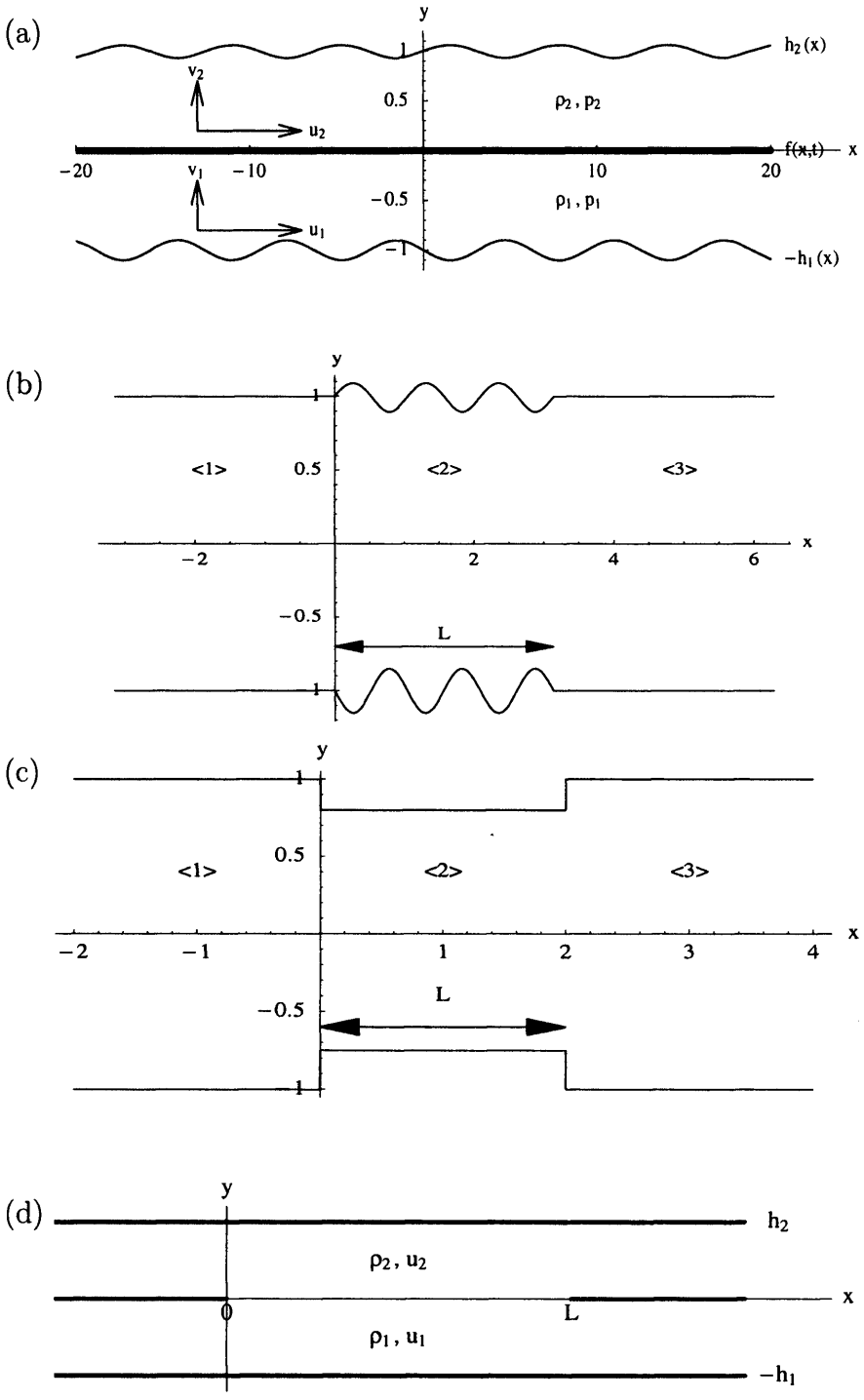

Figure 1.5: Diagrams showing the set-ups considered in Chapters 3-5. (a) is considered in Chapter 3, (b) and (c) in Chapter 4 and (d) in Chapter 5. The symbols on the diagrams are defined in the relevant chapters.

nusoidally shaped. Different numbers of sine periods in the wall shape are considered, with most being found to be unstable.

Secondly, a wall nonhomogeneity shaped like two discrete jumps, i.e. forming a rectangular 'obstacle', is considered. This is illustrated in Figure 1.5(c). Instability, due to feedback between the two ends of the middle section, is found both for channels with a contracted section and those with an expanded section. However, for the expanded-section case, the middle section must be reasonably long before the instability is observed. There is no such restriction for channels with a contracted middle section.

In Chapter 5, another problem with physics similar to that in the previous chapters is considered. In this case the geometry comprises a channel containing two fluids separated by a solid partition everywhere except for in a short finite region, where they are in contact, as shown in Figure 1.5(d). Numerical results are presented which show that the system is globally unstable for all finite aperture lengths which are not too short. This is despite the fact that the local system in the aperture region is only convectively unstable.

The problem is then reformulated by considering disturbances as waves travelling between the ends of the aperture. The system exhibits a feedback between such waves and this idea is used to obtain an infinite-range limit for the stability spectrum. It remains globally unstable in this limit, again despite the fact that the homogeneous system is only convectively unstable.

In Chapter 6, we move away from the problems of fluid-dynamical origin considered in Chapters 3, 4 and 5. In these chapters it was shown that a system which, over an infinite range, is locally convectively unstable everywhere can, over a finite range, support an unstable global mode through feedback between boundary conditions. In Chapter 6 we look at systems, typical of those used to study stability, which are stable over an infinite range but support strong transients as a growth mechanism. When nonhomogeneous boundary condi-

tions are introduced, in this case by confining the system to a finite range, global instability is again observed.

The first system we consider comprises three coupled linear kinematic wave equations. It is shown that each of the three waves which satisfy the equations is stable on an infinite range. One wave is right-going; two are left-going and the parameters of the problem are chosen such that these are in near-resonance. When the system is confined to a short range, unstable eigenmodes are found.

The second system comprises two coupled linear kinematic wave equations. This system is amenable to analytic solution for sufficiently simple initial conditions. Again, solutions decay on an infinite range but, if the coupling parameter is appropriately chosen, solutions can grow when the system is confined. The system is shown not to receive energy through the boundary conditions; this leads to the result that the instability is due to the non-normality of the wave operator.

The Benjamin-Ono equation is used in the stability analysis of deep stratified fluids. Integration across a 'bulk fluid' region satisfying Laplace's equation in such analysis leads to the Benjamin-Ono equation having a Cauchy integral term. Solutions to equations possessing a Cauchy integral term may decay algebraically in space; this is demonstrated by consideration of soliton solutions of the equation at the beginning of Chapter 7.

In the remainder of the chapter, a modified Benjamin-Ono equation with a linear growth rate term and a dissipative term is considered. Firstly, it is shown that 'mechanical' use of the Briggs-Bers (saddle point) criterion for the stability analysis of the system is incorrect. This is because the Cauchy integral term in the equation corresponds to a nonanalytic function of wavenumber in the dispersion relation. The branch cut associated with this makes a more important contribution to the overall stability than the saddle point does.

Having considered the stability problem associated with the homogeneous

version of our modified Benjamin-Ono equation, we construct an inhomogeneous version by making the linear growth rate vary in space. We wish to compute solutions to this problem numerically and so we consider the eigenvalues of a matrix formulation. However, the algebraic decay of solutions discussed above means that the computational domain has to be very large to fully represent the system and it is found that attempts to accurately compute eigenvalues fall foul of the problems discussed earlier for large-matrix eigenvalue calculations.

In Chapter 8 we summarise the work presented in this thesis and suggest some ways in which it might be interesting to continue the ideas developed here.

Chapter 2

The linearised Ginzburg-Landau equation

2.1 Introduction

As an introductory example, we consider a linearised one-dimensional Ginzburg-Landau equation with a spatially-periodic linear growth rate term. The general approaches to the study of the stability of spatially-periodic systems are still being developed (see e.g. [10]). Therefore, in this chapter and the next, we consider representative examples with the hope of identifying the typical features of such systems with regard to the distinction between stability, convective instability and absolute instability.

The Ginzburg-Landau equation is a classical model used in the instability theory of dissipative systems. It describes the typical behaviour of a system near the onset of a Hopf bifurcation (see [23]). The linearised version of this equation has been used as an illustration of absolute and convective instability in open flows (see [33]), end effects and transient growth, as well as of the relationship between discrete spectra of non-self-adjoint operators and absolute and convective instability in the related homogeneous systems (see [14], [18]).

Firstly, we recall the spatially-homogeneous case, which may be analysed completely for a given initial condition and which has a well-defined dispersion relation, as described in Chapter 1. We then include spatial periodicity in the destabilising term and address the question of absolute/convective instability for such strongly nonhomogeneous systems. Strictly speaking, the issue should be resolved using a Green's function approach, similar to that outlined in the introduction, by solution of an initial-and-boundary-value problem. However, this approach may not be feasible in more complicated situations. Instead, we rely on the analysis of the so-called signalling problem in conjunction with parametric continuation from a well-defined state (the system with constant coefficients, in our case). Specifically, we assume that a time-periodic disturbance is being constantly supplied to the system by means of a spatially-localised source. The source of the disturbance does not need to be specified as we are effectively studying an infinite-time limit. We consider the response of the system in the form of spatial eigenfunctions, which in the constant-coefficient system may be written as exponentials. In the case of spatially-periodic coefficients, the exponentials are replaced by more complicated functions determined by Floquet theory. We use parametric continuation to distinguish between eigenfunctions corresponding to upstream- and downstream-propagating disturbances in the far field (away from the disturbance source). We are then able to distinguish between stable and unstable systems. The analogue of the pinch-point condition described in Chapter 1 is then used to pinpoint the onset of absolute instability in this example. In particular, we find that absolute instability appears sooner when an x-periodic component is added to the destabilising term, despite the average value of the term, over a period, being the same. Also, although making the system periodic makes it less stable in general, we find that the system remains convectively unstable when it contains regions where the local value of the destabilising term would correspond

to absolute instability in the homogeneous case, i.e. regions of local absolute instability.

2.2 Formulation

Consider the following one-dimensional linearised Ginzburg-Landau equation:

$$\begin{aligned} u_t + cu_x &= u_{xx} + b(x)u \quad \text{where,} \\ b(x) &= b_0 + \epsilon \sin(xL). \end{aligned} \tag{2.1}$$

This equation includes an advection term cu_x, with c constant, and a term $b(x)u$ which, in the case of constant positive $b(x)$, is a source of instability in the system. As this system is intended as an introductory example, we choose a sinusoidal variation in $b(x)$ for its simplicity. The constant ϵ is initially taken to be small; it measures the size of the variation in $b(x)$ over a period. The length of the period is equal to $2\pi/L$ and is thus fixed by L. Equation (2.1) has no explicit t dependence and so, as suggested in Chapter 1, we take the solution to be of the form $u(x,t) = e^{-i\omega t}\bar{u}(x)$. For this problem we will generally take ω to be real-valued and so this is a spatial stability problem. Substituting into (2.1), we have

$$-i\omega\bar{u}(x) + c\bar{u}'(x) = \bar{u}''(x) + [b_0 + \epsilon \sin(xL)]\bar{u}(x). \tag{2.2}$$

Now we let $\tilde{x} = xL$ and $v(\tilde{x}) = \bar{u}(x)$. This gives

$$-i\omega v(\tilde{x}) + Lcv'(\tilde{x}) = L^2 v''(\tilde{x}) + [b_0 + \epsilon \sin(\tilde{x})]v(\tilde{x}). \tag{2.3}$$

We may divide through by L^2, rescaling c, b_0, ω and ϵ accordingly, rearrange and drop the $\sim$s to obtain

$$v''(x) - cv'(x) + [b_0 + i\omega + \epsilon \sin(x)]v(x) = 0. \tag{2.4}$$

This shows that the system has three significant constant parameters, c, b_0 and ϵ, in addition to the disturbance frequency ω. We can write (2.4) as a

system of first-order equations, by putting

$$v = v_{(1)}, \quad v' = v_{(2)}. \tag{2.5}$$

So

$$\begin{aligned} \mathbf{v}' &= \begin{pmatrix} v'_{(1)} \\ v'_{(2)} \end{pmatrix} = A\mathbf{v} \quad \text{where,} \\ A &= \begin{pmatrix} 0 & 1 \\ -b_0 - i\omega - \epsilon\sin(x) & c \end{pmatrix}. \end{aligned} \tag{2.6}$$

A is a continuous 2π-periodic matrix. Solutions of (2.6) are conventionally studied with the aid of Floquet's theorem, which we discuss in the following section.

2.3 Floquet's theorem[1]

Consider an equation of the form

$$\frac{\mathrm{d}\mathbf{v}}{\mathrm{d}x} = A(x)\mathbf{v}, \quad x \in \mathbb{R}, \tag{2.7}$$

where $A(x)$ is a continuous $n \times n$ matrix which is θ-periodic in x for some constant θ. Here we will always take *θ-periodic* to mean 'periodic with period θ'. $\mathbf{v} = \mathbf{v}(x)$ is a function from $\mathbb{R}$ to $\mathbb{R}^n$ satisfying this equation. A *fundamental matrix*, $\Phi(x)$, of such an equation is an $n \times n$ matrix with n linearly independent solutions of the equation as its columns. Floquet's theorem states that any fundamental matrix of (2.7) can be written as the product of an θ-periodic matrix and a (generally) non-periodic matrix.

Theorem 1 (Floquet) *Consider equation (2.7) with $A(x)$ a continuous, $n \times n$, θ-periodic matrix. Each fundamental matrix $\Phi(x)$ of (2.7) can be written as a product of two $n \times n$ matrices*

$$\Phi(x) = P(x)e^{Bx}, \tag{2.8}$$

[1] see [72]

with $P(x)$ θ-periodic and B a constant $n \times n$ matrix.

Proof

The fundamental matrix $\Phi(x)$ is composed of n linearly independent solutions of (2.7). Putting $\xi = x + \theta$ and using dashes to represent derivatives w.r.t. x or, equivalently, ξ, we have

$$\begin{aligned} \mathbf{v}' &= A(\xi - \theta)\mathbf{v} \\ &= A(\xi)\mathbf{v}, \end{aligned} \tag{2.9}$$

so we see that $\Phi(\xi) = \Phi(x + \theta)$ is also a fundamental matrix. As $\Phi(x)$ and $\Phi(x + \theta)$ each contain n linearly independent solutions to (2.7), which has at most n solutions, they must be linearly dependent. Thus, we have a constant nonsingular $n \times n$ matrix C such that

$$\Phi(x + \theta) = \Phi(x)C. \tag{2.10}$$

That C must be constant is shown in Appendix A.1.1. There exists a constant matrix B such that

$$C = e^{B\theta}. \tag{2.11}$$

The existence of a matrix logarithm is justified in A.1.2. Consider now

$$P(x) = \Phi(x)e^{-Bx}. \tag{2.12}$$

Then

$$\begin{aligned} P(x + \theta) &= \Phi(x + \theta)e^{-B(x+\theta)} \\ &= \Phi(x)Ce^{-B\theta}e^{-Bx} \\ &= \Phi(x)e^{-Bx} \\ &= P(x). \end{aligned} \tag{2.13}$$

So $P(x)$ is θ-periodic and

$$\Phi(x) = P(x)e^{Bx}. \tag{2.14}$$

□

The eigenvalues, η, of C are called *characteristic multipliers*. For each such η we may find complex λ such that $\eta = e^{\lambda\theta}$, unique up to multiples of $2\pi i/\theta$. Such λ are called *characteristic exponents* of C. For any eigenvector, $\mathbf{q}$, of C, we can choose these characteristic exponents such that they coincide with the eigenvalues of B and

$$e^{B\theta}\mathbf{q} = C\mathbf{q} = \eta\mathbf{q} = e^{\lambda\theta}\mathbf{q}. \tag{2.15}$$

As mentioned in Section 2.2, equation (2.4) meets the requirements of Floquet's theorem. The fact that the (real part of the) exponents λ are uniquely determined is important to us as it is these real parts which determine the growth, or otherwise, of solutions of (2.4).

We delay a discussion of the definition, in general, of stability for (2.1) until we have considered the case $\epsilon = 0$.

2.4 The case $\epsilon = 0$

For the case $\epsilon = 0$, we may study solutions analytically. As the system is now homogeneous in space, as well as in time, we may arrive at a dispersion relation for this problem, as discussed in the introduction. We make a wavelike substitution into (2.4), with $\epsilon = 0$, of the form $v(x,t) = v_0 e^{ikx - i\omega t}$. This gives us a dispersion relation of

$$k^2 + cik - (b_0 + i\omega) = 0. \tag{2.16}$$

We begin by considering the temporal stability of a system with this dispersion relation, i.e. (2.4). We will now refer to the k-values as wavenumbers and ω-values as frequencies, as per Chapter 1. For any real wavenumber, the imaginary part of the frequency, ω_i, is given by

$$\omega_i = b_0 - k^2 \tag{2.17}$$

and so, if $b_0 < 0$, waves with any wavenumber will decay in time and the system is stable. For $b_0 > 0$, there will be wavenumbers which correspond to growing solutions and hence instability. In order to determine which parameter combinations correspond to convective instability and which to absolute instability, we consider the spatial problem. Solutions of (2.16) for k are

$$k = \frac{-ci}{2} \pm i\sqrt{\left(\frac{c}{2}\right)^2 - (b_0 + i\omega)}. \tag{2.18}$$

We note that, when $b_0 < 0$, for any real ω we will obtain one k-value with positive imaginary part and one k-value with negative imaginary part. As we know the $b_0 < 0$ situation to be stable, we can say that the wavenumber with positive imaginary part must be downstream-travelling, as it decays in the downstream direction and is stable. The wavenumber with negative imaginary part must be upstream-travelling, as it decays upstream. It is from this situation, which we fully understand, that we continue our solutions first into the convectively unstable régime and then into absolute instability.

From (2.18), we know that solutions to the homogeneous system (2.4 with $\epsilon = 0$) are of the form

$$v(x) = a_1 e^{\left[\frac{c}{2} + \sqrt{(\frac{c}{2})^2 - (b_0 + i\omega)}\right]x} + a_2 e^{\left[\frac{c}{2} - \sqrt{(\frac{c}{2})^2 - (b_0 + i\omega)}\right]x}, \tag{2.19}$$

for constant a_1 and a_2. Firstly, consider $c < 0$. Having said that, when $b_0 < 0$, solutions decay and thus our upstream-travelling and downstream-travelling waves decay in their direction of travel for all real ω, we may now consider the values of ω for which the corresponding waves decay when $b_0 \geq 0$. For the real parts of the two exponents to have opposite sign and thus for the waves to continue to decay in their direction of travel, we require

$$\mathrm{Re}\left[\frac{c}{2} + \sqrt{\left(\frac{c}{2}\right)^2 - (b_0 + i\omega)}\right] > 0. \tag{2.20}$$

Considering the limiting case, $\mathrm{Re}\left[\frac{c}{2} + \sqrt{\left(\frac{c}{2}\right)^2 - (b_0 + i\omega)}\right] = 0$, we have

$$\frac{c}{2} + \sqrt{\left(\frac{c}{2}\right)^2 - (b_0 + i\omega)} = i\Upsilon, \tag{2.21}$$

for some $\Upsilon \in \mathbb{R}$. Rearranging and equating real and imaginary parts, we have $|\omega| = |c\sqrt{b_0}|$. Stability thus occurs, when $b_0 \geq 0$, for

$$|\omega| > -c\sqrt{b_0} \quad \text{(n.b. } c < 0\text{)}. \tag{2.22}$$

Similarly, when $c > 0$, we have stability for

$$|\omega| > c\sqrt{b_0}. \tag{2.23}$$

As suggested in Chapter 1, we have absolute instability when our two (in this case) k-curves pinch the integration contour for k. This occurs when two wavenumbers, which 'originate' in opposite half-planes, become equal. In the introduction, by taking our ω-integration contour (L) above the singularities of the dispersion relation, we were, in effect, giving ω a large imaginary part. In this problem, b_0 and ω only occur in the combination $(b_0 + i\omega)$, so increasing ω_i is the same as decreasing b_0 (which is real). As has already been mentioned, decreasing b_0 below 0 leads to stability and the separation of the two k-curves into opposite half-planes and so our curves clearly do 'originate' in different half-planes. Two k-values will be equal and our k-curves will pinch, when

$$\sqrt{\left(\frac{c}{2}\right)^2 - (b_0 + i\omega)} = 0. \tag{2.24}$$

This happens when $\omega = 0$ and $b_0 = \frac{c^2}{4}$. Thus, for the range $0 < b_0 < \frac{c^2}{4}$, we have instability, but not absolute instability, and we conclude that this is the convective instability range. We note that, with b_0 in this range, there exists a range of real ω for which both wavenumbers (k-values) have negative imaginary part (see Figure 2.1). We conclude that, for such ω, the downstream-travelling wave now grows in the downstream direction, while the upstream-travelling wave still decays upstream, as would be expected with convective instability.

It is also worth noting that, in the case of absolute instability, there exists a frequency ($\omega = 0$ in this case) for which the upstream and downstream waves are indistinguishable.

Numerical calculations can be used to show the effect of varying b_0 on the range of ω for which solutions are stable. As b_0 increases, the range of ω for which solutions are unstable is seen to increase.

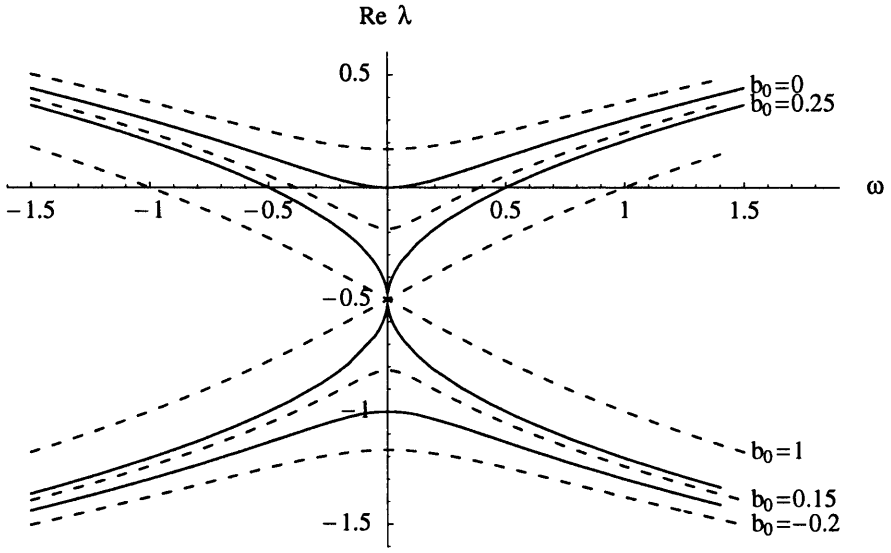

Figure 2.1: The variation of the real part of the characteristic exponents of (2.4) with ω, for several values of b_0. $\epsilon = 0$ and $c = -1$. Note that $\lambda = ik$. The diagram is symmetric about $\mathrm{Re}(\lambda) = -0.5$, so only half of the curves have been labelled.

It is worth noting at this point that, although we have generally only considered the case $c < 0$ here, (2.19) remains essentially the same under the change $c \to -c$, $x \to -x$ and so all the results in this section hold for $c > 0$, but with the direction in space reversed.

Finally, we note that although, for stability problems, we are often interested in making wavelike substitutions similar to those above, for the case $\epsilon = 0$ we can solve the equation for a given initial condition. If $v(x, t = 0) = \delta(x)$ then our system is solved by

$$v(x,t) = \frac{1}{2\sqrt{\pi t}} e^{b_0 t - \frac{(x-ct)^2}{4t}}, \tag{2.25}$$

a translating, spreading Gaussian curve. We note that, if $b_0 < 0$, corresponding to stability, this solution will decay for all values of x. If $0 < b_0 < \frac{c^2}{4}$, corresponding to convective instability, we fix x, setting it equal to zero for simplicity and the solution becomes

$$v(0,t) = \frac{1}{2\sqrt{\pi t}} e^{\left(b_0 - \frac{c^2}{4}\right)t}, \tag{2.26}$$

which decays. However, 'moving along with' the solution, by putting $x = ct$, we obtain

$$v(ct,t) = \frac{1}{2\sqrt{\pi t}} e^{b_0 t}, \tag{2.27}$$

which clearly grows. Thus, in a fixed frame of reference, the solution will decay, but in a moving frame, moving at an appropriate speed, the solution grows. This corresponds exactly to our definition of convective instability. Finally, if $b_0 > \frac{c^2}{4}$, putting $x = 0$ again gives us (2.26) again, which now grows, corresponding to absolute instability.

2.5 The case $\epsilon \neq 0$

Now we reintroduce the $\epsilon \sin(x)$ term into (2.6) and study solutions numerically. We consider solutions with

$$\Phi(0) = \begin{pmatrix} 1 & 0 \\ 0 & 1 \end{pmatrix} = I_2, \tag{2.28}$$

where $\Phi(x)$ is a fundamental matrix of solutions, as described in Section 2.3. This ensures that we get two linearly independent solutions and that the matrix C in (2.10) is equal to $\Phi(2\pi)$. From this, the eigenvalues of C can be obtained and hence the characteristic exponents. We may thus study the effect of the ϵ term on the system.

We begin by considering b_0 and ϵ both small, which we treat as a continuation of the b_0 small, $\epsilon = 0$ case. The results of this are shown in Figure 2.2.

When $\epsilon = 0$ for $b_0 = 0.15$, the system is convectively unstable. We see that increasing ϵ from 0 makes the system more unstable - that is, at $\omega = 0$, the real parts of the characteristic exponents become closer in value, making the most unstable mode more unstable. This indicates that adding any amount of periodic variation to the destabilising term makes the system less stable, despite the average value, over one period, of the term remaining the same. As ϵ is increased further, the characteristic exponent curves eventually meet at about $\epsilon = 0.5$. Although it is not shown, the imaginary parts of the characteristic exponents are both zero at $\omega = 0$. The two characteristic exponents are thus identical for $\epsilon \approx 0.5$, $\omega = 0$, indicating absolute instability.

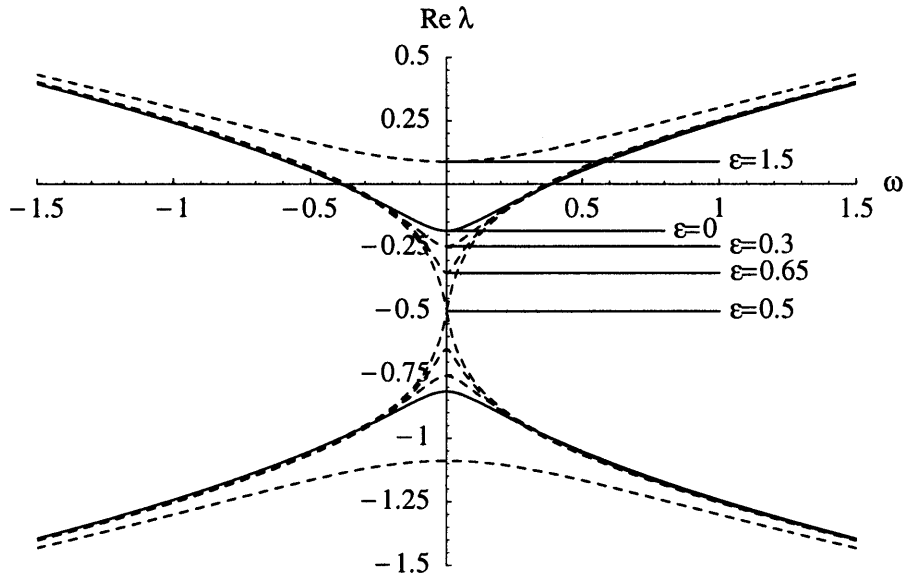

Figure 2.2: The variation of the real part of the characteristic exponents of (2.4) with ω, for several values of ϵ. $b_0 = 0.15$ and $c = -1$. Note that $\lambda = ik$.

However, as ϵ increases still further, we find that eventually the curves begin to move apart again (see the case $\epsilon = 0.65$ in Figure 2.2). It is not, however, immediately clear whether this corresponds to the absolute instability being broken again, as we have relied on continuation from the case $\epsilon = 0$. When we reach absolute instability, the λ-curves meet and may then rejoin differently.

Beyond this, then, (in terms of larger ϵ) we may not have the condition that increasing the imaginary part of ω moves the two curves into opposite half-planes.

Another important point which can be made about Figure 2.2 is that the overall system remains convectively unstable globally, even when regions of space which could be considered to be absolutely unstable are present. For example, when $\epsilon = 0.3$ in Figure 2.2, we can see that the system remains convectively unstable. However, if we define a 'local b_0' to be the value of $b_0 + \epsilon \sin(x)$ at a particular x-station, it is clear that this has a maximum value of 0.45. Comparing this with our absolute instability criterion, for the homogeneous case of $b_0 > \frac{c^2}{4}$ (=0.25 here), we see that there will exist regions of local absolute instability. We know (see Section 1.4.1) that a region of local absolute instability is sometimes sufficient for global instability, but here that is clearly not the case.

Next, we consider Figure 2.3, which shows plots of complex λ as a function of real ω, for several values of ϵ. We begin by noting that our characteristic exponents are repeated infinitely in the λ-plane, separated by an amount $n \in \mathbb{Z}$. This is a consequence of the 2π-periodic coefficients of the equation and may be understood by considering that any matrix like e^{inIx}, with I the identity matrix, may be divided out of $P(x)$ in (2.8) and multiplied into e^{Bx} in the same equation, without changing the validity of Floquet's theorem. This will change the characteristic exponents by n and these 'new' characteristic exponents will be as valid as any others. This phenomenon will be discussed in much more detail for the example in the next chapter.

In the figure, we show only two copies, the one 'nearest' the origin and the copy just above it, in the λ-plane. When $\epsilon = 0$, the important curves to concentrate on are those which pass nearest to -0.5 in the λ-plane. In this ($\epsilon = 0$) case, these are the only ones that really exist, but a copy is shown

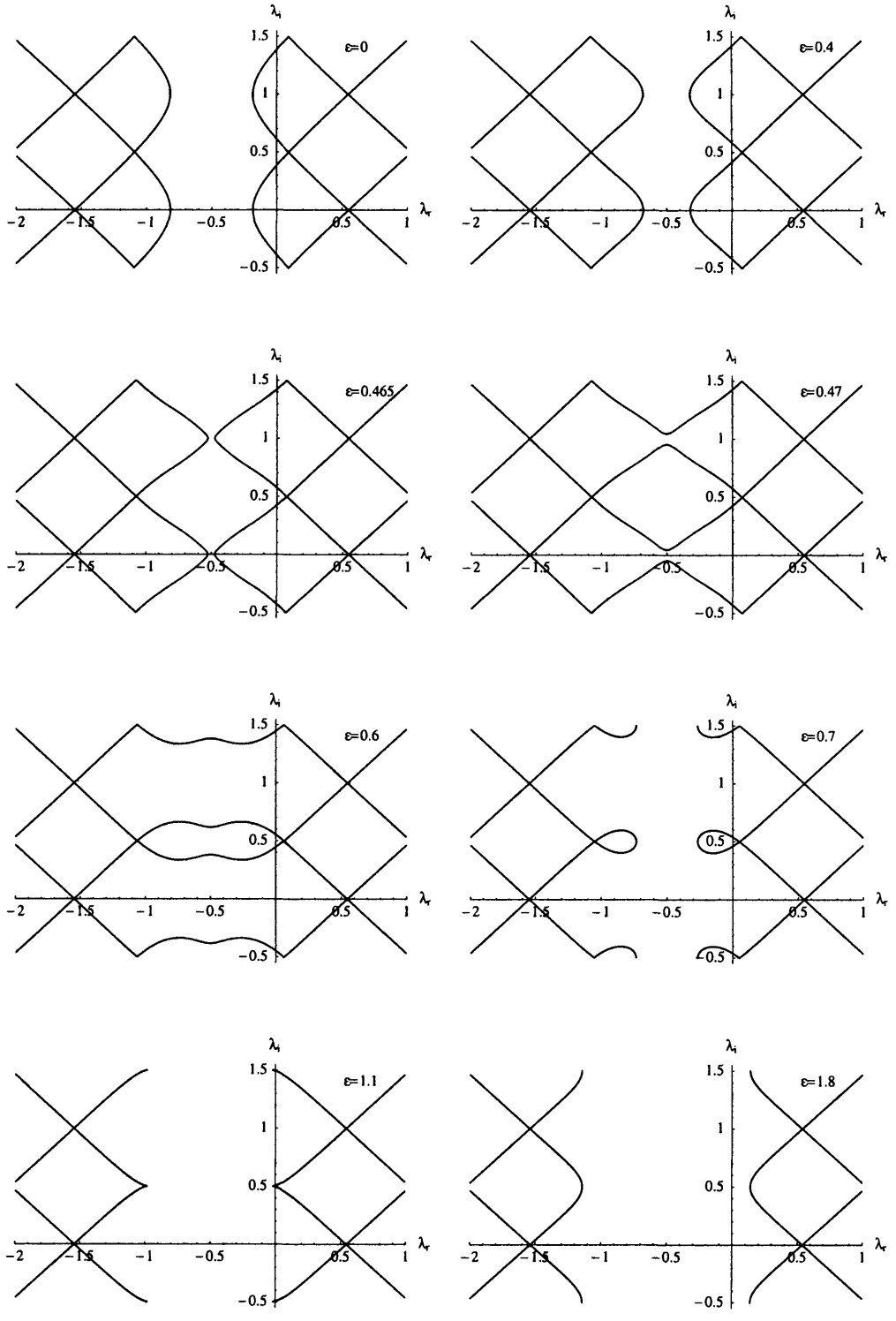
ε=0
ε=0.4
ε=0.465
ε=0.47
ε=0.6
ε=0.7
ε=1.1
ε=1.8
λi
λr
1.5
1
0.5
−0.5
−2
−1.5
−1
−0.5
0.5
1

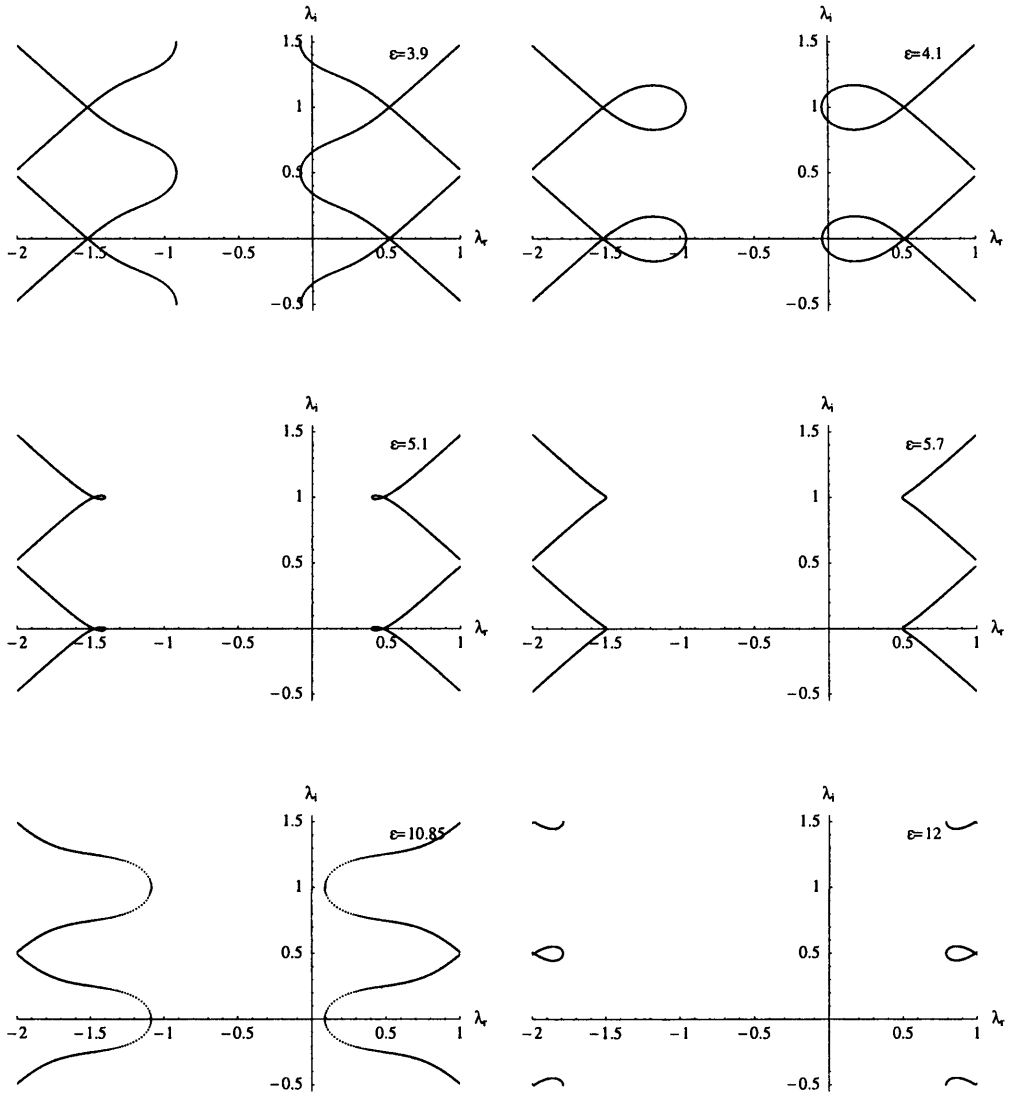

Figure 2.3: Plots of the characteristic exponents of our equation for varying real ω in the complex λ-plane, for several values of ϵ. $c = -1$ and $b_0 = 0.15$. A full explanation of this figure may be found in the text.

above to facilitate comparison with the $\epsilon \neq 0$ cases. Firstly, we note that the upstream-travelling branch curves are those for which $\lambda_r \to -\infty$ as $\lambda_i \to \pm\infty$, by consideration of (2.16). The downstream-travelling branches are those on the curves which have $\lambda_r \to \infty$ as $\lambda_i \to \pm\infty$. The fact that the downstream-travelling branches cross the imaginary λ-axis means that some downstream-travelling signals grow downstream and this situation is, as discussed above, convectively unstable.

As ϵ is increased, upstream-travelling and downstream-travelling curves move towards each other. As ϵ is increased further, we observe that the two sets of curves reconnect, indicating absolute instability. For ϵ larger still, the two sets of curves move apart again. Now, however, each upstream-travelling and downstream-travelling curve has reconnected to a different curve of its own type. By carefully noting which pairs of downstream-travelling and upstream-travelling curves connect at which ϵ values, we see that a pair of upstream-travelling curves and downstream-travelling curves connect to each other and then each reattaches to a new curve of its own type. They then repeat this process. The purpose of the diagram is therefore to demonstrate how we may continue to observe mode reconnections for ϵ of any size as there are infinitely many upstream-travelling curves for each upstream-travelling curve to reconnect with and infinitely many downstream-travelling curves for each downstream-travelling curve to reconnect with. As we have said, increasing ϵ beyond the point at which the curves meet may push them apart again, although this does not necessarily correspond to a return to convective instability.

Justification for choosing to plot the curve only for the value $\omega = 0$ will be given later. When b_0 varies, the changes in shape of the curves are shown in Figure 2.5. We can also demonstrate numerically the fact that the curves can only reconnect for $\omega = 0$. This is our reason for plotting $\omega = 0$ in Figures 2.4

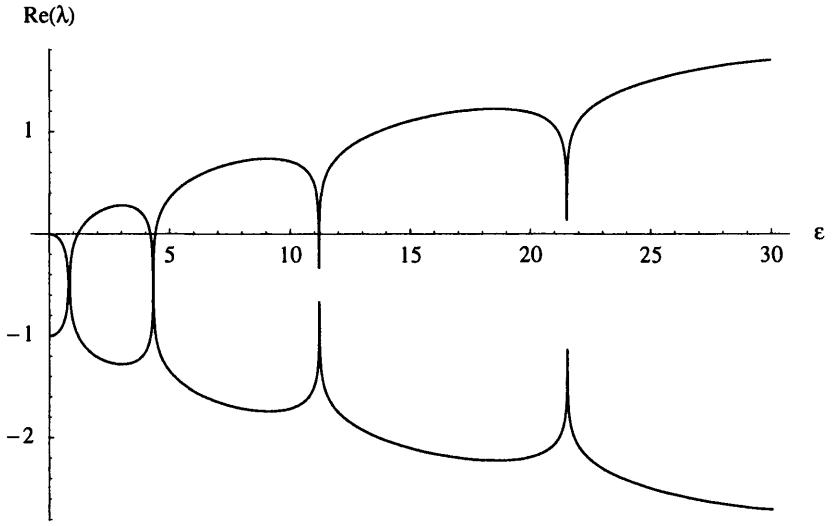

Figure 2.4: The variation of the real part of the characteristic exponents of (2.4) with ϵ. $b_0 = 0$, $\omega = 0$ and $c = -1$. Numerical calculations near each 'spike' in the graph show that they do meet up in the middle.

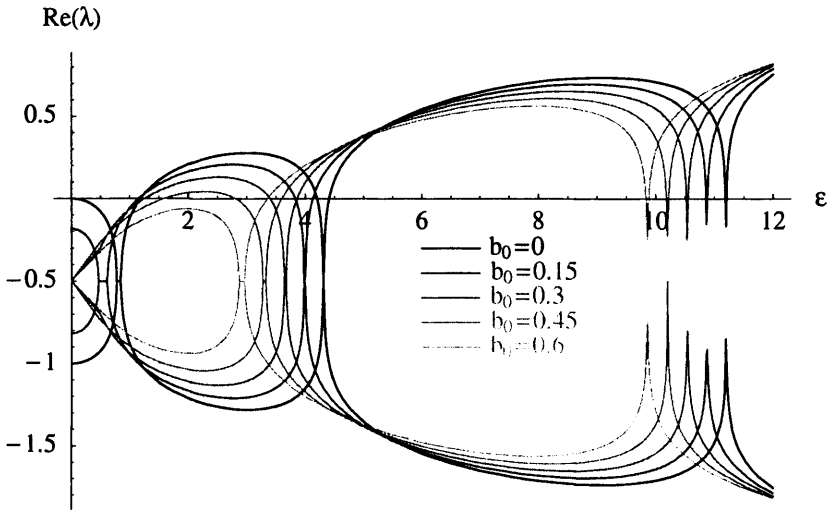

Figure 2.5: The variation of the real part of the characteristic exponents of (2.4) with ϵ for various b_0. $c = -1$ and $\omega = 0$.

and 2.5. When ω is very small, the variation of the characteristic exponents with ϵ is very similar to the case where $\omega = 0$, but the curves never reconnect. This is shown in Figure 2.6.

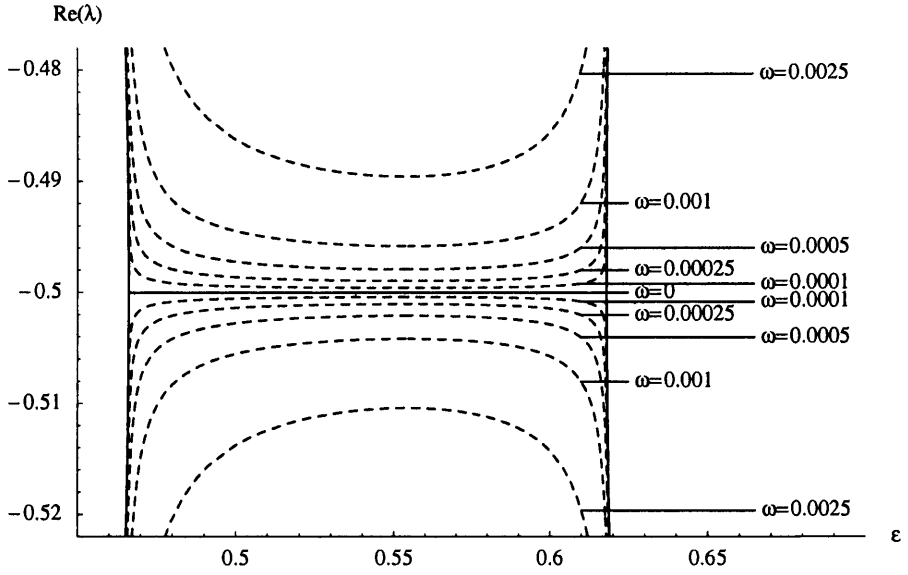

Figure 2.6: The variation of the real part of the characteristic exponents of (2.4) with ϵ for various ω, close to $\omega = 0$. $c = -1$ and $b_0 = 0.15$.

2.6 The Mathieu equation

If we take (2.4) and make a change of variable so that $v(x) = e^{cx}w(x)$ then

$$\begin{aligned} v' &= \tfrac{c}{2}e^{\frac{cx}{2}}w + e^{\frac{cx}{2}}w', \\ v'' &= \tfrac{c^2}{4}e^{\frac{cx}{2}}w + ce^{\frac{cx}{2}}w' + e^{\frac{cx}{2}}w''. \end{aligned} \tag{2.29}$$

This gives

$$w'' + \left[b_0 - \frac{c^2}{4} + i\omega + \epsilon\sin(x)\right]w = 0. \tag{2.30}$$

Equation (2.30) is of the form of the Mathieu equation (see [43]) and a series solution for this equation can be obtained.

We may now set $c = 0$ and relabel b_0 to compensate. In this section, our primary interest has been in determining whether solutions to (2.1) are stable,

convectively unstable or absolutely unstable. As was shown above, the value of ω which is most critical to this determination is $\omega = 0$. This is, in some sense, the most unstable real value of ω. We will thus only consider $\omega = 0$ from now on, which gives

$$w'' + \Big[b_0 + \epsilon \sin(x)\Big] w = 0. \tag{2.31}$$

We proceed to compute the characteristic exponents of (2.31). Removing c as was done above means (consider (2.19)) that if, for example, λ is one characteristic exponent, then $-\lambda$ is the other. We plot the real part of the one with non-negative real part (there clearly must be one), with b_0 and ϵ varied, in Figure 2.7. It is clear that the smallest possible value for the real part of the characteristic exponent with non-negative real part is now zero. For compar-

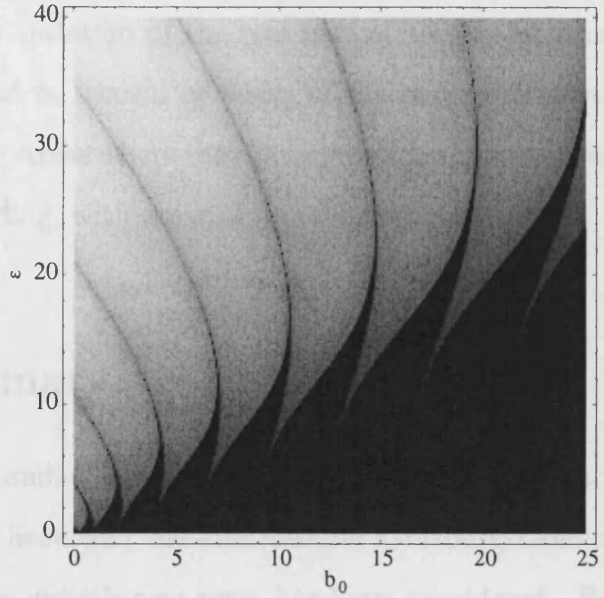

Figure 2.7: The variation of the real part of the characteristic exponents of (2.31) with ϵ and b_0. Areas with larger characteristic exponents are shown with lighter shading, with areas of $\lambda = 0$ being black.

ison, we may alter (2.31) so that the parameters match those of Morse and

Feshbach in [43]. Figure 2.8 shows the result of this. Note that b_0 has been relabelled and h varies like $\sqrt{\epsilon}$.

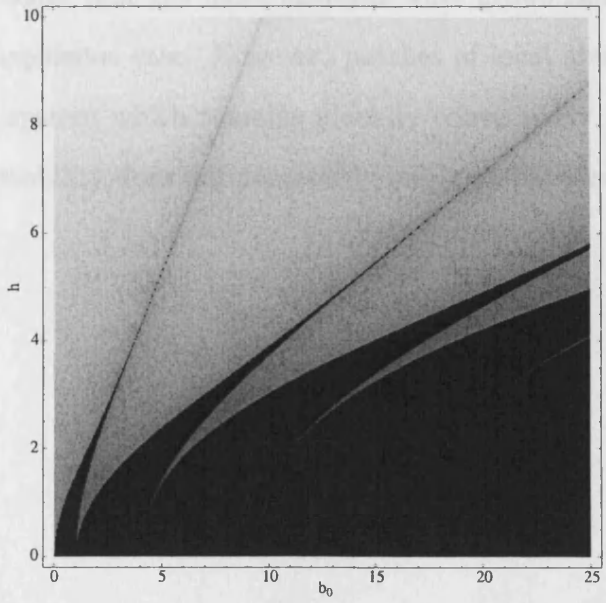

Figure 2.8: The variation of the real part of the characteristic exponents of (2.31) with ϵ and b_0, shown in terms of the parameters used by Morse and Feshbach in [43]. Areas where the characteristic exponents are larger are shown with lighter shading, with areas of $\lambda = 0$ being black.

2.7 Summary

The Ginzburg-Landau equation is a classical model in stability theory. In this chapter, a linearised one-dimensional Ginzburg-Landau equation with spatially-periodic growth rate term has been considered. Results have been obtained by considering continuation from the homogeneous case of a constant growth rate term. The technique which has been used is the study of the signalling problem, here understood as the large-time response of the system to a localised periodic forcing. Floquet's theorem has been used to determine this response for the spatially-periodic system. The homogeneous system may

be made stable, convectively unstable or absolutely unstable by appropriate choices of parameters. Adding the periodicity generally makes the system more unstable, in the sense that the most unstable wave grows faster downstream, than in the homogeneous case. However, patches of local absolute instability can appear in a system which remains globally convectively unstable and so local absolute instability does not necessarily imply global absolute instability.

Chapter 3

A channel-flow problem

3.1 Introduction

We now turn our attention to a problem of fluid-dynamical origin. In this and the next two chapters we will study the stability of two-fluid flows through channels with non-homogeneous geometries. Although our studies will be quite theoretical in their approach, there are several potential applications. In this chapter we will concentrate on a channel whose width varies periodically along its length; this has applications to flow through pipes and ducts, for example, which may have some slight periodicity due to the way in which they are constructed. The reason for our interest in studying the stability of parallel flows in these geometries is, as was mentioned in the introduction, the determination of whether laminar-turbulent transition would occur.

Consider a two-dimensional stratified flow in which two constant-density fluids flow through a channel whose cross-section is small. The cross-section of the channel is not fixed but is allowed to vary along its length. We assume these variations to be fairly small but, in general, of the same order of magnitude as the undistorted channel width. The thinness of the channel allows us to make simplifying assumptions about the system and to arrive at a set of thin-layer

inviscid equations which describe its evolution. For this set of equations it is possible to derive a fairly simple, time independent, analytic solution. We consider this solution to be a base flow through the channel and consider the development of small perturbations by means of a linear stability problem, with the simplicity of the base flow ensuring that this can be done in a symbolic, rather than computed, form.

Analogously with Chapter 2, we begin by considering the stability problem for a channel which is homogeneous along its length. A dispersion relation is derived and the flow régimes corresponding to absolute and convective instability, due to Kelvin-Helmholtz instability (see [23]), are identified by means of the Briggs-Bers criterion. This again enables us to arrive at a system which we understand in the sense that we may say which wavelike disturbances travel upstream and which downstream.

Next, we give the system a sinusoidal periodic spatial variation, comparable with that in Chapter 2. This is done by making the thickness of the channel vary periodically in space. The solution of the full initial-and-boundary-value problem which it would be desirable to use is infeasible and so we again use the signalling problem, considering what the response at large distance would be to a localised time-periodic forcing placed somewhere in the flow. Thus this also is a spatial stability problem. Floquet's theorem is used to calculate the characteristic exponents of solutions which describe the development of wavelike perturbations of the base flow. Using the techniques of Brevdo and Bridges [10], the Briggs-Bers criterion is also applicable here. Essentially, we consider the characteristic exponent spectrum of the periodic problem to be a continuation of the homogeneous case, giving us our upstream-travelling and downstream-travelling branches.

Computation of the characteristic exponent, or wavenumber, spectrum indicates that spatial branches reconnect as soon as any periodic variation is in-

troduced, indicating absolute instability. We confirm this by a multiple scales analysis.

As mentioned above, Floquet's theorem is used to determine the wavenumber spectrum for this problem. The periodic matrix to which the theorem is applied in this section is a continuous function of the frequency, ω, with the consequence that, for this system, we obtain a continuous spectrum, as discussed in Chapter 1. The periodicity of the matrix also leads to the wavenumber curves occurring in an infinite periodic set. This continuous periodic spectrum gives a wide range of observed wavenumbers, which leads to the possibility of resonances between waves. Of particular interest for the system considered here is three-wave resonance. The absolute instability in the system is shown to be due to a three-wave resonance, where one of the three 'waves' is the periodic variation in the channel wall.

Finally in this chapter, we briefly consider the effect of non-sinusoidal periodic wall variation.

3.2 Formulation

We consider the two-dimensional irrotational flow of two fluids in a horizontal channel whose width may vary along its length, as shown in Figure 3.1. u and v are the components of the fluid velocity in the x and y directions, ρ is a density and p is pressure, modified to take gravity into account. A thin-layer, long-wave inviscid approximation is made, so the equations are of the form

$$\frac{\partial u_{1,2}}{\partial t} + u_{1,2}\frac{\partial u_{1,2}}{\partial x} + v_{1,2}\frac{\partial u_{1,2}}{\partial y} = -\frac{1}{\rho_{1,2}}\frac{\partial p_{1,2}}{\partial x}, \tag{3.1}$$

$$\frac{\partial u_{1,2}}{\partial x} + \frac{\partial v_{1,2}}{\partial y} = 0, \tag{3.2}$$

$$\frac{\partial p_{1,2}}{\partial y} = 0. \tag{3.3}$$

(See Appendix A.2.1 for the derivation of these equations). The subscript 2 refers to quantities in the top fluid layer and the subscript 1 refers to those in the bottom fluid layer.

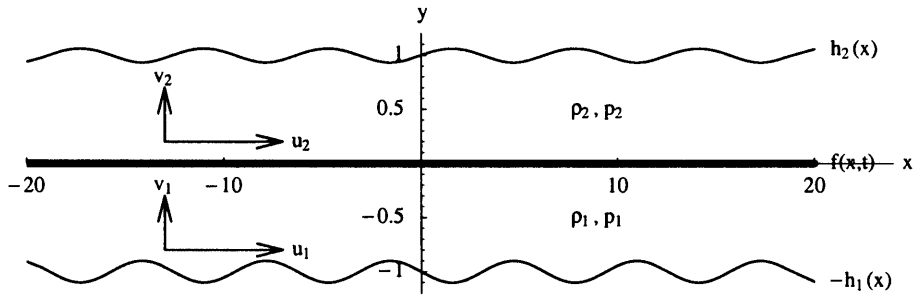

Figure 3.1: The set-up for the channel-flow problem being considered. Note that, although we show the wall shape to vary periodically along its length, we do not require this until Section 3.4.

Far upstream, the flow in each layer is taken to be steady flow in a uniform straight channel, with the following properties:

$$\begin{aligned} h_1(x \to -\infty) &= h_{1\infty}, \quad & u_1(x \to -\infty) &= u_{1\infty}, \\ h_2(x \to -\infty) &= h_{2\infty}, \quad & u_2(x \to -\infty) &= u_{2\infty} \end{aligned} \tag{3.4}$$

and

$$\begin{aligned} v_1(x \to -\infty) &= 0, \quad & p_1(x \to -\infty) &= 0, \\ v_2(x \to -\infty) &= 0, \quad & p_2(x \to -\infty) &= 0. \end{aligned} \tag{3.5}$$

Thus, the thickness of the top and bottom layers far upstream are $h_{2\infty}$ and $h_{1\infty}$ respectively and the corresponding fluid velocities are $u_{2\infty}$ and $u_{1\infty}$. The variables in the varying section of the channel can then be non-dimensionalised against these quantities. The reason for this assumption of uniformity far upstream is that we can fully understand the straight-channel problem and so the assumption means that the fluid enters the system in a 'known' state.

The interface between the fluids is at a level given by $y = f(x,t)$, with the interfacial pressure jump being given by

$$p_2 - p_1 = -g_\rho f + \gamma \frac{\partial^2 f}{\partial x^2}, \tag{3.6}$$

where, again, p_1 and p_2 represent reduced pressure, g_ρ is a constant proportional to the acceleration due to gravity and to the density difference. γ is the non-dimensional surface tension coefficient.

As mentioned above, we take the flow to be irrotational everywhere. Note that, far upstream, the flow is taken to have no x, or y, dependence and hence is irrotational. By means of a scaling argument similar to the one presented in Appendix A.2.1, in our thin-layer system, the condition that the circulation is everywhere zero reduces to a condition that $\frac{\partial u_{1,2}}{\partial y} = 0$. Hence equation (3.1) becomes

$$\frac{\partial u_{1,2}}{\partial t} + u_{1,2}\frac{\partial u_{1,2}}{\partial x} = -\frac{1}{\rho_{1,2}}\frac{\partial p_{1,2}}{\partial x}. \tag{3.7}$$

We consider conditions at the interface of the two fluids. In the bottom fluid, its lower boundary is fixed and its vertical velocity at its upper boundary is given by the material derivative of its thickness

$$\frac{D(h_1 + f)}{Dt} = v_1(y = f(x,t)). \tag{3.8}$$

Integrating the continuity equation (3.2) across fluid 1 vertically and combining this with (3.8) we get

$$\frac{\partial(h_1 + f)}{\partial t} + u_1\frac{\partial(h_1 + f)}{\partial x} + (h_1 + f)\frac{\partial u_1}{\partial x} = 0. \tag{3.9}$$

As h_1 is constant w.r.t. t, this gives

$$\frac{\partial f}{\partial t} + \frac{\partial}{\partial x}\left[u_1 \times (h_1 + f)\right] = 0. \tag{3.10}$$

Similarly, for the upper fluid, we obtain

$$\frac{\partial f}{\partial t} + \frac{\partial}{\partial x}\left[u_2 \times (-h_2 + f)\right] = 0. \tag{3.11}$$

In order to remove terms relating to the interface shape from subsequent stability analysis, we make the simplifying assumption that, for the base flow, the interface is, and remains, horizontal, i.e. $f_0(x,t) = 0$, where the subscript zero

indicates a quantity pertaining to the base flow. As it stands, this condition overspecifies the problem. To account for this, we may choose $h_2(x)$ in such a way that the condition $f_0(x,t) = 0$ is met. Our system then has the correct number of degrees of freedom. From now on, we label quantities $u_{1,2}$, $v_{1,2}$, $p_{1,2}$,... which pertain to the base flow with a further subscript 0. We have

$$\begin{aligned} u_1 = u_{10}(x) &= \tfrac{h_{1\infty}u_{1\infty}}{h_1(x)}, \\ u_2 = u_{20}(x) &= \tfrac{h_{2\infty}u_{2\infty}}{h_2(x)}, \end{aligned} \tag{3.12}$$

from continuity (3.2) and

$$\begin{aligned} p_1 = p_{10}(x) &= \tfrac{\rho_1}{2}\left(u_{1\infty}^2 - u_{10}^2(x)\right), \\ p_2 = p_{20}(x) &= \tfrac{\rho_2}{2}\left(u_{2\infty}^2 - u_{20}^2(x)\right), \end{aligned} \tag{3.13}$$

both from (3.7). These are equal to each other by (3.6), which reduces to $p_{10} = p_{20}$ for the base flow. We can now calculate the shape of the upper boundary, $h_2(x)$. From (3.13) we obtain

$$\left(\frac{u_{20}(x)}{u_{2\infty}}\right)^2 = 1 + \frac{\rho_1 u_{1\infty}^2}{\rho_2 u_{2\infty}^2}\left(\frac{u_{10}^2(x)}{u_{1\infty}^2} - 1\right) \tag{3.14}$$

and thus, from (3.12),

$$h_2(x) = \frac{h_{2\infty}}{\sqrt{1 + \frac{\rho_1 u_{1\infty}^2}{\rho_2 u_{2\infty}^2}\left(\frac{h_{1\infty}^2}{h_1^2(x)} - 1\right)}}. \tag{3.15}$$

The channel geometry given by (3.15) may seem artificial, but we are prepared to sacrifice generality for the value of having an explicit analytic expression for the base state. This greatly improves the clarity of subsequent results. It is also worth noting that this form of h_2 can give fairly symmetrical variations in the channel walls. For example, in Figure 3.1, $-h_1(x)$ is shown as sinusoidal and $h_2(x)$ is shown as given by (3.15).

In order to perform a stability analysis on our system, which has no explicit

t dependence, we consider small disturbances of the form

$$\begin{aligned} u_1 &= u_{10}(x) + \delta e^{-i\omega t} U_1(x) + O(\delta^2), \\ u_2 &= u_{20}(x) + \delta e^{-i\omega t} U_2(x) + O(\delta^2), \\ p_1 &= p_{10}(x) + \delta e^{-i\omega t} P_1(x) + O(\delta^2), \\ p_2 &= p_{20}(x) + \delta e^{-i\omega t} P_2(x) + O(\delta^2), \\ f &= \delta e^{-i\omega t} F(x) + O(\delta^2), \end{aligned} \tag{3.16}$$

where δ is a small parameter. This gives instability if solutions of the system have ω with positive imaginary part. It is implicit from the long-wave approximation used in deriving the base flow that the spatial variation of disturbances is not too fast, i.e. that the 'wavelengths' are long. This point will be returned to in the discussion of results. Combining (3.6), (3.7), (3.10), (3.11) and (3.16) and linearising, we obtain

$$\begin{aligned} \tfrac{1}{h_1}(i\omega F - u_{10}' F - u_{10} F' - U_1 h_1') &= U_1' \\ \tfrac{1}{h_2}(-i\omega F + u_{20}' F + u_{20} F' - U_2 h_2') &= U_2' \\ i\omega U_2 \rho_2 - \rho_2 U_2 u_{20}' - \tfrac{\rho_2 u_{20}}{h_2}(-i\omega F + u_{20}' F + u_{20} F' - U_2 h_2') & \\ -i\omega U_1 \rho_1 + \rho_1 U_1 u_{10}' + \tfrac{\rho_1 u_{10}}{h_1}(i\omega F - u_{10}' F - u_{10} F' - U_1 h_1') &= -gF' + \gamma F''', \end{aligned} \tag{3.17}$$

where primes denote derivatives w.r.t. x (see Appendix A.2.2). In order to apply Floquet's theorem to this system later, we require the system to be expressed as a first order linear matrix equation. To this end, we introduce symbols $G = F'$ and $H = G' = F''$ and obtain

$$\begin{pmatrix} U_1 \\ U_2 \\ F \\ G \\ H \end{pmatrix}' = A(x) \begin{pmatrix} U_1 \\ U_2 \\ F \\ G \\ H \end{pmatrix}, \tag{3.18}$$

where $A(x) =$

$$\begin{pmatrix} \frac{-h_1'}{h_1} & 0 & \frac{i\omega-u_{10}'}{h_1} & \frac{-u_{10}}{h_1} & 0 \\ 0 & \frac{-h_2'}{h_2} & \frac{-i\omega+u_{20}'}{h_2} & \frac{u_{20}}{h_2} & 0 \\ 0 & 0 & 0 & 1 & 0 \\ 0 & 0 & 0 & 0 & 1 \\ \frac{-i\omega\rho_1 h_1+\rho_1 u_{10}' h_1}{\gamma h_1} & \frac{i\omega\rho_2 h_2-\rho_2 u_{20}' h_2}{\gamma h_2} & \frac{i\omega\rho_1 u_{10}-\rho_1 u_{10} u_{10}'}{\gamma h_1}+ & \frac{g_\rho}{\gamma}+\frac{-\rho_1 u_{10}^2}{\gamma h_1} & 0 \\ -\frac{\rho_1 u_{10} h_1'}{\gamma h_1} & +\frac{\rho_2 u_{20} h_2'}{\gamma h_2} & \frac{i\omega\rho_2 u_{20}-\rho_2 u_{20} u_{20}'}{\gamma h_2} & +\frac{-\rho_2 u_{20}^2}{\gamma h_2} & \end{pmatrix}.$$

3.3 The case of a straight channel

We begin by considering the case of a straight channel, with $h_1(x) = h_{1\infty}$. This gives $h_2(x) = h_{2\infty}$ and all other variables characterising the base flow are constants. With no explicit x dependence in the elements of the matrix A in (3.18), we may put

$$[U_1, U_2, F] = e^{ikx}\,[U_{1,0}, U_{2,0}, F_0]\,, \tag{3.19}$$

to obtain a normal mode calculation, as described in the introduction. This gives us the following dispersion relation (see Appendix A.2.3):

$$\frac{\rho_1}{h_{1\infty}}(\omega - ku_{1\infty})^2 + \frac{\rho_2}{h_{2\infty}}(\omega - ku_{2\infty})^2 = g_\rho k^2 + \gamma k^4. \tag{3.20}$$

This is second order w.r.t. ω and fourth order w.r.t. k and so we have two temporal modes and four spatial branches. We will concentrate only on the spatial branches, i.e. the case of ω real. For the following illustrations, we choose the parameters of the problem to be

$$\begin{gathered} h_{1\infty} = h_{2\infty} = u_{2\infty} = 1,\ u_{1\infty} = 0.8, \\ \gamma = 0.5,\ g_\rho = 0, \\ \rho_1 = \rho_2 = 1. \end{gathered} \tag{3.21}$$

The variation of the imaginary part of k, for real ω, is shown in Figure 3.2. This clearly shows that the system has branches with nonzero $\mathrm{Im}(k)$. In order

to examine the stability of the system, Figure 3.3 shows the trajectories of the spatial branches, $k(\omega)$, in the complex k-plane. To distinguish between the branches, a small positive amount is added to ω_i, the imaginary part of ω. As mentioned in Chapter 2, this has the effect of pushing upstream-travelling branches into the lower half-k-plane and downstream-travelling branches into the upper half-k-plane and is sufficient to distinguish those that lie close to the real k-axis. Only $\omega_r \geq 0$ is shown. The dots in the diagram show the value of k when $\omega_r = 0$.

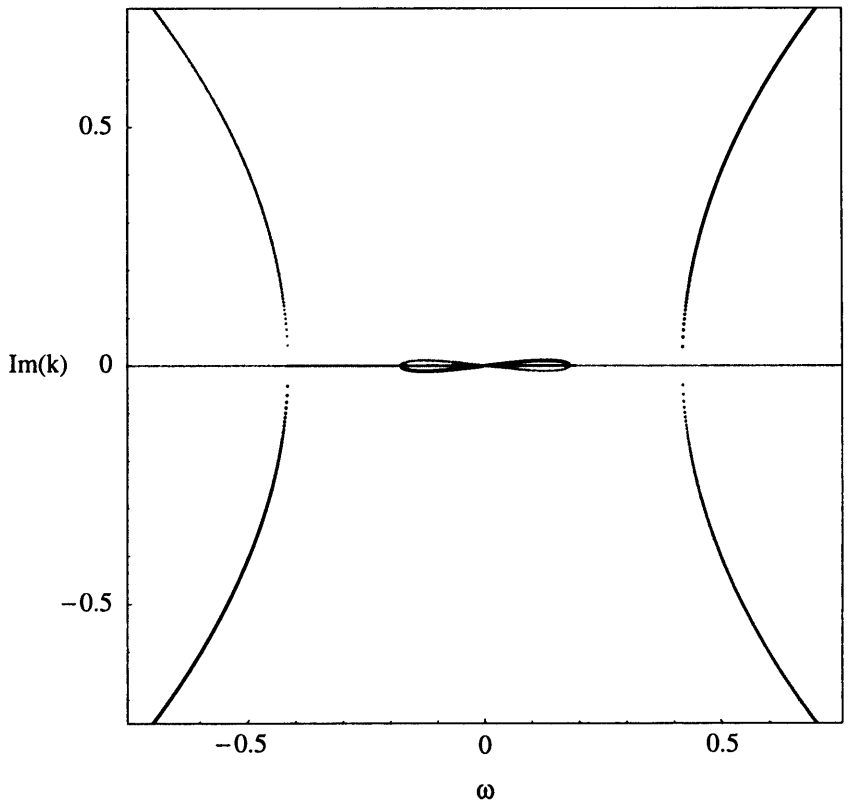

Figure 3.2: Variation of the imaginary part of k, with ω, for the normal modes of the straight-channel system. The lines are different shades to help distinguish them. $\omega_i = 0$.

Trajectory 1 is a downstream-travelling branch and, as $k_i < 0$ for small ω, is unstable. Trajectory 2 is also downstream-travelling, but is stable. Trajec-

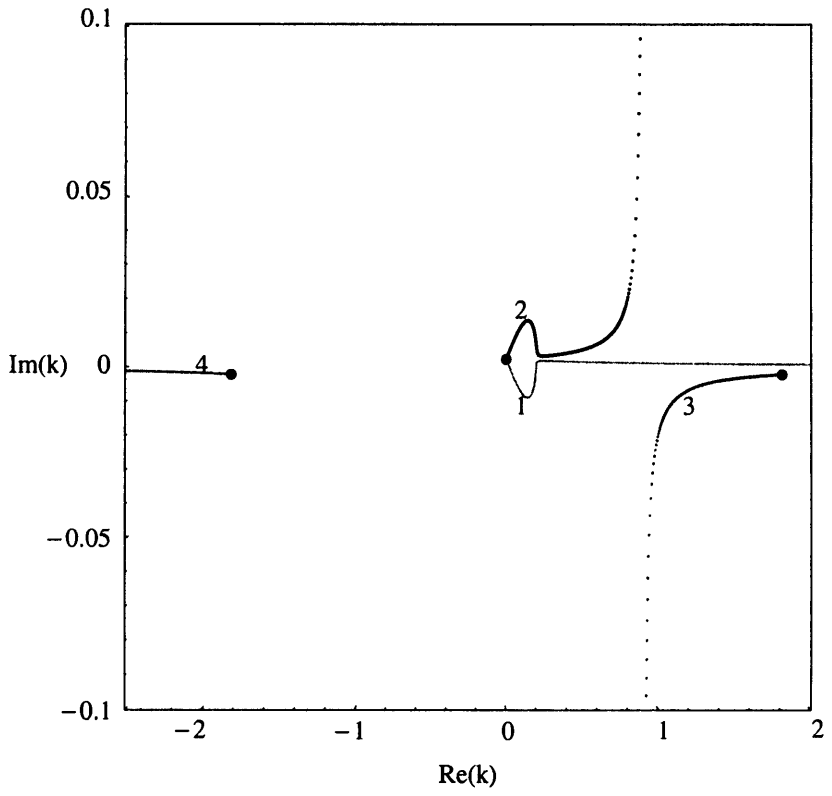

Figure 3.3: The trajectories of k, as ω varies, in the complex plane. $\omega_r \geq 0$. The black dots at the ends of the lines show the positions of the branches for $\omega_r = 0$. The trajectories are plotted as dots, rather than lines, to prevent incorrect connections between trajectories from being shown. $\omega_i = 0.002$.

tories 3 and 4 correspond to waves travelling upstream. Varying ω_i shows that no pinching of branches occurs for $\omega_i > 0$ and so the system is only convectively unstable. This can be seen in Figure 3.4, which shows the movement of the branches into different half-planes as ω_i is made larger.

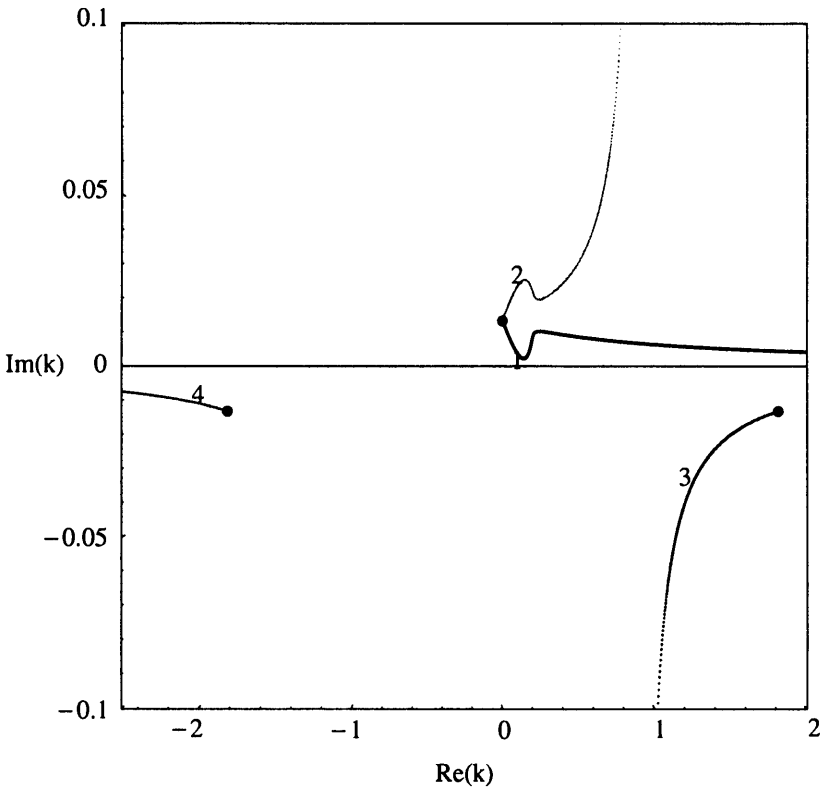

Figure 3.4: The trajectories of k, as ω varies, in the complex plane. $\omega_r \geq 0$. The dots show the positions of the branches for $\omega_r = 0$. $\omega_i = 0.012$.

Finally, we note that this combination of parameters gives neutrally stable solutions. By continuing our branch numbering down to $\omega_i = 0$ from the $\omega_i = 0.002$ case shown in Figure 3.3, root 4, the majority of root 1 and sections of the trajectories of roots 2 and 3 lie along the real axis, indicating this neutral stability. The presence of neutral modes is also clear from Figure 3.2.

It is worth noting, however, that the convective instability of the system is dependent on the choice of parameters as, if parameters are chosen such that

the 'bulge' in root 1 meets root 3, then absolute instability occurs. This is illustrated in Figures 3.5 and 3.6, where we have reduced $u_{1\infty}$ to 0.4, keeping all other parameters the same.

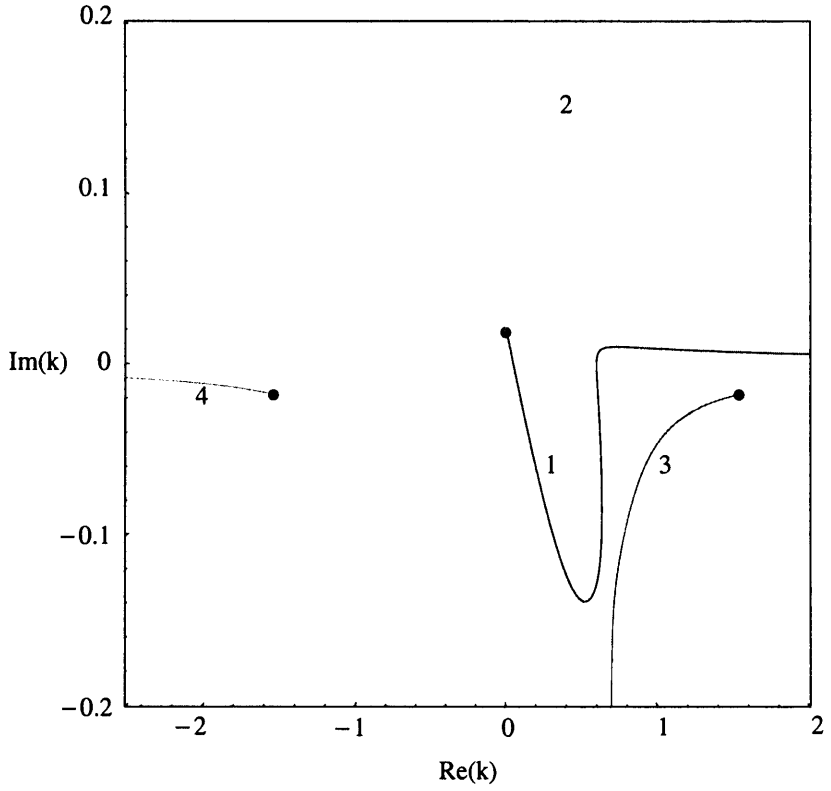

Figure 3.5: The trajectories of k, as ω varies, in the complex plane, when $u_{1\infty}$ is reduced to 0.4. $\omega_r \geq 0$. The dots show the positions of the branches for $\omega_r = 0$. $\omega_i = 0.015$.

The merger of the two branches, marked 1 and 3 in Figure 3.5, for positive ω_i, indicates absolute instability (Chapter 1). We keep $u_{1\infty}$ at 0.8 for the remainder of this chapter, and in subsequent chapters, to 'keep some distance from' this possibility.

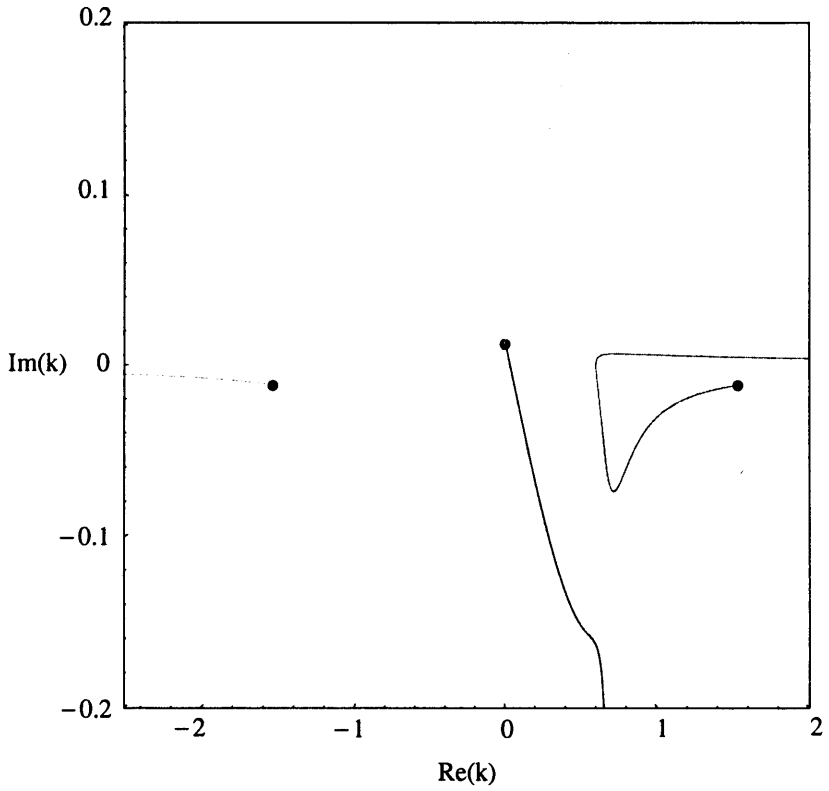

Figure 3.6: The trajectories of k, as ω varies, in the complex plane, when $u_{1\infty}$ is reduced to 0.4. $\omega_r \geq 0$. The dots show the positions of the branches for $\omega_r = 0$. $\omega_i = 0.01$. The downstream-travelling branch marked 1 in Figure 3.5 has merged with the upstream-travelling branch marked 3 for $\omega_i > 0$, indicating absolute instability.

3.4 Flow in a periodically-varying channel

We now allow the lower boundary of the system to be a function of x (only). This will also determine the upper boundary of the system, via (3.15). We put

$$h_1(x) = h_{1\infty} + \epsilon \sin(x), \tag{3.22}$$

where ϵ is assumed to be small, i.e. $|\epsilon| < h_{1\infty}$. Now, combining (3.12), (3.15) and (3.18) and defining $\mathbf{u}$ by $\mathbf{u} = (U_1\ U_2\ F\ G\ H)^T$, the superscript T indicating 'transpose', we obtain

$$\frac{\mathrm{d}\mathbf{u}}{\mathrm{d}x} = A(x)\mathbf{u}, \tag{3.23}$$

with $A(x)$ a known function of $u_{1\infty}$, $u_{2\infty}$, $h_{1\infty}$, $h_{2\infty}$, ρ_1, ρ_2, g_ρ, γ, ω, ϵ and x (see Appendix A.2.4). The space coordinate x only appears in $A(x)$ through the sine function and its derivatives, so $A(x)$ is 2π-periodic in x. We may therefore apply Floquet's theorem to (3.23) and obtain solutions of the form

$$\Phi(x) = P(x)e^{Bx}, \tag{3.24}$$

where $\Phi(x)$ is a fundamental matrix of (3.23), $P(x)$ is 2π-periodic and B is a constant matrix. In order to calculate B, we begin with $\Phi(0) = I_5$, the 5×5 identity matrix. Then (3.23) is solved numerically, by means of a fourth-order Runge-Kutta integration, to find $C = \Phi(2\pi)$. Floquet's theorem then says that the characteristic exponents, λ_j, of C, defined such that $\rho_j = e^{2\pi\lambda_j}$ is an eigenvalue of C, and unique up to the addition of multiples of i, can be chosen to coincide with the eigenvalues of B. We thus expect solutions of (3.23) to vary as $e^{\lambda_j x}$, where λ_j are the eigenvalues of B.

An important point when considering solutions (3.24) of our equation is that $P(x)$, a 2π-periodic function of x, has a Fourier series expansion equal to

$$P(x) = \sum_{n=-\infty}^{\infty} \Upsilon_n e^{-iI_5 nx}, \tag{3.25}$$

say, so we may write

$$\Phi(x) = \sum_{n=-\infty}^{\infty} \Upsilon_n e^{(B-iI_5n)x}. \tag{3.26}$$

Assuming that the matrix coefficients Υ_n are, in general, not zero, we find that we are actually searching for the eigenvalues of $B - iI_5n$ for all n. Subtracting iI_5n from a matrix decreases each of its eigenvalues by in, so the eigenvalues/branches we are searching for can therefore only be determined up to the addition of integer multiples of i. An alternative viewpoint is to say that any matrix of the form e^{iI_5nx} can be 'removed from' (divided out of) $P(x)$ and 'given to' (multiplied into) e^{Bx}, without altering the validity of (3.24). This is a consequence of the periodic coefficients of the equation.

We begin defining by wavenumbers k by $\lambda = ik$ and treating these as a continuation from the wavenumbers in the straight channel, $\epsilon = 0$, case. We look at the case $\epsilon = 0.1$. Although this may be considered quite a large variation in the channel thickness, given that the base flow equations made use of a thin-layer approximation, we take this value of ϵ for clarity of results and will demonstrate later that the results apply for any small positive value. Figure 3.7 shows the variation of k_i, with ω, for ω real. This may be compared with Figure 3.2 for the $\epsilon = 0$ case. Immediately obvious is the appearance of two loops in the branch curves, at around $\omega = \pm 0.3$. Some idea of the origin of these loops can be obtained by considering Figure 3.8. The lines in these diagrams are coloured different shades of grey, in order to help distinguish them. However, wherever two branches intersect in these diagrams, two entirely different branch curves appear after the intersection. It is thus not meaningful to associate curves of one shade on one side of an intersection with curves of the same shade on the other side. By adding a small imaginary part to ω and separating the curves, we can meaningfully assign one shade to an entire curve. This is done later, when the influence on the stability of the system of the branch reconnections which create the loops is considered.

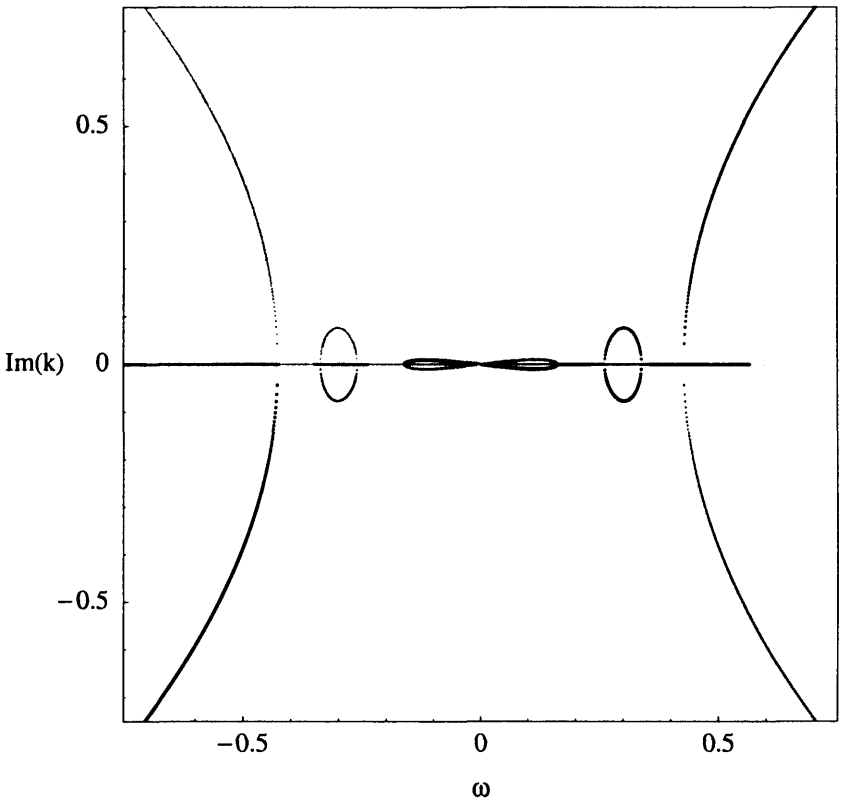

Figure 3.7: Variation of the imaginary part of k, with ω, for the branch curves when $\epsilon = 0.1$. $\omega_i = 0$. See the text for a note about the shading of the lines.

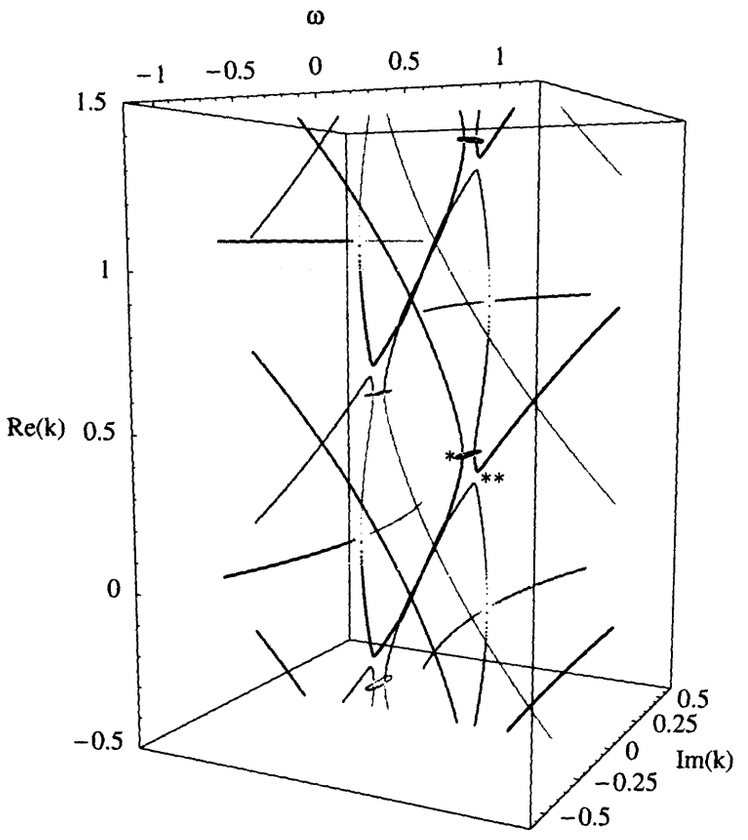

Figure 3.8: Variation of k in the complex plane, with ω, for the branch curves when $\epsilon = 0.1$. $\omega_i = 0$. The branches repeat infinitely with period 1 in k_r. Two copies are shown. See the text for a note about the shading of the lines.

We compare Figure 3.8 with Figure 3.9. Figure 3.9 shows the same set of curves as Figure 3.8, generated numerically, for $\epsilon = 0$. The fact that the curves were generated in the same way as for the $\epsilon \neq 0$ curves ensures that we see the same 1-periodicity in the branches. This facilitates comparison between the two and, although we are adding branches which may not be there in the case $\epsilon = 0$, we will see later that the branches will be there for any non-zero ϵ, however small.

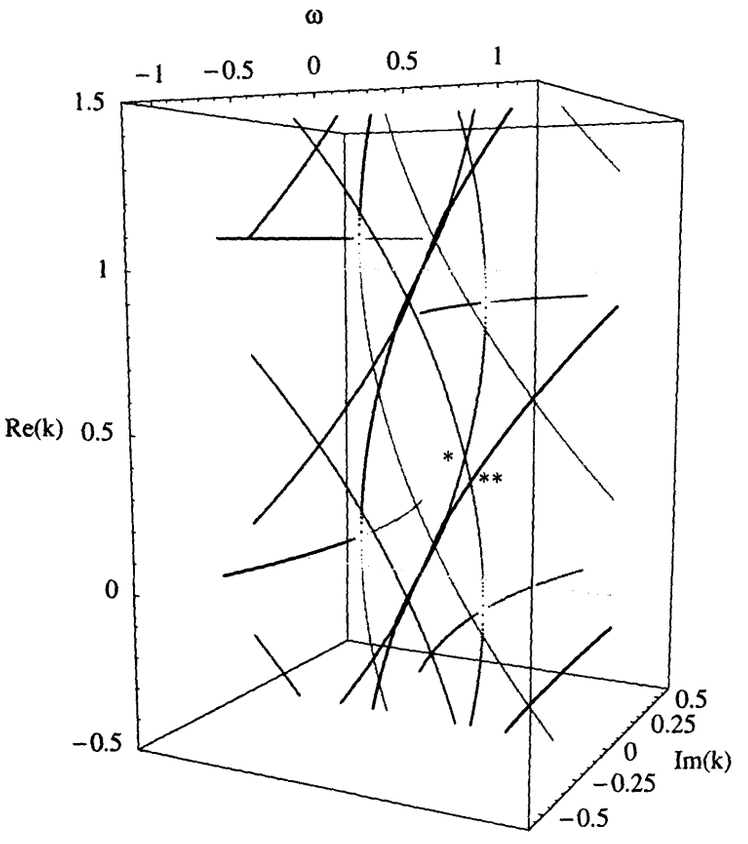

Figure 3.9: Variation of k in the complex plane, with ω, for the branch curves when $\epsilon = 0$. $\omega_i = 0$. The curves shown are repeated, with period 1 in k_r, for comparison with Figure 3.8. Two copies are shown.

We can see which two branch curves, when $\epsilon = 0.1$, interact to create the loop (marked *). We can also see how two nearby branch curves (marked **) swap and move away from each other. This behaviour is similar for all sets of

curves while ϵ remains small. An important point to note about the interaction which creates the loop is that it occurs between two copies of the 'same' curve, with one shifted by 1 in k_r. By 'the same' we mean that they correspond to parabolas of the same sign in the $k_r - \omega_r$-plane. The two branches which separate come from two parabolas (in the $k_r - \omega_r$-plane) with opposite sign, one of which is also 1-shifted in k_r, relative to the original ($\epsilon = 0$) curves. Note that both the loop and the curve separation are due to the interaction between roots corresponding to waves travelling in opposite directions: in the former case roots 3 and 1 and, in the latter, roots 3 and 2. This is illustrated in Figure 3.10 which shows the branch curves which lie in the $k_r - \omega_r$-plane. Note that, as $\omega_r(k_r)$ is shown, we have only two values of ω_r for each k_r.

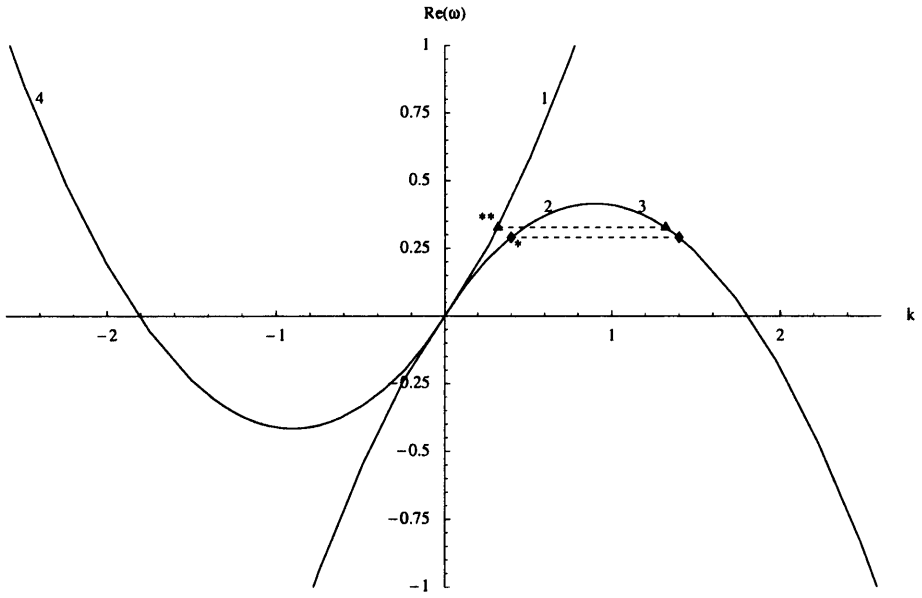

Figure 3.10: Variation of real ω with real k, for the branch curves when $\epsilon = 0$. The two places, for positive ω and k, at which the branch curves are separated by exactly 1 are shown by the ▲s and ♦s and the points marked * and ** correspond to those in Figures 3.8 and 3.9. The numbering of the curves corresponds to that in Figure 3.3.

In the '3D' curves we can see that one of the branches is always zero (this

and its 1-shifted copy are shown as the palest grey lines in Figure 3.9). This is to be expected as our calculations from (3.23) return five values, where the dispersion relation for $\epsilon = 0$, equation (3.20) has only four roots for k. Thus $A(x)$ contains more information than is necessary. The zero root is left in as it provides a convenient reference axis $k = 0$. It also suggests that the channel supports standing waves of any frequency.

We will show later that the loop in the branch curves occurs for any ϵ, however small. To support this idea, Figure 3.11 shows the loop for $\epsilon = 0.001$. The scales on the axes give an idea of its size.

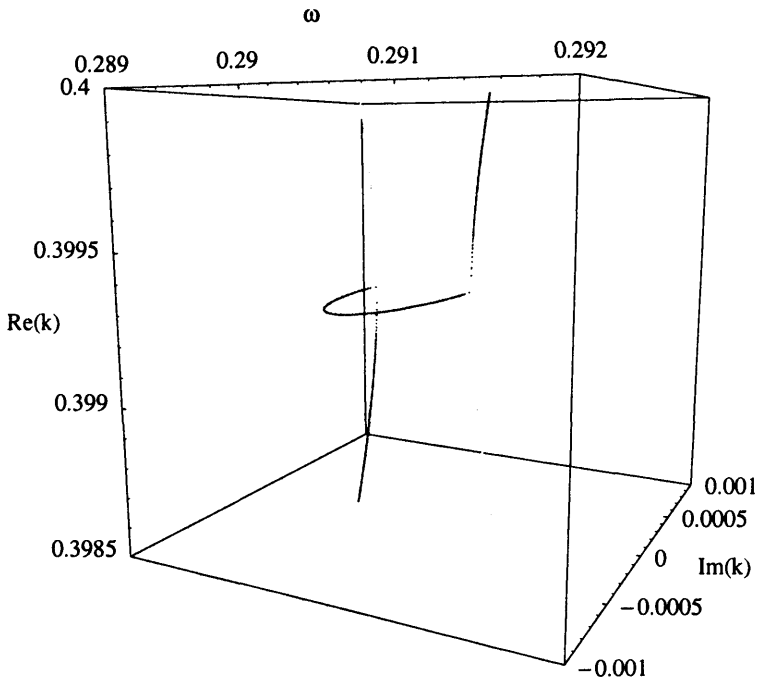

Figure 3.11: Close-up view of one of the loops in the branch curves formed when small $\epsilon > 0$. $\epsilon = 0.001$.

Also of interest is the behaviour of the loops as ϵ becomes large. They continue to grow, maintaining a similar shape until ϵ becomes quite large. Figure 3.12 shows the size of the loops when $\epsilon = 0.3$. Eventually, they connect to the parabola-like roots with large k_i for large $|\omega_r|$, as shown in Figure

3.13. At this stage, the branch curves are quite complicated and will not be considered further. Note that the long-wave approximation used to derive the base flow equations is not applicable when the wall shape changes rapidly with the streamwise coordinate and this is the case when ϵ is made large.

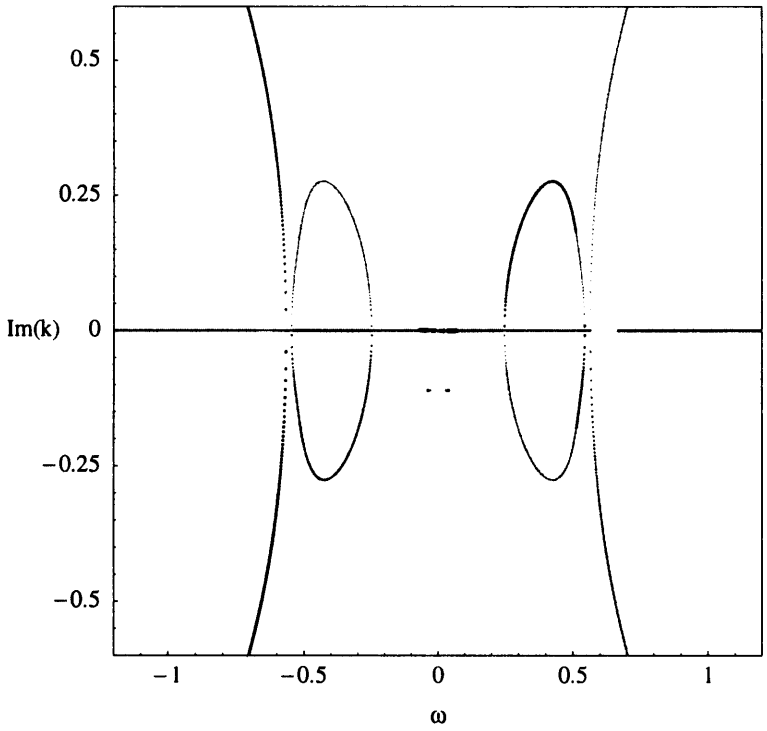

Figure 3.12: Variation of k_i with real ω for $\epsilon = 0.3$.

We now consider the effect of the branch interactions which create the loops on the stability of the system. Figure 3.14, similar to Figure 3.4, shows the position of the branches, in the complex k-plane, when $\omega_i = 0.015$ and $\epsilon = 0$. The branches are repeated, 1-periodically, in a similar way to Figure 3.9 and for the same reason. The labelling is as in Figures 3.3 and 3.4, with root number 4 being just off the left hand edge of the diagram. Root 1 and its copies, and the copies of root 4, tend to asymptotic lines parallel to the real axis, as $\omega_r \to \infty$. However, only a limited range of ω can be shown, as the numerical routine used to generate the data breaks down for large $|\omega_r|$.

Figure 3.15 shows what happens to the branches when 'roughness' is added

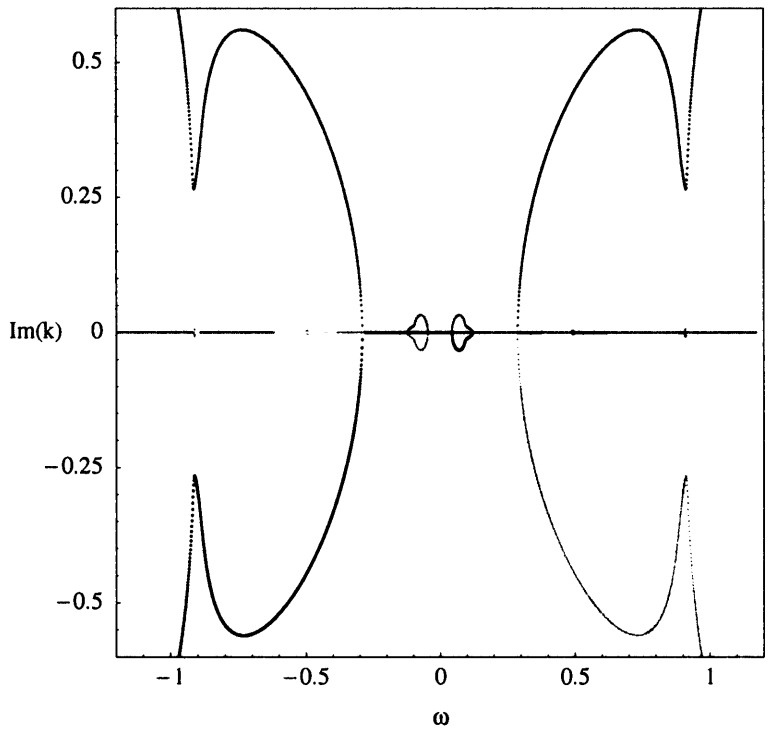

Figure 3.13: Variation of k_i with real ω for $\epsilon = 0.45$. The loops in the branch curves have joined to the parabola-like curves.

to the walls. Here $\epsilon = 0.1$. The formation of the loop, manifested as upward and downward spikes in the curves at around $k_r = 0.4 + n$, $n \in \mathbb{Z}$, is apparent. Also apparent is the movement of the copies of root 1 and those of root 3 towards each other, for k_r about $0.3 + n$. When ω_i is reduced slightly, we see that the two branches join up at this point. Figure 3.16 shows this for $\omega_i = 0.01$, in which the branches cannot be labelled consistently with Figures 3.14 and 3.15. We thus have two roots, originating in different half-planes, which join up in the complex k-plane for positive ω_i, which indicates (see Chapter 1) absolute instability. We note that at least one of these absolutely unstable wavenumbers, i.e. $k_r \approx 0.4$, corresponds to a 'long wave', i.e. one whose wavelength is much larger than the channel thickness and so the long-wave approximation made in Section 3.2 is valid.

We now briefly comment on the likely physical meaning of this instability.

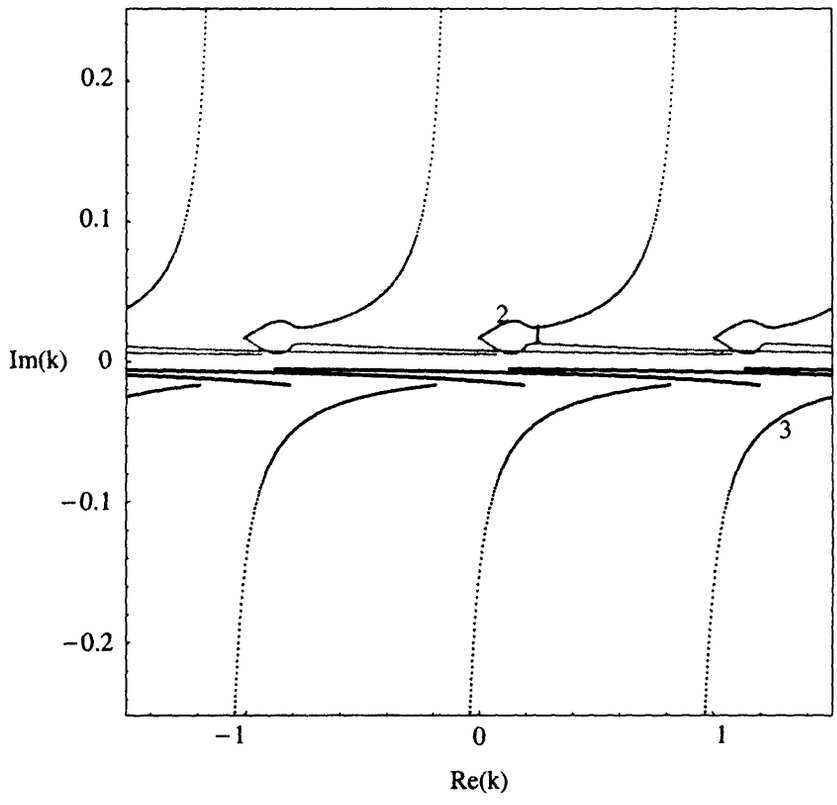

Figure 3.14: The trajectories of k, as ω_r varies, in the complex plane when $\epsilon = 0$. $\omega_r \geq 0$ and $\omega_i = 0.015$. The numbering is as in Figure 3.10.

Our 'disturbance vector', $\mathbf{u}$, corresponds, physically, to a combination of the two fluid velocities and the surface shape. If, for certain wavenumbers, the components of this vector grow (in modulus) in time, we expect to see these velocities and surface shape change in time. The most obvious physical quantity, from the point of view of someone looking at the system, is the surface shape. We would thus expect the surface shape to change from being flat to being a growing-in-time wave pattern, the shape of which depends on the unstable wavenumbers. It is likely that, in an experimental problem, the surface would then break up, destroying our model.

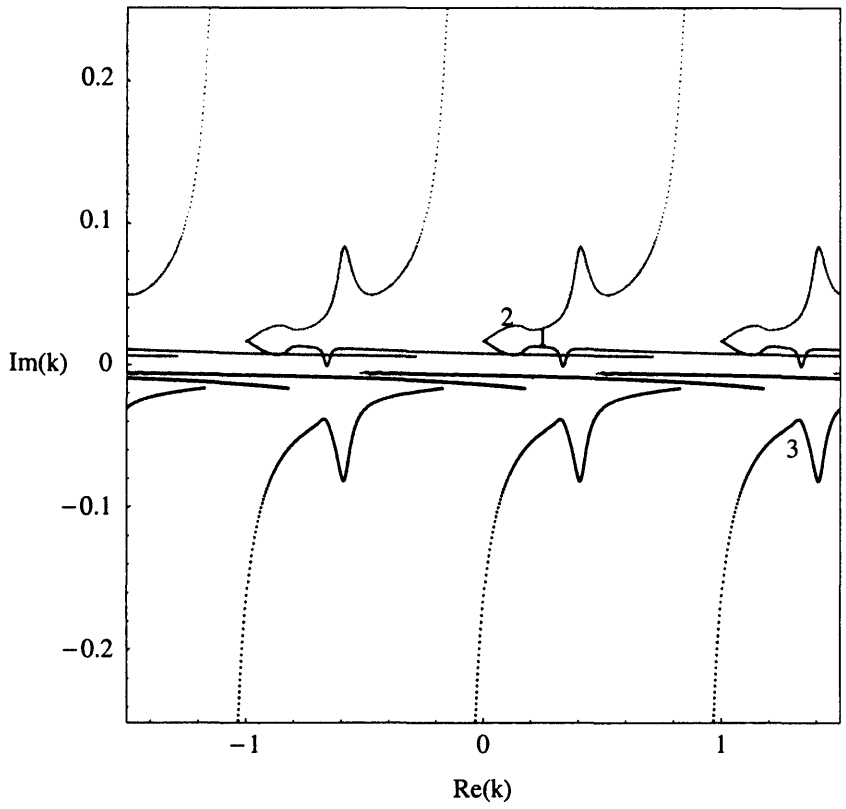

Figure 3.15: The trajectories of k, as ω_r varies, in the complex plane when $\epsilon = 0.1$. $\omega_r \geq 0$ and $\omega_i = 0.015$.

We now examine the size of the loop. Figure 3.17 shows the result of measuring, numerically, the maximum value of k_i across the loop, for various

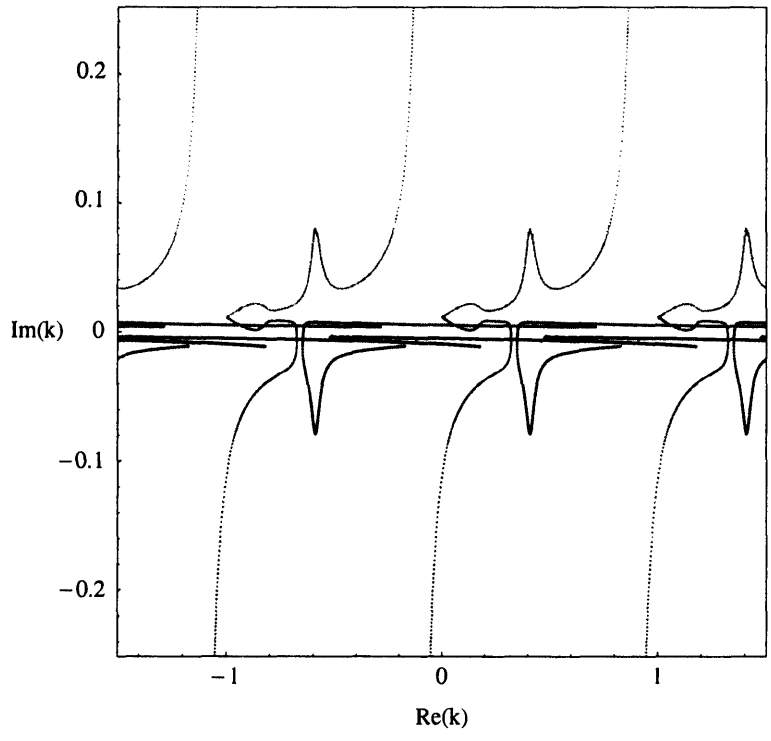

Figure 3.16: The trajectories of k, as ω varies, in the complex plane when $\epsilon = 0.1$. $\omega_r \geq 0$ and $\omega_i = 0.01$.

very small ϵ. A straight line through the origin is fitted to the data, with equation

$$k_{i,max} = 0.75702\epsilon. \tag{3.27}$$

The R^2 and adjusted R^2 values for this fit are equal to unity, to greater precision than that of the measured data.

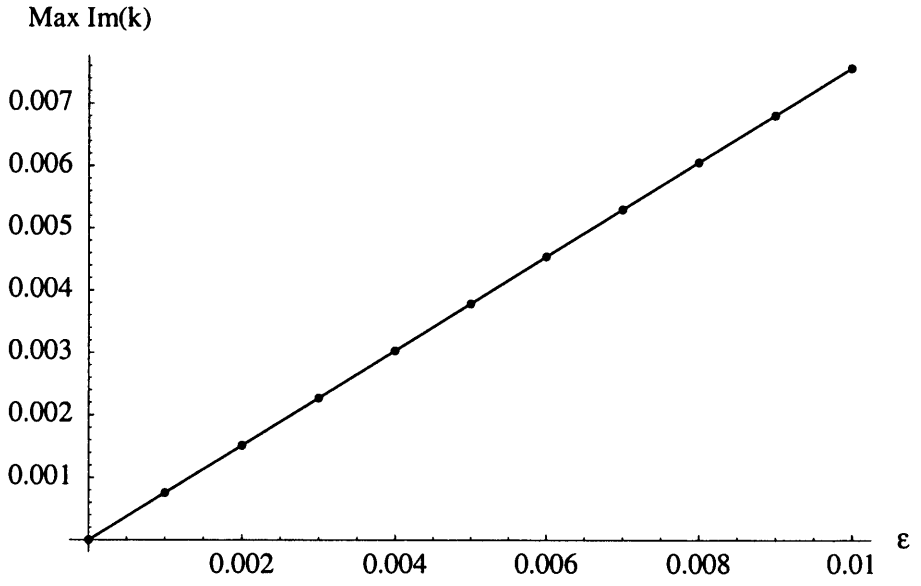

Figure 3.17: The maximum value of k_i across the loop in the branch curves, measured numerically, for various very small ϵ. The best-fit line has equation $k_{i,max} = 0.75702\epsilon$.

3.5 Method of multiple scales analysis of the instability

We use the method of multiple scales to analyse this loop growth with ϵ. We wish to treat the $\epsilon = 0$ case as a leading order approximation and the ϵ small and positive case as a perturbation of this. From the form of $A(x)$, (Appendix

A.2.4), we may write (Appendix A.2.5):

$$A(x) = A^{(0)} + \epsilon A^{(1+)}e^{ix} + \epsilon A^{(1-)}e^{-ix} + O(\epsilon^2). \tag{3.28}$$

We expect the order-ϵ terms to have influence on length scales of order $1/\epsilon$. To capture this influence, we define the slow-scale variable $X = \epsilon x$ and so

$$\mathbf{u} = \mathbf{u}_0(x, X) + \epsilon \mathbf{u}_1(x, X) + O(\epsilon^2), \tag{3.29}$$

$$\frac{\mathrm{d}\mathbf{u}}{\mathrm{d}x} = \frac{\partial \mathbf{u}_0}{\partial x}(x, X) + \epsilon \frac{\partial \mathbf{u}_1}{\partial x}(x, X) + \epsilon \frac{\partial \mathbf{u}_0}{\partial X}(x, X) + O(\epsilon^2), \tag{3.30}$$

so, from (3.23) at order 1, we have

$$\frac{\partial \mathbf{u}_0}{\partial x}(x, X) - A^{(0)}\mathbf{u}_0(x, X) = 0, \tag{3.31}$$

with solutions

$$\mathbf{u}_0 = \sum_{j=0}^{4} \mathbf{q}_j(X) e^{ik_j x}, \tag{3.32}$$

where the ik_j are the eigenvalues of $A^{(0)}$ and the $\mathbf{q}_j$ are the corresponding eigenvectors, defined up to multiplication by a scalar dependent on the initial conditions. At order ϵ, we have

$$\frac{\partial \mathbf{u}_1}{\partial x}(x, X) + \frac{\partial \mathbf{u}_0}{\partial X}(x, X) = A^{(0)}\mathbf{u}_1(x, X) + A^{(1+)}\mathbf{u}_0(x, X)e^{ix} + A^{(1-)}\mathbf{u}_0(x, X)e^{-ix}, \tag{3.33}$$

or

$$\begin{aligned} \frac{\partial \mathbf{u}_1}{\partial x}(x, X) - A^{(0)}\mathbf{u}_1(x, X) \;=\; & -\sum_{j=0}^{4} \mathbf{q}_j'(X) e^{ik_j x} + A^{(1+)} \sum_{j=0}^{4} \mathbf{q}_j(X) e^{i(k_j+1)x} \\ & + A^{(1-)} \sum_{j=0}^{4} \mathbf{q}_j(X) e^{i(k_j-1)x}. \end{aligned} \tag{3.34}$$

As discussed in Appendix A.2.6, in order to eliminate the secular terms which vary like $xe^{ik_j x}$ from the solution of (3.34), we begin by writing, for each m, the coefficients on the right hand side of (3.34) which vary like $e^{ik_m x}$, added together, as $\mathbf{Q}e^{ik_m x}$ for some constant vector $\mathbf{Q}$. Figure 3.9 shows that, for

almost any ω, the eigenvalues ik_j are distinct. Thus the eigenvectors of $A^{(0)}$, $\mathbf{q}_j$, are linearly independent and so we may write $\mathbf{Q}$ as a linear combination of them. We must ensure that the coefficient of $\mathbf{q}_m$ in this expansion is zero.

If, for a particular ω and m, ik_m is such that $i(k_m+1)$ and $i(k_m-1)$ do not correspond to any other eigenvalues, then we may ensure that the coefficient on the right hand side of (3.34) parallel to $\mathbf{q}_m$ is zero by putting $\mathbf{q}'_m(X)$ equal to zero, i.e. $\mathbf{q}_m(X)$ is a constant.

If, however, ω is such that $ik_1 = i(k_0+1)$, say, then to eliminate the secular terms we must have

$$-\mathbf{q}'_0(X) + A^{(1-)}\mathbf{q}_1(X) \in \text{span}\{\mathbf{q}_1(X), \mathbf{q}_2(X), \mathbf{q}_3(X), \mathbf{q}_4(X)\}. \tag{3.35}$$

We know from (3.31) that the $\mathbf{q}_j$ must remain eigenvectors of $A^{(0)}$. Therefore they can vary only up to scalar multiplication. For each j, we put $\mathbf{q}_j(X) = l_j(X)\underline{\mathbf{q}}_j$, with $l_j(X)$ a scalar function of X and $\underline{\mathbf{q}}_j$ a constant unit vector. We now find a vector $\underline{\mathbf{o}}_0$, by Gram-Schmidt orthogonalisation for example, which is perpendicular to $\mathbf{q}_1$, $\mathbf{q}_2$, $\mathbf{q}_3$ and $\mathbf{q}_4$. Thus (3.35) reads

$$-l'_0(X)\underline{\mathbf{q}}_0.\underline{\mathbf{o}}_0 + l_1(X)\left(A^{(1-)}\underline{\mathbf{q}}_1\right).\underline{\mathbf{o}}_0 = 0. \tag{3.36}$$

We now use the fact that $i(k_1-1) = ik_0$ to show that the following must also be true:

$$-\mathbf{q}'_1(X) + A^{(1+)}\mathbf{q}_0(X) \in \text{span}\{\mathbf{q}_0(X), \mathbf{q}_2(X), \mathbf{q}_3(X), \mathbf{q}_4(X)\} \tag{3.37}$$

and so

$$-l'_1(X)\underline{\mathbf{q}}_1.\underline{\mathbf{o}}_1 + l_0(X)\left(A^{(1+)}\underline{\mathbf{q}}_0\right).\underline{\mathbf{o}}_1 = 0, \tag{3.38}$$

with $\underline{\mathbf{o}}_1$ perpendicular to $\mathbf{q}_0$, $\mathbf{q}_2$, $\mathbf{q}_3$ and $\mathbf{q}_4$. Combining the two scalar differential equations (3.36) and (3.38) gives

$$l''_0(X) - \left[\frac{\left((A^{(1+)}\underline{\mathbf{q}}_0).\underline{\mathbf{o}}_1\right)\left((A^{(1-)}\underline{\mathbf{q}}_1).\underline{\mathbf{o}}_0\right)}{(\underline{\mathbf{q}}_0.\underline{\mathbf{o}}_0)(\underline{\mathbf{q}}_1.\underline{\mathbf{o}}_1)}\right] l_0(X) = 0 \tag{3.39}$$

and the same equation for $l_1(X)$. The terms $\underline{\mathbf{q}}_0.\underline{\mathbf{o}}_0$ and $\underline{\mathbf{q}}_1.\underline{\mathbf{o}}_1$ are not zero by the fact that the eigenvectors form a spanning set. Thus we expect the solutions to (3.23) to vary like

$$e^{ik_1x \pm \sqrt{W}\epsilon x}, \tag{3.40}$$

where W is the term in square brackets in (3.39).

We now find $\sqrt{W}$ at the point at which two roots meet to form a loop, labelled * in Figure 3.9. For this we find solutions of the dispersion relation (3.20) with parameter values (3.21), ik_0 and ik_1, in the right range of (real) ω, such that $ik_1 = i(k_0 + 1)$. We get

$$\begin{aligned} \omega &\approx 0.290386, \\ k_0 &\approx 0.399331, \\ k_1 &\approx 1.399331 \end{aligned} \tag{3.41}$$

and

$$\sqrt{W} \approx 0.75700, \tag{3.42}$$

in good agreement with (3.27). This analysis has demonstrated that a loop will appear for any small, positive value of ϵ. At the point marked ** in Figure 3.9, two branches which touch when $\epsilon = 0$ move away from each other. This point is

$$\begin{aligned} \omega &\approx 0.327141, \\ k_0 &\approx 0.319327, \\ k_1 &\approx 1.319327, \end{aligned} \tag{3.43}$$

so

$$\sqrt{W} \approx 0.23481i, \tag{3.44}$$

which explains the movement of the two branch curves away from each other, again for any $\epsilon > 0$.

Finally, we consider the shape of the loops. We put

$$\omega = \omega_0 + \epsilon\omega_1, \tag{3.45}$$

$$A(x) = A^{(0)} + \epsilon A^{(1+)}e^{ix} + \epsilon A^{(1-)}e^{-ix} + \epsilon\omega_1 A^{(\omega)} + O(\epsilon^2), \tag{3.46}$$

where $\omega_0 \approx 0.290386$ is the value of ω at which the loop first appears. $A^{(0)}$, $A^{(1+)}$ and $A^{(1-)}$ are now taken to be functions of ω_0 and $A^{(\omega)}$ has the form given in Appendix A.2.7. At order 1, the solutions to (3.23) remain the same as before, given by (3.32). At order ϵ, (3.33) becomes

$$\begin{aligned} \tfrac{\partial \mathbf{u}_1}{\partial x}(x,X) + \tfrac{\partial \mathbf{u}_0}{\partial X}(x,X) &= A^{(0)}\mathbf{u}_1(x,X) + A^{(1+)}\mathbf{u}_0(x,X)e^{ix} + \\ &\quad A^{(1-)}\mathbf{u}_0(x,X)e^{-ix} + \omega_1 A^{(\omega)}\mathbf{u}_0(x,X), \end{aligned} \tag{3.47}$$

so

$$\begin{aligned} \tfrac{\partial \mathbf{u}_1}{\partial x} - A^{(0)}\mathbf{u}_1(x,X) &= \sum_j \left(\omega_1 A^{(\omega)}\mathbf{q}_j(X) - \mathbf{q}_j'(X)\right) e^{ik_j x} + \\ &\quad A^{(1+)}\sum_j \mathbf{q}_j(X)e^{i(k_j+1)x} + A^{(1-)}\sum_j \mathbf{q}_j(X)e^{i(k_j-1)x}. \end{aligned} \tag{3.48}$$

Applying the same logic as before, if ik_m is such that the corresponding root does not interfere with any other then $\mathbf{q}_m(X) = \textit{constant}$ is again a solution. If, however, we have that $ik_1 = i(k_0 + 1)$, the equivalent of (3.35) reads

$$\omega_1 A^{(\omega)}\mathbf{q}_0(X) - \mathbf{q}_0'(X) + A^{(1-)}\mathbf{q}_1(X) \in \text{span}\{\mathbf{q}_1(X), \mathbf{q}_2(X), \mathbf{q}_3(X), \mathbf{q}_4(X)\}. \tag{3.49}$$

We again put $\mathbf{q}_j(X) = l_j(X)\underline{\mathbf{q}}_j$ and obtain

$$l_0(X)\omega_1\left(A^{(\omega)}\underline{\mathbf{q}}_0\right).\underline{\mathbf{o}}_0 - l_0'(X)\underline{\mathbf{q}}_0.\underline{\mathbf{o}}_0 + l_1(X)\left(A^{(1-)}\underline{\mathbf{q}}_1\right).\underline{\mathbf{o}}_0 = 0, \tag{3.50}$$

with $\underline{\mathbf{o}}_0$ as before. The equivalent from considering terms varying like $e^{ik_1 x}$ is

$$l_1(X)\omega_1\left(A^{(\omega)}\underline{\mathbf{q}}_1\right).\underline{\mathbf{o}}_1 - l_1'(X)\underline{\mathbf{q}}_1.\underline{\mathbf{o}}_1 + l_0(X)\left(A^{(1+)}\underline{\mathbf{q}}_0\right).\underline{\mathbf{o}}_1 = 0. \tag{3.51}$$

Combining these two equations we obtain

$$\begin{aligned} & l_0''(X)(\underline{\mathbf{q}}_0.\underline{\mathbf{o}}_0)(\underline{\mathbf{q}}_1.\underline{\mathbf{o}}_1) \\ -l_0'(X)\left[\omega_1(\underline{\mathbf{q}}_0.\underline{\mathbf{o}}_0)\left(A^{(\omega)}\underline{\mathbf{q}}_1\right).\underline{\mathbf{o}}_1+\omega_1(\underline{\mathbf{q}}_1.\underline{\mathbf{o}}_1)\left(A^{(\omega)}\underline{\mathbf{q}}_0\right).\underline{\mathbf{o}}_0\right]+ & \\ +l_0(X)\left[-\left(A^{(1+)}\underline{\mathbf{q}}_0\right).\underline{\mathbf{o}}_1\times\left(A^{(1-)}\underline{\mathbf{q}}_1\right).\underline{\mathbf{o}}_0\right. & \\ \left.+\omega_1^2\left(A^{(\omega)}\underline{\mathbf{q}}_0\right).\underline{\mathbf{o}}_0\times\left(A^{(\omega)}\underline{\mathbf{q}}_1\right).\underline{\mathbf{o}}_1\right] &= 0 \end{aligned} \tag{3.52}$$

and the same equation for $l_1(X)$. Note that when $\omega_1 = 0$, this reduces to (3.39).

Equation (3.52), despite the complexity of the coefficients, is a second-order linear differential equation with constant (w.r.t. X) coefficients. In [7], the dispersion relation

$$D(k,\omega) = k^2 - \omega^2 - \gamma^2 = 0, \tag{3.53}$$

with γ constant, is considered as an example. If we temporarily consider a substitution of the form $e^{i\kappa X}$ for $l_0(X)$, (3.52) begins to look a little like (3.53). A change of variables to two variables of the form $\phi_{1,2} = \mu_{1,2}\kappa + \nu_{1,2}\omega$ can then be used to reduce the equation to something of exactly this form and we expect the results in [7] to hold.

Solutions to (3.23) will vary like

$$e^{ik_1x+J(\omega_1)\epsilon x}, \tag{3.54}$$

where

$$\begin{aligned} J(\omega_1) &= \omega_1\left(\frac{\left(A^{(\omega)}\underline{\mathbf{q}}_0\right).\underline{\mathbf{o}}_0}{2\underline{\mathbf{q}}_0.\underline{\mathbf{o}}_0}+\frac{\left(A^{(\omega)}\underline{\mathbf{q}}_1\right).\underline{\mathbf{o}}_1}{2\underline{\mathbf{q}}_1.\underline{\mathbf{o}}_1}\right)\pm \\ & \sqrt{\omega_1^2\left(\frac{\left(A^{(\omega)}\underline{\mathbf{q}}_0\right).\underline{\mathbf{o}}_0}{2\underline{\mathbf{q}}_0.\underline{\mathbf{o}}_0}-\frac{\left(A^{(\omega)}\underline{\mathbf{q}}_1\right).\underline{\mathbf{o}}_1}{2\underline{\mathbf{q}}_1.\underline{\mathbf{o}}_1}\right)^2+\frac{\left(A^{(1+)}\underline{\mathbf{q}}_0\right).\underline{\mathbf{o}}_1\times\left(A^{(1-)}\underline{\mathbf{q}}_1\right).\underline{\mathbf{o}}_0}{(\underline{\mathbf{q}}_0.\underline{\mathbf{o}}_0)(\underline{\mathbf{q}}_1.\underline{\mathbf{o}}_1)}}. \end{aligned} \tag{3.55}$$

The function $J(\omega_1)$, shifted by ω_0 in the ω_r direction, is plotted as the curve in Figure 3.18. Some numerical points from the full solution, i.e. that computed using Floquet's theorem, are shown as dots.

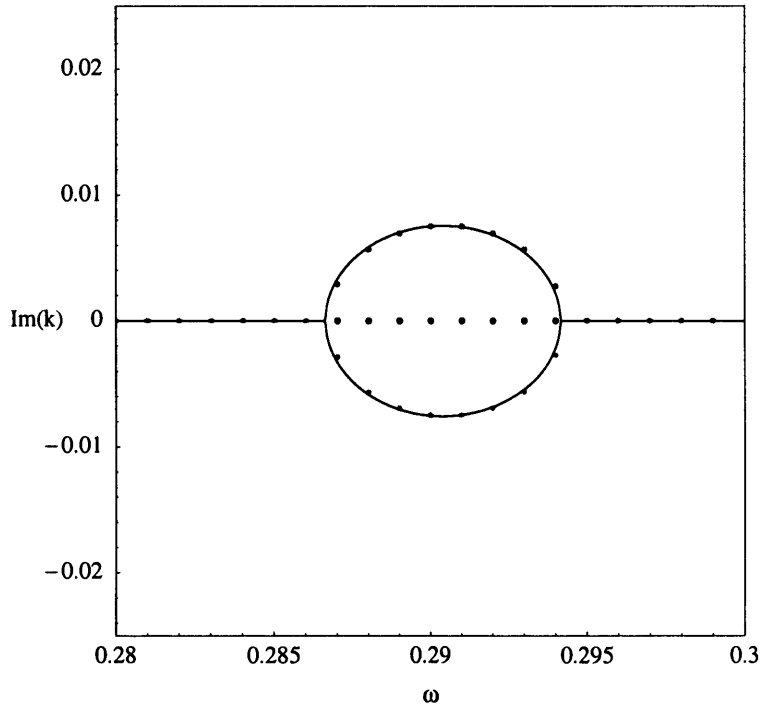

Figure 3.18: The shape of the loop, for $\epsilon = 0.01$. The solid line shows its shape as given by (3.55) and the dots show data generated numerically.

Figure 3.18 shows that the size and shape of the loop match the numerical data over the whole range of ω_1. However, it is clear that the 'centre' of the loop shifts slightly, in the positive ω direction, as ϵ increases and our model does not account for this. An explanation for this is given by Figure 3.19. This shows numerical data for the shift of the loop σ, measured by measuring the ω which gives maximum k_i, against ϵ in a log-log plot. log here is taken to be $\log_e$.

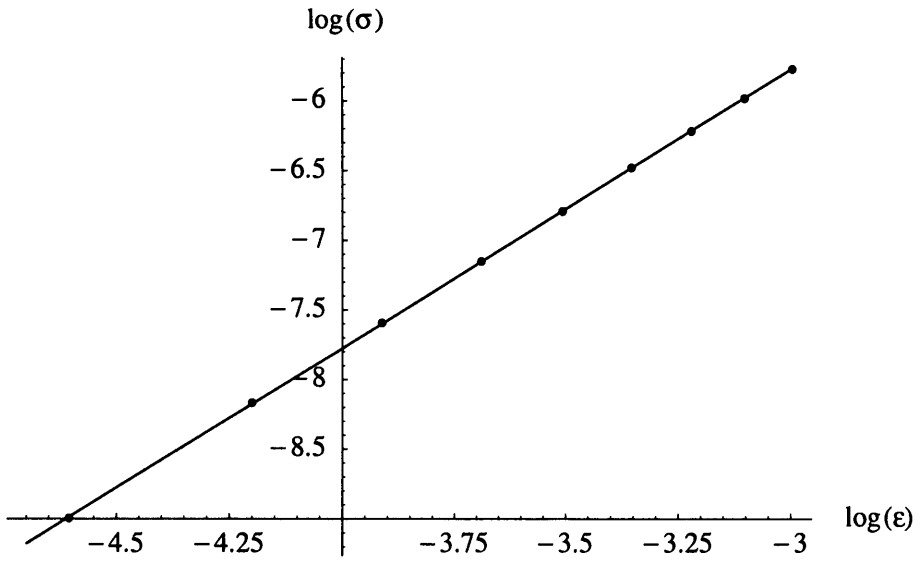

Figure 3.19: The shift of the loop σ, for varying ϵ between 0.01 and 0.05. The line shown has a slope of exactly 2.

The line shown in the figure has slope exactly 2, with its 'intercept' chosen so that it is a good fit for the data. This provides good evidence that the shifting of the loop is a second-order effect in ϵ. Unfortunately, the coefficient of ϵ^2 in a numerical best-fit of this data is about 1.23, so the shift will be quite significant for all but very small ϵ.

We may also study the stability of our system in terms of the influence of the branch reconnections which form the loop and of the influence of the separation of the branches, for non-zero epsilon, marked ** in Figure 3.9.

Figure 3.20 shows the loop, as given by (3.54) and (3.55), in the complex k-plane, with ω_i varying. As ω_i is increased, the branch curves which go to make up the loop separate into different half-planes and we conclude that the process leading to the loop formation does not cause absolute instability.

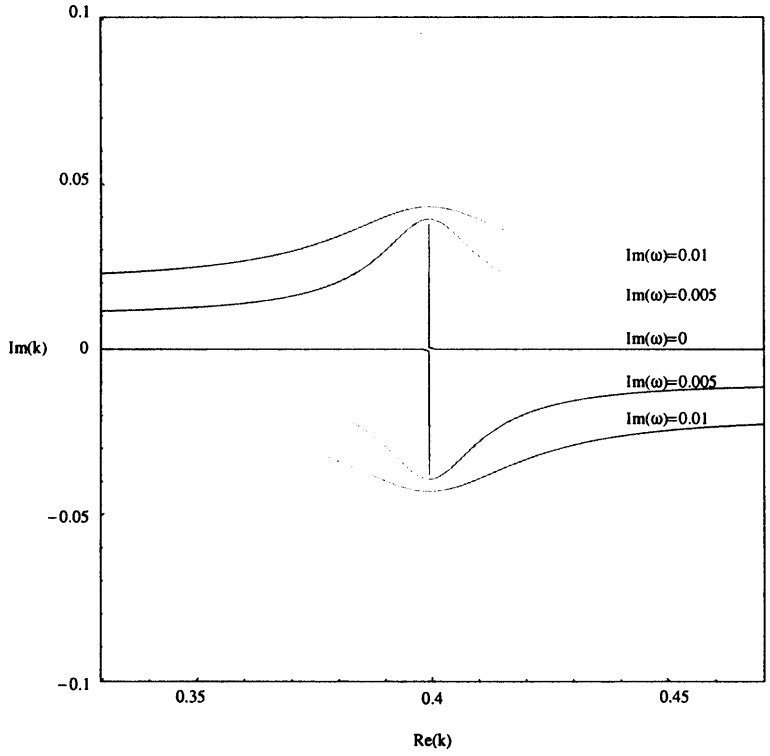

Figure 3.20: The loop in the branch curves, as predicted from the method of multiple scales analysis, for $\omega_i = 0$, 0.005 and 0.01. $\epsilon = 0.05$. The curves get lighter with increasing ω_r.

We now turn our attention to the separation of the branch curves which occurs for slightly higher ω_r, shown in Figures 3.21 and 3.22. Figure 3.22 shows that when $\omega_i = 0.005$ there is a branch curve connecting the two half-planes. Thus the absolute instability is due to the separation of the branch curves.

It is worth noting that the behaviour of the loop and separation point at ω_0 is consistent with all the quotient-like terms in $J(\omega_1)$ (equation 3.55) being

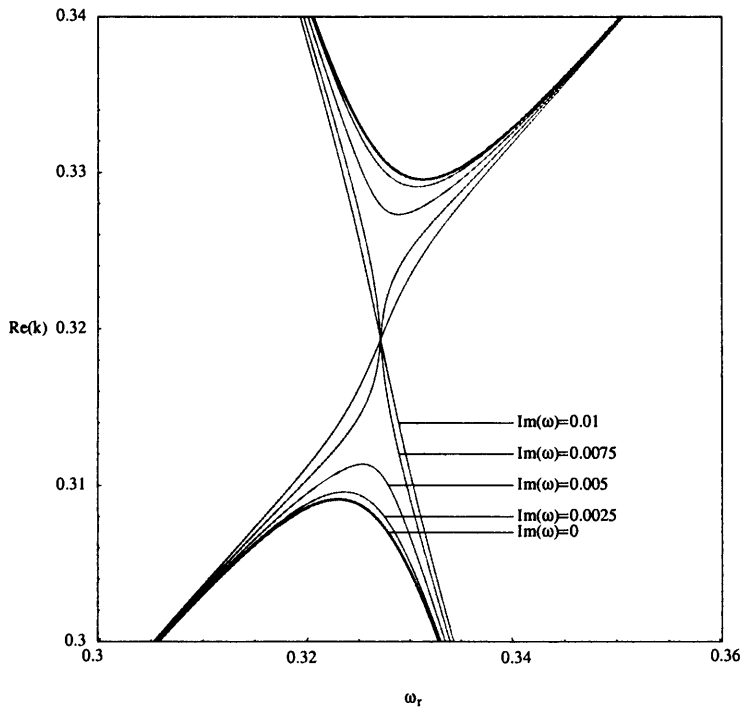

Figure 3.21: The separation of the branch curves, as predicted from the method of multiple scales analysis, for ω_i between 0 and 0.01, shown as the variation of k_r with ω. $\epsilon = 0.05$. The curves get lighter with increasing ω_r.

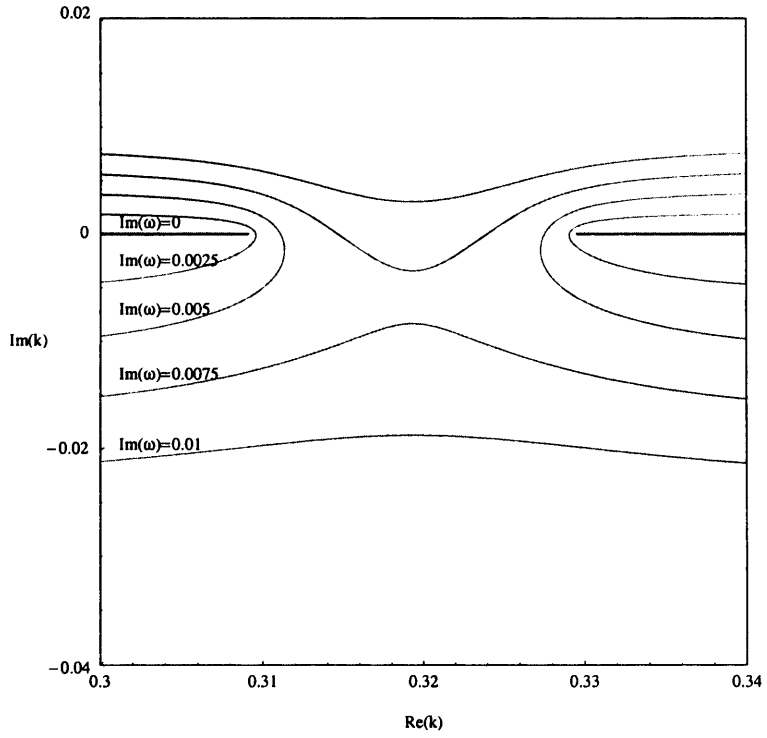

Figure 3.22: The separation of the branch curves, as predicted from the method of multiple scales analysis, for ω_i between 0 and 0.01, shown in the complex k-plane. $\epsilon = 0.05$. The curves get lighter with increasing ω_r.

real. This can be shown to be the case. We first note that $A^{(0)}$ is of the form

$$A^{(0)} = ZA_{(I)}Z^{-1}, \tag{3.56}$$

where

$$Z = \begin{pmatrix} 1 & 0 & 0 & 0 & 0 \\ 0 & 1 & 0 & 0 & 0 \\ 0 & 0 & 1 & 0 & 0 \\ 0 & 0 & 0 & i & 0 \\ 0 & 0 & 0 & 0 & 1 \end{pmatrix} \tag{3.57}$$

and $A_{(I)}$ is a purely imaginary matrix. $A^{(0)}$ itself could be made purely imaginary by using the substitutions $F' = iG$, $G' = iH$ in Section 3.2, in place of $F' = G$, $G' = H$. As things are, if the eigenvalues of $A^{(0)}$ and so $A_{(I)}$ are imaginary, then the eigenvectors of $A_{(I)}$ will have each component real. So each eigenvector $\mathbf{q}_j$ of $A^{(0)}$ will be of the form

$$Zx_{(I)}, \tag{3.58}$$

where $x_{(I)}$ is an eigenvector of $A_{(I)}$. Thus all the components of $\mathbf{q}_j$ will be real, except for the fourth, which will be imaginary. $\underline{\mathbf{o}}_0$ and $\underline{\mathbf{o}}_1$ can be written in this form too. We note next that $A^{(\omega)}$ has the same form as $A^{(0)}$ in (3.56) and $A^{(1+)}$ and $A^{(1-)}$ have similar forms, although with a purely-real matrix 'in the middle'. Thus terms like $A^{(\omega)}\underline{\mathbf{q}}_j$ in (3.55) will be of the form (real, real, real, imaginary, real) and terms like $A^{(1+)}\underline{\mathbf{q}}_j$ or $A^{(1-)}\underline{\mathbf{q}}_j$ will be (imaginary, imaginary, imaginary, real, imaginary). Looking at the form of the quotient-like terms in (3.56) it is clear that they will all equate to real numbers.

This point is made because, looking at the derivations in the appendix it is expected that similar forms for the terms in $J(\omega_1)$ could be found for other systems with order-ϵ space-periodic variation in the parameters.

3.6 Three-wave interactions

A three-(or more) wave interaction or resonance is a phenomenon which can occur in nonlinear partial differential systems where certain conditions on the frequencies and wavenumbers of particular waves are met. Here we will consider only the three-wave case as it is the one relevant to the problem discussed in this chapter. Assuming the usual convention (see Chapter 1) of making wavelike substitutions in to an equation of the form $u(x,t) = u_0 e^{ikx-i\omega t}$, with wavenumbers k and frequencies ω, the conditions may be expressed as

$$\begin{aligned} k_1 \pm k_2 &= k_3, \\ \omega_1 \pm \omega_2 &= \omega_3 \quad \text{with}, \\ \omega_j &= \omega_j(k_j), \end{aligned} \tag{3.59}$$

for $j = 1, 2, 3$, for a set of three waves in a system. An early description of this type of phenomenon, may be found in Phillips [48], for a four-wave interaction amongst surface waves on deep water. McGoldrick [41] discovered a three-wave interaction between capillary-gravity waves. Examples of simple systems exhibiting this behaviour may be found in [20] and [23].

As was mentioned above, these resonances are found in nonlinear systems. For small disturbances, i.e. in situations where wave amplitudes are small, the nonlinear terms will be very small. As was suggested above, a substitution of the form $u(x,t) = u_0 e^{ikx-i\omega t}$ satisfying the linear terms of the equation is made. By considering u_0 to be a slowly-varying function of time, a sum over such waves can be considered as a solution to the system forced by the very small nonlinear terms, i.e. the full system. When three waves exist in the system such that (3.59) is satisfied, the amplitude of one is then forced by the other two through this nonlinear term.

In systems in which a continuous spectrum of modes/branches exists it is clear that there is the potential for (3.59) to be satisfied. The system considered

in this chapter is one such system and indeed (3.59) is satisfied with k_3 and ω_3 describing the fixed walls of the channel. We will thus label k_3 as k_{wall}, because it is the wavenumber corresponding to the periodic wall variation. Here $k_{wall} = 1$; $\omega_3 = 0$ because the wall does not change with time. Thus, it is no surprise that the wavenumbers causing instability correspond to two copies of the branch curves, separated by exactly 1, at the same frequency. The previous section can therefore be considered as an example to clarify the description above.

Hasselmann [27] notes that the 'sum' interaction in (3.59) is unstable and the 'difference' interaction neutrally stable. However, due to the invariance of our system, (3.20), under the transformation $k \rightarrow -k$, $\omega \rightarrow -\omega$, both of the interactions (at * and at **) can be considered as both sum and difference.

The relationships between wavenumbers and frequencies can be demonstrated further by changing the value of k_{wall}. Firstly, we put $h_1 = h_{1\infty} + \epsilon \sin(0.75x)$ and change h_2 accordingly, to keep the base-state interface flat. The result is that the branch curves are now separated by $k_{wall} = 0.75$, as shown in Figure 3.23. The interactions still occur in the corresponding places.

We now change k_{wall} to 0.4. This results in the branch curves shown in Figure 3.24. We can see that the situation becomes more complicated. Interactions occur not only where the branch curves are separated by $k_{wall} = 0.4$, but also when they are separated by $2k_{wall} = 0.8$. Figure 3.25 shows a close-up of part of this figure, to enable easier identification and classification of the interactions. The interactions between branches separated by k_{wall} are marked '$\Delta = 1$' in Figure 3.25, while those between branches separated by $2k_{wall}$ are marked '$\Delta = 2$'. The pluses and minuses following these describe which curves the interaction occurs between. A + corresponds to a curve which looks, on a large scale, like $\mathrm{Re}(k) = +\omega^2$ and a $-$ one that looks like $\mathrm{Re}(k) = -\omega^2$.

Classification of these interactions is as follows: '$\Delta = 1-,-$', which de-

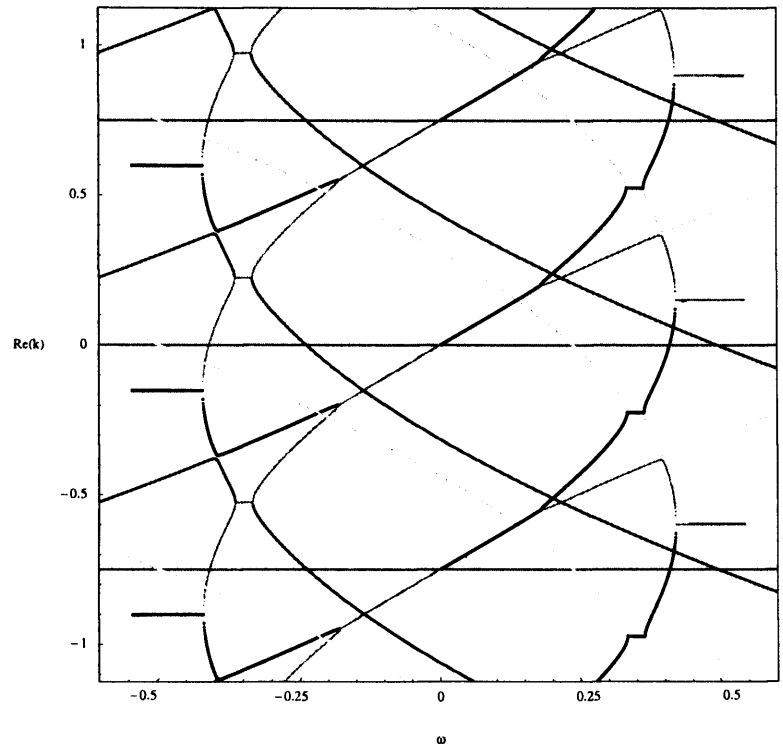

Figure 3.23: The branch curves for a system with $k_{wall} = 0.75$. $\epsilon = 0.03$.

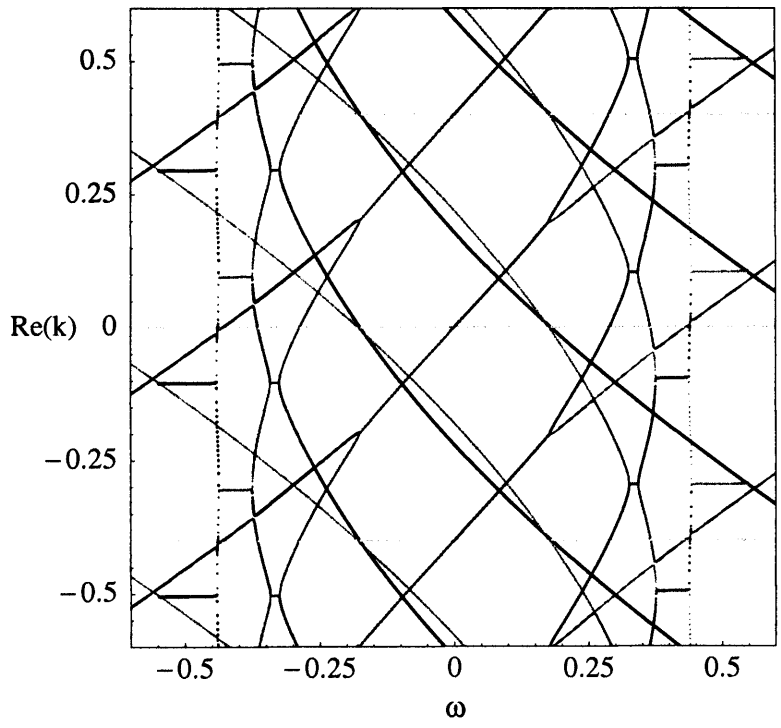

Figure 3.24: The branch curves for a system with $k_{wall} = 0.4$. $\epsilon = 0.08$.

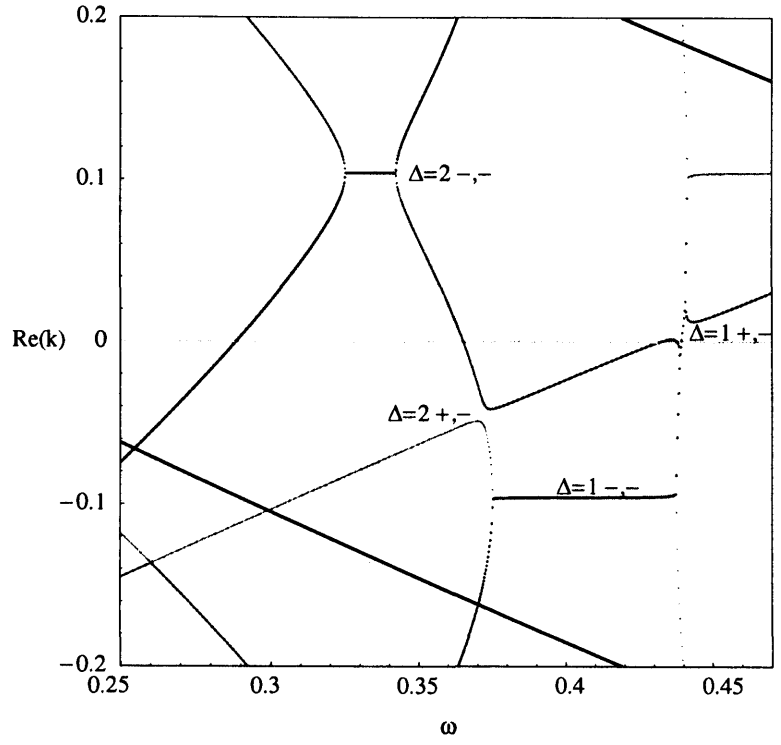

Figure 3.25: A close-up of part of Figure 3.24.

scribes the approximately-horizontal straight line in the diagram, is a loop (when complex k is considered). It roughly corresponds to the loop discovered in the original case, when $k_{wall} = 1$. '$\Delta = 2-,-$', also an approximately-horizontal line, is a new interaction, a smaller loop. '$\Delta = 2+,-$' is a separation similar to, but not corresponding to, the separation for $k_{wall} = 1$ (for $k_{wall} = 1$ there were no '$\Delta = 2$' interactions, thus it cannot correspond). It is similar to the $k_{wall} = 1$ case, however, in that it describes the reconnection of an upstream-travelling and downstream-travelling branch for $w_i > 0$ and thus indicates absolute instability. The '$\Delta = 1+,-$' interaction is the one which corresponds to the separation for $k_{wall} = 1$. The figure indicates that it has become a loop and thus no longer implies absolute instability. An explanation for this can be found by considering Figure 3.10. If the dashed horizontal lines on this figure are gradually shortened in length from 1 down to 0.4, while keeping their ends on the curved lines, we see that the line connecting curves 1 and

3 will pass over the turning point of the curve, so that it links curves 1 and 2. As these are both downstream-travelling branches, interaction between them cannot lead to absolute instability. Another thing to notice from this figure and Figure 3.24 is that interactions seem to occur whenever two curves are separated by an integer multiple of the wall wavenumber and they are in the $k_r > 0, \omega > 0$ quadrant or, correspondingly, the $k_r < 0, \omega < 0$ quadrant. This suggests that '$\Delta = 3$' connections may exist as well: an additional separation appears to occur at $\omega \approx 0.26$, which has $k_r \approx -0.14$. This may also signify absolute instability.

We now consider more complicated, but still periodic, wall geometries, such as that given by setting h_1 equal to

$$h_{gauss}(x) = e^{-\left(50\frac{x}{2\pi}\right)^2} - \frac{1}{2}, \tag{3.60}$$

on $-\pi < x \leq \pi$, repeated with period 2π, in x. This is shown in Figure 3.26. $h_2(x)$ is set accordingly, to keep the base-state interface flat. The function $h_{gauss}(x)$ may be viewed as the sum of its Fourier cosine components, shown in Figure 3.27. As would be expected from the theory of Fourier series, the low-wavenumber components dominate. The lowest wavenumber in the expansion of this 2π-periodic function is $n = 1$. It is expected, then, that this component would create interactions wherever branch curves, at the same frequency, were separated by 1, or any multiple of 1 (in the upper-right or lower-left quadrants of Figure 3.10). Therefore the interactions due to other components, $n = 2, 3, \ldots$, would coincide with those already due to $n = 1$. The key to the branch curve interactions of periodic wall geometries would therefore be the lowest-wavenumber Fourier branch of the wall shape, i.e. the one corresponding to its period.

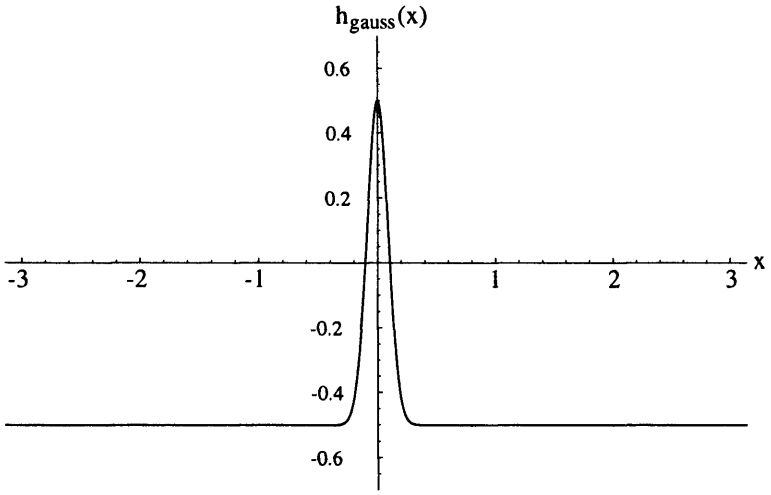

Figure 3.26: $h_{gauss}(x) = e^{-\left(50\frac{x}{2\pi}\right)^2} - \frac{1}{2}$ for $-\pi < x \leq \pi$.

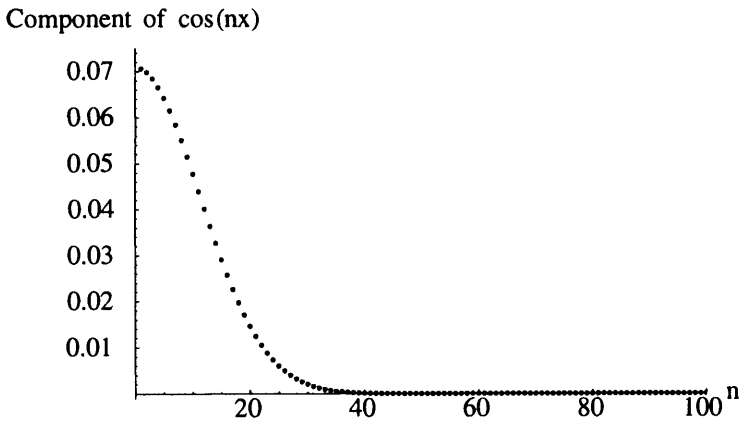

Figure 3.27: The first hundred Fourier cosine components of $h_{gauss}(x)$, except the constant term, which depends only on the position of the curve below the x-axis.

3.7 Summary

The stability of stratified thin-layer two-fluid flow in a channel has been considered. By defining the upper channel wall shape in terms of the lower channel wall shape, it is possible to determine an analytic base flow. The spatial stability problem for the homogeneous (straight channel) case has been considered for a set of parameters which make it convectively unstable. The walls have then been made to vary periodically in space and Floquet's theorem has been used to find the wavenumbers of wavelike perturbations of the base flow and investigate the signalling problem. Sinusoidal wall variations of any magnitude make the flow absolutely unstable. This is due to a three-wave resonance, with one 'wave' being the channel wall. For the non-sinusoidal periodic wall case, the dominant Fourier series component of the wall shape should be sufficient to make the flow absolutely unstable.

Chapter 4

Channels with a short-range depth variation

4.1 Introduction

We now turn our attention to two problems for which the physical set-up is similar to that investigated in Chapter 3, but for which the variation of channel width is confined to a finite x-range. The remainder of the channel is straight and the sections upstream and downstream of the inhomogeneity will be referred to as 'straight sections'. This problem is again relevant to real-world flows through pipes and ducts and solving a stability problem corresponds to attempting to determine whether laminar-turbulent transition would occur.

As discussed in Chapter 1, when considering a stability problem we can search for a spectrum of frequencies signifying instability. This could be a continuous spectrum or a discrete spectrum (or both). In the problems considered in Chapters 2 and 3, we have been looking for continuous spectra. As discussed in the introduction, for systems such as the one we have described, it is common to identify a discrete spectrum of modes and we do so here.

Firstly, we consider the case where the wall-shape nonhomogeneity is si-

nusoidal in form. Three sub-cases are considered: a single sine-period, a half sine-period and the case of several periods. All three are found to make the flow absolutely unstable. In the half-period case, this seems only to occur when the wall shape represents a contraction of the channel, for which a single unstable mode is found. For the several-period case, several unstable modes are found.

Cavity tones are a well-known phenomenon in acoustics (see e.g. [31]). They can occur when a fluid such as air, flowing through a channel, passes a cavity such as a finite-range enlargement of the channel width. The flow may become unstable, creating trapped waves between the ends of the cavity. These waves can have important engineering implications as they may lead to sound pollution or potentially dangerous structural vibration. It is therefore interesting to consider how a cavity-like set-up affects the stability of our two-fluid flow. In this chapter we study not only expansions of the channel width, but also contractions.

To this end, we consider a rectangular inhomogeneity in the wall shape, i.e. a pair of discrete jumps in the channel depth. Jump conditions at the two jumps are derived and demonstrated to correspond well with smoother transitions, in the appropriate limit. Instability is again found, appearing to occur for an expanded section of any length; this is confirmed by asymptotics for small length. For a contracted section, instability only occurs when the length is sufficiently large. Some analysis is then done of the nature of the spatial variation of the unstable eigenfunctions.

4.2 Formulation

One consequence of looking at a finite-range nonhomogeneity is that it gives us a definite 'starting point' for the system, i.e. it removes the translational sym-

metry in the streamwise direction. In the systems discussed in previous chapters we have allowed upstream-travelling and downstream-travelling branches in any part of the system. In channel flows with a finite-range inhomogeneity, it is sensible to restrict this by means of the physical argument that the nonhomogeneity should not be subjected to disturbances coming in from infinity, in either direction. All disturbances must then 'travel away from' the inhomogeneity. This means that we cannot allow downstream-travelling branches upstream of the inhomogeneity or upstream-travelling branches downstream of it. The restriction is what gives us a discrete spectrum: we will see that we cannot find a wavenumber for each frequency, or vice versa, satisfying the system of equations - only certain frequencies may be found with this property.

Our strategy for finding such frequencies is as follows: for each complex frequency, consider which combinations of upstream-travelling disturbances are possible at the upstream end of the inhomogeneity. Compute how such disturbances would change as they are transmitted across the inhomogeneity and check whether, at its downstream end, they correspond to a downstream-travelling disturbance. If so, the frequency is a mode which satisfies the system. This is equivalent, of course, to finding singularities of the scattering matrix.

The physical situations considered in this chapter are similar to those in the previous chapter. It is important to note that, in the straight sections, any disturbance of given frequency is a sum of exponentials with respect to the streamwise coordinate and hence we can use the straight-channel dispersion relation (3.20) to find four wavenumbers for each frequency. As discussed in Chapter 3, two will be upstream-travelling waves and two downstream-travelling waves and these may be distinguished by continuation from the case of ω_i large and positive. To compute the changes across the inhomogeneity we use the nonhomogeneous equations (3.17). A consequence of having four roots of the dispersion relation is that it is now convenient to reduce the system

(3.17) to fourth order. This may be done by observing that the fluid velocity $u_2(x)$ can be written in terms of $u_1(x)$ and other variables. We combine (3.10) and (3.11) and integrate to give

$$u_2(x) = \frac{u_1(x) \times (h_1(x) + f(x)) - u_{1\infty}h_{1\infty} - u_{2\infty}h_{2\infty}}{f(x) - h_2(x)}. \tag{4.1}$$

The rest of the derivation is similar to the fifth-order case and is considered in Appendix A.3.1. It is, however, worth stating here that the fourth-order equivalent of (3.23) reads

$$\mathbf{u}_4' = A_4(x)\mathbf{u}_4, \tag{4.2}$$

with the 'disturbance vector', $\mathbf{u}_4$, equal to

$$\mathbf{u}_4 = (U_1 \; F \; G \; H)^T. \tag{4.3}$$

As mentioned above, whereas in previous chapters the distinction between upstream- and downstream-travelling branches has only been made to show that the branches can satisfy the Briggs-Bers criterion, here we require that certain branches do not occur in certain sections. The distinction is made by putting ω_i large, which pushes downstream-travelling branches into the upper half-k-plane and upstream-travelling ones into the lower half-k-plane. By parametric continuation we may make the upstream/downstream distinction for any ω_i. Note however that, for certain values of ω, one downstream-travelling branch does not decay downstream. This branch can be seen in Figure 3.2 as the branch which, for $\omega \approx 0.1$, lies below the line Im(k)=0. In the homogeneous case, it corresponds to convective instability. We allow such a phenomenon here because we are only looking for specific frequencies which satisfy the system. If such frequencies have negative imaginary part, all signals decay with time. Neutral modes would thus dominate. If the frequencies have positive imaginary part, then the system is unstable. In the unstable case, the inhomogeneous section is taken to act as a forcing driving the rest of the

system. The response to the forcing is convected downstream and grows with time. We thus expect that waves which grow away from the inhomogeneous section, i.e. in space, may be observed. It seems reasonable to think that this situation could occur as a result of an initial-value problem with a spatially compact initial condition, provided that only the region in which the initial disturbance has had time to have influence is considered. We note that, for the examples in this chapter, instability is global in the sense that a discrete eigenvalue with $\omega_i > 0$ provides disturbance growth in the entire channel.

It is important to note that the dispersion relation has branch points, k_b say, where

$$\left.\frac{\partial \omega}{\partial k}\right|_{k=k_b} = 0. \tag{4.4}$$

We must thus choose a branch cut coming from such points. For the set of parameters chosen in Chapter 3, there are two such points on the real k-axis, for $\omega \approx \pm 0.4151$. When performing our continuation from ω_i large, to distinguish upstream- from downstream-travelling branches, it is important that we do not cross such a branch cut. In fact, the natural choice for a branch cut here is along the positive (for the branch point with $\omega = +0.4151$) real ω-axis. This is sufficient as a choice because we are only interested in modes which grow, i.e. have $\omega_i > 0$. It is assumed that there may be neutral modes (with real ω) which would dominate any decaying solutions.

Finally, we note that the straight-channel dispersion relation is invariant under the transformation $\omega \to -\omega$, $k \to -k$. To save on computation we will restrict ourselves to $\omega_r > 0$.

4.3 Channels with a short-range sinusoidal variation

We now consider channels with a short-range variation in depth, similarly to before, but with a single period or half-period of sinusoidal variation in depth. Figure 4.1 shows the general geometry under consideration for systems with a limited-range depth variation.

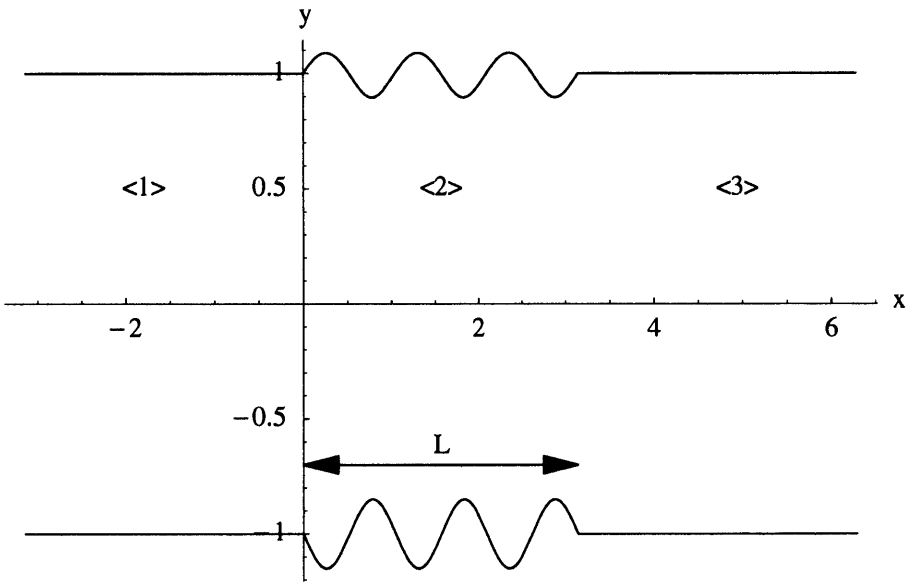

Figure 4.1: The general set-up considered for channels with a short-range depth variation. Other parameters and flow variables are as in Figure 3.1. For convenience of reference in the text, we divide the channel into three sections. Section $\langle 1 \rangle$ is the straight upstream section, section $\langle 2 \rangle$ has varying depth and section $\langle 3 \rangle$ is the straight downstream section.

Initially, we put $L = 2\pi$ and assume the magnitude of the variation to be ϵ so

$$h_1(x) = \begin{cases} 1 + \epsilon \sin(x) & 0 < x < 2\pi \\ 1 & \text{elsewhere.} \end{cases} \tag{4.5}$$

$h_2(x)$ is again defined in terms of $h_1(x)$, by means of (3.15), in order to keep

the base-state interface flat. The sharp corners in the wall shapes, at $x = 0$ and $x = L$, raise two possible questions. The first concerns whether sharp corners are valid in the long-wave/thin-layer approximation used in this, and the previous, chapter. It is assumed, however, that the corners could be smoothed sufficiently to remove this issue, without significantly changing the results obtained. This will be commented on further for the example considered in Section 4.4. The second question is whether a jump condition is required for the disturbances as they cross $x = 0$ and $x = L$. To check this, we assume that the interface slope, G, is continuous across a short range extending either side of $x = 0$ (or $x = L$). This may then be used to show that the other disturbance variables, i.e. U_1, F and H, are also continuous, so no jump condition is required. A similar analysis to this is performed in Section 4.4.

As mentioned in Section 4.2, we search numerically across the $\omega_r > 0$, $\omega_i > 0$ quarter-plane, starting with ω_i large and using continuation to distinguish upstream- and downstream-travelling branches. Parameters for the problem are the same as those chosen in Chapter 3, i.e. $u_{1\infty} = 0.8$, $u_{2\infty} = 1$, $\gamma = 0.5$, $g_\rho = 0$, $\rho_1 = \rho_2 = 1$, so that 'downstream' means 'to the right'. Figure 4.2 shows the results of the search, with $\epsilon = 0.2$. There appears to be exactly one frequency $\omega_0 \approx 0.462834 + 0.000785i$ for $\omega_r > 0$ and $\omega_i > 0$ which solves the system; thus, the spectrum is discrete.

We may then consider how this ω_0 varies as a function of ϵ. The results of this are shown in Figure 4.3. By considering a curve fit to data similar to those shown in the figure, for very small ϵ, we see that ω_0 tends to a real-valued limit as $\epsilon \to 0$ and that difference between the real part of ω_0 and the value of ω_0 in this limit varies like ϵ^4. The variation of the imaginary part is of even higher order.

We now consider the situation where $L = \pi$, so that there is only a half-period of sinusoidal variation in the channel walls. Numerical results imme-

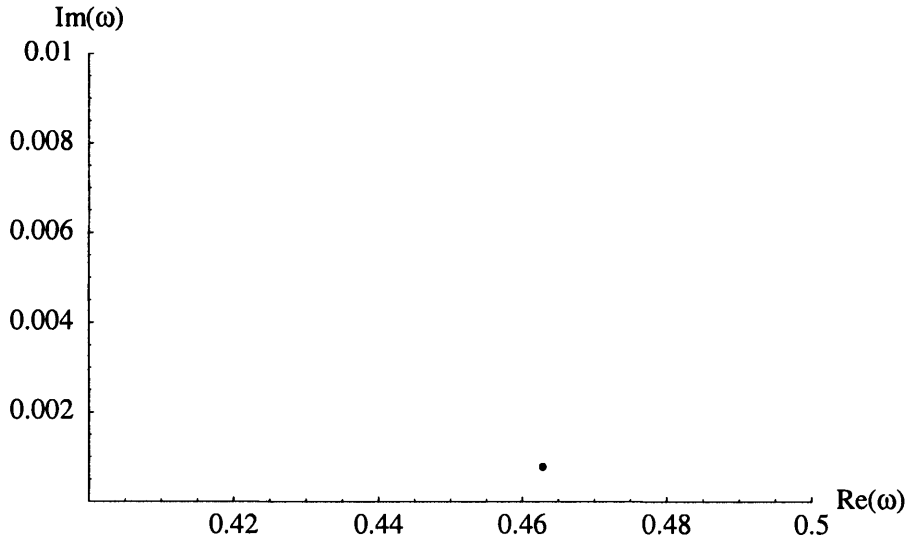

Figure 4.2: A complex ω-plane plot of the (single) solution to the limited-range sinusoidal-depth-variation problem for $\epsilon = 0.2$. It is plotted in this way to emphasise the fact that a search over a large area of the ω-plane was used to locate the frequency of the mode. In fact, a much larger region was searched than is shown.

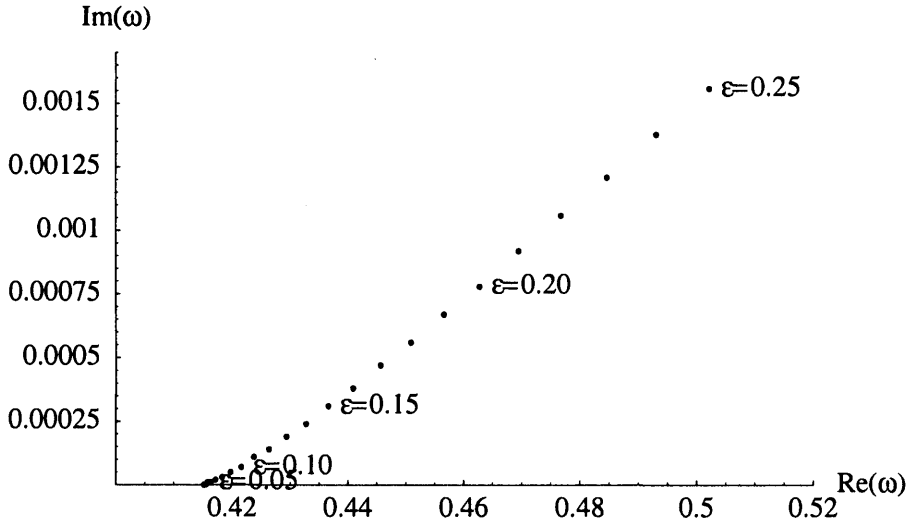

Figure 4.3: The movement of ω_0 in the complex ω-plane, as a function of ϵ when $L = 2\pi$. The labelling extends to all points in the obvious way.

diately indicate that there are no solutions for positive ϵ, but that some exist for $\epsilon < 0$. Thus, only channels having a contraction, in the sense that they become thinner for a short x-range, appear to support these branches. Figure 4.4 is the equivalent of Figure 4.3 for this situation. Finally, we note that for

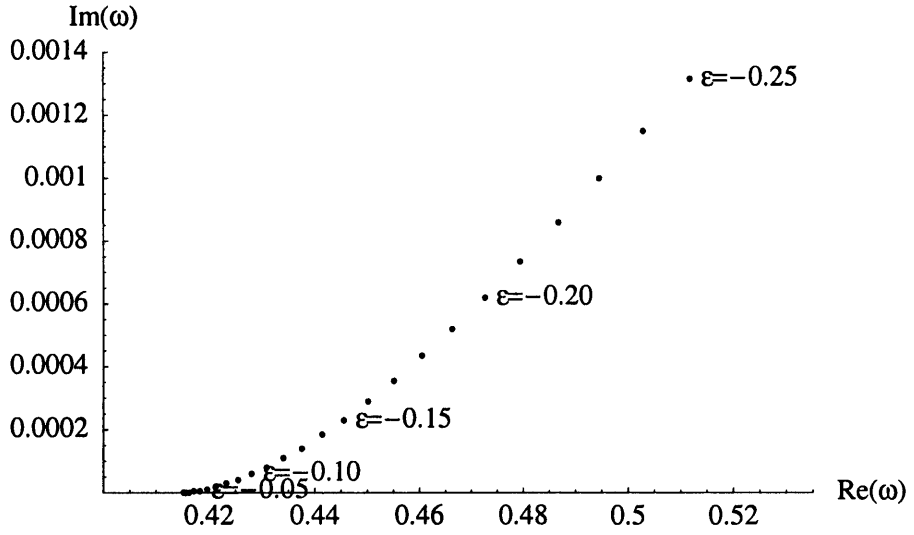

Figure 4.4: The movement of ω_0 in the complex ω-plane, as a function of ϵ when $L = \pi$. The labelling extends to all points in the obvious way.

a larger number of periods of wall variation, we appear to get more than one ω which solves the system. For small $n \in \mathbb{N}$, it appears that, when $L = 2\pi n$, n solutions $\omega_{0,j}$, $j = 1 \ldots n$ of the system appear. The 'motion' of these $\omega_{0,j}(\epsilon)$ in the ω-plane is more complicated than in the simpler situations. The case $L = 10\pi$, $\epsilon = 0.2$ is shown in Figure 4.5.

Returning to the half-period ($L = \pi$) case, the variation of ω_r appears, from curve fitting to the data in Figure 4.4, to be second-order in $-\epsilon$. Despite this, it appears that finding asymptotic solutions which match the parameters given above is a difficult task and so we move on to simpler geometries.

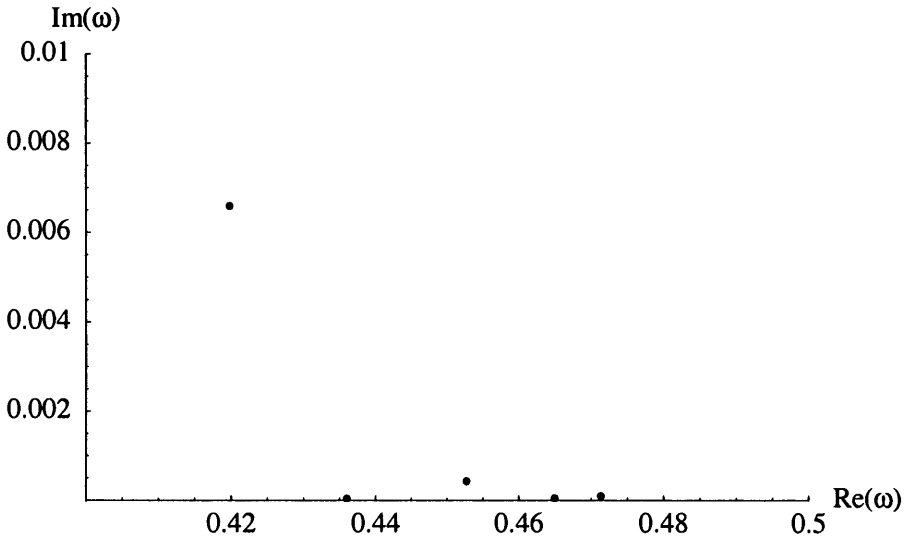

Figure 4.5: Solutions to the limited-range depth problem for $L = 10\pi$, in the complex ω-plane, for $\epsilon = 0.2$.

4.4 Flow past rectangular steps

Consider a two-fluid channel flow past an isolated rectangular step on each side of the channel. A typical set-up is shown in Figure 4.6.

The differential system describing the flow in each of the sections marked $\langle 1 \rangle$, $\langle 2 \rangle$ and $\langle 3 \rangle$ is essentially as before. As each of these sections is straight, each disturbance is a sum of harmonic waves whose wavenumbers may be found, for a given frequency, by means of the dispersion relation for a straight channel, (3.20). While we may use this equation unmodified in sections $\langle 1 \rangle$ and $\langle 3 \rangle$, using $u_{1\infty}$, $u_{2\infty}$, $h_{1\infty}$, $h_{2\infty}$ as the base-flow velocities and depths in these sections, it is clear that in section $\langle 2 \rangle$ the corresponding equation is

$$\frac{\rho_1}{h_{1\langle 2 \rangle}}(\omega - k u_{1\langle 2 \rangle})^2 + \frac{\rho_2}{h_{2\langle 2 \rangle}}(\omega - k u_{2\langle 2 \rangle})^2 = gk^2 + \gamma k^4, \tag{4.6}$$

where quantities marked with a subscript $\langle 2 \rangle$ correspond to the base flow in section $\langle 2 \rangle$ determined, when $h_{1\langle 2 \rangle}$ is specified, by (3.12) and (3.15). ω will be the same as in sections $\langle 1 \rangle$ and $\langle 3 \rangle$, but the values of k will be different. As discussed in Section 4.2, for the system to be fully satisfied and physically

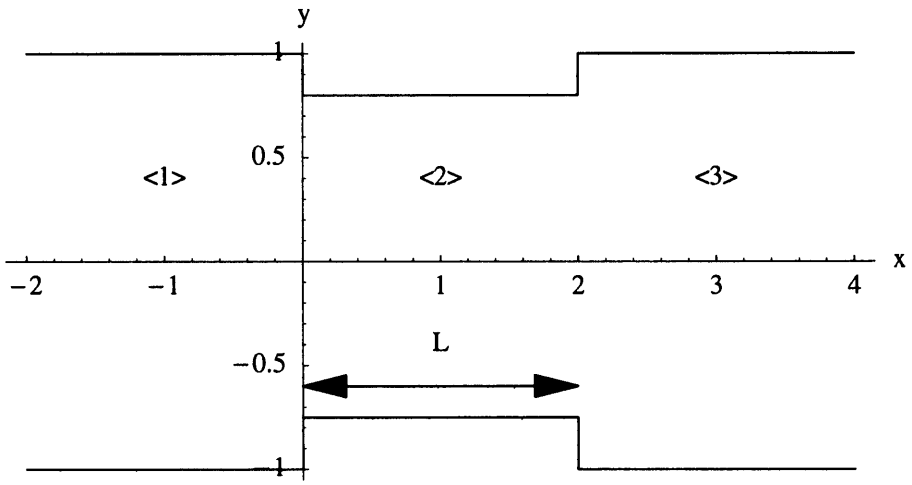

Figure 4.6: The set-up for flow past a rectangular step. Other parameters and flow variables are as for Figure 3.1. Section ⟨1⟩ extends infinitely upstream and section ⟨3⟩ infinitely downstream. Section ⟨2⟩ has a different depth and the jumps at $x = 0$ and $x = L$ are taken to occur over an infinitesimal x-range.

reasonable, only the two upstream-travelling branches for a given frequency are allowed in section ⟨1⟩ and the two downstream-travelling ones in section ⟨3⟩. All wavenumbers (k-values) satisfying (4.6) are allowed in section ⟨2⟩.

We must also take into account the discrete jumps at $x = 0$ and $x = L$. The disturbance vector (see equation 4.3) will not be continuous across such jumps and we must determine a set of physically-reasonable conditions for the change in the disturbance vector across each jump. To do this, we create a matrix, B_{jump}, such that

$$\mathbf{u}_4^+ = B_{jump}\mathbf{u}_4^-, \tag{4.7}$$

where $\mathbf{u}_4^-$ and $\mathbf{u}_4^+$ are the disturbance vectors before and after the step respectively. B_{jump} will depend on parameters such as h_1^- and h_1^+, the depth of the lower fluid before and after the jump. We consider an approximate integral of our system across a very short x-range, $(-\epsilon, \epsilon)$, where the jump is assumed to be at $x = 0$. Any terms which tend to zero as $\epsilon \to 0$ are taken to be continuous

across the jump.

We begin by saying that G, the slope of the interface, should be continuous across a jump. Thus

$$G^+ = G^- \tag{4.8}$$

and so, as $G = F'$ we have

$$\int_{-\epsilon}^{\epsilon} G\mathrm{d}x = \int_{-\epsilon}^{\epsilon} F'\mathrm{d}x = [F]_{-\epsilon}^{\epsilon} = F^+ - F^-, \tag{4.9}$$

but, as G is continuous across the jump, $\int_{-\epsilon}^{\epsilon} G\mathrm{d}x$ can only be $O(\epsilon)$ and thus tends to zero. We have

$$F^+ = F^-, \tag{4.10}$$

as well. We now consider the change in U_1. Equation (A.17) gives us

$$i\omega F - (u_{10}F)' = (U_1 h_1)', \tag{4.11}$$

which gives, upon integration,

$$\int_{-\epsilon}^{\epsilon} i\omega F\mathrm{d}x - (u_{10}^+ - u_{10}^-)F^- = U_1^+ h_1^+ - U_1^- h_1^-. \tag{4.12}$$

The part under the integral sign will tend to zero as $\epsilon \longrightarrow 0$ and so we get

$$U_1^+ = \frac{h_1^-}{h_1^+} U_1^- + \frac{u_{10}^- - u_{10}^+}{h_1^+} F^-. \tag{4.13}$$

The final part of the jump matrix B_{jump} follows similarly, although many more terms are involved. The form of B_{jump} is thus given by

$$\begin{pmatrix} \frac{h_1^-}{h_1^+} & \frac{u_1^- - u_1^+}{h_1^+} & 0 & 0 \\ 0 & 1 & 0 & 0 \\ 0 & 0 & 1 & 0 \\ B_{jump,(41)} & B_{jump,(42)} & 0 & 1 \end{pmatrix}, \tag{4.14}$$

where

$$B_{jump,(41)} = \frac{1}{\gamma}\left(\frac{u_2^+ \rho_2 h_1^-}{h_2^+} + \frac{\rho_1 u_1^+ h_1^-}{h_1^+} - \frac{u_2^- \rho_2 h_1^-}{h_2^-} - \rho_1 u_1^-\right) \tag{4.15}$$

and

$$B_{jump,(42)} = \frac{1}{\gamma}\left(\frac{\rho_2 u_2^+(u_1^+-u_2^+)}{h_2^+} - \frac{\rho_2 u_2^-(u_1^--u_2^-)}{h_2^-} + (u_1^- - u_1^+)\left(\frac{u_2^+\rho_2}{h_2^+} + \frac{u_1^+\rho_1}{h_1^+}\right)\right). \tag{4.16}$$

Justification for the assumption that $G^+ = G^-$, and hence the form of B_{jump} given above, can be found in the numerical results to be discussed below. First we consider the complex frequencies which satisfy our system of equations, with the jump conditions as above. The results of this, with the parameters $h_{1\infty} = 1$, $h_{2\infty} = 1$, $u_{1\infty} = 0.8$, $u_{2\infty} = 1$, $\rho_1 = 1$, $\rho_2 = 1$, $\gamma = 0.5$, $g_\rho = 0$, $L = 6.7$, and the height of the obstacle in the lower wall, Δh_1, equal to 0.2, are shown in Figure 4.7. We immediately note that such a flow can have more than one complex ω with $\omega_i > 0$, unlike in the case considered in the previous chapter for a half-period sinusoidally-shaped obstacle.

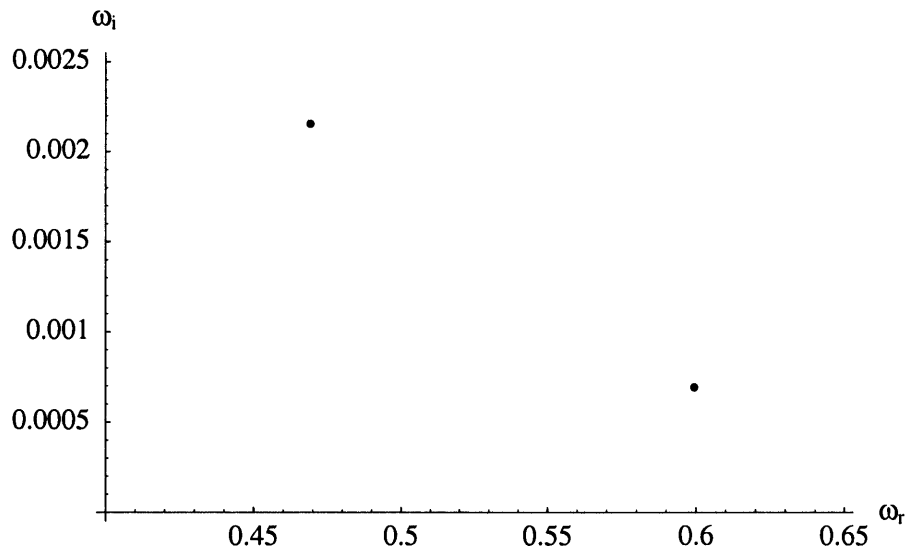

Figure 4.7: The complex frequencies which satisfy our system of flow past rectangular obstacles on the channel walls. The length and height of the lower-wall obstacle, in our nondimensional units, are 6.7 and 0.2 respectively. All other flow parameters are the same as for previous problems.

We can now provide some evidence that we have made the correct choice of jump conditions. Consider flow past an obstacle which is approximately

step-shaped, but with the ends rounded off so that solutions to the system can be found by integrating directly. We look at the limit as the ends become a discontinuous step. The channel geometry is as shown in Figure 4.8. The function which describes the hump shape, between 0 and ηL, is taken to be

$$h(x) = \begin{cases} -h_{1\infty} & x < 0 \\ -h_{1\infty} + \Delta h_1 \left(\left(\frac{2x}{\eta L}\right)^3 - \frac{1}{2}\left(\frac{2x}{\eta L}\right)^4 \right) & 0 < x < \frac{\eta L}{2} \\ -h_{1\infty} + \Delta h_1 \left(1 + \left(\frac{2x}{\eta L}\right)\left(\left(\frac{2x}{\eta L}\right) - 2\right)^3 \right) & \frac{\eta L}{2} < x < \eta L \\ -h_{1\infty} + \Delta h_1 & x > \eta L. \end{cases} \tag{4.17}$$

This function of $\frac{2x}{\eta L}$ is chosen because it is continuous up to its third derivative. The same function, reflected and translated in x, is used to describe the other end of the step, for $L < x < (1+\eta)L$. Δh_1 is the height of the step.

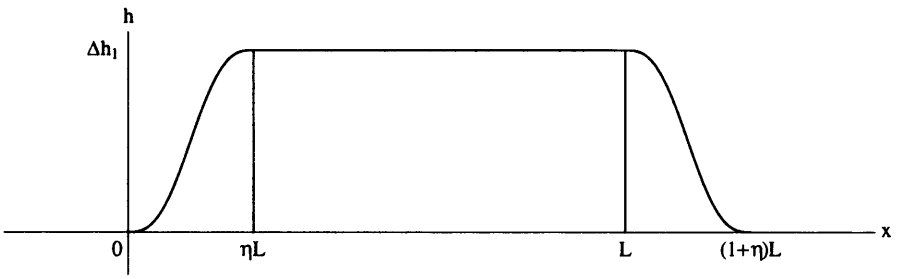

Figure 4.8: The shape of a rounded obstacle past which fluid flows. We consider the limiting case of $\eta \to 0$ and demonstrate that it corresponds with the jump conditions for a rectangular obstacle.

The frequencies, with $\omega_r > 0$ and $\omega_i > 0$, which solve the system, as η is varied, are shown in Figure 4.9. By curve-fitting to the points we extrapolate back to $\eta = 0$ and find frequencies of $\omega = 0.59955 + 0.00069408i$ and $\omega = 0.46904 + 0.0021566i$. These are in good agreement with the jump-condition calculated values of $\omega = 0.59955 + 0.0069409i$ and $\omega = 0.46905 + 0.0021564i$, shown in Figure 4.7.

We conclude from this that the matrix B_{jump} describes a physically rea-

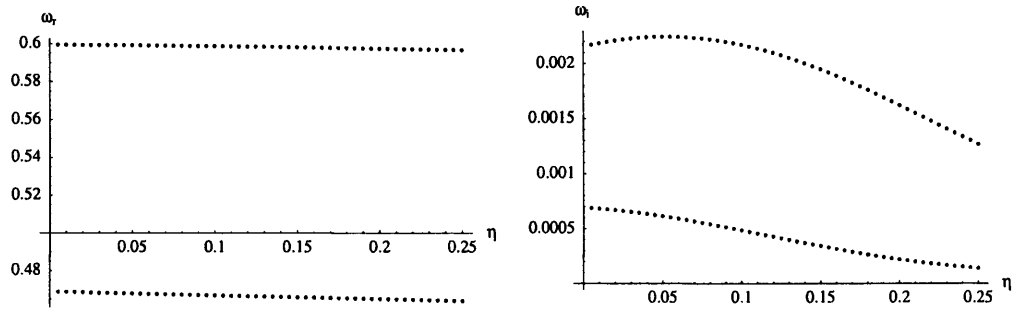

Figure 4.9: The real and imaginary parts of the variation of ω with η, the 'smoothness' of the ends of the obstacle. The height, Δh_1, of the obstacle is 0.2, and the length, L, is 6.7. Other parameters are as for other problems.

sonable jump condition. It appears, however, to allow some reflection at the ends of section $\langle 2 \rangle$ and an explanation for the observed instability is as follows: a disturbance travelling downstream in section $\langle 2 \rangle$ is (partly) reflected at the downstream end and sends a signal back upstream. This too is reflected, at the upstream end, through the jump conditions, creating a feedback loop. If this feedback exists for a frequency with positive imaginary part, then the overall disturbance in section $\langle 2 \rangle$ will grow in time. Section $\langle 2 \rangle$ can then act as an oscillator driving growing signals travelling up and down the channel. The frequency hence represents an unstable global mode. As suggested in Section 4.1, the downstream influence may not even decay downstream in space, although we will later show that, for channels such as the one just considered, which have a contracted section, the downstream influence does indeed decay downstream.

The good correlation between systems with discrete jumps at $x = 0$ and $x = L$ and those with smoothed ends provides evidence for the assumption in Section 4.3 that ends could be smoothed without significantly affecting results.

4.4.1 Channels with a contraction

We have already considered an example of a channel with a contraction above (with $L = 6.7$ and $\Delta h_1 = 0.2$). We now wish to further investigate the variation with L. We keep $\Delta h_1 = 0.2$ and vary L from 0 to 50. Other parameters are as for other problems ($h_{1\infty} = 1$, $h_{2\infty} = 1$, $u_{1\infty} = 0.8$, $u_{2\infty} = 1$, $\rho_1 = 1$, $\rho_2 = 1$, $\gamma = 0.5$, $g_\rho = 0$). The results are shown in Figure 4.10. We see that short lengths can create the largest instability (i.e. largest ω_i). The flow is unstable for all L considered, but the size of the largest ω_i (the most unstable mode) decreases as L increases. A new unstable mode appears every time L is increased by approximately 4.4.

It is interesting to note how the frequencies 'move around' in the complex ω-plane. Thus we plot, for several values of L, the position of the frequencies which satisfy the system (i.e. equation (3.20) in sections $\langle 1 \rangle$ and $\langle 3 \rangle$ and equation (4.6) in section $\langle 2 \rangle$ with the boundary and jump conditions described) in Figure 4.11. We see that an unstable mode appears immediately, i.e. for L small, and moves up and rightwards for increasing L, as would be expected from Figure 4.10. It then moves down and up in a zigzag fashion while moving slowly rightwards. As L is increased further, another mode appears and then another and so on. All progress slowly rightwards, with up-down zigzags of decreasing magnitude appearing to tend ultimately towards (real) $\omega \approx 0.65$. A close-up of the $L = 200$ case is shown in Figure 4.12

Looking at Figures 4.10 to 4.12, we see that modes exist with real parts only between $\omega_r \approx 0.41$ and $\omega_r \approx 0.65$. It is interesting to try to use this observation to say more about the way in which the branches satisfy the system of equations. Consider the four roots of the 'dispersion relation for section $\langle 2 \rangle$', (4.6). The real and imaginary parts of these are shown, for positive real ω, in Figures 4.13 and 4.14. These essentially represent the continuous spectrum which would be seen in an infinite pipe with the depths and velocities of the

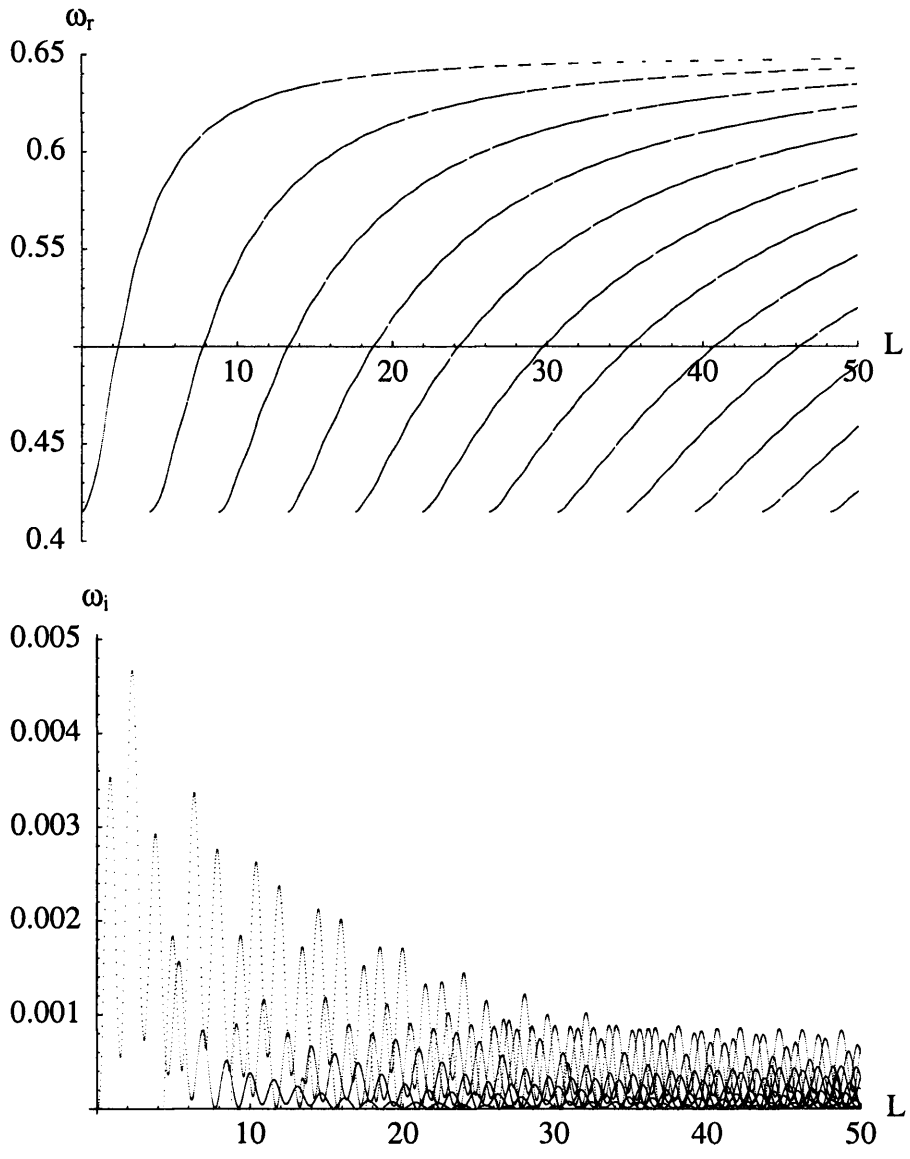

Figure 4.10: The real and imaginary parts of ω, as L is varied, for a channel with a step-shaped contracted section. The height, Δh_1, of the obstacle is 0.2. Other parameters are as for other problems. Each curve represents an unstable mode. The gaps in the ω_r curves appear because we only consider $\omega_i > 0$ due to the branch cut along the ω_r axis in the dispersion relations (3.20) and (4.6); when the modes pass below this axis we do not show them on either graph.

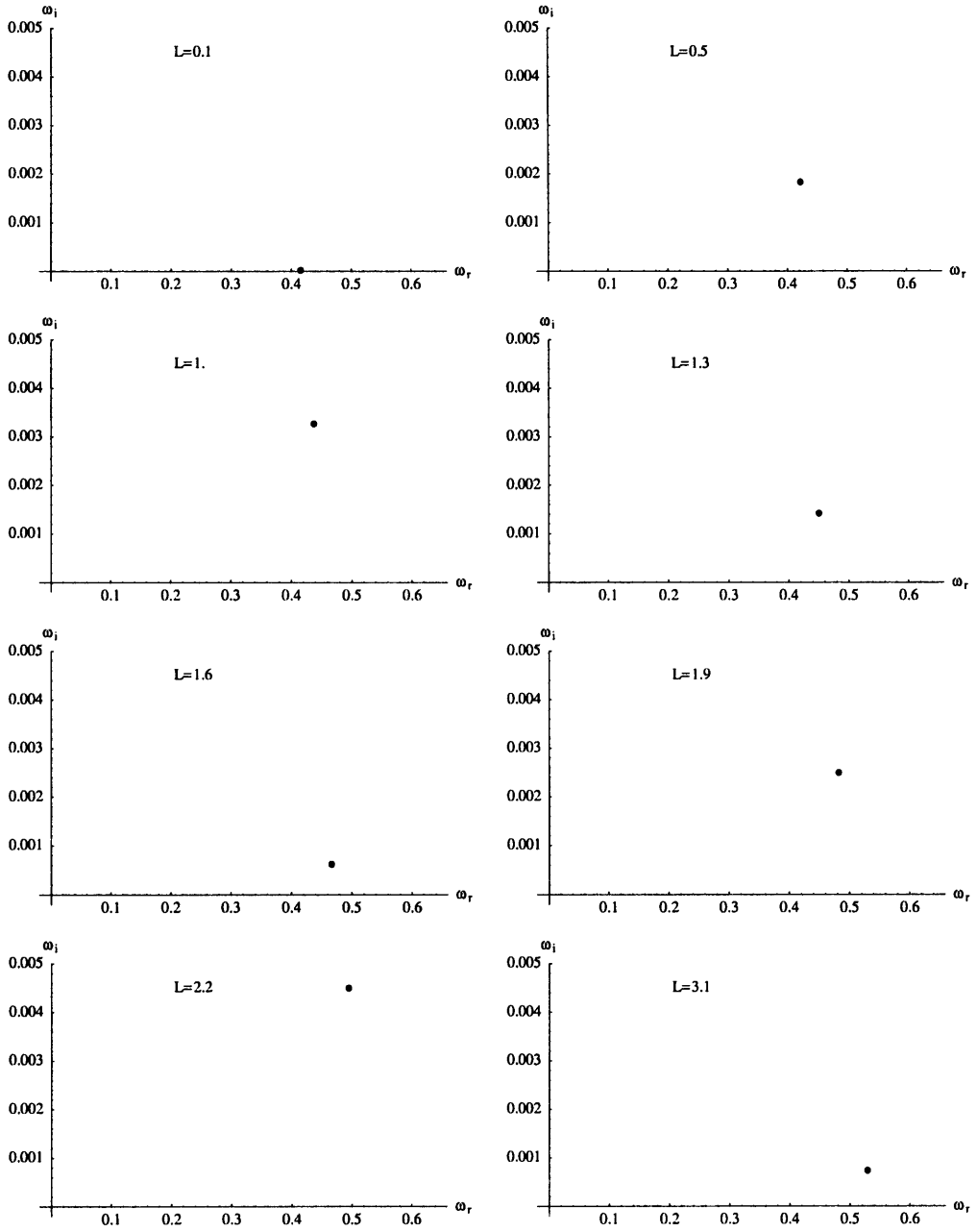
ωi
0.005
0.004
0.003
0.002
0.001
L=0.1
0.1 0.2 0.3 0.4 0.5 0.6
ωr
ωi
0.005
0.004
0.003
0.002
0.001
L=0.5
0.1 0.2 0.3 0.4 0.5 0.6
ωr
ωi
0.005
0.004
0.003
0.002
0.001
L=1.
0.1 0.2 0.3 0.4 0.5 0.6
ωr
ωi
0.005
0.004
0.003
0.002
0.001
L=1.3
0.1 0.2 0.3 0.4 0.5 0.6
ωr
ωi
0.005
0.004
0.003
0.002
0.001
L=1.6
0.1 0.2 0.3 0.4 0.5 0.6
ωr
ωi
0.005
0.004
0.003
0.002
0.001
L=1.9
0.1 0.2 0.3 0.4 0.5 0.6
ωr
ωi
0.005
0.004
0.003
0.002
0.001
L=2.2
0.1 0.2 0.3 0.4 0.5 0.6
ωr
ωi
0.005
0.004
0.003
0.002
0.001
L=3.1
0.1 0.2 0.3 0.4 0.5 0.6
ωr

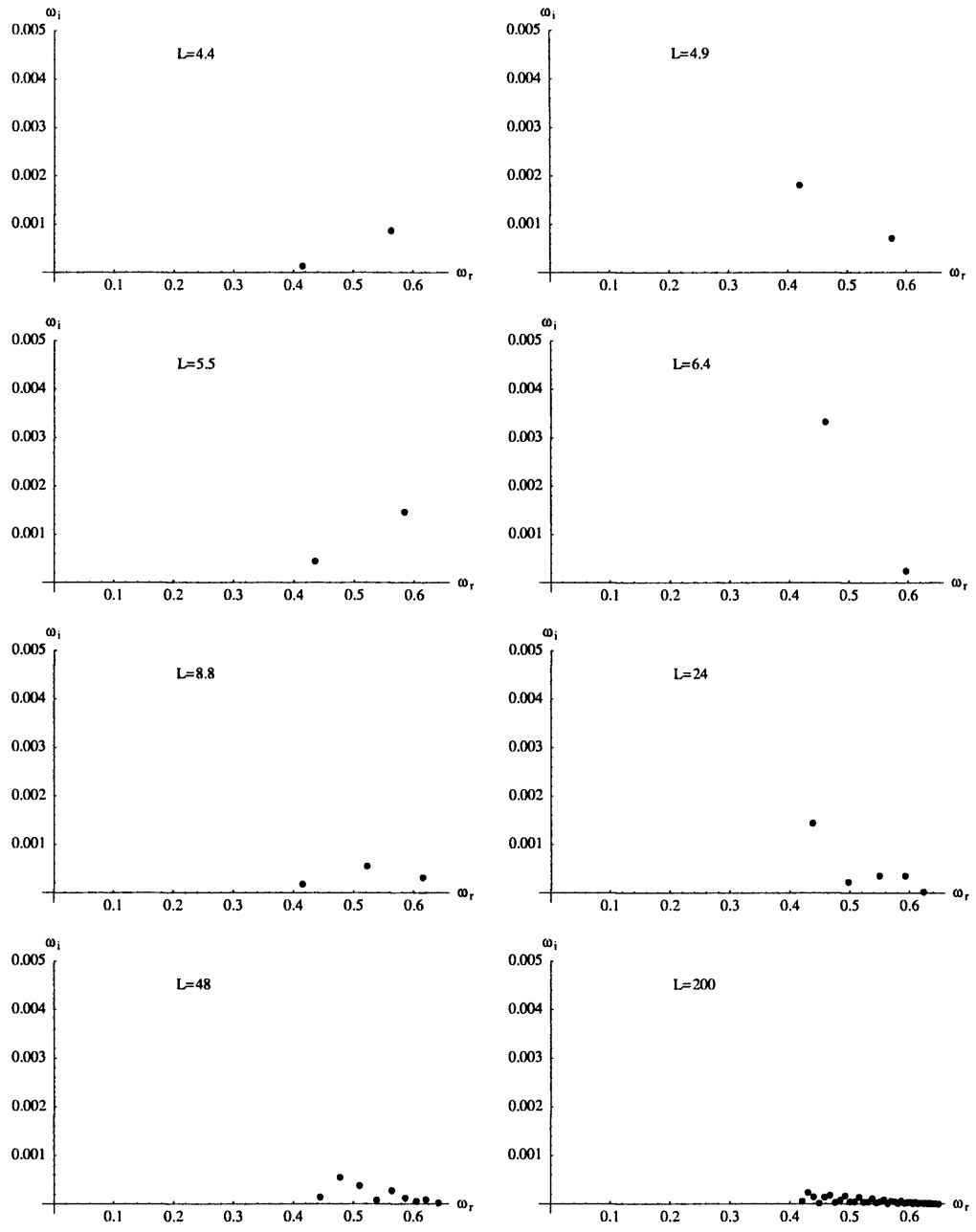

Figure 4.11: The motion of modes satisfying the system described in the text, for systems with a contracted section, as the length of the contraction is varied. The full set of parameters used and a discussion may be found in the text.

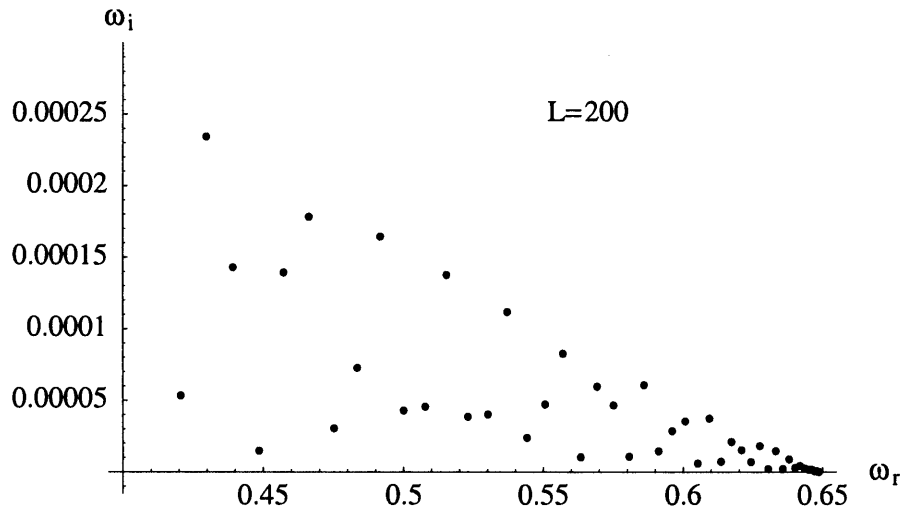

Figure 4.12: A close-up of the $L = 200$ case in Figure 4.11.

base flow as they are in section $\langle 2 \rangle$. We see that $\omega = 0.648893$, close to the apparent largest ω_r for which solutions to the full system, i.e. that of a pipe with a contraction, occur, is significant. For a range of real ω less than this, all four branches are neutral. This suggests that the waves which transmit disturbances across section $\langle 2 \rangle$ of the full system are approximately neutral. (Recall that, in Figure 4.14, $\omega \in \mathbb{R}$, which is not quite true in the full system.) Figures 4.13 and 4.14 also illustrate that the layout of the branches in the contracted section is the same as for the 'normal-width' system, i.e. there have been no new branch reconnections. This confirms that the middle section is locally convectively unstable.

We now consider the waves transmitted, for frequencies satisfying the system, in sections $\langle 1 \rangle$ and $\langle 3 \rangle$. Here the dispersion relation is (3.20). Figures 4.15 and 4.16 are equivalent to 4.13 and 4.14 for this dispersion relation. We see that now the value $\omega = 0.415127$, close to the smallest ω_r for which solutions to the full system are seen, is significant. For ω_r larger than this, two of the modes are non-neutral but have equal real parts. We conclude that the eigenfunc-

tions corresponding to instability in this system comprise one rapidly-decaying and one slowly-decaying wave in the upstream section, four near-neutral waves in section ⟨2⟩ and one rapidly-decaying and one slowly-decaying wave in the downstream section. The real parts of the wavenumbers corresponding to these waves are fairly small and so the long-wave approximation used in the derivation of the base flow equations remains valid.

We now attempt an asymptotic analysis of the short-length case. Good agreement, to second order in L, can be achieved; see Appendix A.3.2. We arrive at (A.104 again)

$$\begin{pmatrix} m_{d,1} \\ -l_{u,1} \\ -2\sqrt{\omega_2} \\ -\Psi_{n,1} \end{pmatrix} = (\mathbf{q}_{d,0}\ \mathbf{q}_{u,0}\ \mathbf{q}_{nu,1,\omega}\ \mathbf{q}_0)^{-1} C_{jump}^{-1} E_1 C_{jump} \mathbf{q}_0,$$

where all symbols are as given in the appendix. Putting in values gives $\omega_2 = 0.03780$, in good agreement with the curve fit to Figure 4.17. However, this only describes the real part of the variation of ω with L. To get the imaginary part, $O(L^3)$ asymptotics would need to be considered and we do not do so here.

The variation of ω with Δh_1, the height of the obstacle on the lower wall, is considered in Figure 4.18. We see that, as the obstacle becomes larger, the system admits more unstable solutions and that these solutions each become generally more unstable.

4.4.2 Channels with an expansion

An obvious alternative to studying channels with a contracted section 'in the middle' is to study channels with an expanded section. The computation is much the same as before, but with $\Delta h_1 = -1$. All other parameters are kept the same. This set-up appears not to be unstable for small L. However,

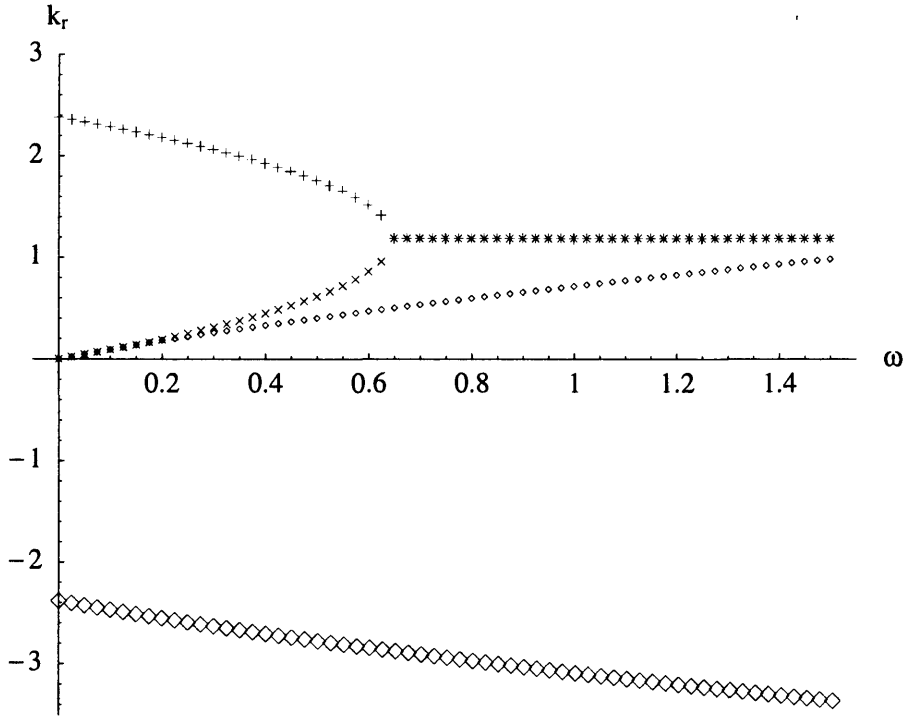

Figure 4.13: The dispersion relation, (4.6), corresponding to an infinite channel with the same depths and base-flow velocities as are in the middle section of our channel with a rectangular contraction, using the set of parameters used in Section 4.4.1. Here the real part of k is plotted for real ω. Although the branches are continuous functions of ω, we plot them discretely using symbols which allow them to be distinguished where they overlap one another. The continuation of each branch is as it would be were a small positive imaginary part added to ω. The branches marked $\times$ and $+$ meet at k_b from (4.4) when $\omega = 0.648893$.

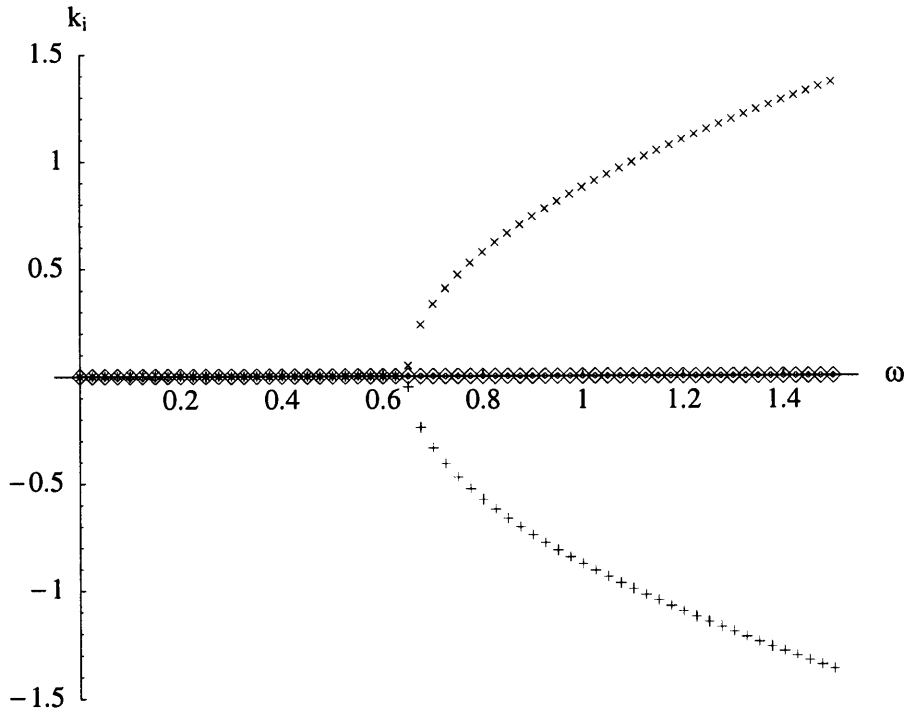

Figure 4.14: As Figure 4.13 but with the imaginary part of k plotted for real ω.

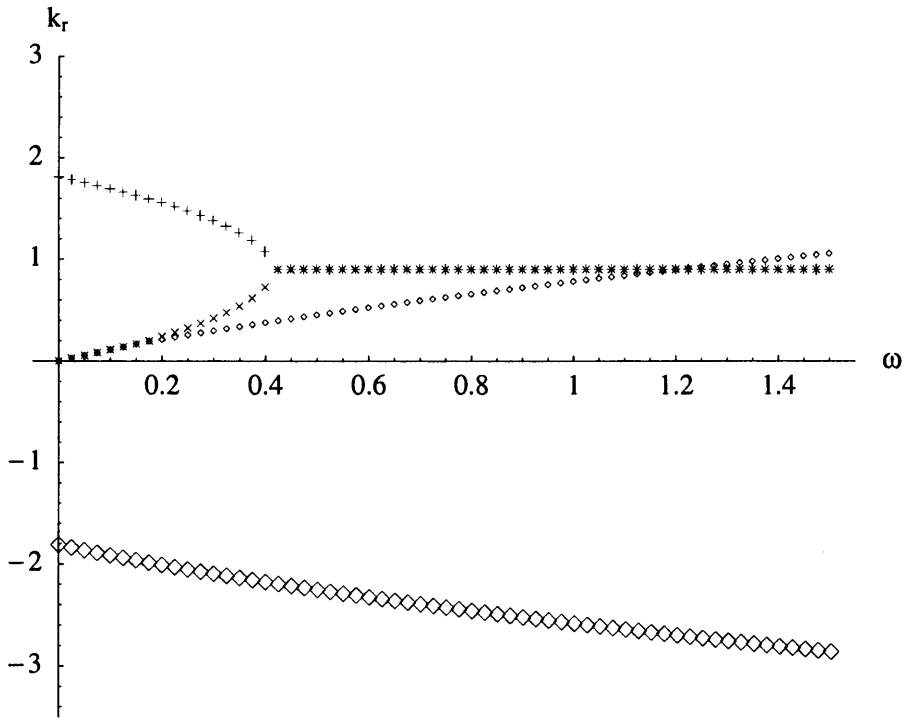

Figure 4.15: The dispersion relation, (3.20), corresponding to an infinite channel with the same depths and base-flow velocities as are in the straight sections, $\langle 1 \rangle$ and $\langle 3 \rangle$, of our channel, with $h_{1\infty} = 1$, $h_{2\infty} = 1$, $u_{1\infty} = 0.8$, $u_{2\infty} = 1$, $\rho_1 = 1$, $\rho_2 = 1$, $\gamma = 0.5$, $g_\rho = 0$. Here the real part of k is plotted for real ω. Although the branches are continuous functions of ω, we plot them discretely using symbols which allow them to be distinguished where they overlap one another. The continuation of each branch is as it would be were a small positive imaginary part added to ω. The branches marked $\times$ and $+$ meet at k_b from (4.4) when $\omega = 0.415127$.

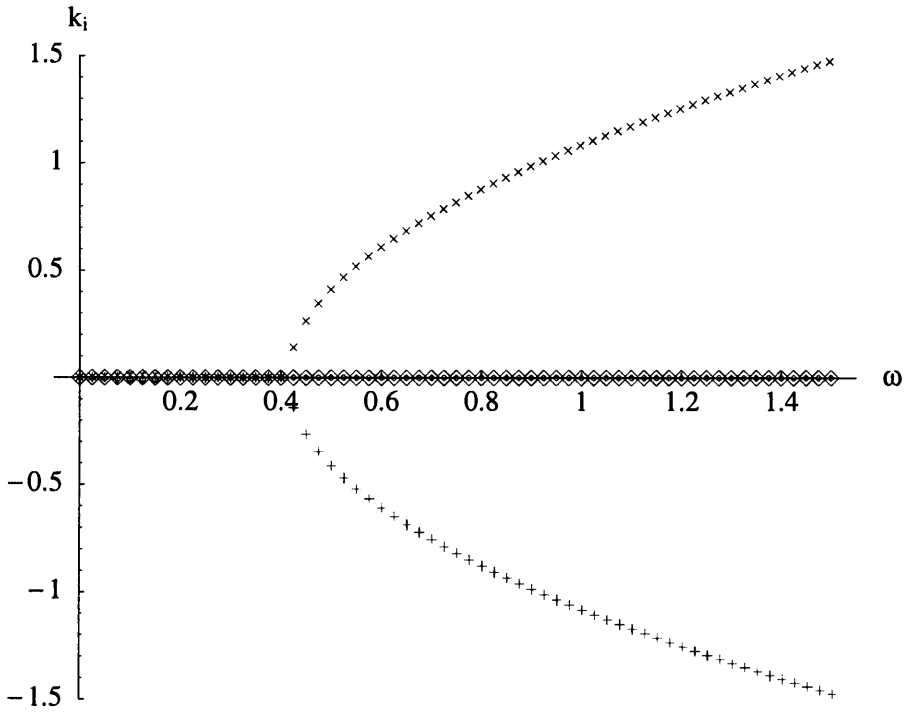

Figure 4.16: As Figure 4.15 but with the imaginary part of k plotted for real ω.

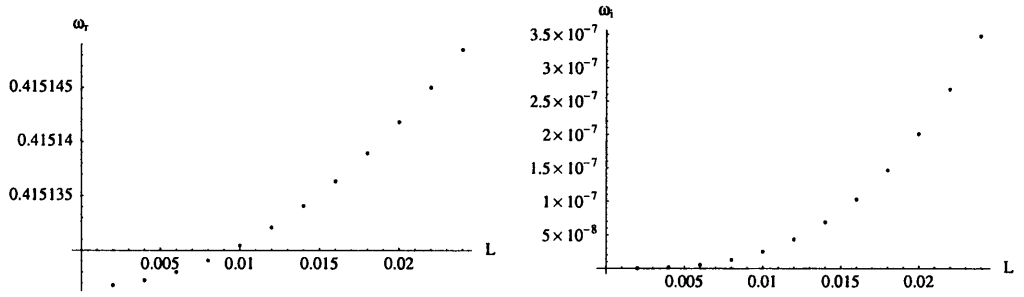

Figure 4.17: The real and imaginary parts of the variation of ω with L, for L small. The height, Δh_1, of the obstacle is 0.2 and other parameters are as for other problems. Fitting curves of the form $a + bx^c$ to the real and imaginary parts separately, we arrive at $0.41513 + 0.03782L^{1.999} + (-9.05 \times 10^{-12} + 0.02495L^{2.998})i$.

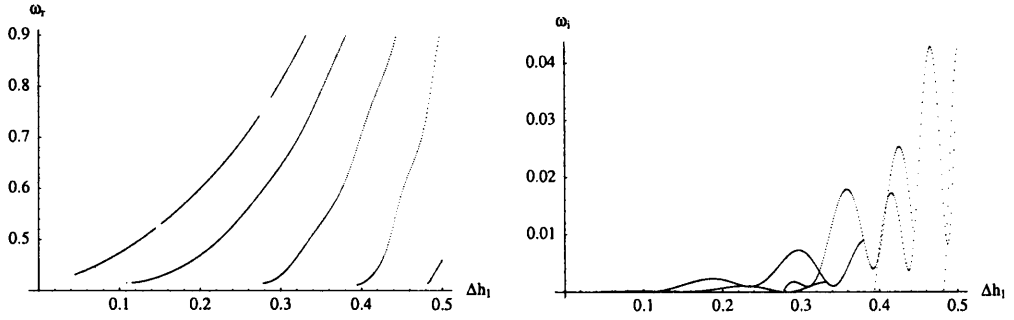

Figure 4.18: The variation of the real and imaginary parts of ω with Δh_1. $L = 6.7$. The gaps in the ω_r curves occur when ω_i goes below 0, which we do not consider.

instability occurs for lengths beyond $L \approx 57$, with the system becoming more unstable as the length of the expanded section increases (Figure 4.19). The results here agree with [65], which considers them in terms of feedback between the ends of the expanded section.

Similarly to the contraction case above, we now attempt to gain further understanding by looking at the range of observed frequencies satisfying the system, for various L. The 'motion' of these frequencies, in the ω-plane, is shown in Figure 4.20. A first mode appears for $L \approx 57$, moves up and rightwards and then down and disappears, i.e. moves below the real ω-axis. This means it becomes a decaying mode and we do not consider it further. A second mode appears and behaves similarly. After this, two modes appear for similar L values, before moving rightwards and disappearing. Eventually several modes appear and, although each mode ultimately disappears, there are always some modes for any L larger than about 62. Increasing numbers of modes appear, with the overall level of instability increasing; see Figure 4.19. For very large length, the modes appear to begin to approximate two lines of a continuous spectrum.

In order to perform an analysis of the form of the eigenfunctions corre-

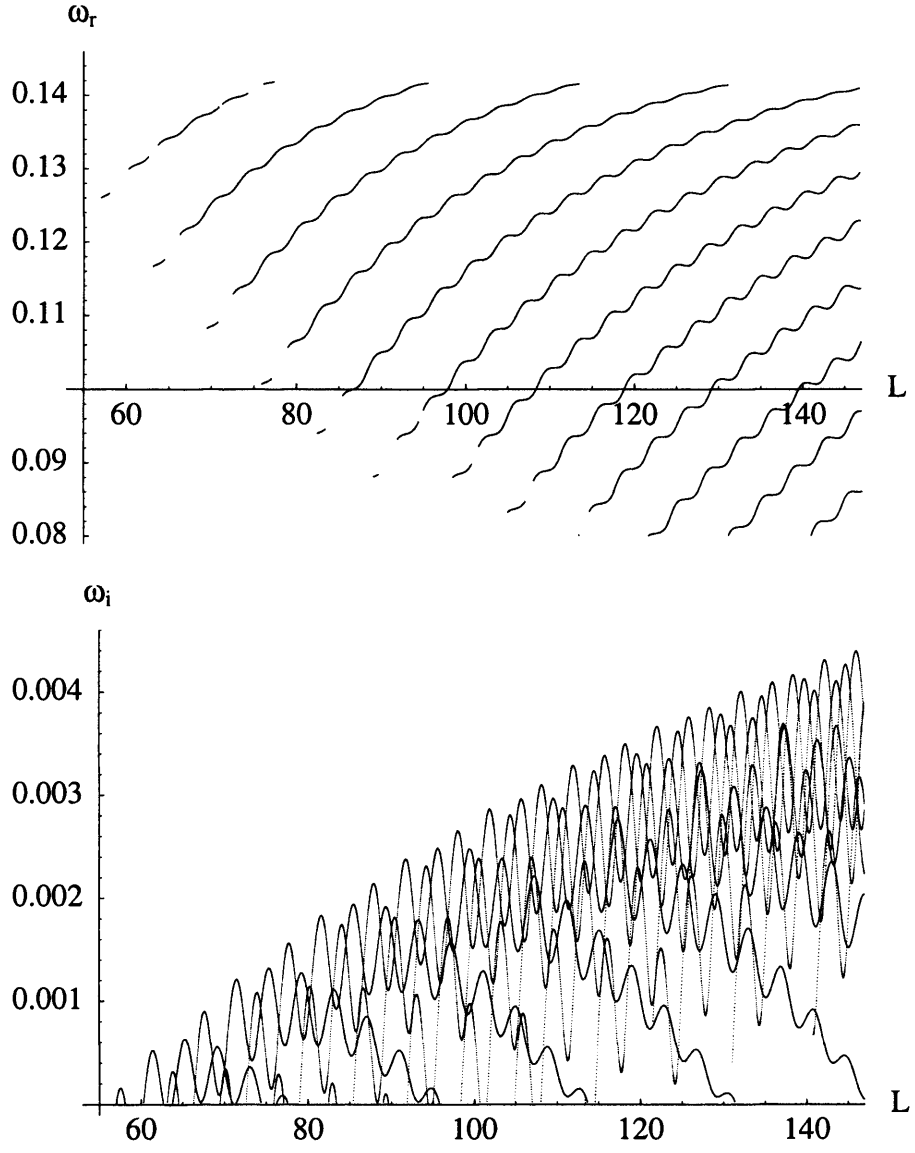

Figure 4.19: The real and imaginary parts of ω, as L is varied, for a channel with a step-shaped expanded section. $\Delta h_1 = -1$ and other parameters are as for other problems.

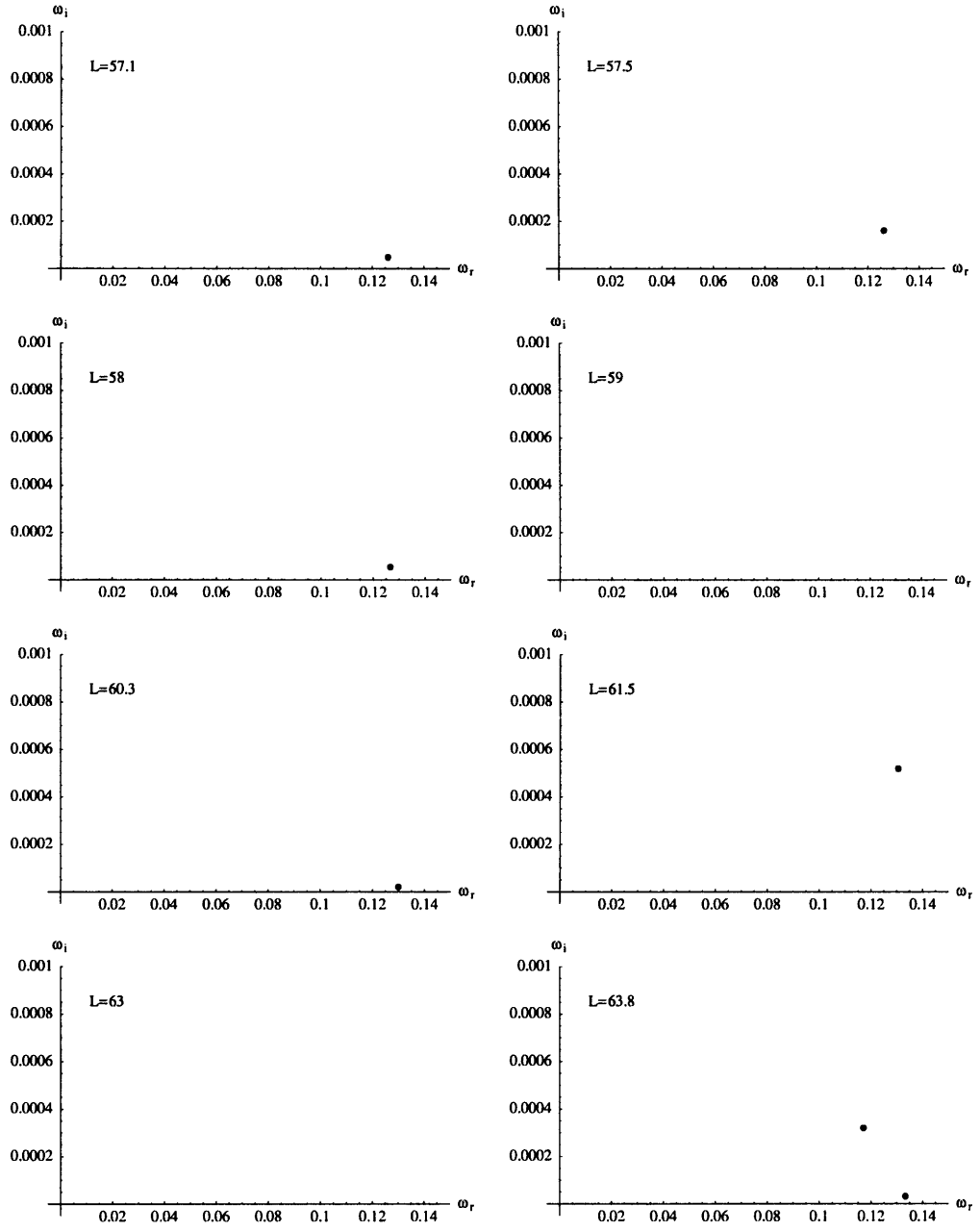
ωi
0.001
0.0008
0.0006
0.0004
0.0002
L=57.1
0.02 0.04 0.06 0.08 0.1 0.12 0.14
ωr
ωi
0.001
0.0008
0.0006
0.0004
0.0002
L=57.5
0.02 0.04 0.06 0.08 0.1 0.12 0.14
ωr
ωi
0.001
0.0008
0.0006
0.0004
0.0002
L=58
0.02 0.04 0.06 0.08 0.1 0.12 0.14
ωr
ωi
0.001
0.0008
0.0006
0.0004
0.0002
L=59
0.02 0.04 0.06 0.08 0.1 0.12 0.14
ωr
ωi
0.001
0.0008
0.0006
0.0004
0.0002
L=60.3
0.02 0.04 0.06 0.08 0.1 0.12 0.14
ωr
ωi
0.001
0.0008
0.0006
0.0004
0.0002
L=61.5
0.02 0.04 0.06 0.08 0.1 0.12 0.14
ωr
ωi
0.001
0.0008
0.0006
0.0004
0.0002
L=63
0.02 0.04 0.06 0.08 0.1 0.12 0.14
ωr
ωi
0.001
0.0008
0.0006
0.0004
0.0002
L=63.8
0.02 0.04 0.06 0.08 0.1 0.12 0.14
ωr

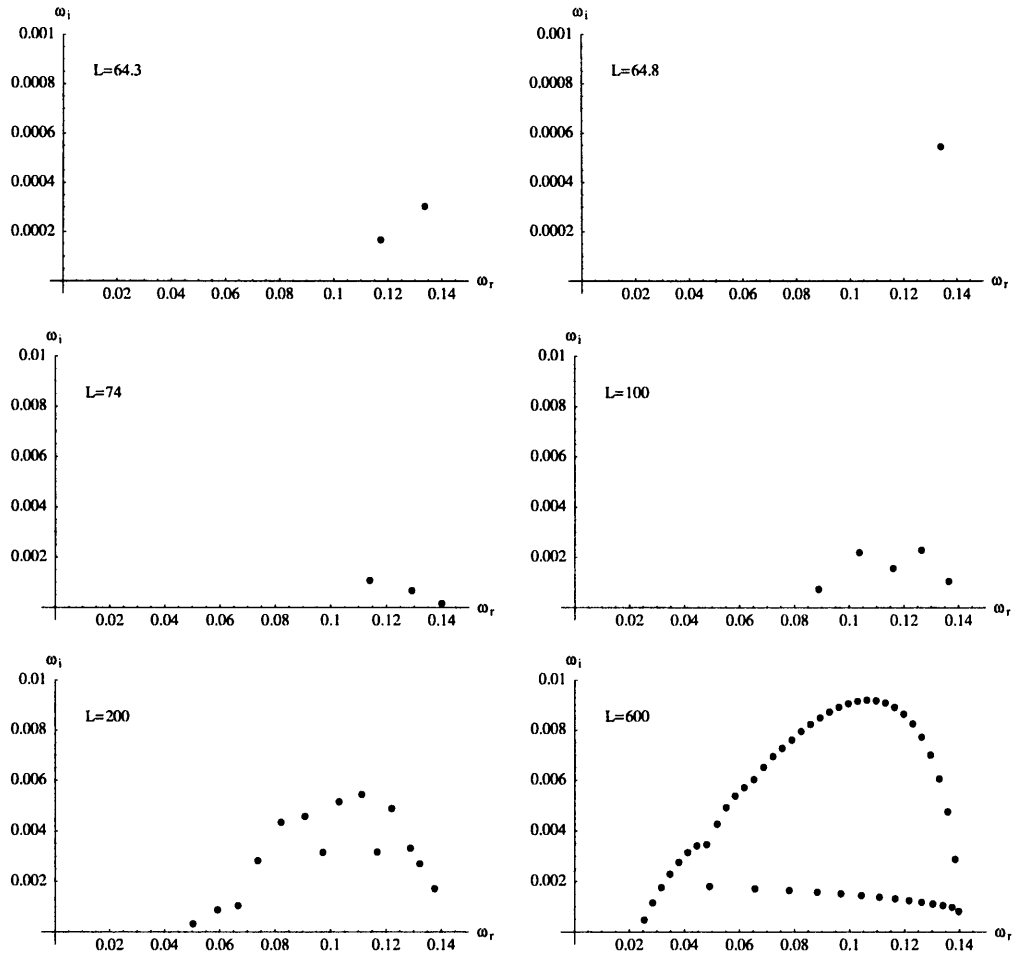

Figure 4.20: The motion of modes satisfying the system described in the text, for systems with a expanded section, as the length of the expansion is varied. The full set of parameters used and a discussion may be found in the text.

sponding to unstable modes, as was done in the previous section, we now plot the dispersion relation (4.6) for the base-flow velocity and depth of the expanded section in Figures 4.21 to 4.24. It is, however, more difficult to determine what the requirements on the waves comprising the eigenfunction are. Frequencies satisfying the system seem to have real part between 0 and ~ 0.14. Their imaginary part seems to be less than ~ 0.01, although it is unclear if this remains true as $L \to \infty$. In section $\langle 1 \rangle$, looking at Figure 4.16, there will be two near-neutral waves. In section $\langle 2 \rangle$ (Figure 4.24), all four waves will be fairly near-neutral. In section $\langle 3 \rangle$ we can see that one wave will decay downstream. The other, for the values of ω_i which are slightly larger than 0, will grow downstream. However, Figure 3.4, for which $\omega_i = 0.012$, suggests that for the largest ω_i observed, this too may decay downstream. Again, we note that the real parts of the wavenumbers are fairly small and the long-wave approximation remains valid.

Figures 4.23 and 4.24 also demonstrate that, as was the case for a channel with a contracted section, the flow in the middle section of this set-up has the same layout of branches as the 'normal-width' case. We conclude that it is also locally convectively unstable.

As discussed above, the instability in these systems can be explained in terms of a feedback loop formed using the jump conditions at $x = 0$ and $x = L$. The mechanism for the feedback in an expanded section is the same as that described above for a contracted section. Here, however, we will, for some disturbances, observe growth downstream. The apparent discrepancy between our explanation of section $\langle 2 \rangle$ as an oscillator driving influences elsewhere and the infinite growth downstream in space may be explained as follows: the oscillator viewpoint is derived from the idea of an initial disturbance reflected back and forth in the middle section. It is thus an initial-value problem. As was explained in Chapter 1, the eigenvalue approach to these systems describes the

infinite-time asymptotics. We may thus understand our predicted downstream-growing eigenfunction as an infinite-time limit of the oscillator description.

4.5 Summary

Using a fluid-dynamical model similar to that considered in the previous chapter, two set-ups have been considered for two-fluid flow through a straight channel with a finite-range nonhomogeneous section. Unlike in Chapter 3, we have only allowed disturbances which emanate from the nonhomogeneity, disallowing those coming from infinity. In the first set-up, the nonhomogeneity was sinusoidal in form. In all the cases considered, except that of a half-sine-period expansion, global instability has been found. For a multiple-period wall deformation, multiple instability modes have been found. In the second set-up considered, the nonhomogeneity was rectangular, corresponding to a short-range, sudden, contraction or expansion of the channel. Instability has been observed for a contraction of any length and increasing the length, in general, decreased the instability. For an expanded section, there was a minimum length for instability to be seen, but increasing length gave increasing instability. It is worth emphasising once again that the globally unstable modes in these examples are not related to a region of local absolute instability in the flow.

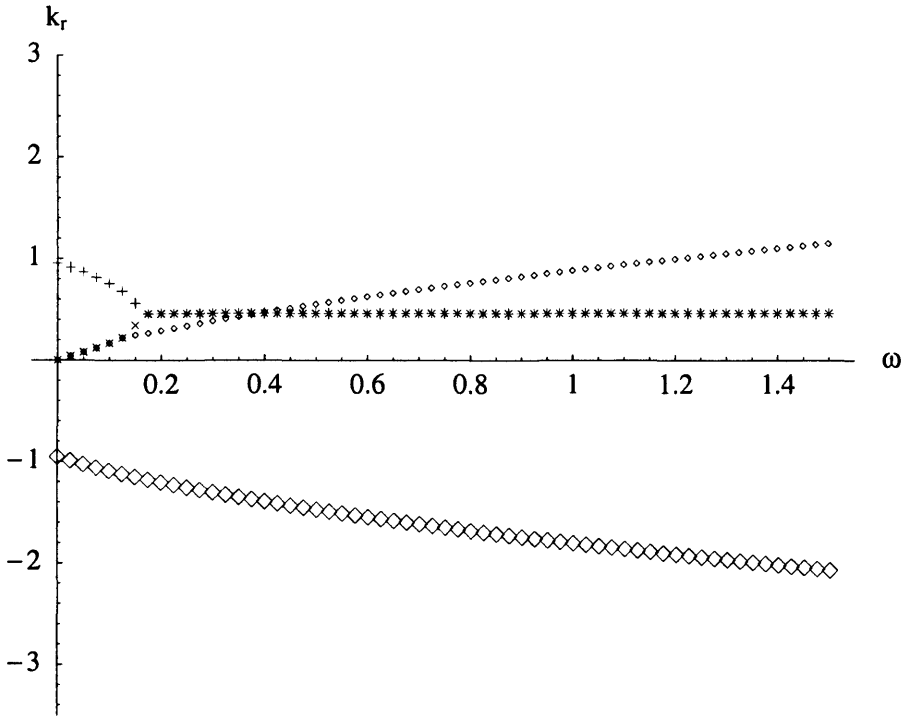

Figure 4.21: The dispersion relation, (4.6), corresponding to an infinite channel with the same depths and base-flow velocities as are found in the middle section of our channel with a rectangular expansion, using the set of parameters used in Section 4.4.2. Here, the real part of k is plotted for real ω. Although the branches are continuous functions of ω, we plot them discretely using symbols which allow them to be distinguished where they overlap one another. The continuation of each branch is as it would be were a small positive imaginary part added to ω. The branches marked $\times$ and $+$ meet at k_b from (4.4) when $\omega = 0.156982$ and those marked $\times$ and with a small $\diamond$ meet at $\omega = 0.139673$.

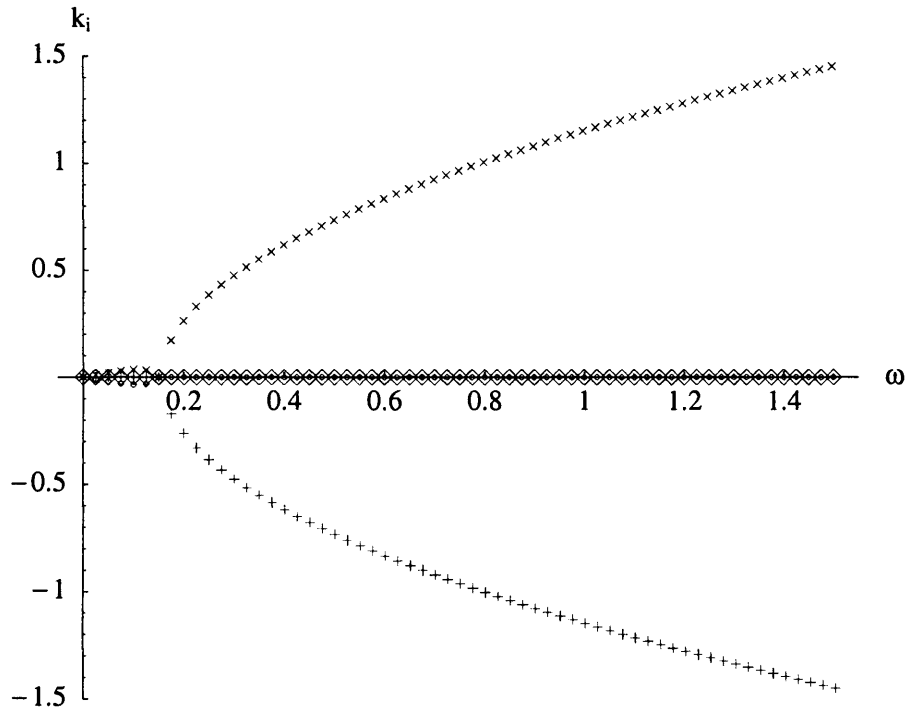

Figure 4.22: As Figure 4.21 but with the imaginary part of k plotted for real ω.

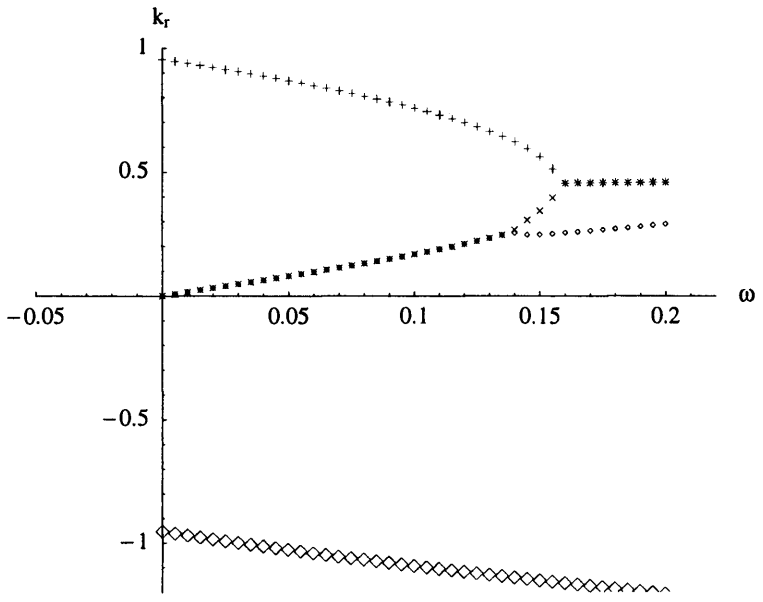

Figure 4.23: A close-up view of part of Figure 4.21.

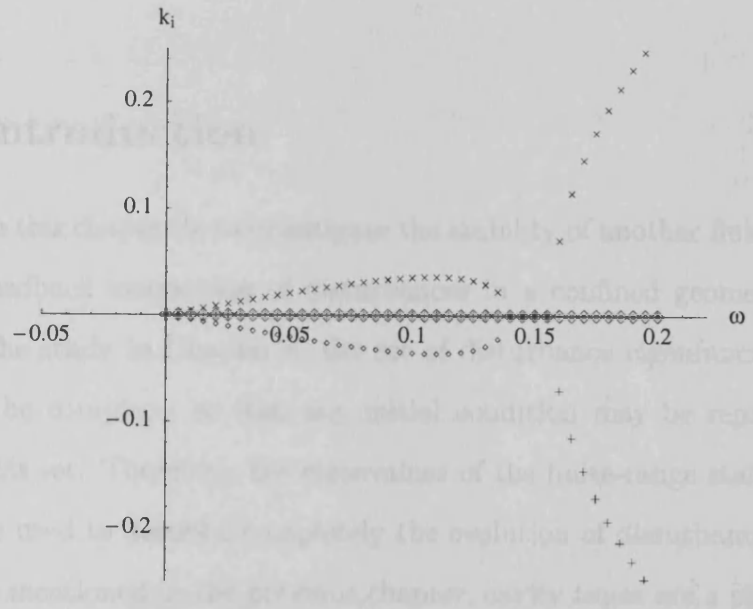

Figure 4.24: A close-up view of part of Figure 4.22.

Chapter 5

Flow past an aperture

5.1 Introduction

The aim in this chapter is to investigate the stability of another fluid flow with possible feedback interaction of disturbances in a confined geometry. Compared to the study in Chapter 4, the set of disturbance eigenfunctions is expected to be complete, so that any initial condition may be represented in terms of this set. Therefore, the eigenvalues of the finite-range stability problem can be used to describe completely the evolution of disturbances.

As was mentioned in the previous chapter, cavity tones are a phenomenon which can have important consequences in engineering applications. When fluid flows over an aperture in a wall, it is known that disturbances may propagate back and forth across the aperture at certain frequencies (see [31]). This fluid-structure interaction can potentially lead to sound pollution and damaging structural vibration. The problem we study in this chapter is related to this. Here, however, we are interested in looking for instability when different fluids flow above and below the cavity.

The set-up is again physically similar to that in Chapters 3 and 4. Two-fluid flow in a narrow straight channel is considered. The two fluids have a

rigid partition between them in the two semi-infinite regions $-\infty < x < 0$ and $L < x < \infty$ and are in contact in the range $0 < x < L$. The solutions to the stability problem for this set-up are then determined by the end conditions at $x = 0$ and $x = L$, where we assume that the fluid-fluid interface remains smoothly attached to the ends of the partition. However, unlike the case in the previous chapter, flow in the semi-infinite regions is sufficiently simple to support only neutral disturbances and we do not have to concern ourselves with whether such disturbances should be upstream-travelling or downstream-travelling.

Firstly, some numerical results are shown. After this, an alternative formulation of the problem is derived by analysing the waves travelling between the ends of the system. This leads to some results for special cases where the frequency is restricted, including an approximation for the rate at which such a frequency tends to its infinite-range limit.

We show that the idea of feedback between waves propagating in opposite directions can be used to deduce an approximation for the distribution of the eigenvalues when the spatial range is large. The disturbances in the unpartitioned section may be viewed as combinations of waves whose wavenumbers are obtained from the straight-channel dispersion relation. This idea leads to a criterion for the waves to satisfy the end conditions. By considering the coefficient, in the long-length limit, of the most dominant wave in this criterion, we are able to find approximate solutions to the system and end conditions.

The significance of feedback in the disturbed flow can once again be seen by comparing the distribution of eigenvalues when the length tends to infinity in this problem and in the Ginzburg-Landau modes discussed in Chapters 1 and 2. If the disturbed flow is free from feedback, as in the Ginzburg-Landau model, the finite-range problem produces only eigenvalues in the lower half-ω-plane, unless the flow is absolutely unstable. In a feedback system, unstable

eigenvalues can be found for sufficiently large length even if the flow remains locally convectively unstable.

At the end of the chapter, a comparison is made, in the long-length case, with the examples from the previous chapter.

5.2 Formulation

We consider a flow in a channel containing two fluids with rigid, straight, outer walls. Between the fluids we suppose there to be a rigid partition, in which there is an aperture of finite length. The properties of the fluid-fluid interface in the aperture region are determined by surface tension, in the long wave approximation. We also make the assumption that the ends of the fluid-fluid interface remain smoothly attached to the ends of the partition. This can be regarded as a simple version of a flexible wall between two fluids and may be compared to the model used in, for example, [63] for a flexible wall. The reason for requiring the interface to remain attached to the solid walls is that this leads to reasonably simple end conditions for reflecting disturbances. The set-up is as shown in Figure 5.1.

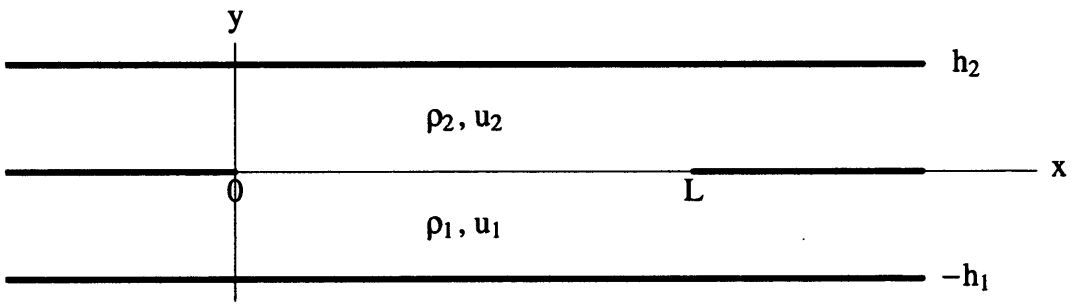

Figure 5.1: The set-up being considered, with a finite aperture between two fluids in the range $0 < x < L$.

It is clear that, in the range $0 < x < L$, the set-up is exactly as in each of the sections $\langle 1 \rangle$, $\langle 2 \rangle$ and $\langle 3 \rangle$ of the channel considered in Chapter 4. The

base flow is uniform and small disturbances can be written in the form $e^{ikx-i\omega t}$, where k and ω satisfy the dispersion relation (3.20 with $h_{1\infty}$ and $h_{2\infty}$ replaced)

$$\frac{\rho_1}{h_1}(\omega - u_{1\infty}k)^2 + \frac{\rho_2}{h_2}(\omega - u_{2\infty}k)^2 = g_\rho k^2 + \gamma k^4. \tag{5.1}$$

Note that we are now using $u_{1\infty}$ and $u_{2\infty}$ to represent base-flow velocities. Consider the flow in the the two semi-infinite regions separated by solid walls. The base flow here is as in the section $0 < x < L$, i.e. uniform flow. To derive equations describing the evolution of small disturbances, we begin with the usual thin-layer inviscid approximation (Section 3.2, Appendix A.2.1)

$$\frac{\partial u_{1,2}}{\partial t} + u_{1,2}\frac{\partial u_{1,2}}{\partial x} + v_{1,2}\frac{\partial u_{1,2}}{\partial y} = -\frac{1}{\rho_{1,2}}\frac{\partial p_{1,2}}{\partial x}, \tag{5.2}$$

$$\frac{\partial u_{1,2}}{\partial x} + \frac{\partial v_{1,2}}{\partial y} = 0, \tag{5.3}$$

$$\frac{\partial p_{1,2}}{\partial y} = 0. \tag{5.4}$$

We now repeat an argument that was used in Section 3.2. We again wish the flow to be everywhere irrotational; the condition for the circulation to be zero is $\frac{\partial u_{1,2}}{\partial y} = 0$, by means of the scaling argument used in that section. Thus $u_{1,2}$ are functions of x and t only.

Integrating the continuity equation (5.3), at any x-station, w.r.t. y, between the upper and lower walls of the straight sections of the channel and using the fact that $v = 0$ at these walls, we have

$$\int_{-h_1}^{0} \frac{\partial u_1}{\partial x} dy = (0 - (-h_1))\frac{\partial u_1}{\partial x} = 0, \tag{5.5}$$

for the lower fluid and a similar expression for the upper one. We conclude that

$$\frac{\partial u_{1,2}}{\partial x} = 0. \tag{5.6}$$

This, combined with the condition $\frac{\partial u_{1,2}}{\partial y} = 0$, reduces the momentum equation to

$$\frac{\partial u_{1,2}}{\partial t} + \frac{1}{\rho_{1,2}}\frac{\partial p_{1,2}}{\partial x} = 0, \tag{5.7}$$

which essentially gives us a way to calculate the pressure distribution for any given velocity distribution. Thus matching at $x = 0$ and $x = L$ is trivial: the upper and lower fluids, in the sections where they are separated by rigid walls, move with no x- or y-variation in their velocity and adopt the velocity of the edges of the $0 < x < L$ region.

We can now deduce 'end' conditions for the finite-length aperture section. As, by our assumption, the fluid-fluid interface remains smoothly attached to the rigid wall at its ends, we choose

$$F(0) = G(0) = F(L) = G(L) = 0, \tag{5.8}$$

where F and G are the height of the interface and its x-derivative, as in Chapters 3 and 4. Thus, our system of small disturbances is governed by

$$\frac{\mathrm{d}\mathbf{u_4}}{\mathrm{d}x} = A_4\mathbf{u_4},\ \mathbf{u_4}(0) = (\Gamma_1\ 0\ 0\ \Gamma_2)^T,\ \mathbf{u_4}(L) = (\Gamma_3\ 0\ 0\ \Gamma_4)^T, \tag{5.9}$$

with A_4 as in (A.58) and where the values of Γ_1, Γ_2, Γ_3 and Γ_4 are unimportant. Solutions to our system, on the range $(0, L)$, are given by

$$\mathbf{u_4} = \sum_{j=1}^{4} a_j \mathbf{q}_j(\omega) e^{ik_j(\omega)x}, \tag{5.10}$$

where ik_j are the eigenvalues of the matrix A_4 (roots of the dispersion relation (5.1) for a given ω) and $\mathbf{q}_j$ are the corresponding eigenvectors. We begin by evaluating some numerical results, putting in our usual set of parameters ($u_{1\infty} = 0.8$, $u_{2\infty} = 1$, $h_1 = h_2 = 1$, $\rho_1 = \rho_2 = 1$, $g_\rho = 0$, $\gamma = 0.5$) and varying L. We note that these parameters, when applied to the infinite-range interface case discussed in Section 3.3, corresponded to convective instability. We conclude that, if the middle section were infinite in extent, the flow would be convectively unstable.

The numerical results are shown in Figure 5.2. We see that, for short L, the system is neutrally stable. As L is increased, instability first occurs at about $L = 3.46$. Note that, as in the previous chapter, there is no distinction

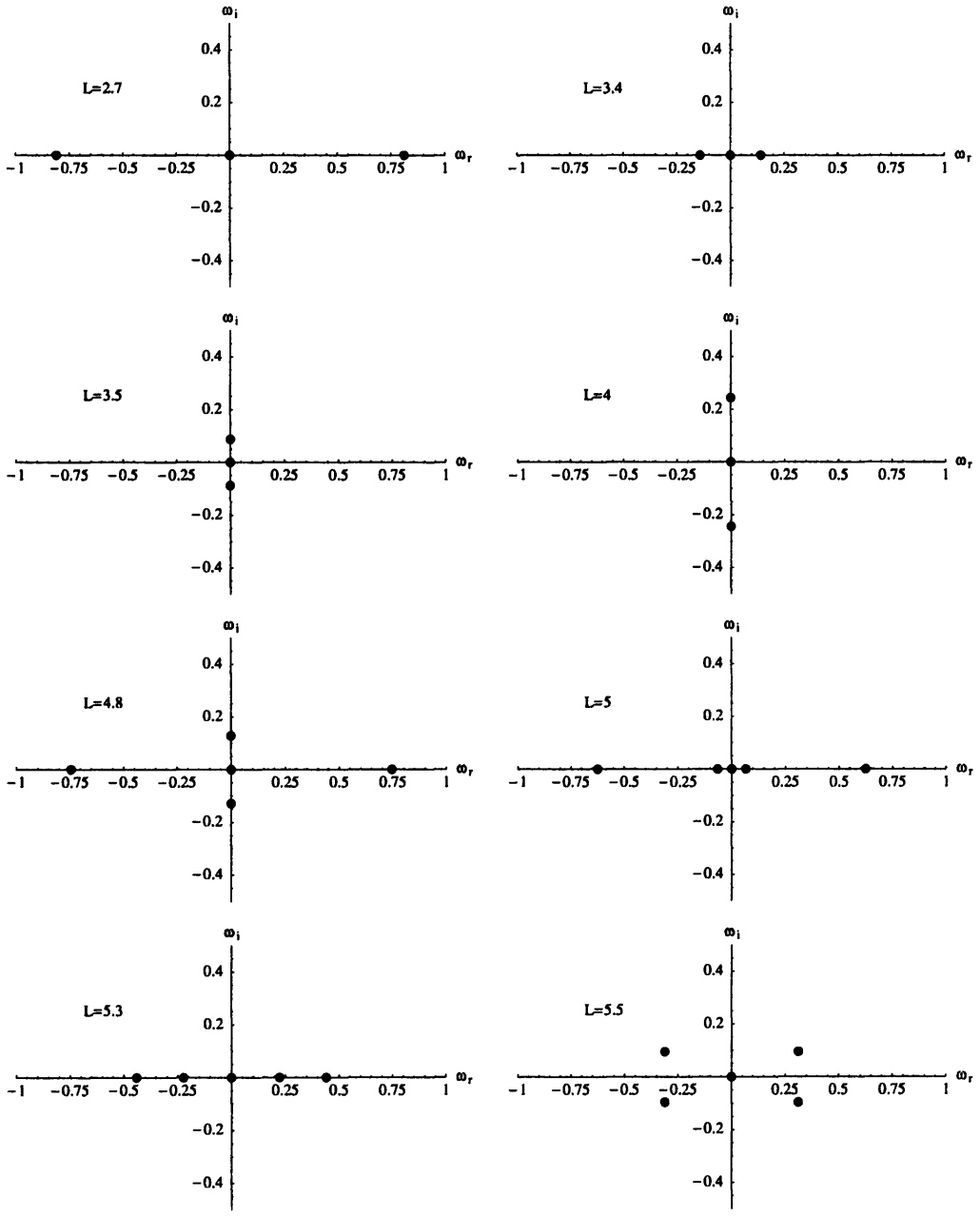

Figure 5.2: The complex ω-plane, showing eigenvalues of our system for various lengths L.

here between convective and absolute instability and every growing mode will behave like absolute instability, growing at any spatial location. Increasing L further causes the system then, temporarily, to become more unstable, before becoming neutrally stable again as more neutral eigenvalues 'arrive' from $\omega_r = \pm\infty$. The pairs of eigenvalues move towards each other and then move out into the plane as they meet.

We note also that the eigenvalues appear to be symmetric in both real and imaginary parts. This will be shown to be the case in Section 5.4, but, from now on, we will concentrate on the first quadrant of the plane. We expect also that, as L increases, there will be an increasing number of eigenvalues. We show this in Figure 5.3.

The figure shows that the number of eigenvalues does indeed keep increasing with increasing L, increasing by 1 every time L increases by about 3.5. By looking at the cases for $L \geq 20$ we see that the positions of the roots become approximately periodic in L. This will be discussed further in the next section. We now look at some results for L large, Figure 5.4.

We compare Figure 5.4 with the dispersion relation for real k, Figure 5.5. We see that, even for $L \approx 500$, the purely-imaginary eigenvalues are not necessarily close to 0. In the next section, we will see that, in fact, the purely-imaginary eigenvalues do tend to zero as $L \to \infty$, albeit very slowly, although the dispersion curve for $k \in \mathbb{R}$ is not the limit of the other eigenvalues.

We now discuss an explanation for the instability observed in Figures 5.2, 5.3 and 5.4. A growing global mode can be observed in a system which, if infinite, would be convectively unstable. This is due to feedback between the end conditions in the finite-range case. A signal travelling downstream (rightwards) will grow as the system is 'convectively unstable'. It will be reflected at the downstream end, through the end conditions, and travel back upstream. If its upstream decay is sufficiently slow, it can then be reflected

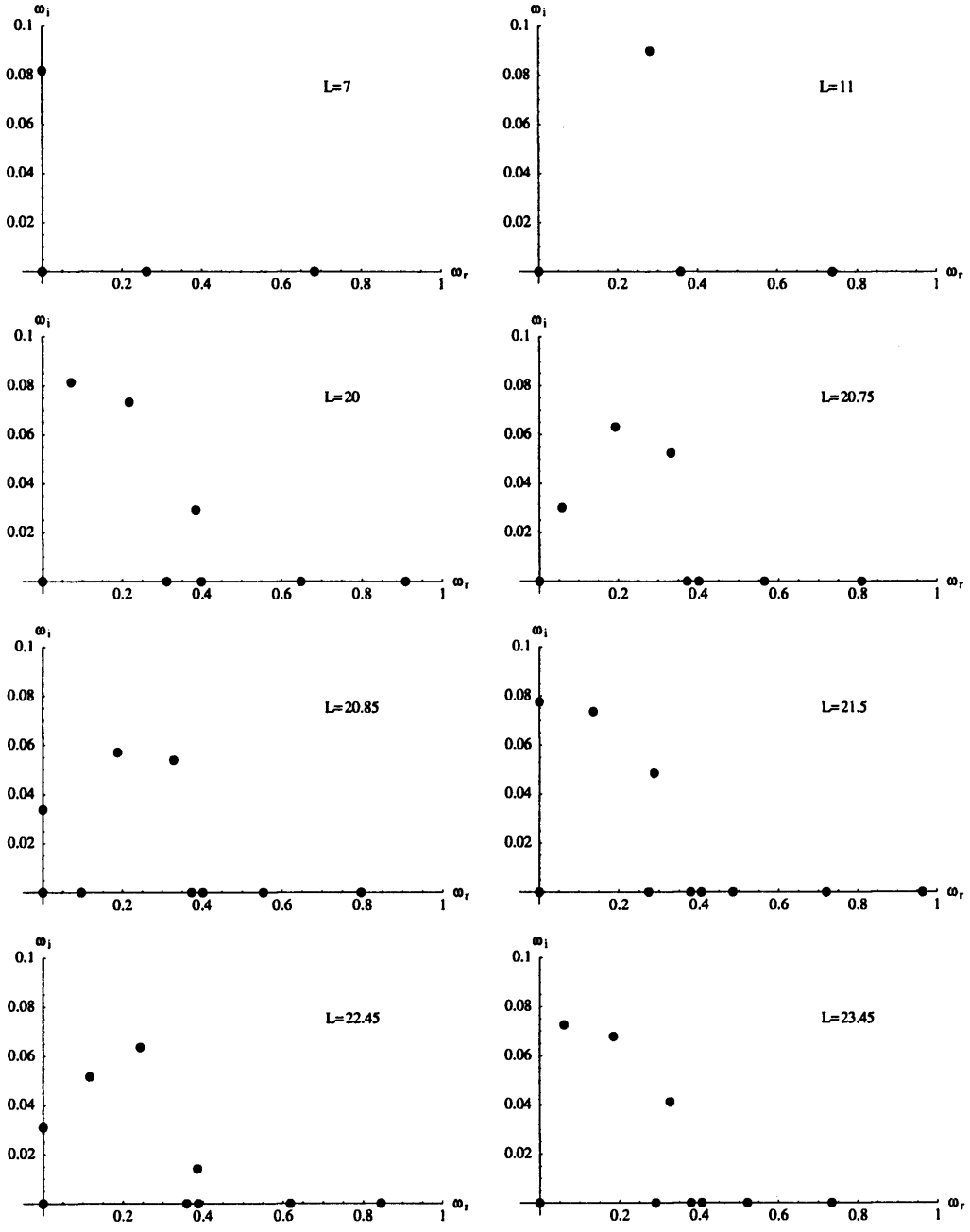

Figure 5.3: The complex ω-plane, showing eigenvalues of our system for various lengths L, larger than before.

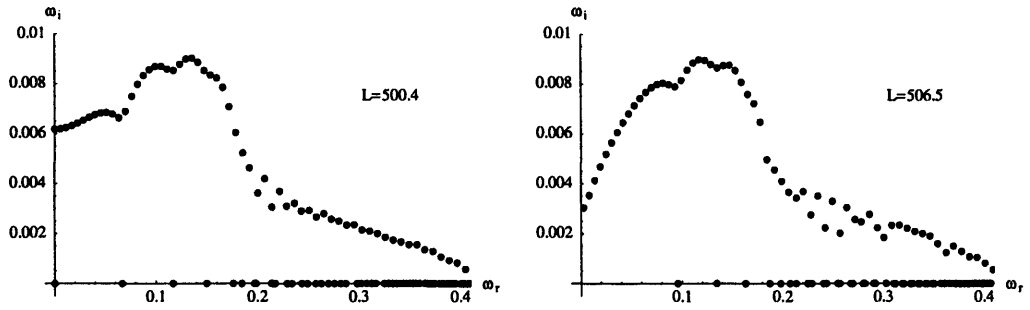

Figure 5.4: The complex ω-plane, showing eigenvalues of our system for two large values of L.

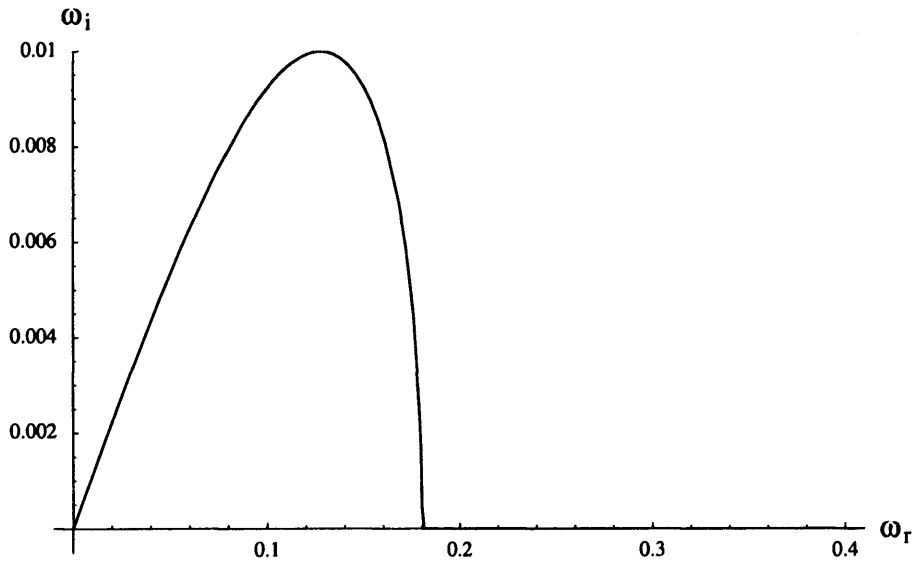

Figure 5.5: The dispersion relation for the infinite-range system, i.e. the straight-channel system considered in Chapter 3, showing complex ω as a function of real k.

again at the upstream end, leading to a feedback loop and global growth in time. Hence, a growing global mode will be observed.

We now briefly show that the phenomenon of being convectively unstable in the infinite-range case and unstable in the finite-range case does not hold for systems which do not exhibit feedback. In Section 2.4, we showed that the linearised Ginzburg-Landau equation (equation (2.1) with $\epsilon = 0$)

$$u_t + cu_x = u_{xx} + b_0 u, \tag{5.11}$$

was convectively unstable for $0 < b_0 < \frac{c^2}{4}$. In Section 1.5, we considered the same equation, with the coefficients labelled differently, in a finite range. The resulting solution, with coefficients labelled as in (5.11), for the range $0 < x < \pi$ is

$$u(x,t) = e^{\left(-c^2/4 - n^2 + b_0\right)t} e^{\frac{cx}{2}} \sin(nx), \tag{5.12}$$

for any n. This decays in time when the condition for convective instability in the infinite-range case is met and so is stable. This is, therefore, an example of a system with no feedback which is convectively unstable for an infinite-range problem and stable when confined to a finite range.

5.3 A scalar formulation

We now describe an alternative formulation of the problem, in terms of scalar quantities. In order that the disturbances propagating in the range $0 < x < L$ can match with those outside this range, we require that the surface height and slope equal zero at $x = 0$ and $x = L$, as before. Solutions to our system are given by (5.10). Thus, at $x = 0$ we have

$$\begin{pmatrix} \mathbf{q}_1 & \mathbf{q}_2 & \mathbf{q}_3 & \mathbf{q}_4 \end{pmatrix} \begin{pmatrix} a_1 \\ a_2 \\ a_3 \\ a_4 \end{pmatrix} = \begin{pmatrix} \Gamma_{0,1} \\ \Gamma_{0,2} \\ \Gamma_{0,3} \\ \Gamma_{0,3} \end{pmatrix}, \tag{5.13}$$

with $\Gamma_{0,2} = 0$, $\Gamma_{0,3} = 0$ and any $\Gamma_{0,1}$ and $\Gamma_{0,4}$. At $x = L$, we have

$$\begin{pmatrix} \mathbf{q}_1 & \mathbf{q}_2 & \mathbf{q}_3 & \mathbf{q}_4 \end{pmatrix} \begin{pmatrix} e^{ik_1 L} & 0 & 0 & 0 \\ 0 & e^{ik_2 L} & 0 & 0 \\ 0 & 0 & e^{ik_3 L} & 0 \\ 0 & 0 & 0 & e^{ik_4 L} \end{pmatrix} \begin{pmatrix} a_1 \\ a_2 \\ a_3 \\ a_4 \end{pmatrix} = \begin{pmatrix} \Gamma_{L,1} \\ \Gamma_{L,2} \\ \Gamma_{L,3} \\ \Gamma_{L,4} \end{pmatrix}, \tag{5.14}$$

with $\Gamma_{L,2} = 0$, $\Gamma_{L,3} = 0$ and any $\Gamma_{L,1}$ and $\Gamma_{L,4}$. We write this as

$$R_{\mathbf{q}} D_e \begin{pmatrix} a_1 \\ a_2 \\ a_3 \\ a_4 \end{pmatrix} = \begin{pmatrix} \Gamma_{L,1} \\ \Gamma_{L,2} \\ \Gamma_{L,3} \\ \Gamma_{L,4} \end{pmatrix}, \tag{5.15}$$

for notational convenience. Combining the important parts of (5.13) and (5.15) we get

$$\begin{aligned} \left(\begin{pmatrix} 0 & 1 & 0 & 0 \\ 0 & 0 & 1 & 0 \\ 0 & 0 & 0 & 0 \\ 0 & 0 & 0 & 0 \end{pmatrix} R_{\mathbf{q}} + \begin{pmatrix} 0 & 0 & 0 & 0 \\ 0 & 0 & 0 & 0 \\ 0 & 1 & 0 & 0 \\ 0 & 0 & 1 & 0 \end{pmatrix} R_{\mathbf{q}} D_e \right) \begin{pmatrix} a_1 \\ a_2 \\ a_3 \\ a_4 \end{pmatrix} &= \begin{pmatrix} \Gamma_{0,2} \\ \Gamma_{0,3} \\ \Gamma_{L,2} \\ \Gamma_{L,3} \end{pmatrix} \\ &= \begin{pmatrix} 0 \\ 0 \\ 0 \\ 0 \end{pmatrix}, \end{aligned} \tag{5.16}$$

or

$$\begin{pmatrix} q_{1,(2)} & q_{2,(2)} & q_{3,(2)} & q_{4,(2)} \\ q_{1,(3)} & q_{2,(3)} & q_{3,(3)} & q_{4,(3)} \\ q_{1,(2)} e^{ik_1 L} & q_{2,(2)} e^{ik_2 L} & q_{3,(2)} e^{ik_3 L} & q_{4,(2)} e^{ik_4 L} \\ q_{1,(3)} e^{ik_1 L} & q_{2,(3)} e^{ik_2 L} & q_{3,(3)} e^{ik_3 L} & q_{4,(3)} e^{ik_4 L} \end{pmatrix} \begin{pmatrix} a_1 \\ a_2 \\ a_3 \\ a_4 \end{pmatrix} = \begin{pmatrix} 0 \\ 0 \\ 0 \\ 0 \end{pmatrix}, \tag{5.17}$$

where the subscripts on the q_js in parentheses indicate components within the vector $\mathbf{q}_j$. We label the above matrix Ξ. Thus, our problem is completely specified as: ω is a root if the matrix Ξ, depending on the corresponding ks and qs, is singular.

We now note that, as the second component of $\mathbf{u}$ (i.e. F) is the surface displacement, and the third component (G) is its slope, in Fourier space we are able to say that $q_{j,(3)} = ik_j q_{j,(2)}$. We also note that

$$\Xi = \begin{pmatrix} 1 & 1 & 1 & 1 \\ ik_1 & ik_2 & ik_3 & ik_4 \\ e^{ik_1 L} & e^{ik_2 L} & e^{ik_3 L} & e^{ik_4 L} \\ ik_1 e^{ik_1 L} & ik_2 e^{ik_2 L} & ik_3 e^{ik_3 L} & ik_4 e^{ik_4 L} \end{pmatrix} \begin{pmatrix} q_{1,(2)} & 0 & 0 & 0 \\ 0 & q_{2,(2)} & 0 & 0 \\ 0 & 0 & q_{3,(2)} & 0 \\ 0 & 0 & 0 & q_{4,(2)} \end{pmatrix}. \tag{5.18}$$

The diagonal matrix above is nonsingular when $q_{1,(2)}q_{2,(2)}q_{3,(2)}q_{4,(2)} \neq 0$, which is, in general, the case. It now suffices to make the left-hand matrix on the r.h.s. of (5.18) singular. Its determinant is

$$\begin{aligned} \Theta \;=\; & -(k_2 - k_3)(k_1 - k_4)\left(e^{i(k_2+k_3)L} + e^{i(k_1+k_4)L}\right) \\ & +(k_1 - k_3)(k_2 - k_4)\left(e^{i(k_1+k_3)L} + e^{i(k_2+k_4)L}\right) \\ & -(k_1 - k_2)(k_3 - k_4)\left(e^{i(k_1+k_2)L} + e^{i(k_3+k_4)L}\right). \end{aligned} \tag{5.19}$$

It is clear that $\Theta = 0$, with Θ as given by (5.19), is the complete specification of the problem with no approximations made.

5.4 The modes with $\omega_r = 0$

In this section, we choose to consider only roots with $\omega_r = 0$. These do not always exist, as is shown by Figure 5.8. However, there appear to be a large number of fairly-wide ranges of L-values where a mode with $\omega_r = 0$ does exist. Substitution of the $\omega_r = 0$ approximation into (5.19) simplifies the equation and some results, such as an analytic description of the aforementioned approximate periodicity of the modes, may be obtained. Choosing to investigate

modes with $\omega_r = 0$ has another significant advantage: consider the dispersion relation (equation 5.1 again)

$$\frac{\rho_1}{h_1}(\omega - ku_{1\infty})^2 + \frac{\rho_2}{h_2}(\omega - ku_{2\infty})^2 = g_\rho k^2 + \gamma k^4,$$

or,

$$\frac{\rho_1}{h_{1\infty}}((-\omega) - (-k)\,u_{1\infty})^2 + \frac{\rho_2}{h_{2\infty}}((-\omega) - (-k)\,u_{2\infty})^2 = g_\rho\,(-k)^2 + \gamma\,(-k)^4\,. \tag{5.20}$$

Labelling complex conjugates with a superscript asterisk, we also obtain

$$\frac{\rho_1}{h_{1\infty}}(\omega^* - k^*u_{1\infty})^2 + \frac{\rho_2}{h_{2\infty}}(\omega^* - k^*u_{2\infty})^2 = g_\rho\,(k^*)^2 + \gamma\,(k^*)^4\,, \tag{5.21}$$

where use has been made of the fact that $(z^*)^n = (z^n)^*$ for any $z \in \mathbb{C}$ and $n \in \mathbb{N}$. From these we note that firstly, if ω is an eigenvalue, then so will be $-\omega$, ω^* and hence $-\omega^*$, as suggested in Section 5.1. Secondly, comparing the last two of the equations above, if $-\omega = \omega^*$ (i.e. $\omega_r = 0$), then both $-k$ and k^* will be roots. Thus our k-values will occur in 'real-conjugate' pairs. (We take the 'real-conjugate' of z to mean $-z^*$.) This leads to three possibilities:

- All four roots are imaginary,
- two roots are purely imaginary and two are not, but occur as a 'real-conjugate' pair,
- the roots occur as two non-purely-imaginary 'real-conjugate' pairs.

We will only consider the last of these here, as it seems to be the usual case for the set of parameters chosen for this problem. We label, without loss of generality, k_1 and k_2 as a 'real-conjugate' pair and k_3 and k_4 as a 'real-conjugate' pair.

To proceed further, we use the fact that our dispersion relation is a quartic in k and so may be rewritten as

$$(k - k_1)(k - k_2)(k - k_3)(k - k_4) = 0. \tag{5.22}$$

which has a coefficient of k^3 equal to $-k_1 - k_2 - k_3 - k_4$. By comparing this with the other form of the dispersion relation (5.1), we conclude that

$$k_1 + k_2 + k_3 + k_4 = 0. \tag{5.23}$$

As we know that $k_1 + k_2 = 2i\mathrm{Im}(k_1) = 2i\mathrm{Im}(k_2)$ and $k_3 + k_4 = 2i\mathrm{Im}(k_3) = 2i\mathrm{Im}(k_4)$, we also conclude that

$$\mathrm{Im}(k_1) = \mathrm{Im}(k_2) = -\mathrm{Im}(k_3) = -\mathrm{Im}(k_4). \tag{5.24}$$

Thus, we can say that

$$\begin{aligned}
&k_1 + k_2 \in i\mathbb{R}, && k_1 + k_3 \in \mathbb{R},\\
&k_1 + k_4 \in \mathbb{R}, && k_2 + k_3 \in \mathbb{R},\\
&k_2 + k_4 \in \mathbb{R}, && k_3 + k_4 \in i\mathbb{R},\\
&k_1 - k_2 \in \mathbb{R}, && k_3 - k_4 \in \mathbb{R},\\
&\mathrm{Re}(k_1 - k_3) = -\mathrm{Re}(k_2 - k_4), && \mathrm{Im}(k_1 - k_3) = \mathrm{Im}(k_2 - k_4),\\
&\mathrm{Re}(k_1 - k_4) = -\mathrm{Re}(k_2 - k_3), && \mathrm{Im}(k_1 - k_4) = \mathrm{Im}(k_2 - k_3).
\end{aligned} \tag{5.25}$$

We conclude that $(k_1 - k_3)(k_2 - k_4)$ is purely real (and negative) and the same applies to $(k_1 - k_4)(k_2 - k_3)$. Taking the terms of our determinant, Θ, from (5.19), in order, we get four exponential terms, each periodic in L, with real coefficients and then two purely growing/decaying exponentials in L, again with real coefficients. Let

$$\begin{aligned}
\kappa_1 &= i(k_1 + k_2),\\
\kappa_2 &= k_1 + k_3,\\
\kappa_3 &= k_1 + k_4,\\
r_1 &= -2(k_1 - k_2)(k_3 - k_4),\\
r_2 &= 2(k_1 - k_3)(k_2 - k_4),\\
r_3 &= -2(k_2 - k_3)(k_1 - k_4)
\end{aligned} \tag{5.26}$$

and we now have

$$\Theta = r_2 \cos(\kappa_2 L) + r_3 \cos(\kappa_3 L) + r_1 \cosh(\kappa_1 L). \tag{5.27}$$

$\Theta = 0$, with Θ as given by (5.27), is a complete formulation of the problem when ω is purely imaginary.

5.4.1 Approximate periodicity in the ω-plane

We now use (5.27) to make some comments about the approximate periodicity, in L, of the purely-imaginary modes. As an example, we look, by trial and error, for two solutions with $L \approx 500$ and with one value of ω equal to $0.002i$. We choose 497.8383 and 501.3076, as shown in Figure 5.6.

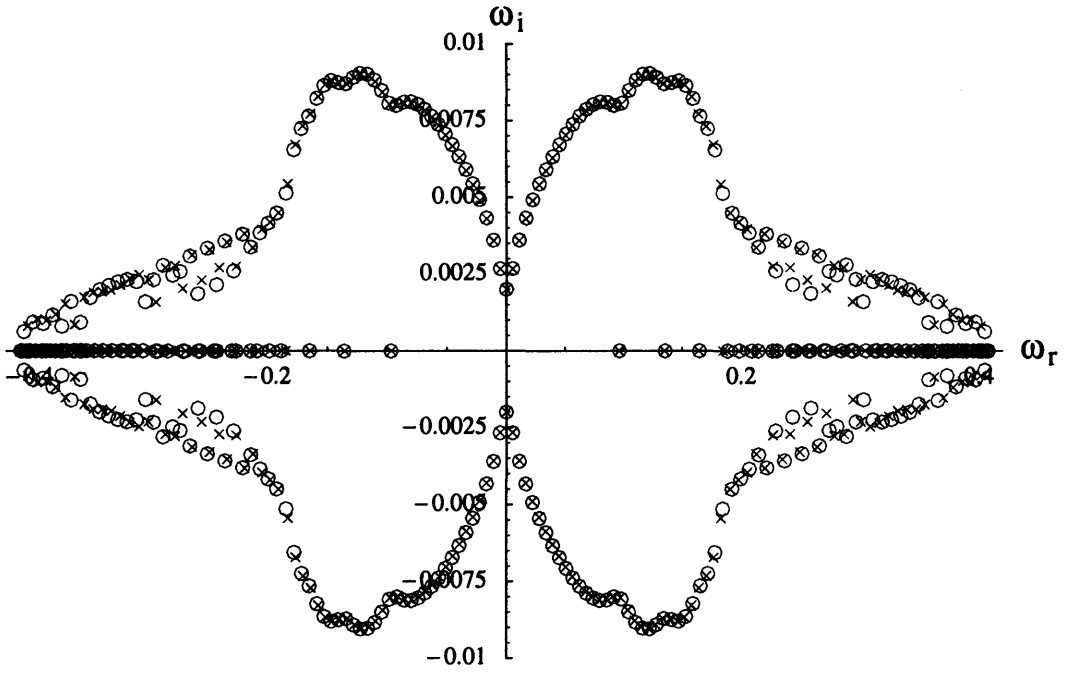

Figure 5.6: The ω-plane eigenvalues of the finite-range problem describing our system. The octagons are for $L = 497.8383$, the crosses for $L = 501.3076$. Both have $\omega = 0.002i$ as an eigenvalue. We can see that many of the other eigenvalues, especially those with $|\omega_r| < 0.15$, coincide in the two cases; this is what we refer to as the 'approximate periodicity in L' of the modes.

For this value of ω, we have $k_1 = -1.811080 - 0.00219512i$, $k_2 = 1.811080$ - $0.00219512i$, $k_3 = -0.000243916 + 0.00219512i$ and $k_4 = 0.000243916 +$

$0.00219512i$. This gives us

$$\begin{aligned} r_1 &= -0.00353400, \quad r_2 = -6.558291, \quad r_3 = 6.561824, \\ \kappa_1 &= 0.00439023, \quad \kappa_2 = -1.811324, \quad \kappa_3 = -1.810836. \end{aligned} \tag{5.28}$$

We can use these values to plot Θ against L, as shown in Figure 5.7. In the top diagram, we can see that this value of ω will give us roots ($\Theta = 0$) for approximately evenly-spaced values of L. This shows the approximate periodicity in L of the purely-imaginary roots. The middle diagram demonstrates that there are solutions to our system for L approximately 497.8 and 501.3, which should, of course, be the case. The bottom diagram shows that, eventually, we expect there to be an $L \approx 1840$ beyond which the root $\omega = 0.002i$ is never achieved. This is evidence of the purely-imaginary ωs eventually tending to zero. We will return to this later.

First we observe that, for this set of parameters, r_2 and r_3 are very close in magnitude and for $L = 500$, $|r_1 \cosh(\kappa_1 L)| < 0.02$. If we ignore the contribution from this term, we have, approximately, the trigonometric cosine 'addition formula', giving us a short-range variation with L like $(|\kappa_2| + |\kappa_3|)L/2$. This predicts a 'period' of

$$\frac{2\pi}{(|\kappa_2| + |\kappa_3|)/2} = 3.4688. \tag{5.29}$$

This compares well with our measured 'period' of 501.3076-497.8383 = 3.4693.

5.4.2 The large-L limit

We now look at the long-length limit. To get an initial idea, we begin by looking at the variation of the purely-imaginary ωs, where they exist, with L. This is shown below, in Figure 5.8.

We wish to consider the dispersion relation for ω small and imaginary. To this end, we substitute expansions of the form

$$\begin{aligned} \omega &= \omega_0 + \epsilon\omega_\epsilon, \\ k &= k_0 + \epsilon k_\epsilon + \epsilon^2 k_{\epsilon^2} + \ldots, \end{aligned} \tag{5.30}$$

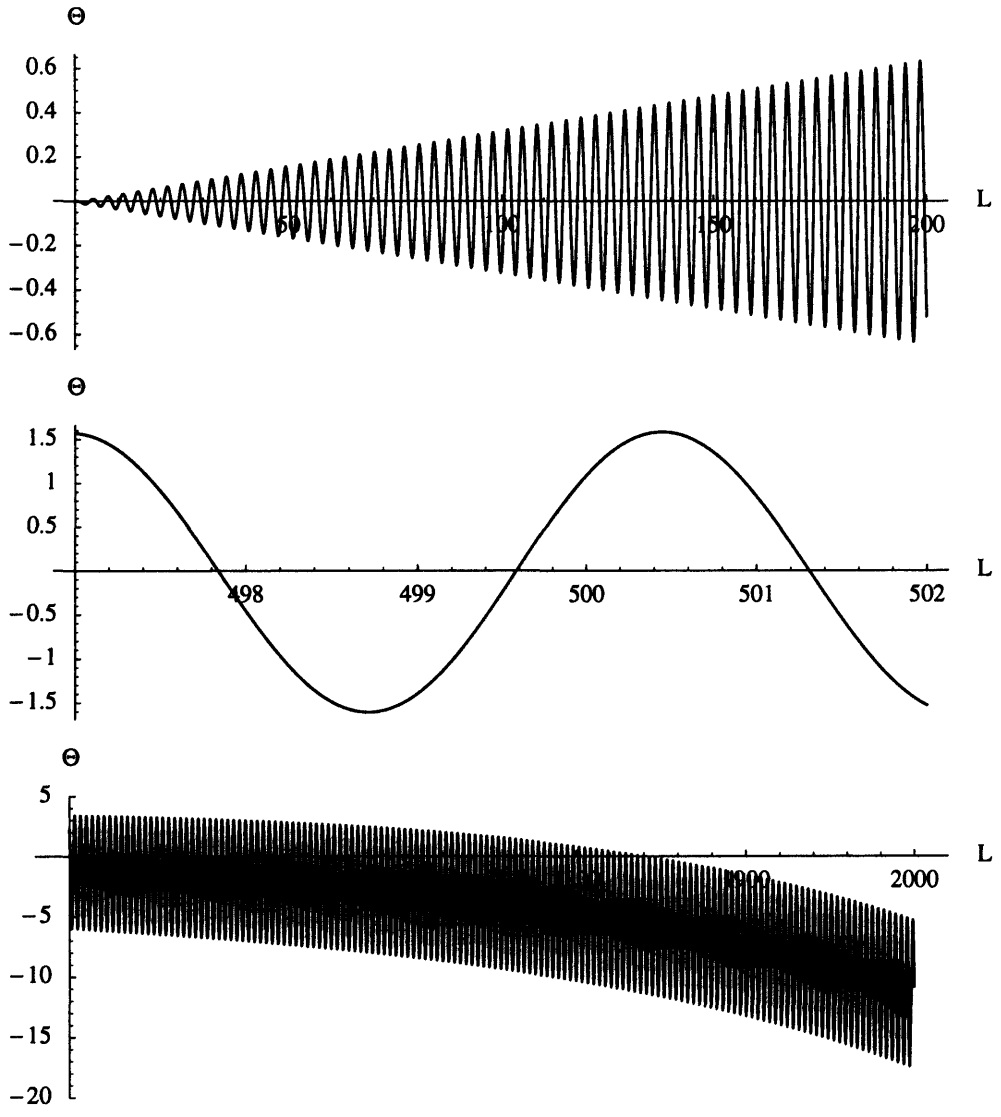

Figure 5.7: Θ against L for $\omega = 0.002i$.

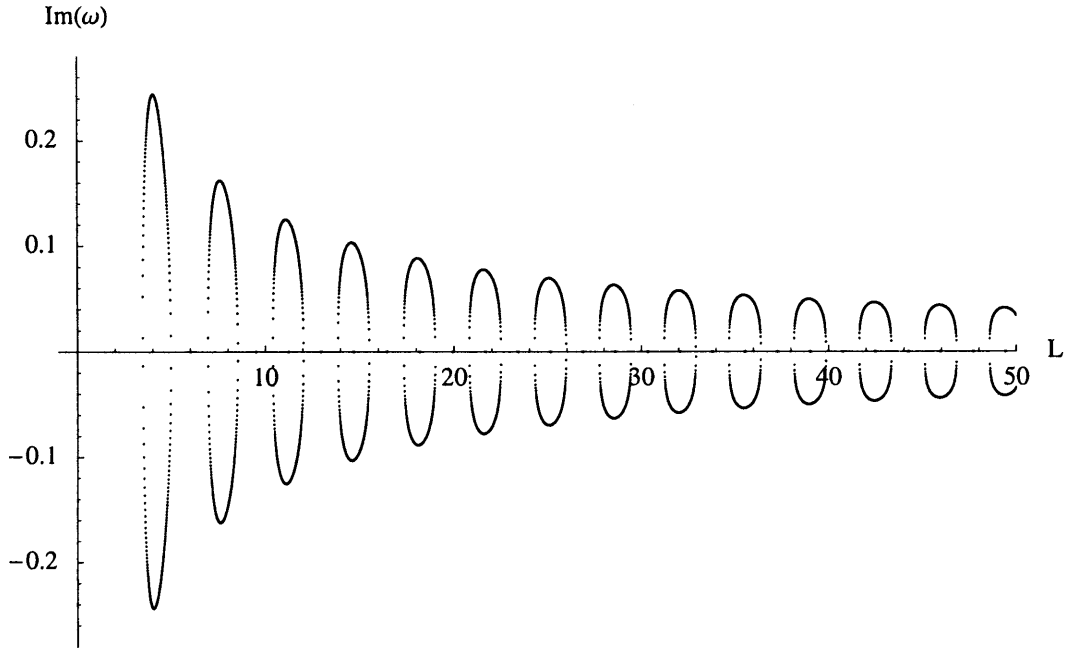

Figure 5.8: The variation of the purely-imaginary ωs with L.

into the dispersion relation (5.1). At $O(1)$, we obtain the same equation with k replaced by k_0 and ω replaced by ω_0, which we set to zero from here onwards. Thus

$$k_0^4 + g_\gamma k_0^2 - \rho_{h,1} u_{1\infty}^2 k_0^2 - \rho_{h,2} u_{2\infty}^2 k_0^2 = 0, \tag{5.31}$$

where the substitutions $g_\gamma = g_\rho/\gamma$, $\rho_{h,1} = \rho_1/(h_{1\infty}\gamma)$ and $\rho_{h,2} = \rho_2/(h_{2\infty}\gamma)$ have been made for clarity. We thus have a double root for k_0 at 0 and two more at $\pm\sqrt{\rho_{h,1}u_{1\infty}^2 + \rho_{h,2}u_{2\infty}^2 - g_\gamma}$.

At $O(\epsilon)$, we have

$$4k_0^3 k_\epsilon + 2(g_\gamma - \rho_{h,1}u_{1\infty}^2 - \rho_{h,2}u_{2\infty}^2)k_0 k_\epsilon + (2\rho_{h,1}u_{1\infty} + 2\rho_{h,2}u_{2\infty})\omega_\epsilon k_0 = 0. \tag{5.32}$$

For our roots with $k_0 \neq 0$, we may rearrange this to give

$$\begin{aligned} k_\epsilon &= \frac{(2\rho_{h,1}u_{1\infty}+2\rho_{h,2}u_{2\infty})k_0}{2(\rho_{h,1}u_{1\infty}^2+\rho_{h,2}u_{2\infty}^2-g_\gamma)k_0-4k_0^3}\omega_\epsilon \\ &= -\frac{\rho_{h,1}u_{1\infty}+\rho_{h,2}u_{2\infty}}{\rho_{h,1}u_{1\infty}^2+\rho_{h,2}u_{2\infty}^2-g_\gamma}\omega_\epsilon. \end{aligned} \tag{5.33}$$

However, for the linear asymptotics where $k_0 = 0$, we must look at $O(\epsilon^2)$:

$$(\rho_{h,1}u_{1\infty}^2 + \rho_{h,2}u_{2\infty}^2 - g_\gamma)k_\epsilon^2 - 2\omega_\epsilon(\rho_{h,1}u_{1\infty} + \rho_{h,2}u_{2\infty})k_\epsilon + \omega_\epsilon^2(\rho_{h,1} + \rho_{h,2}) = 0, \tag{5.34}$$

where the substitution $k_0 = 0$, which removes the terms containing k_{ϵ^2}, has already been made. We have

$$k_\epsilon = \omega_\epsilon \frac{\rho_{h,1}u_{1\infty}+\rho_{h,2}u_{2\infty}}{\rho_{h,1}u_{1\infty}^2+\rho_{h,2}u_{2\infty}^2-g_\gamma} \pm \omega_\epsilon \frac{\sqrt{(\rho_{h,1}+\rho_{h,2})g_\gamma-\rho_{h,1}\rho_{h,2}(u_{1\infty}-u_{2\infty})^2}}{\rho_{h,1}u_{1\infty}^2+\rho_{h,2}u_{2\infty}^2-g_\gamma}. \tag{5.35}$$

We note that the first part of this is just $-(k_\epsilon$ from before). This is necessary to ensure that the sum of the roots is zero. We expect the part under the square-root to be negative, in order to ensure a 'real-conjugate' pair of roots when ω_ϵ is imaginary. We therefore label our roots

$$\begin{aligned}
k_1 &= -\sqrt{\rho_{h,1}u_{1\infty}^2 + \rho_{h,2}u_{2\infty}^2 - g_\gamma} - \epsilon\omega_\epsilon \frac{\rho_{h,1}u_{1\infty}+\rho_{h,2}u_{2\infty}}{\rho_{h,1}u_{1\infty}^2+\rho_{h,2}u_{2\infty}^2-g_\gamma}, \\
k_2 &= \sqrt{\rho_{h,1}u_{1\infty}^2 + \rho_{h,2}u_{2\infty}^2 - g_\gamma} - \epsilon\omega_\epsilon \frac{\rho_{h,1}u_{1\infty}+\rho_{h,2}u_{2\infty}}{\rho_{h,1}u_{1\infty}^2+\rho_{h,2}u_{2\infty}^2-g_\gamma}, \\
k_3 &= 0 + \epsilon\omega_\epsilon \left(\frac{\rho_{h,1}u_{1\infty}+\rho_{h,2}u_{2\infty}}{\rho_{h,1}u_{1\infty}^2+\rho_{h,2}u_{2\infty}^2-g_\gamma} + \frac{\sqrt{(\rho_{h,1}+\rho_{h,2})g_\gamma-\rho_{h,1}\rho_{h,2}(u_{1\infty}-u_{2\infty})^2}}{\rho_{h,1}u_{1\infty}^2+\rho_{h,2}u_{2\infty}^2-g_\gamma} \right), \\
k_4 &= 0 + \epsilon\omega_\epsilon \left(\frac{\rho_{h,1}u_{1\infty}+\rho_{h,2}u_{2\infty}}{\rho_{h,1}u_{1\infty}^2+\rho_{h,2}u_{2\infty}^2-g_\gamma} - \frac{\sqrt{(\rho_{h,1}+\rho_{h,2})g_\gamma-\rho_{h,1}\rho_{h,2}(u_{1\infty}-u_{2\infty})^2}}{\rho_{h,1}u_{1\infty}^2+\rho_{h,2}u_{2\infty}^2-g_\gamma} \right),
\end{aligned} \tag{5.36}$$

giving

$$\begin{aligned}
\kappa_1 &= i(k_1 + k_2) = -2i\epsilon\omega_\epsilon \frac{\rho_{h,1}u_{1\infty}+\rho_{h,2}u_{2\infty}}{\rho_{h,1}u_{1\infty}^2+\rho_{h,2}u_{2\infty}^2-g_\gamma}, \\
\kappa_2 &= k_1 + k_3 = \begin{array}{l} -\sqrt{\rho_{h,1}u_{1\infty}^2 + \rho_{h,2}u_{2\infty}^2 - g_\gamma} \\ +\epsilon\omega_\epsilon \frac{\sqrt{(\rho_{h,1}+\rho_{h,2})g_\gamma-\rho_{h,1}\rho_{h,2}(u_{1\infty}-u_{2\infty})^2}}{\rho_{h,1}u_{1\infty}^2+\rho_{h,2}u_{2\infty}^2-g_\gamma}, \end{array} \\
\kappa_3 &= k_1 + k_4 = \begin{array}{l} -\sqrt{\rho_{h,1}u_{1\infty}^2 + \rho_{h,2}u_{2\infty}^2 - g_\gamma} \\ -\epsilon\omega_\epsilon \frac{\sqrt{(\rho_{h,1}+\rho_{h,2})g_\gamma-\rho_{h,1}\rho_{h,2}(u_{1\infty}-u_{2\infty})^2}}{\rho_{h,1}u_{1\infty}^2+\rho_{h,2}u_{2\infty}^2-g_\gamma}, \end{array}
\end{aligned}$$

$$
\begin{aligned}
r_1 &= -2(k_1-k_2)(k_3-k_4) &&= 0 - 8\epsilon\omega_\epsilon\sqrt{\tfrac{(\rho_{h,1}+\rho_{h,2})g_\gamma-\rho_{h,1}\rho_{h,2}(u_{1\infty}-u_{2\infty})^2}{\rho_{h,1}u_{1\infty}^2+\rho_{h,2}u_{2\infty}^2-g_\gamma}},\\
r_2 &= 2(k_1-k_3)(k_2-k_4) &&= -2(\rho_{h,1}u_{1\infty}^2+\rho_{h,2}u_{2\infty}^2-g_\gamma)\\
&&&\quad -4\epsilon\omega_\epsilon\sqrt{\tfrac{(\rho_{h,1}+\rho_{h,2})g_\gamma-\rho_{h,1}\rho_{h,2}(u_{1\infty}-u_{2\infty})^2}{\rho_{h,1}u_{1\infty}^2+\rho_{h,2}u_{2\infty}^2-g_\gamma}}\\
&&&\quad +O(\epsilon^2),\\
r_3 &= -2(k_1-k_4)(k_2-k_3) &&= 2(\rho_{h,1}u_{1\infty}^2+\rho_{h,2}u_{2\infty}^2-g_\gamma)\\
&&&\quad -4\epsilon\omega_\epsilon\sqrt{\tfrac{(\rho_{h,1}+\rho_{h,2})g_\gamma-\rho_{h,1}\rho_{h,2}(u_{1\infty}-u_{2\infty})^2}{\rho_{h,1}u_{1\infty}^2+\rho_{h,2}u_{2\infty}^2-g_\gamma}}\\
&&&\quad +O(\epsilon^2).
\end{aligned}
\tag{5.37}
$$

We evaluate these for the case $\omega_\epsilon = i$, $\epsilon = 0.002$ (also $u_{1\infty} = 0.8$, $u_{2\infty} = 1$, $\rho_{h,1} = \rho_{h,2} = 2$, $g_\gamma = 0$) as a check and get

$$
\begin{aligned}
\kappa_1 &= 0.00439024, \quad \kappa_2 = -1.81132, \quad \kappa_3 = -1.81083,\\
r_1 &= -0.00353381, \quad r_2 = -6.55823, \quad r_3 = 6.56177,
\end{aligned}
\tag{5.38}
$$

in good agreement with (5.28). Our dispersion relation is (5.27 again)

$$\Theta = r_2\cos(\kappa_2 L) + r_3\cos(\kappa_3 L) + r_1\cosh(\kappa_1 L).$$

We are now in a position to estimate the largest value of L for which there can be roots of Θ. We know

$$|r_2\cos(\kappa_2 L) + r_3\cos(\kappa_3 L)| < |r_2| + |r_3|. \tag{5.39}$$

Thus, when

$$|r_1\cosh(\kappa_1 L)| > |r_2| + |r_3|, \tag{5.40}$$

there can never be any more solutions. We put $\omega_\epsilon = i$ and make the following assumptions, both of which hold for the parameter values chosen for this problem:

$$
\begin{aligned}
&\rho_{h,1}u_{1\infty}^2 + \rho_{h,2}u_{2\infty}^2 > g_\gamma,\\
&\tfrac{\rho_{h,1}\rho_{h,2}(u_{1\infty}-u_{2\infty})^2-(\rho_{h,1}+\rho_{h,2})g_\gamma}{\rho_{h,1}u_{1\infty}^2+\rho_{h,2}u_{2\infty}^2-g_\gamma} > 0.
\end{aligned}
\tag{5.41}
$$

Then, from (5.37),

$$\begin{aligned} |r_2| + |r_3| \;&\leq\; 4(\rho_{h,1}u_{1\infty}^2 + \rho_{h,2}u_{2\infty}^2 - g_\gamma) \\ &\quad +8\epsilon\sqrt{\tfrac{\rho_{h,1}\rho_{h,2}(u_{1\infty}-u_{2\infty})^2-(\rho_{h,1}+\rho_{h,2})g_\gamma}{\rho_{h,1}u_{1\infty}^2+\rho_{h,2}u_{2\infty}^2-g_\gamma}} + O(\epsilon^2). \end{aligned} \tag{5.42}$$

$\epsilon > 0$ and the positive square root is chosen. Also,

$$\begin{aligned} |r_1\cosh(\kappa_1 L)| \;&=\; 8\epsilon\sqrt{\tfrac{\rho_{h,1}\rho_{h,2}(u_{1\infty}-u_{2\infty})^2-(\rho_{h,1}+\rho_{h,2})g_\gamma}{\rho_{h,1}u_{1\infty}^2+\rho_{h,2}u_{2\infty}^2-g_\gamma}} \\ &\quad \times \cosh(2\epsilon\tfrac{\rho_{h,1}u_{1\infty}+\rho_{h,2}u_{2\infty}}{\rho_{h,1}u_{1\infty}^2+\rho_{h,2}u_{2\infty}^2-g_\gamma}L). \end{aligned} \tag{5.43}$$

We now drop terms $O(\epsilon^2)$ and, for convenience, make the following substitutions:

$$\begin{aligned} A_s \;&=\; 4(\rho_{h,1}u_{1\infty}^2 + \rho_{h,2}u_{2\infty}^2 - g_\gamma), \\ B_s \;&=\; 8\sqrt{\tfrac{\rho_{h,1}\rho_{h,2}(u_{1\infty}-u_{2\infty})^2-(\rho_{h,1}+\rho_{h,2})g_\gamma}{\rho_{h,1}u_{1\infty}^2+\rho_{h,2}u_{2\infty}^2-g_\gamma}}, \\ C_s \;&=\; 2\tfrac{\rho_{h,1}u_{1\infty}+\rho_{h,2}u_{2\infty}}{\rho_{h,1}u_{1\infty}^2+\rho_{h,2}u_{2\infty}^2-g_\gamma}, \end{aligned} \tag{5.44}$$

which are all real and positive by our assumptions. We now require that

$$\epsilon B_s\cosh(C_s\epsilon L) > A_s + \epsilon B_s, \tag{5.45}$$

i.e.

$$\epsilon B_s\cosh(C_s\epsilon L) - (A_s + \epsilon B_s) > 0, \tag{5.46}$$

or,

$$\frac{\epsilon B_s}{2}\left(e^{2C_s\epsilon L}+1\right) - (A_s+\epsilon B_s)e^{C_s\epsilon L} > 0. \tag{5.47}$$

This is a quadratic in $e^{C_s\epsilon L}$. So

$$\begin{aligned} &\left(e^{C_s\epsilon L} - \tfrac{A_s+\epsilon B_s+\sqrt{(A_s+\epsilon B_s)^2-2\epsilon B_s}}{\epsilon B_s}\right) \\ &\times\left(e^{C_s\epsilon L} - \tfrac{A_s+\epsilon B_s\sqrt{(A_s+\epsilon B_s)^2-2\epsilon B_s}}{\epsilon B_s}\right) \;>\; 0. \end{aligned} \tag{5.48}$$

Note that, for $x, n, m \in \mathbb{R}$, $(x-m)(x-n) > 0$ is satisfied when $x > \max(m, n)$. In our case

$$e^{C_s \epsilon L} > \frac{A_s + \epsilon B_s + \sqrt{(A_s + \epsilon B_s)^2 - 2\epsilon B_s}}{\epsilon B_s}. \tag{5.49}$$

So,

$$L > \frac{1}{C_s \epsilon} \log \left(\frac{A_s + \epsilon B_s + \sqrt{(A_s + \epsilon B_s)^2 - 2\epsilon B_s}}{\epsilon B_s} \right), \tag{5.50}$$

where log is $\log_e$. In our specific example, we have $A_s = 13.12$, $B_s = 1.7669$, $C_s = 2.19512$. This gives

$$L > 2030.17, \tag{5.51}$$

10.3% larger than our measured value. Finally, we plot the minimum length for a particular ϵ, using our standard parameters for $u_{1\infty}$, etc. This demonstrates that, although the purely-imaginary ω tends to 0 as $L \to \infty$, it does so very slowly indeed. Also, we can see from the dots that (5.50) is a fairly good approximation across a wide range of ϵ.

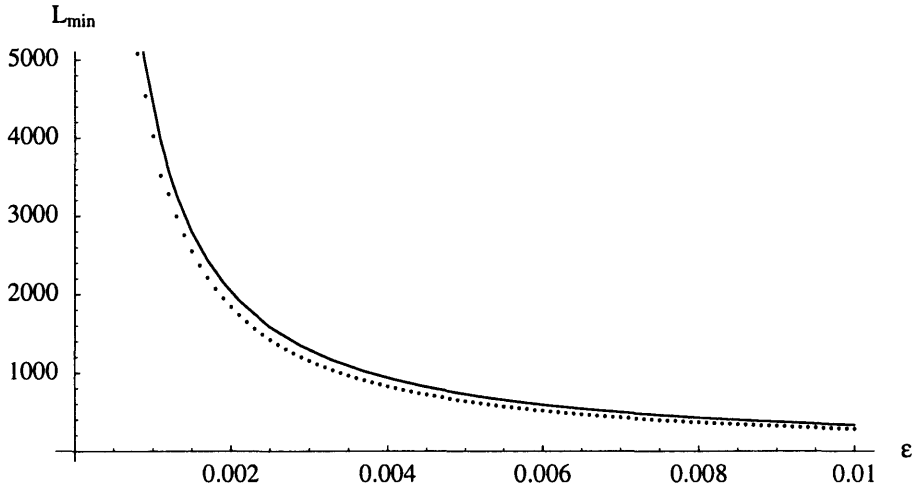

Figure 5.9: The minimum length, L_{min}, such that the purely-imaginary ω is less than ϵ, as a function of ϵ. (The inverse function would be more interesting, but an explicit formula is harder to derive.) Some numerical values of the largest length such that the corresponding values of ϵ are reached are also shown as dots.

5.5 The case $\omega \in \mathbb{R}$

When $\omega \in \mathbb{R}$, our dispersion relation is a quartic in k with real roots. For the set of parameters we have considered elsewhere for this problem, we typically get a complex-conjugate pair, which we label as k_1 and k_2, and two real roots, k_3 and k_4.

We have

$$\begin{gathered} k_1 + k_2 \in \mathbb{R}, \\ k_1 + k_4 = -(k_2 + k_3) = -(k_1 + k_3)^* = -(k_2 + k_4)^*, \\ k_2 - k_3 = (k_1 - k_3)^*, \\ k_2 - k_4 = (k_1 - k_4)^*. \end{gathered} \tag{5.52}$$

Thus, if we define

$$\begin{aligned} \kappa_1 &= k_1 + k_2, \\ \kappa_2 &= k_1 + k_3, \\ \kappa_3 &= k_1 + k_4, \\ r_1 &= -2(k_1 - k_2)(k_3 - k_4), \\ r_2 &= 2(k_1 - k_3)(k_2 - k_4), \\ r_3 &= -2(k_2 - k_3)(k_1 - k_4), \end{aligned} \tag{5.53}$$

(note that κ_1 is different to that used in Section 5.4) then,

$$\begin{aligned} \kappa_1 &\in \mathbb{R}, \\ \kappa_3 &= -\kappa_2^*, \\ r_1 &\in i\mathbb{R}, \\ r_3 &= -r_2^* \end{aligned} \tag{5.54}$$

and

$$\Theta = r_1 \cos(\kappa_1 L) + r_2 \cos(\kappa_2 L) + r_3 \cos(\kappa_3 L). \tag{5.55}$$

Now

$$\begin{aligned} r_2 \cos(\kappa_2 L) + r_3 \cos(\kappa_3 L) &= -2ir_{2,r} \sin(\kappa_{2,r} L) \sinh(\kappa_{2,i} L) \\ &\quad +2ir_{2,i} \cos(\kappa_{2,r} L) \cosh(\kappa_{2,i} L) \end{aligned} \tag{5.56}$$

and, as $r_1 = ir_{1,i}$, $\kappa_1 = \kappa_{1,r}$, we have

$$\begin{aligned} -i\Theta &= r_{1,i}\cos(\kappa_{1,r}L) - 2r_{2,r}\sin(\kappa_{2,r}L)\sinh(\kappa_{2,i}L) \\ &\quad +2r_{2,i}\cos(\kappa_{2,r}L)\cosh(\kappa_{2,i}L). \end{aligned} \tag{5.57}$$

Also, $r_{1,i} = -2r_{2,i}$. Therefore, we wish to find solutions to

$$\cos(\kappa_{2,r}L)\cosh(\kappa_{2,i}L) - \cos(\kappa_{1,r}L) - \frac{r_{2,r}}{r_{2,i}}\sin(\kappa_{2,r}L)\sinh(\kappa_{2,i}L) = 0. \tag{5.58}$$

For L large, we ignore the cos term and use the fact that $\tanh(x) \to \mathrm{sgn}(x)$ as $x \to \pm\infty$ so

$$\tan(\kappa_{2,r}L) = \frac{r_{2,i}}{r_{2,r}}\mathrm{sgn}(\kappa_{2,i}), \tag{5.59}$$

i.e.

$$L = \frac{\mathrm{sgn}(\kappa_{2,i})}{\kappa_{2,r}}\tan^{-1}\left(\frac{r_{2,i}}{r_{2,r}}\right). \tag{5.60}$$

For our previous set of data with $L = 501.3076$ we have ω=0.16427916 as a root. This gives $k_1 = 0.184103 - 0.00835848i$, $k_2 = 0.184103 + 0.00835848i$, $k_3 = -1.97639$, $k_4 = 1.60818$. So

$$\begin{aligned} \kappa_2 &= -1.79228 - 0.00835848i, \\ r_2 &= -6.15327 + 0.0599231i, \end{aligned} \tag{5.61}$$

which predicts $L = 501.3077$, in reasonable agreement. Note that we choose $\tan^{-1}$ in the range $\left(286 - \frac{1}{2}\right)\pi < \tan^{-1}(x) < \left(286 + \frac{1}{2}\right)\pi$. We expect roughly periodic roots in L with period $\pi/|\kappa_{2,r}| \approx 1.753$ in our case. Two 'periods' would have $\Delta L = 3.506$, which compares well with the difference between our octagons and crosses, which had (measured) $\Delta L = 3.469$ and both had roots at approximately $\omega = 0.16427916$.

5.6 The general case of L large

Consider (5.19) for general k,

$$\begin{aligned} \Theta &= -(k_2 - k_3)(k_1 - k_4)\left(e^{i(k_2+k_3)L} + e^{i(k_1+k_4)L}\right) \\ &\quad +(k_1 - k_3)(k_2 - k_4)\left(e^{i(k_1+k_3)L} + e^{i(k_2+k_4)L}\right) \\ &\quad -(k_1 - k_2)(k_3 - k_4)\left(e^{i(k_1+k_2)L} + e^{i(k_3+k_4)L}\right). \end{aligned}$$

We order our four roots such that $k_{1,i} \leq k_{2,i} \leq k_{3,i} \leq k_{4,i}$. Thus $k_{1,i} < 0$ and we expect this to make the dominant contribution. So,

$$\begin{aligned}\Theta &= e^{ik_1L}[-(k_2-k_3)(k_1-k_4)\left(e^{i(k_2+k_3-k_1)L}+e^{ik_4L}\right)\\ &\quad +(k_1-k_3)(k_2-k_4)\left(e^{ik_3L}+e^{i(k_2+k_4-k_1)L}\right)\\ &\quad -(k_1-k_2)(k_3-k_4)\left(e^{ik_2L}+e^{i(k_3+k_4-k_1)L}\right)].\end{aligned} \tag{5.62}$$

Now,

$$\begin{aligned} k_{2,i} &\leq k_{3,i} \leq k_{4,i},\\ k_{2,i} &\leq k_{3,i} \leq k_{2,i}+k_{3,i}-k_{1,i},\\ k_{2,i} &\leq k_{3,i} \leq k_{2,i}+k_{4,i}-k_{1,i},\\ k_{2,i} &\leq k_{3,i} \leq k_{3,i}+k_{4,i}-k_{1,i},\end{aligned} \tag{5.63}$$

from which we conclude that the terms varying like e^{ik_2L} and e^{ik_3L} are the next most important. Keeping only these and setting $\Theta = 0$ we get

$$-(k_1-k_3)(k_2-k_4)\,e^{ik_3L}+(k_1-k_2)(k_3-k_4)\,e^{ik_2L}=0, \tag{5.64}$$

or,

$$e^{i(k_2-k_3)L}=\frac{(k_1-k_3)(k_2-k_4)}{(k_1-k_2)(k_3-k_4)}, \tag{5.65}$$

or,

$$i(k_2-k_3)L=\log\left(\frac{(k_1-k_3)(k_2-k_4)}{(k_1-k_2)(k_3-k_4)}\right)+2n\pi i, \tag{5.66}$$

i.e.

$$k_2-k_3=\frac{-i}{L}\log\left(\frac{(k_1-k_3)(k_2-k_4)}{(k_1-k_2)(k_3-k_4)}\right)+\frac{2n\pi}{L}, \tag{5.67}$$

and when L is large, we conclude that the imaginary parts of k_2 and k_3 will be approximately equal and the real parts will differ by a multiple of $2\pi/L$. This is because

$$\frac{(k_1-k_3)(k_2-k_4)}{(k_1-k_2)(k_3-k_4)}$$

is bounded for ω small. It is worth noting at this point that, had we chosen our x-range for this problem to be $-L < x < 0$ and thus been concerned with the wavenumbers with largest, rather than smallest (most negative) imaginary

parts, we would have arrived at the same condition. By choosing the x-range to be $0 < x < L$ we have chosen downstream-growing waves as being important.

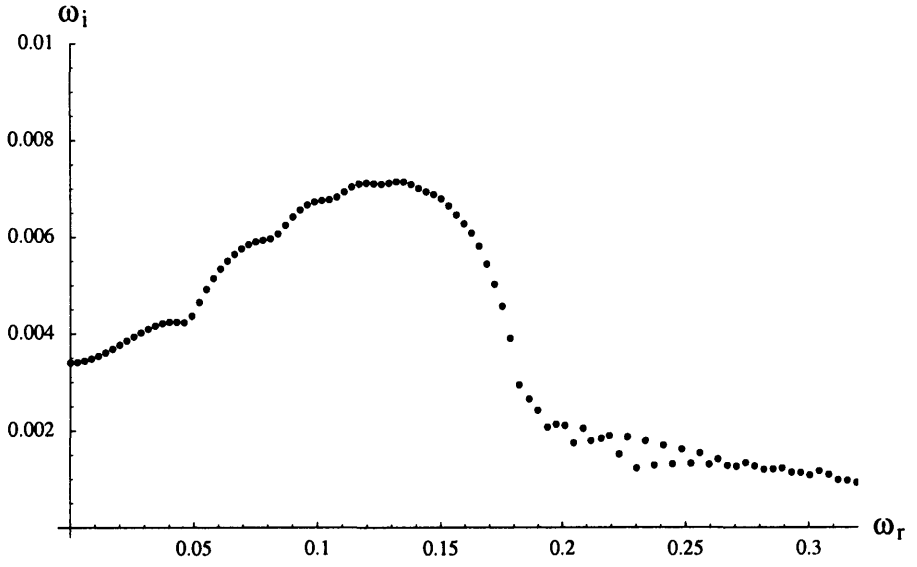

Figure 5.10: The eigenvalues, ω, in the complex plane, for $L = 1000$.

As an example, we consider two modes for $L = 1000$. These are at $\omega = 0.120451 + 0.00711885i$ and $\omega = 0.123457 + 0.00710552i$. The first gives

$$\begin{aligned} k_1 &= 1.66763 - 0.00927327i, \\ k_2 &= -1.93489 - 0.00687864i, \\ k_3 &= 0.133785 - 0.00314921i, \\ k_4 &= 0.133478 + 0.0193011i, \end{aligned} \tag{5.68}$$

and we have

$$\begin{aligned} k_2 - k_3 &= -2.06868 - 0.00372942i, \\ \frac{-i}{L}\log\left(\frac{(k_1-k_3)(k_2-k_4)}{(k_1-k_2)(k_3-k_4)}\right) &= -0.00157515 - 0.00366935i. \end{aligned} \tag{5.69}$$

Therefore, the log term accounts for the fact that $\mathrm{Im}(k_2 - k_3) = 0$ is a somewhat poor approximation. Note that $-329\frac{2\pi}{L} = -2.06717$ which, when the correction due to the log term is added, gives a good approximation to $\mathrm{Re}(k_2 - k_3)$.

For the second value of ω, we have

$$\begin{aligned} k_1 &= 1.66371 - 0.0093035i, \\ k_2 &= -1.93779 - 0.00684659i, \\ k_3 &= 0.137145 - 0.0032068i, \\ k_4 &= 0.136943 + 0.0193569i \end{aligned} \tag{5.70}$$

and

$$\begin{aligned} k_2 - k_3 &= -2.07494 - 0.0036398i, \\ \frac{-i}{L}\log\left(\frac{(k_1-k_3)(k_2-k_4)}{(k_1-k_2)(k_3-k_4)}\right) &= -0.00157043 - 0.00366296i. \end{aligned} \tag{5.71}$$

Now, $-330\frac{2\pi}{L} = -2.07345$, which suggests that n is 1 larger (in magnitude) here. In fact, the change in $\mathrm{Re}(k_2 - k_3)$ is 0.006260, close to $\frac{2\pi}{L} = 0.006283$.

We now note that, for our second set of data, $n/L = -0.33$. Fixing this as $k_2 - k_3$ we get, in the infinite-range limit, $\omega = 0.12275802 + 0.0053534647i$ as a root. Substituting the corresponding ks into the r.h.s. of (5.67) we get

$$k_2 - k_3 = -2.07502 - 0.0036667i, \tag{5.72}$$

a substantial improvement on our original guess of $-0.33 \times 2\pi = -2.07345$. This scheme will subsequently be referred to as the 'second approximation'. The numerical answer is as in (5.71).

As a way of slightly improving our scheme, we note that, looking at (5.67),

$$\begin{aligned} |\mathrm{Re}(k_1 - k_3)| &\gg |\mathrm{Im}(k_1 - k_3)|, & \mathrm{Re}(k_1 - k_3) &> 0, \\ |\mathrm{Re}(k_2 - k_4)| &\gg |\mathrm{Im}(k_2 - k_4)|, & \mathrm{Re}(k_2 - k_4) &< 0, \\ |\mathrm{Re}(k_1 - k_2)| &\gg |\mathrm{Im}(k_1 - k_2)|, & \mathrm{Re}(k_1 - k_2) &> 0, \\ |\mathrm{Im}(k_3 - k_4)| &\gg |\mathrm{Re}(k_3 - k_4)|, & \mathrm{Im}(k_3 - k_4) &< 0, \end{aligned} \quad \text{and} \tag{5.73}$$

for the range of ωs where we have solutions. This means the term inside the log term is almost purely imaginary, with negative coefficient. Thus, the log part will have an imaginary part of roughly $-\pi/2$. We may make a slight correction of $-\frac{\pi}{2L}$ to the real part of $k_2 - k_3$. Finally, we use this slightly improved scheme

to plot our first and second approximations for several values of n. We see that there is good agreement between the second approximations and the numerical results.

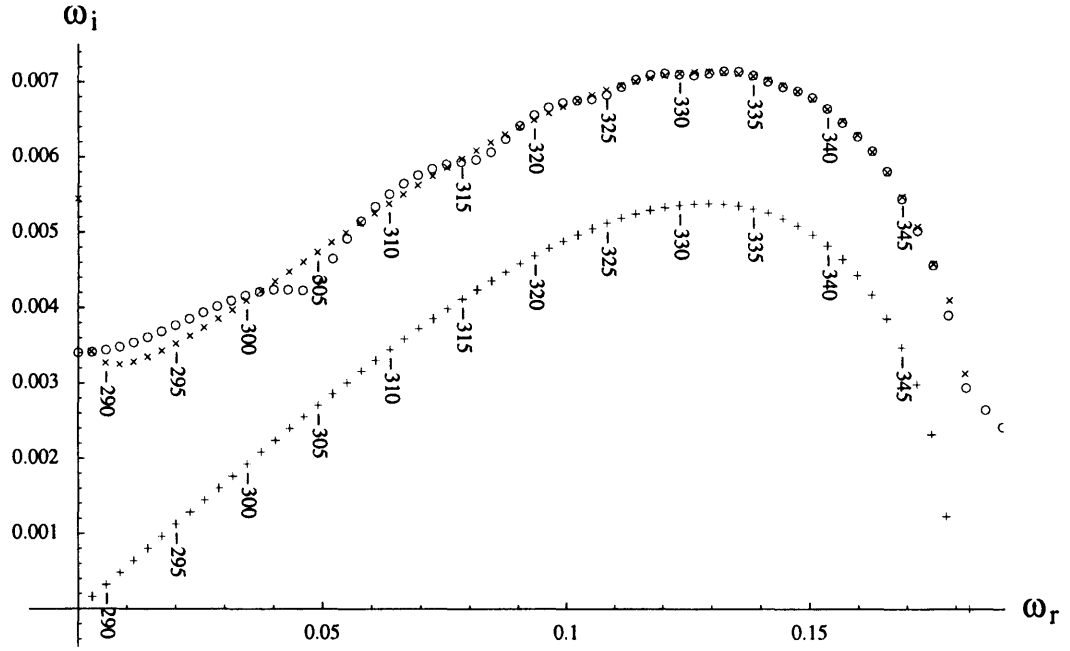

Figure 5.11: The first (+) and second (×) approximations to the eigenvalue solutions to our system, according to the scheme described in the text. The numbers next to every fifth point are the corresponding values of n. The numerical results for ω with strictly positive imaginary part are shown as octagons.

We summarise the consequences of equation (5.67) in the limit $L \to \infty$ as follows: as mentioned before, we expect the term which forms the argument of the log function to be bounded. This means that, as $L \to \infty$, $\mathrm{Im}(k_2 - k_3) \to 0$. We expect the infinite-range limit of this problem to approach the curve given by this criterion. Firstly, we examine which wavenumber is which. Looking at equations (5.68) and (5.70) we see that k_1 corresponds to the curve marked 3 in Figure 3.3, k_2 curve 4, k_3 curve 1 and k_4 curve 2.

Thus k_1 is, by the choice of preferring downstream-growing modes discussed above, downstream-growing. It is upstream-travelling. k_2 is also downstream-growing and upstream-travelling. k_3 however, although it grows downstream, is downstream-travelling. Therefore, our criterion for the infinite-range limit is equivalent to saying that the upstream-travelling k_2 must grow as much as the downstream-travelling k_3, in the same direction. It is easy to see, then, how they can 'cancel each other out'.

The curve given by the condition $\mathrm{Im}(k_2 - k_3) = 0$ is shown in Figure 5.12. It is equivalent to drawing a continuous curve through the +s in Figure 5.11. We saw above, of course, that the shape is approximately correct, but the imaginary part is smaller than in the $L = 1000$ case. This is not entirely surprising, as we may compare it to the results of Section 5.4, for which solutions were found to tend to their limiting value very slowly.

An important point to note about this system is that, for any L, it is rendered unstable by means of global modes. Thus, in the infinite-range limit, as the modes approach the curve shown in Figure 5.12, remaining unstable, we expect perturbations still to grow everywhere. This is in contrast with the homogeneous system, i.e. that without rigid partitions anywhere, in Section 3.3, which is convectively unstable. The system discussed in this chapter exhibits feedback between the ends, determining its stability properties for any length of nonhomogeneity. We conclude that stability properties of a nonhomogeneous system exhibiting feedback, in the infinite-range limit, may be different from the stability properties of the homogeneous equivalent.

It is worth briefly comparing this with the linearised Ginzburg-Landau equation. The equivalent of (5.12) for the range $0 < x < L$ (as opposed to $0 < x < \pi$) is

$$u(x,t) = \exp\left[\left(-c^2/4 - \left(\frac{n\pi}{L}\right)^2 + b_0\right)t\right] e^{\frac{cx}{2}} \sin\left(\frac{n\pi}{L}x\right). \tag{5.74}$$

With the same condition for convective instability as before, it is clear that

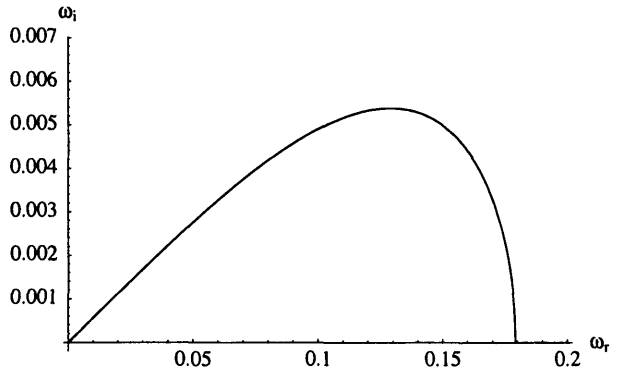

Figure 5.12: The curve, in the ω-plane, obtained by equating the imaginary parts of the two wavenumbers k_2 and k_3, as defined in the text. It is equal to the continuous stability spectrum for the nonhomogeneous system with an aperture, in the infinite-range limit.

this system remains stable for any length. We conclude that a system without feedback, which is convectively unstable in the homogeneous case, will remain stable in the nonhomogeneous case in the limit of long length.

5.7 Large-L comparison with Chapter 4

We now wish to compare the results of this chapter, for L large, with those of the second part of the previous chapter, also in the long-length limit. We begin with the contracted channel from Chapter 4. It is clear that we should consider the straight-channel results of this chapter for channels of two different widths: one with the same width as sections $\langle 1 \rangle$ and $\langle 3 \rangle$ from Chapter 4 (Figure 4.6) and one with the same width as section $\langle 2 \rangle$.

As as mentioned in Section 5.2, all the channels considered so far in this chapter have had the same width and base-flow velocity as those in sections $\langle 1 \rangle$ and $\langle 3 \rangle$ of the channels in the previous chapter. Thus, Figure 5.6 is an example of some large-L results for this case. Comparing this with Figure 4.11

for the $L = 200$ case, we see very little similarity. For example, in Figure 4.11, solutions are only found for $\omega_r > 0.415$ and this is not the case in Figure 5.6. We conclude that the mechanisms for instability in the contracted-channel case probably do not correspond to the mechanisms for instability in a fixed-width system with a finite-length aperture and the same width as sections $\langle 1 \rangle$ and $\langle 3 \rangle$.

Although it is not shown in Figure 5.6, it is worth noting that the solutions in this case do not extend beyond $\omega_r \approx 0.415$. We now perform the finite-length aperture calculation for a fixed-width channel with the same width and base-flow velocities as section $\langle 2 \rangle$ in the contracted-channel case from the previous chapter; the result is shown in Figure 5.13. We can see that here, the range of ω_r extends to $\omega_r \approx 0.649$, as it does in Figure 4.11 in the $L = 200$ case. We also note that, although the size of the imaginary parts are quite different (the lengths are different too) in the range $0.415 < \omega_r < 0.649$, the patterns of modes in Figures 5.13 and 4.12 have some similarities. For example, the larger values of ω_i occur for smaller ω_r. A difference between the two is that, of course, for the variable-width-channel case, there are no modes with $\omega_r < 0.415$. We conclude that, when $0.415 < \omega_r < 0.649$, the mechanisms of instability may be similar in the two cases but, when $\omega_r < 0.415$, either the change in shape of the channel, or the constraint on the directions in which waves may travel, prevents modes being observed in a variable-width channel.

We now move our attention to the comparison of the results in this chapter with those for a channel with an expanded section from the previous chapter (Section 4.4.2). Again, Figure 5.6 has the same parameters as sections $\langle 1 \rangle$ and $\langle 3 \rangle$ for the channel in the previous chapter. We now plot its equivalent, for the parameters for section $\langle 2 \rangle$ in the previous chapter, in Figure 5.14. These may both be compared with the $L = 600$ case in Figure 4.20. Again, we see that the variable-width problem bears more resemblance to the finite-length aperture

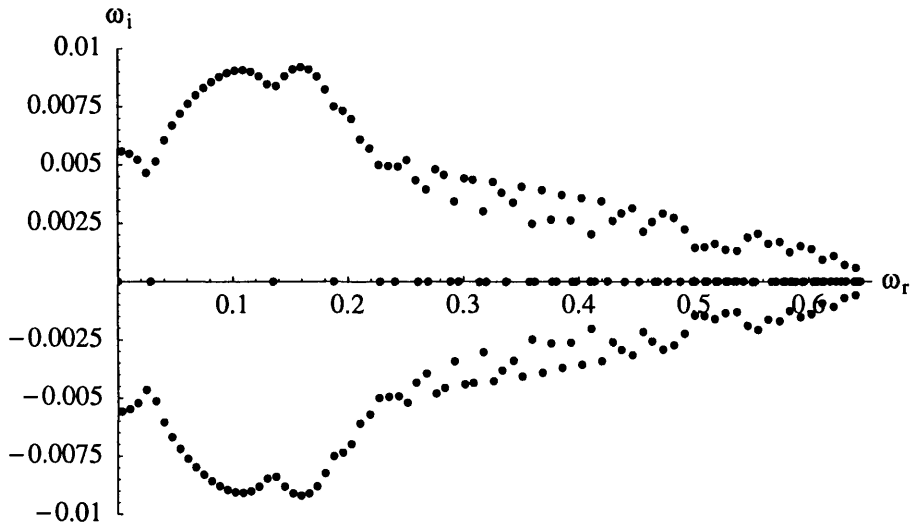

Figure 5.13: The eigenvalues, ω, in the complex plane, which solve the stability problem for a fixed-width channel with a finite-range aperture, with channel dimensions and flow velocities equal to those in the middle section of the contracted-channel problem considered in Chapter 4. Here $L = 500$.

problem with the same parameters as the middle section than it does to the finite-length aperture problem with the same parameters as the semi-infinite sections. Here, however, it seems that neither the variation in width, nor the constraint on the directions in which waves may travel has a great effect on the distribution.

5.8 Summary

The stability of two-fluid flow through a rigid pipe has been considered. The fluids are separated by a solid wall, in which there is a finite-length aperture. The physics is similar to that considered in Chapters 3 and 4 and again instability is found, due to feedback between the ends. This is an example of an infinite-range problem which is convectively unstable leading to a finite-range problem which is unstable. That this is not always the case is demonstrated

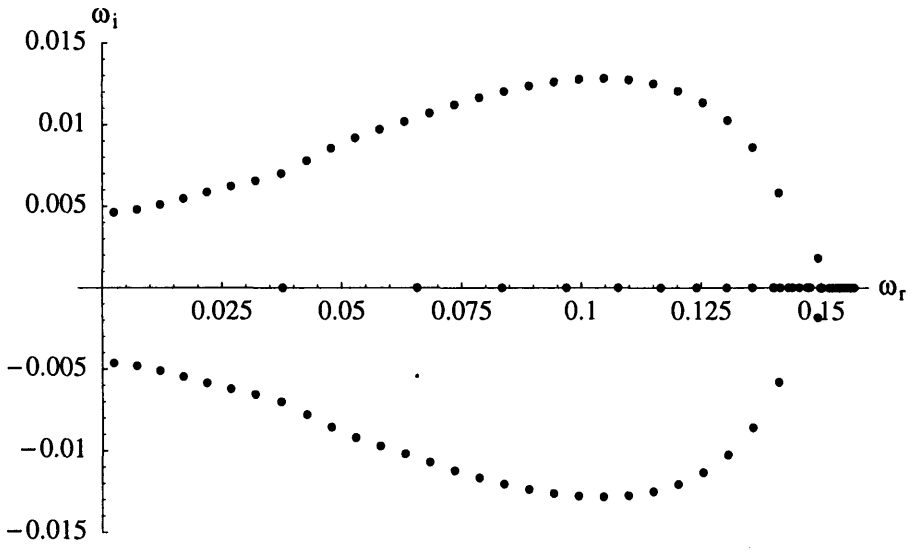

Figure 5.14: The eigenvalues, ω, in the complex plane, which solve the stability problem for a fixed-width channel with a finite-length aperture, with channel dimensions and flow velocities equal to those in the middle section of the expanded-channel problem considered in Chapter 4. Here $L = 400$.

by consideration of the linearised Ginzburg-Landau equation.

Some analysis has then been performed of special cases with purely-real or purely-imaginary frequencies, which are more amenable to simple solution than the full problem.

Next, an infinite-aperture-length limit for the spectrum of unstable modes has been derived. It has been shown that unstable global modes will continue to occur in this limit, meaning that the infinite-range system has different stability properties to the corresponding homogeneous system. This has again been compared to the linearised Ginzburg-Landau equation.

Finally, some comparisons have been made with the eigenvalue spectra for the problems considered in Chapter 4.

Chapter 6

Instability due to feedback between stable waves

6.1 Introduction

In Chapters 4 and 5, we have seen that a global instability mode can arise in a nominally convectively unstable flow provided two conditions are satisfied: (i) the flow supports both upstream- and downstream-travelling waves with instability properties sufficient for feedback, and (ii) sufficiently strong nonhomogeneity is found in the flow to provide wave scattering and receptivity for waves of different families. The feedback between waves of such families is a key element in this kind of instability.

In this chapter we will consider the evolution of signals which, amplified over a finite range in space or a finite interval of time, may be sufficient to set up an end-to-end interaction in a system with strong nonhomogeneity. A system confined to a finite range is an example of such a strongly-nonhomogeneous system. We will call this phenomenon transient feedback and will attempt to demonstrate global instability due to it.

As mentioned in Chapter 1, it is well known that a finite range of local ab-

solute instability can lead to global instability (see e.g. [35]). As was demonstrated in the previous chapters, however, with feedback modes, convective instability can be sufficient. Here we will study systems which, if infinite in extent, would be considered stable, i.e. disturbances would decay everywhere. We choose systems which can support strong transients and hope to use these transients to provide sufficient growth of disturbances to form a feedback loop and thus create global instability.

In this chapter we will study two such systems. The first comprises three linear kinematic wave equations with coupled wave operators. The parameters of this coupling can be varied to create arbitrarily-large transients when the waves which solve the equations are close to resonance. The system is shown to be unstable when confined to a finite range of appropriate length, despite the infinite-range problem being stable. Some asymptotics are done on the distribution of unstable modes for such a system when two of the waves are in resonance, when the 'mode number' is large. Some comments are made about the near-resonant case and about the near-periodicity of modes in the frequency plane.

The second system studied here comprises two linear kinematic wave equations, again with coupled wave operators. This system is sufficiently simple to admit solutions to an initial value problem on an infinite range. On a restricted range, it is found to be unstable when the coupling parameter, which again allows for transient growth, is sufficiently large in magnitude. An energy integral of the system is used to demonstrate that the end conditions do not feed energy into the system. Finally, the two systems are compared.

The content of this chapter was presented as a joint paper with my supervisor, Dr Sergei Timoshin, in [64].

6.2 A three-wave system exhibiting instability due to transient growth

The first system we consider consists of the following set of linear kinematic wave equations:

$$\begin{aligned} \frac{\partial u}{\partial t} - c_1 \frac{\partial u}{\partial x} + \beta_1 u &= a_1 v, \\ \frac{\partial v}{\partial t} - c_2 \frac{\partial v}{\partial x} + \beta_2 v &= a_2 w, \\ \frac{\partial w}{\partial t} + c_3 \frac{\partial w}{\partial x} + \beta_3 w &= 0, \end{aligned} \tag{6.1}$$

with c_1, c_2, c_3, β_1, β_2 and β_3 taken to be real and positive. These equations are chosen as a representative example of a simple differential system, rather than as a model of any particular physical system. From these, in an infinite (homogeneous) system we can derive a dispersion relation. We put $u = u_0 e^{i(kx-\omega t)}$, $v = v_0 e^{i(kx-\omega t)}$ and $w = w_0 e^{i(kx-\omega t)}$, as is usual for such problems. Substitution into (6.1) gives

$$\begin{aligned} -i\omega u_0 - ikc_1 u_0 + \beta_1 u_0 &= a_1 v_0, \\ -i\omega v_0 - ikc_2 v_0 + \beta_2 v_0 &= a_2 w_0, \\ -i\omega w_0 + ikc_3 w_0 + \beta_3 w_0 &= 0. \end{aligned} \tag{6.2}$$

Substituting the first into the second of these gives

$$(-i\omega - ikc_2 + \beta_2) \frac{1}{a_1} (-i\omega - ikc_1 + \beta_1) u_0 = a_2 w_0 \tag{6.3}$$

and this into the third equation gives

$$(-i\omega + ikc_3 + \beta_3) \frac{1}{a_2} (-i\omega - ikc_2 + \beta_2) \frac{1}{a_1} (-i\omega - ikc_1 + \beta_1) u_0 = 0, \tag{6.4}$$

or,

$$(\omega + kc_1 + i\beta_1)(\omega + kc_2 + i\beta_2)(\omega - kc_3 + i\beta_3) = 0. \tag{6.5}$$

The roots $\omega_1 = -kc_1 - i\beta_1$ and $\omega_2 = -kc_2 - i\beta_2$ correspond to leftward-travelling waves and $\omega_3 = kc_3 - i\beta_3$ to a rightward-travelling one. It is clear

that, for any real wavenumber k, as β_1, β_2 and β_3 are positive real numbers, all waves will decay in time. It is important to remember that each of u, v and w can be written as a linear combination of the waves corresponding to these roots. For example,

$$u(x,t) = e^{-\beta_1 t} u_1(x + c_1 t) + e^{-\beta_2 t} u_2(x + c_2 t) + e^{-\beta_3 t} u_3(x - c_3 t). \quad (6.6)$$

This will be the case unless the left-going waves are in resonance, which will occur when $\beta_1 = \beta_2$ and $c_1 = c_2$, In this case the solutions will have a term varying like $te^{\beta_1 t}$, for example,

$$u(x,t) = e^{-\beta_1 t} u_1(x + c_1 t) + te^{-\beta_1 t} u_2(x + c_1 t) + e^{-\beta_3 t} u_3(x - c_3 t). \quad (6.7)$$

We note that, although the dispersion relation is independent of the coupling coefficients a_1 and a_2, the solutions (6.6) and (6.7) depend on their presence. For example, if $a_1 = 0$, we have as a general solution for u

$$u(x,t) = e^{-\beta_1 t} u_1(x + c_1 t) \quad (6.8)$$

only. This is similar for v, if $a_2 = 0$. From (6.6) and (6.7) we conclude that, in any infinite system governed by (6.1), disturbances will always (eventually) decay.

We now proceed to place some inhomogeneities in our system. We do this in the simplest way, by enclosing it in a box, $0 < x < L$. We also consider the boundary conditions of the system to act only on u. This enables us to rewrite (6.1) as

$$\widetilde{D}_1 \widetilde{D}_2 \widetilde{D}_3[u] = 0, \quad (6.9)$$

with, for example, $\widetilde{D}_1 = \frac{\partial}{\partial t} - c_1 \frac{\partial}{\partial x} + \beta_1$ and similarly for $\widetilde{D}_2$ and $\widetilde{D}_3$. The boundary conditions we choose at the ends are those which model the semi-infinite regions $(-\infty, 0)$ and (L, ∞) containing very heavy damping. Thus we

have

$$\begin{aligned} u(0,t) &= 0, \\ u(L,t) &= 0, \\ \tfrac{\partial u}{\partial x}(L,t) &= 0. \end{aligned} \tag{6.10}$$

Note that, as our system is third-order in x, we have three boundary conditions. As our new system only has explicit dependence on x, and not on t, we consider disturbances to be of the form

$$u(x,t) = e^{-i\omega t}\bar{u}(x) \tag{6.11}$$

in the case with no resonance between leftward-travelling waves, with the eigenvalue, ω, in (6.11) to be determined. At each frequency ω, we take the x-variation to be in the form of three waves with wavenumbers satisfying (6.5). Equation (6.6), with (6.11), becomes

$$\bar{u}(x) = A_1 e^{\frac{\beta_1 - i\omega}{c_1}x} + A_2 e^{\frac{\beta_2 - i\omega}{c_2}x} + A_3 e^{-\frac{\beta_3 - i\omega}{c_3}x} \tag{6.12}$$

for constant A_1, A_2 and A_3, say. Our boundary conditions (6.10) are

$$\begin{gathered} A_1 + A_2 + A_3 = 0, \\ A_1 e^{\frac{\beta_1 - i\omega}{c_1}L} + A_2 e^{\frac{\beta_2 - i\omega}{c_2}L} + A_3 e^{-\frac{\beta_3 - i\omega}{c_3}L} = 0, \\ A_1 \tfrac{\beta_1 - i\omega}{c_1} e^{\frac{\beta_1 - i\omega}{c_1}L} + A_2 \tfrac{\beta_2 - i\omega}{c_2} e^{\frac{\beta_2 - i\omega}{c_2}L} - A_3 \tfrac{\beta_3 - i\omega}{c_3} e^{-\frac{\beta_3 - i\omega}{c_3}L} = 0. \end{gathered} \tag{6.13}$$

Eliminating A_3, we obtain

$$\begin{gathered} A_1\left(e^{\frac{\beta_1 - i\omega}{c_1}L} - e^{-\frac{\beta_3 - i\omega}{c_3}L}\right) = A_2\left(e^{-\frac{\beta_3 - i\omega}{c_3}L} - e^{\frac{\beta_2 - i\omega}{c_2}L}\right), \\ A_1\left(\tfrac{\beta_1 - i\omega}{c_1} e^{\frac{\beta_1 - i\omega}{c_1}L} + \tfrac{\beta_3 - i\omega}{c_3} e^{-\frac{\beta_3 - i\omega}{c_3}L}\right) = -A_2\left(\tfrac{\beta_3 - i\omega}{c_3} e^{-\frac{\beta_3 - i\omega}{c_3}L} + \tfrac{\beta_2 - i\omega}{c_2} e^{\frac{\beta_2 - i\omega}{c_2}L}\right), \end{gathered} \tag{6.14}$$

or

$$\begin{gathered} A_1\left(e^{\mu_1 L} - 1\right) = A_2\left(1 - e^{\mu_2 L}\right), \\ A_1\left(\tfrac{\beta_1 - i\omega}{c_1} e^{\mu_1 L} + \tfrac{\beta_3 - i\omega}{c_3}\right) = -A_2\left(\tfrac{\beta_3 - i\omega}{c_3} + \tfrac{\beta_2 - i\omega}{c_2} e^{\mu_2 L}\right), \end{gathered} \tag{6.15}$$

with

$$\begin{aligned} \mu_1 &= \tfrac{\beta_1 - i\omega}{c_1} + \tfrac{\beta_3 - i\omega}{c_3}, \\ \mu_2 &= \tfrac{\beta_2 - i\omega}{c_2} + \tfrac{\beta_3 - i\omega}{c_3}. \end{aligned} \tag{6.16}$$

Thus,

$$\left(e^{\mu_1 L}-1\right)\left(\frac{\beta_3-i\omega}{c_3}+\frac{\beta_2-i\omega}{c_2}e^{\mu_2 L}\right)=\left(e^{\mu_2 L}-1\right)\left(\frac{\beta_1-i\omega}{c_1}e^{\mu_1 L}+\frac{\beta_3-i\omega}{c_3}\right). \tag{6.17}$$

The first thing to note about this system is that there is obviously a solution when

$$\frac{\beta_1-i\omega}{c_1}=\frac{\beta_2-i\omega}{c_2}, \tag{6.18}$$

i.e.

$$\omega=i\frac{\beta_1 c_2-\beta_2 c_1}{c_1-c_2}. \tag{6.19}$$

However, this amounts to two waves being identical in (6.12), so that it is no longer a solution of the form (6.6). We must therefore search for a solution of the resonant form for this. We note that ω is purely imaginary and that ω_i can be either positive (unstable) or negative (stable). We will return to this later, as we wish to discuss solutions to the resonant equation beforehand.

There are, however, many other roots of (6.17) which are not solutions of (6.19). We begin by demonstrating that, for certain combinations of parameters, the system can be stable. This is shown in Figure 6.1(a). Note that the results are shown in terms of $\lambda=-i\omega$, so $\omega_r=-\lambda_i$ and $\omega_i=\lambda_r$; the eigenvalues with $\lambda_r<0$ correspond to exponential decay in time. We can see also that the results are symmetric in λ_i.

Figure 6.1(b) shows, however, that for other combinations of parameters the system may be unstable. We note that the terms

$$s_1=\frac{\beta_1-i\omega}{c_1},\quad s_2=\frac{\beta_2-i\omega}{c_2},\quad s_3=-\frac{\beta_3-i\omega}{c_3} \tag{6.20}$$

in (6.12) satisfy $\mathrm{Re}(s_1)>0$, $\mathrm{Re}(s_2)>0$, $\mathrm{Re}(s_3)<0$, even for unstable modes ($\omega_i>0$). Thus the waves u_1, u_2 and u_3 still all decay in the direction of their propagation. Figure 6.2 shows, for two (unstable) modes, how the three waves which comprise u 'fit into' the range $(0,L)$.

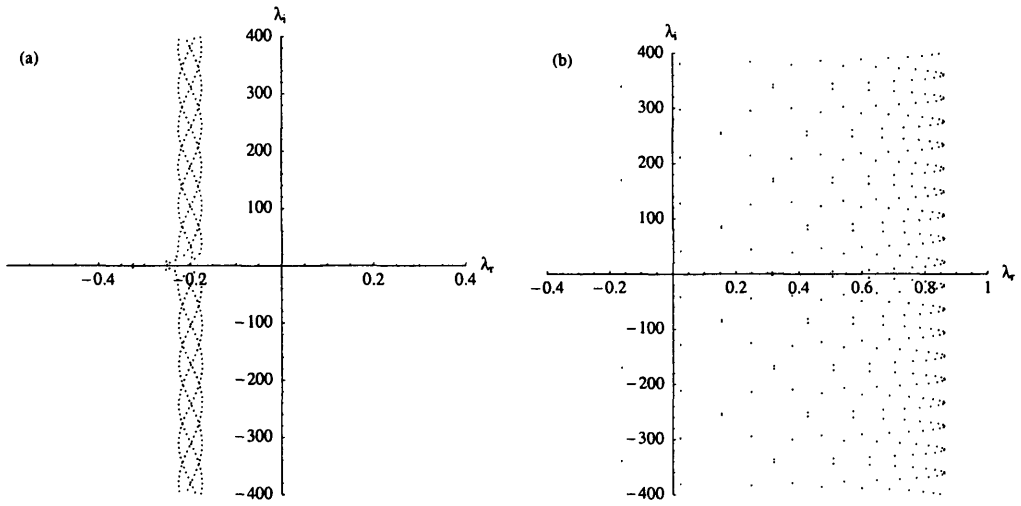

Figure 6.1: Solutions to the finite-range system, for the parameters (a) $\beta_1 = 3$, $\beta_2 = 0.5$, $\beta_3 = 0.7$, $c_1 = 0.4$, $c_2 = 0.25$, $c_3 = 0.55$, $L = 0.5$ and (b) $\beta_1 = 0.5$, $\beta_2 = 0.5$, $\beta_3 = 0.2$, $c_1 = 0.27$, $c_2 = 0.25$, $c_3 = 0.5$, $L = 0.5$. The results are shown in terms of $\lambda = -i\omega$.

We seek an explanation for the instability for case (b) in Figure 6.1 in terms of the near-resonance between the left-going waves. When there is an exact resonance between our left-going waves, the solution to our general equation is of the form

$$\bar{u}(x) = (A_1 + A_2 x)e^{\frac{\beta_1 - i\omega}{c_1}x} + A_3 e^{-\frac{\beta_3 - i\omega}{c_3}x}. \tag{6.21}$$

This clearly shows a spatial transient for the components corresponding to left-going waves. When the end conditions (6.10) are applied, we have

$$\begin{gathered} A_1 + A_3 = 0, \\ A_1 e^{\frac{\beta_1 - i\omega}{c_1}L} + A_2 L e^{\frac{\beta_1 - i\omega}{c_1}L} + A_3 e^{-\frac{\beta_3 - i\omega}{c_3}L} = 0, \\ A_1 \frac{\beta_1 - i\omega}{c_1} e^{\frac{\beta_1 - i\omega}{c_1}L} + A_2 e^{\frac{\beta_1 - i\omega}{c_1}L} + A_2 L \frac{\beta_1 - i\omega}{c_1} e^{\frac{\beta_1 - i\omega}{c_1}L} - A_3 \frac{\beta_3 - i\omega}{c_3} e^{-\frac{\beta_3 - i\omega}{c_3}L} = 0, \end{gathered} \tag{6.22}$$

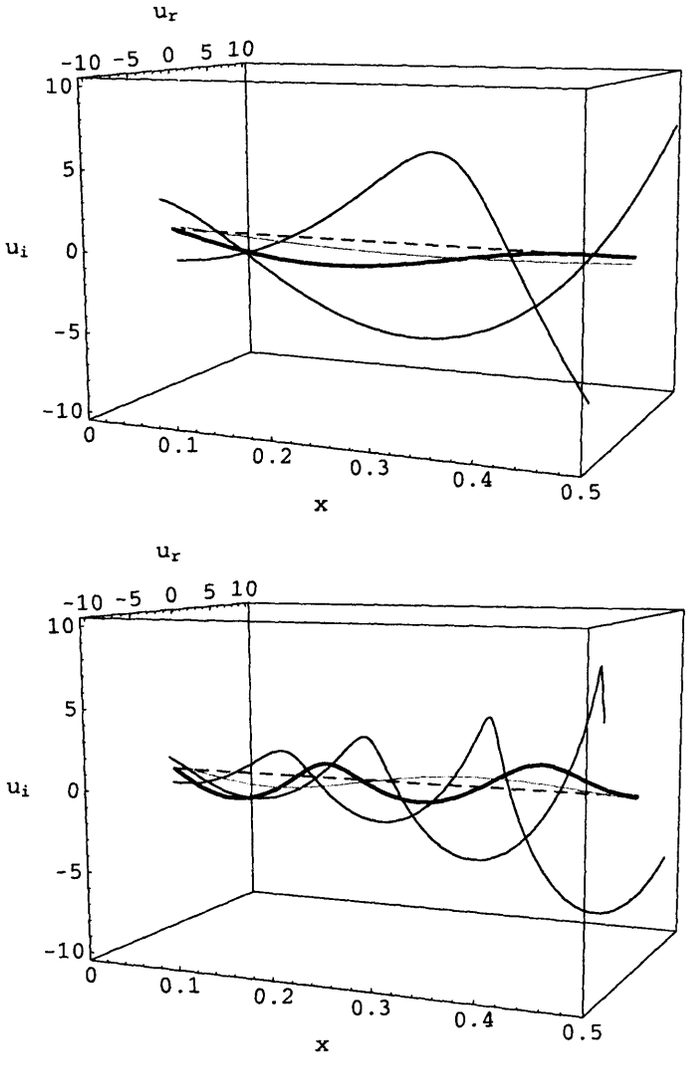

Figure 6.2: Two diagrams showing how the three waves which comprise u 'fit into' our range $(0, L)$. The thin lines represent the three waves, with the grey line being the right-going one. The thick line is the sum of the three and the dashed line is the $u = 0$ axis. We have parameters $\beta_1 = 0.5$, $\beta_2 = 0.5$, $\beta_3 = 0.2$, $c_1 = 0.27$, $c_2 = 0.25$, $c_3 = 0.5$ and $L = 0.5$. The upper diagram is for the mode $\omega = 0.315 + 2.552i$ and the lower one, the mode $\omega = 0.623 + 6.919i$.

or

$$\begin{aligned} A_1\left(e^{\frac{\beta_1-i\omega}{c_1}L}-e^{-\frac{\beta_3-i\omega}{c_3}L}\right) &= -A_2Le^{\frac{\beta_1-i\omega}{c_1}L}, \\ A_1\left(\tfrac{\beta_1-i\omega}{c_1}e^{\frac{\beta_1-i\omega}{c_1}L}+\tfrac{\beta_3-i\omega}{c_3}e^{-\frac{\beta_3-i\omega}{c_3}L}\right) &= -A_2\left(e^{\frac{\beta_1-i\omega}{c_1}L}+L\tfrac{\beta_1-i\omega}{c_1}e^{\frac{\beta_1-i\omega}{c_1}L}\right). \end{aligned} \tag{6.23}$$

μ_1 is as given by (6.16) and

$$\begin{aligned} A_1\left(e^{\mu_1 L}-1\right) &= -A_2Le^{\mu_1 L}, \\ A_1\left(\tfrac{\beta_1-i\omega}{c_1}e^{\mu_1 L}+\tfrac{\beta_3-i\omega}{c_3}\right) &= -A_2\left(e^{\mu_1 L}+L\tfrac{\beta_1-i\omega}{c_1}e^{\mu_1 L}\right), \end{aligned} \tag{6.24}$$

or

$$\left(e^{\mu_1 L}-1\right)\left(e^{\mu_1 L}+L\frac{\beta_1-i\omega}{c_1}e^{\mu_1 L}\right) = Le^{\mu_1 L}\left(\frac{\beta_1-i\omega}{c_1}e^{\mu_1 L}+\frac{\beta_3-i\omega}{c_3}\right), \tag{6.25}$$

i.e.

$$\left(e^{\mu_1 L}-1\right)\left(1+L\frac{\beta_1-i\omega}{c_1}\right) = L\left(\frac{\beta_1-i\omega}{c_1}e^{\mu_1 L}+\frac{\beta_3-i\omega}{c_3}\right), \tag{6.26}$$

so

$$e^{\mu_1 L}-1-L\frac{\beta_1-i\omega}{c_1} = L\frac{\beta_3-i\omega}{c_3}, \tag{6.27}$$

that is

$$e^{\mu_1 L} = 1+L\left(\frac{\beta_1-i\omega}{c_1}+\frac{\beta_3-i\omega}{c_3}\right) = 1+\mu_1 L. \tag{6.28}$$

We put $z=\mu_1 L$ and so we are searching for solutions to

$$e^z = 1+z. \tag{6.29}$$

The solutions to this equation, for complex z, are shown in Figure 6.3. It is easy to derive an asymptotic approximation for the roots located far from the origin. Consider a root, z_0, of (6.29), which we can write as

$$z_0 = \log(z_0+1), \tag{6.30}$$

where log is $\log_e$. Then, choosing the same branch for log, the 'next root up', z_1, exists such that

$$z_1 = \log(z_1+1)+2\pi i, \tag{6.31}$$

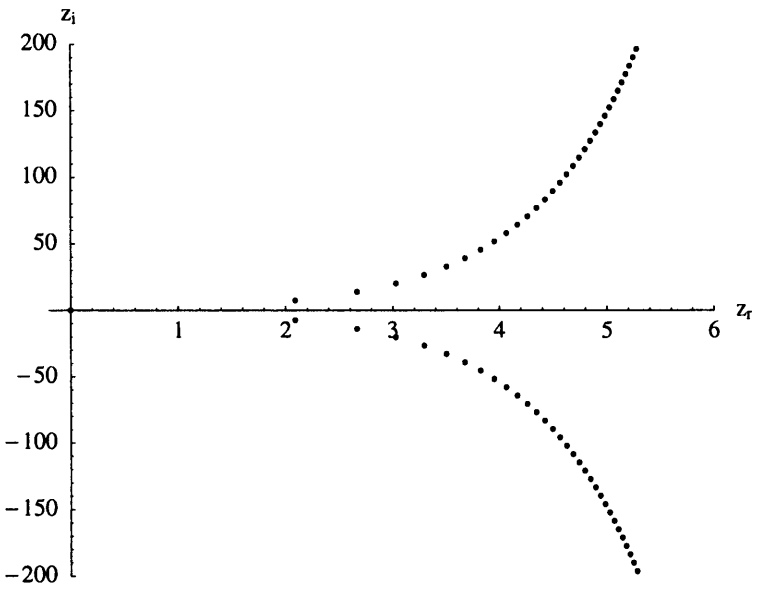

Figure 6.3: Solutions to $e^z = 1 + z$.

so

$$z_1 = z_0 + \log(z_1 + 1) - \log(z_0 + 1) + 2\pi i = z_0 + \log\left(\frac{z_1 + 1}{z_0 + 1}\right) + 2\pi i. \quad (6.32)$$

Similarly,

$$\begin{aligned} z_2 &= z_1 + \log\left(\tfrac{z_2+1}{z_1+1}\right) + 2\pi i \\ &= z_0 + \log\left(\tfrac{z_2+1}{z_1+1}\right) + \log\left(\tfrac{z_1+1}{z_0+1}\right) + 4\pi i \\ &= z_0 + \log\left(\tfrac{z_2+1}{z_0+1}\right) + 4\pi i. \end{aligned} \quad (6.33)$$

It is clear how this extends to

$$z_n = z_0 + \log\left(\frac{z_n + 1}{z_0 + 1}\right) + 2n\pi i. \quad (6.34)$$

Taking this expression for z_n and substituting it into the r.h.s. of the same equation gives

$$z_n = z_0 + \log\left(1 + \frac{\log\left(\tfrac{z_n+1}{z_0+1}\right) + 2n\pi i}{z_0 + 1}\right) + 2n\pi i. \quad (6.35)$$

We assume, to be justified in a moment, that the $\log\left(\tfrac{z_n+1}{z_0+1}\right)$ part of this equation grows no faster than $O(n)$ as $n \to \infty$. Thus,

$$\mathrm{Im}(z_n) = 2n\pi + O\left(\log(n)\right) \quad (6.36)$$

as $n \to \infty$. To examine the real part of z_n, consider (6.35) written as

$$z_n = z_0 + \log(n) + \log\left(\frac{1}{n}\left(z_0 + 1 + \log\left(\frac{z_n+1}{z_0+1}\right)\right) + 2\pi i\right) - \log(z_0+1) + 2n\pi i \tag{6.37}$$

and we have that

$$\mathrm{Re}(z_n) = \log(n) + O(1) \tag{6.38}$$

as $n \to \infty$. This, with (6.36), justifies our assumption. Considering (6.36) and (6.38), we have obtained the desired asymptotic approximation to solutions of (6.29).

We briefly return to the case of resonant solutions due to (6.19). This has a purely imaginary solution for ω and so can only be a solution of our resonant equation, (6.29), for the case $\mu_1 = 0$. This is equivalent to

$$\omega = -i\frac{\beta_1 c_3 + \beta_3 c_1}{c_1 + c_3}, \tag{6.39}$$

which is imaginary with negative imaginary part. Thus, any solution due to resonance of the form (6.19) must be stable if it exists.

We are now in a position to look at the near-resonant case. (6.17), multiplied through by L, may also be written as

$$\left(e^{\zeta_1-\zeta_3} - 1\right)\left(\zeta_2 e^{\zeta_2-\zeta_3} - \zeta_3\right) = \left(e^{\zeta_2-\zeta_3} - 1\right)\left(\zeta_1 e^{\zeta_1-\zeta_3} - \zeta_3\right), \tag{6.40}$$

where $\zeta_1 = s_1 L$, $\zeta_2 = s_2 L$ and $\zeta_3 = s_3 L$. We assume that ζ_1 and ζ_2 are close, by making c_1 and c_2 close and β_1 and β_2 close, i.e.

$$\begin{aligned} c_2 &= c_1 + \epsilon c_\epsilon, \\ \beta_2 &= \beta_1 + \epsilon \beta_\epsilon. \end{aligned} \tag{6.41}$$

We also expand ω as a power series

$$\omega = \omega_0 + \epsilon\omega_1 + \epsilon^2\omega_2 + O(\epsilon^3), \tag{6.42}$$

where ϵ is a small parameter. To keep things as simple as possible, we encapsulate the dependence on the various parts of ω into new quantities:

$$\begin{aligned} \zeta_0 &= \tfrac{\beta_1 - i\omega_0}{c_1} L, \\ \zeta_{\omega 1} &= \tfrac{-i\omega_1}{c_1} L, \\ \zeta_{\omega 2} &= \tfrac{-i\omega_2}{c_1} L. \end{aligned} \tag{6.43}$$

This gives

$$\begin{aligned} \zeta_1 &= \zeta_0 + \epsilon\zeta_{\omega 1} + \epsilon^2\zeta_{\omega 2} + O(\epsilon^3), \\ \zeta_2 &= \zeta_0 + \epsilon\left(\tfrac{\beta_\epsilon L - c_\epsilon\zeta_0}{c_1} + \zeta_{\omega 1}\right) + \epsilon^2\left(-\tfrac{c_\epsilon}{c_1^2}\left(\beta_\epsilon L - c_\epsilon\zeta_0 + c_1\zeta_{\omega 1}\right) + \zeta_{\omega 2}\right) + O(\epsilon^3), \\ \zeta_3 &= \tfrac{1}{c_3}\left(\beta_1 L - \beta_3 L - c_1\zeta_0\right) - \epsilon\tfrac{c_1}{c_3}\zeta_{\omega 1} - \epsilon^2\tfrac{c_1}{c_3}\zeta_{\omega 2} + O(\epsilon^3). \end{aligned} \tag{6.44}$$

We then note that, when $\epsilon = 0$, $\zeta_1 = \zeta_2$ and we have the resonant case, solved by solutions to $e^z = 1 + z$. Thus,

$$e^{\zeta_0 - \frac{1}{c_3}(\beta_1 L - \beta_3 L - c_1\zeta_0)} = 1 + \zeta_0 - \frac{1}{c_3}\left(\beta_1 L - \beta_3 L - c_1\zeta_0\right), \tag{6.45}$$

always. We use this to expand our dispersion relation (6.40). We note that, at order 1, each side of (6.40) is the same. Thus, the dispersion relation is solved identically. At order ϵ, the equation reduces to (6.45), which we know to be true. However, at order ϵ^2, we obtain

$$\begin{aligned} &\tfrac{1}{2c_1^2c_3^3}\left(\beta_3 L - \beta_1 L + (c_1 + c_3)\zeta_0\right)\left(c_3 + \beta_3 L - \beta_1 L + (c_1 + c_3)\zeta_0\right) \\ &\times \left(\beta_\epsilon L - c_\epsilon\zeta_0\right)\left(\beta_\epsilon c_3 L - c_3 c_\epsilon\zeta_0 + 2c_1(c_1 + c_3)\zeta_{\omega 1}\right) = 0. \end{aligned} \tag{6.46}$$

Each bracketed expression, apart from the last, contains ω_0, through ζ_0, only once. Rearranging each of these for such ω_0, we see that no bracketed expression can be equal to zero for all ω_0 which satisfy our (resonant) equation.

Therefore, the last bracketed expression must equal 0. This gives us

$$\zeta_{\omega 1} = \frac{c_3 c_\epsilon \zeta_0 - \beta_\epsilon c_3 L}{2c_1 (c_1 + c_3)}. \tag{6.47}$$

We rewrite this in terms of ω_0 and ω_1 to obtain

$$\omega_1 = -ic_3 \frac{\beta_\epsilon c_1 - \beta_1 c_\epsilon + ic_\epsilon \omega_0}{2c_1 (c_1 + c_3)}. \tag{6.48}$$

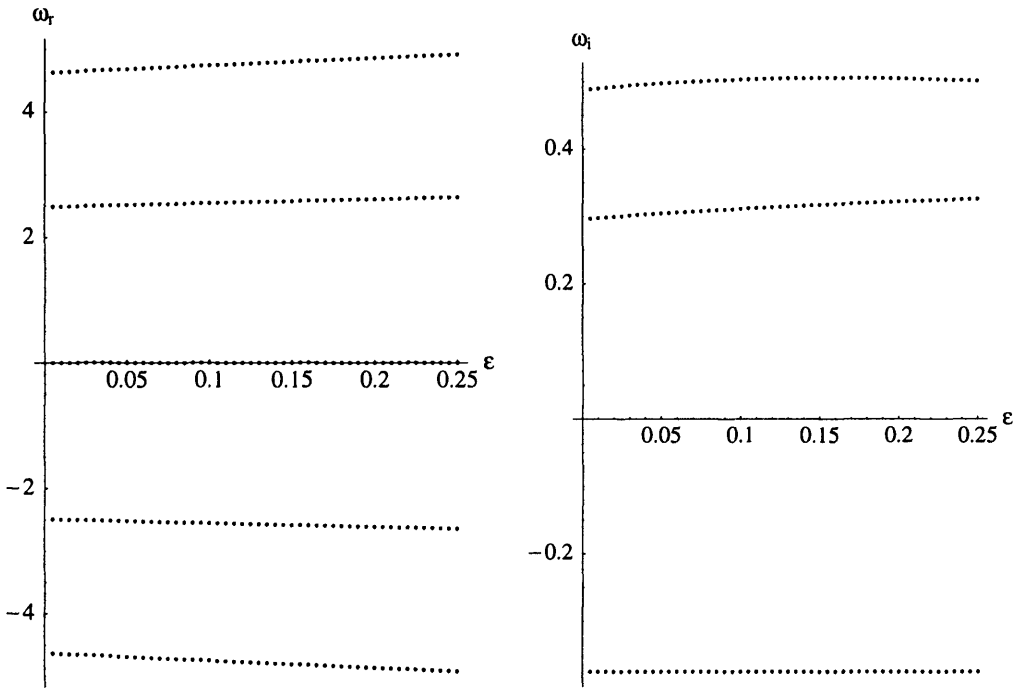

Figure 6.4: Solutions of the dispersion relation for our transiently-growing system, plotted for $\beta_2 = \beta_1 + \epsilon\beta_\epsilon$ and $c_2 = c_1 + \epsilon c_\epsilon$. Here we show the real (left) and imaginary (right) parts of ω against ϵ for $\beta_1 = 0.5$, $\beta_\epsilon = 0.1$, $\beta_3 = 0.2$, $c_1 = 0.25$, $c_\epsilon = 0.2$, $c_3 = 0.5$ and $L = 0.5$.

A numerical run for the set of parameters $\beta_1 = 0.5$, $\beta_\epsilon = 0.1$, $\beta_3 = 0.2$, $c_1 = 0.25$, $c_\epsilon = 0.2$, $c_3 = 0.5$ and $L = 0.5$ is shown in Figure 6.4. Fitting a fourth-order polynomial in ϵ to the small-ϵ end of each data set with $\omega_r > 0$

we get

$$\begin{aligned}\omega &= (4.62635 + 0.488023i) + (1.23370 + 0.230129i)\epsilon \\ &\quad -(0.209755 + 0.826815i)\epsilon^2 - (0.0028336 - 0.612822i)\epsilon^3 \\ &\quad +(0.118440 - 0.557211i)\epsilon^4\end{aligned} \tag{6.49}$$

and

$$\begin{aligned}\omega &= (2.48716 + 0.296281i) + (0.663244 + 0.179007i)\epsilon \\ &\quad -(0.146603 + 0.276306i)\epsilon^2 + (0.0235386 + 0.192975i)\epsilon^3 \\ &\quad +(0.0100579 - 0.123306i)\epsilon^4.\end{aligned} \tag{6.50}$$

Using (6.48) on the leading order terms ω_0 of each of these we obtain

$$\omega_1 = 1.23369 + 0.230139i \tag{6.51}$$

and

$$\omega_1 = 0.663243 + 0.179008i, \tag{6.52}$$

in very good agreement with the order-ϵ terms, ω_1, from the computed results.

6.3 The case of ω_r large or β_j small

We now consider eigenvalues with large values of ω_r. To this end, we introduce 'fast' time and space scales governed by a small parameter δ so that $x = \delta X$ and $t = \delta T$. Making this substitution into our equations (6.1) and assuming that coupling occurs sufficiently strongly to remain important on this scale, we obtain

$$\begin{aligned}\tfrac{1}{\delta}\tfrac{\partial u}{\partial T} - \tfrac{c_1}{\delta}\tfrac{\partial u}{\partial X} + \beta_1 u &= \tfrac{a_1}{\delta} v, \\ \tfrac{1}{\delta}\tfrac{\partial v}{\partial T} - \tfrac{c_2}{\delta}\tfrac{\partial v}{\partial X} + \beta_2 v &= \tfrac{a_2}{\delta} w, \\ \tfrac{1}{\delta}\tfrac{\partial w}{\partial T} + \tfrac{c_3}{\delta}\tfrac{\partial w}{\partial X} + \beta_3 w &= 0,\end{aligned} \tag{6.53}$$

or

$$\begin{aligned} \frac{\partial u}{\partial T} - c_1 \frac{\partial u}{\partial X} + \delta\beta_1 u &= a_1 v, \\ \frac{\partial v}{\partial T} - c_2 \frac{\partial v}{\partial X} + \delta\beta_2 v &= a_2 w, \\ \frac{\partial w}{\partial T} + c_3 \frac{\partial w}{\partial X} + \delta\beta_3 w &= 0. \end{aligned} \tag{6.54}$$

We expect our equations to be solved by frequencies of the order of $\frac{1}{\delta}$. When

We expect our equations to be solved by frequencies of the order of $\frac{1}{\delta}$. When delta is made very small, i.e. when we look at leading order in the above equations, we see that this has the effect of removing β_1, β_2 and β_3 from the equations. This follows all the way through to the dispersion relation

$$\begin{aligned} &\left(e^{\omega(\chi_1+\chi_3)} - 1\right) \\ &\times \left(\omega\chi_3 + \omega\chi_2 e^{\omega(\chi_2+\chi_3)}\right) \end{aligned} = \begin{aligned} &\left(e^{\omega(\chi_2+\chi_3)} - 1\right) \\ &\times \left(\omega\chi_3 + \omega\chi_1 e^{\omega(\chi_1+\chi_3)}\right), \end{aligned} \tag{6.55}$$

where

$$\chi_1 = \frac{-iL}{c_1\delta}, \quad \chi_2 = \frac{-iL}{c_2\delta}, \quad \chi_3 = \frac{-iL}{c_3\delta}. \tag{6.56}$$

We expect solutions to this to approximate solutions to our complete system when the mode number is large (i.e. ω_r is large). However, (6.55) does not take account of effects which, in the complete system, would be $O(1)$, which may be quite large. This is shown in Figure 6.5, which is Figure 6.1(a), with $\beta_1 = \beta_2 = \beta_3 = 0$.

We immediately see similarities in the structure of Figure 6.1(a), for large ω_r, and that of Figure 6.5, but differences of order 1 in the values taken. Figure 6.5 is useful, however, as we may say more about systems with $\beta_1 = \beta_2 = \beta_3 = 0$. (6.55) is equivalent to

$$\chi_3 e^{\omega\chi_1} + \chi_2 e^{\omega(\chi_1+\chi_2+\chi_3)} - \chi_2 e^{\omega\chi_2} = \chi_3 e^{\omega\chi_2} + \chi_1 e^{\omega(\chi_1+\chi_2+\chi_3)} - \chi_1 e^{\omega\chi_1}, \tag{6.57}$$

or

$$(\chi_2 - \chi_3)\, e^{\omega(-\chi_1-\chi_3)} - \chi_2 = (\chi_1 - \chi_3)\, e^{\omega(-\chi_2-\chi_3)} - \chi_1. \tag{6.58}$$

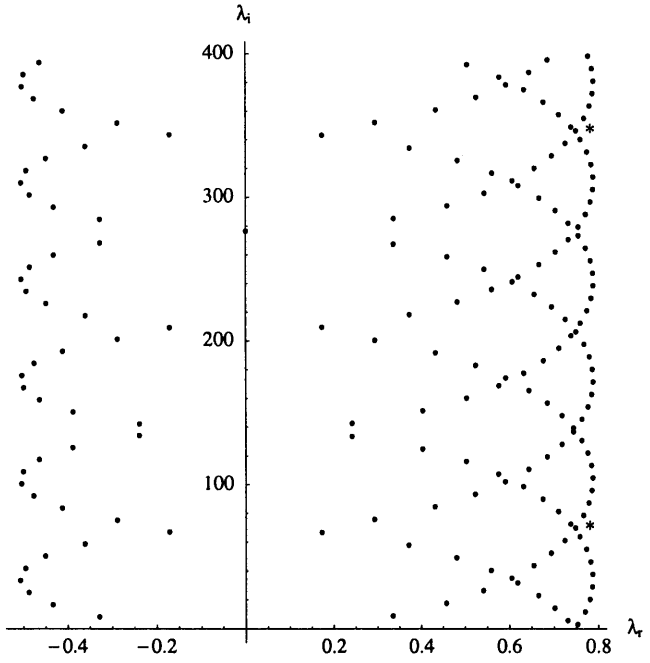

Figure 6.5: Solutions to our system with $\beta_1 = \beta_2 = \beta_3 = 0$. $c_1 = 0.4$, $c_2 = 0.25$, $c_3 = 0.55$, $L = 0.5$. The lower half-plane is a mirror image of the upper half-plane and is not shown. Again, we show results in terms of $\lambda = -i\omega$.

From this we see that, given a root ω_0 and a quantity $\omega_0 + \Delta\omega$, if both $\Delta\omega\,(-\chi_1 - \chi_3)$ and $\Delta\omega\,(-\chi_2 - \chi_3)$ are multiples of $2\pi i$, then $\omega_0 + \Delta\omega$ is another root. If χ_1, χ_2 and χ_3 all happen to be rational numbers, as they have been in every computed example so far, then we may write

$$\begin{aligned} \Delta\omega\,(-\chi_1 - \chi_3) &= \Delta\omega\left(-\tfrac{\chi_{1n}}{\chi_{1d}} - \tfrac{\chi_{3n}}{\chi_{3d}}\right) = 2n_1\pi i, \\ \Delta\omega\,(-\chi_2 - \chi_3) &= \Delta\omega\left(-\tfrac{\chi_{2n}}{\chi_{2d}} - \tfrac{\chi_{3n}}{\chi_{3d}}\right) = 2n_2\pi i, \end{aligned} \tag{6.59}$$

with χ_{1n}, χ_{2n}, $\chi_{3n} \in -i\mathbb{N}$, χ_{1d}, χ_{2d}, χ_{3d}, n_1, $n_2 \in \mathbb{N}$. Quotients are assumed to be in lowest terms. This is equivalent to

$$\begin{aligned} \Delta\omega\left(-\tfrac{\chi_{1n}\chi_{3d}+\chi_{1d}\chi_{1n}}{\chi_{1d}}\right) &= 2n_1\pi i\chi_{3d}, \\ \Delta\omega\left(-\tfrac{\chi_{2n}\chi_{3d}+\chi_{2d}\chi_{1n}}{\chi_{2d}}\right) &= 2n_2\pi i\chi_{3d}. \end{aligned} \tag{6.60}$$

Putting

$$\Delta\omega = 2\pi\chi_{3d}\mathrm{lcm}(\chi_{1d}, \chi_{2d}), \tag{6.61}$$

clearly satisfies our equations. For the example given in Figure 6.5, we have

$$\begin{aligned} c_1 &= 0.4 = \tfrac{2}{5}, \\ c_2 &= 0.25 = \tfrac{1}{4}, \\ c_3 &= 0.55 = \tfrac{11}{20}, \\ L &= 0.5 = \tfrac{1}{2}. \end{aligned} \tag{6.62}$$

Thus $\chi_1 = -i\frac{5}{4}$, $\chi_2 = -i\frac{2}{1}$ and $\chi_3 = -i\frac{10}{11}$. This gives

$$\Delta\omega = 2\pi \times 11 \times 4 = 88\pi. \tag{6.63}$$

The two *'s on Figure 6.5 are separated by exactly this amount. Looking in their vicinity shows that the set of roots is indeed periodic with this period.

Another advantage of the $\beta_1 = \beta_2 = \beta_3 = 0$ case is that we may easily find an asymptotic limit as χ_1 and χ_2 become close. (6.57) may be rewritten as

$$(\chi_1 + \chi_3)\, e^{\omega(\chi_1 - \chi_2)} = (\chi_3 + \chi_2) + (\chi_1 - \chi_2)\, e^{\omega(\chi_1 + \chi_3)}. \tag{6.64}$$

We let $\epsilon = \chi_1 - \chi_2$ be small and $\Lambda = \chi_1 + \chi_3$ be relatively large. Then we have

$$\Lambda e^{\omega\epsilon} = (\Lambda - \epsilon) + \epsilon e^{\omega\Lambda}. \tag{6.65}$$

ϵ is small so

$$\Lambda\,(1 + \omega\epsilon) = (\Lambda - \epsilon) + \epsilon e^{\omega\Lambda}, \tag{6.66}$$

or

$$1 + \omega\Lambda = e^{\omega\Lambda} \tag{6.67}$$

and we expect our solutions to approach those in the resonant case. This can be shown numerically in both the $\beta_j = 0$ and $\beta_j \neq 0$ cases as is done in Figures 6.6 and 6.7.

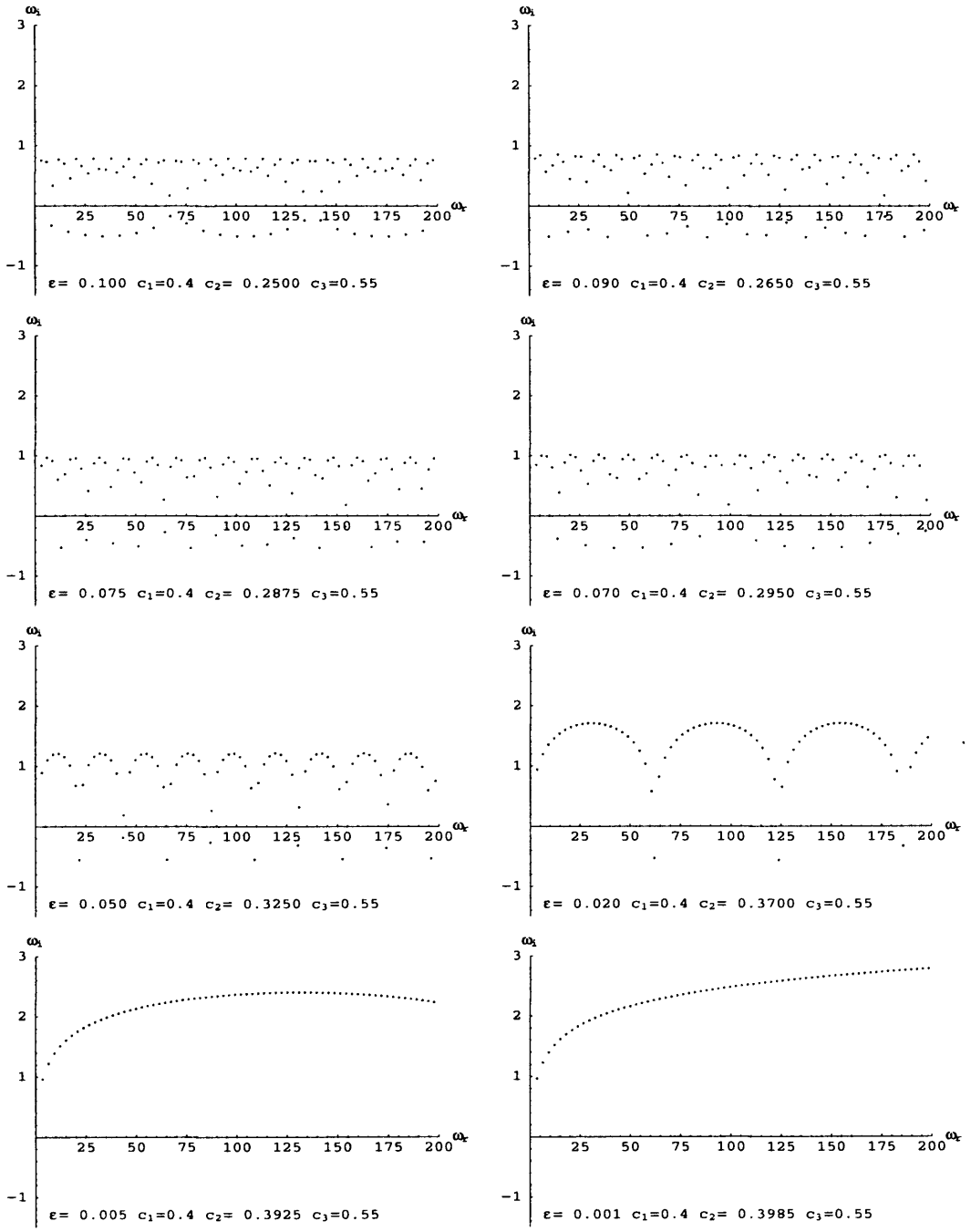

Figure 6.6: Solutions to the equations with $\beta_j = 0$ as c_2 approaches c_1. We see that the sets of roots start to approach those in the resonant case. Note that, at around $\epsilon = 0.07$, we can make out apparent patterns in the points both on scales of $\Delta\omega_r \approx 15$ and on scales of the entire length of the diagram. $L = 0.5$ for each graph.

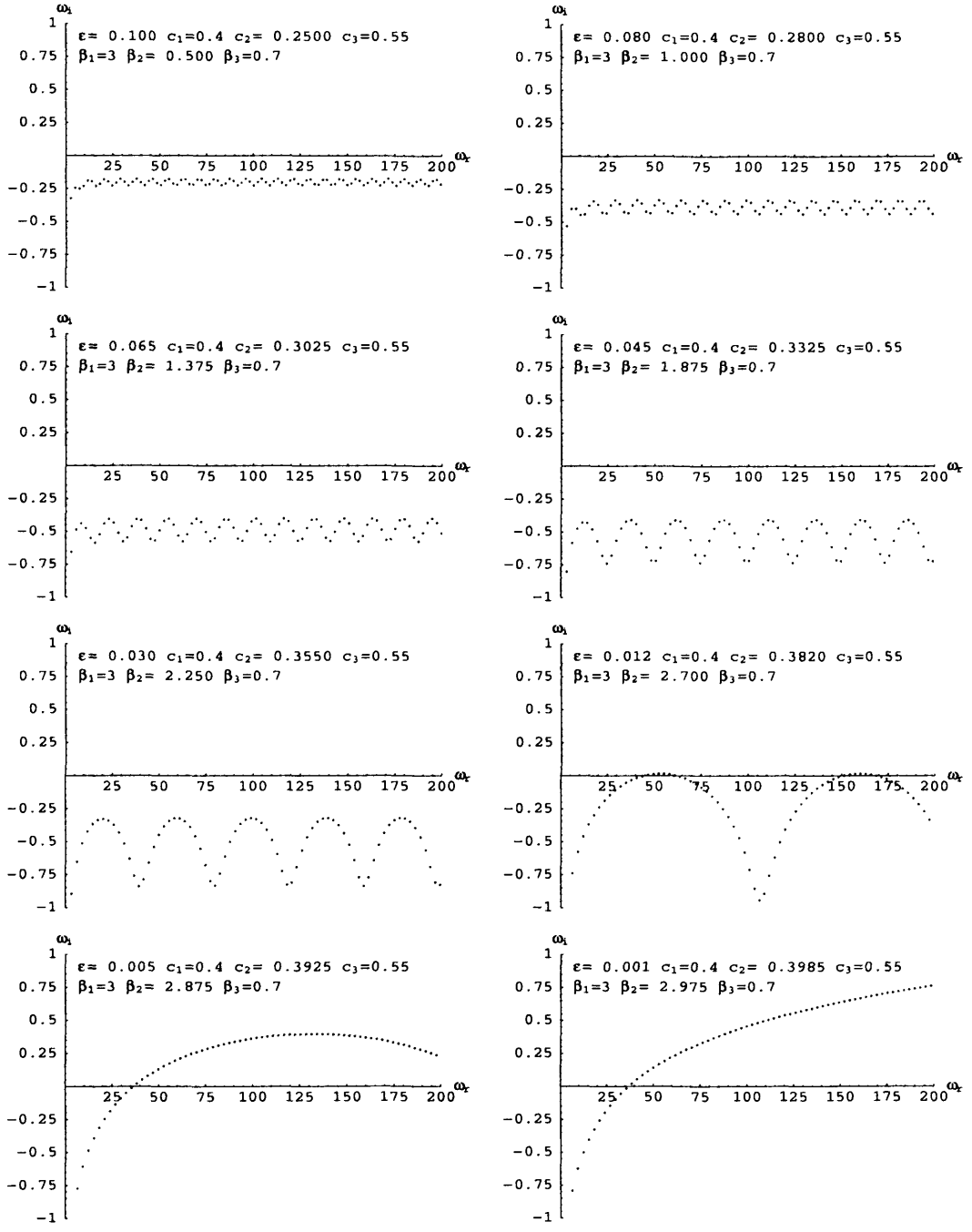

Figure 6.7: Solutions to the equations with $\beta_j \neq 0$ as β_2 approaches β_1 and c_2 approaches c_1. We see that the sets of roots start to approach those in the resonant case. $L = 0.5$ for each graph.

6.4 A two-wave system exhibiting instability due to transient growth

In the previous example of a system with transient growth leading to instability, the spatial and temporal transient growths were interchangeable. This was even done at the beginning of the section (compare equations (6.7) and (6.21)). We now consider a system of two-wave system where the transients are purely temporal. Our system is

$$\begin{aligned} \frac{\partial u}{\partial t} - c_1 \frac{\partial u}{\partial x} + \beta_1 u &= a_1 v, \\ \frac{\partial v}{\partial t} + c_2 \frac{\partial v}{\partial x} + \beta_2 v &= 0. \end{aligned} \tag{6.68}$$

In this we assume that c_1, c_2, β_1 and β_2 are real and positive. We note that given initial conditions $u = u_{init}(x)$ and $v = v_{init}(x)$ at $t = 0$, say, we may write a complete solution as follows

$$v(x,t) = e^{-\beta_2 t} v_{init}(x - c_2 t). \tag{6.69}$$

Substituting this into our equation for u,

$$\frac{\partial u}{\partial t} - c_1 \frac{\partial u}{\partial x} + \beta_1 u = a_1 e^{-\beta_2 t} v_{init}(x - c_2 t). \tag{6.70}$$

We make the substitutions $y_1 = x + c_1 t$ and $y_2 = x - c_2 t$. We obtain

$$(-c_2 - c_1)\frac{\partial u}{\partial y_2} + \beta_1 u = a_1 e^{-\beta_2 \frac{y_1 - y_2}{c_1 + c_2}} v_{init}(y_2), \tag{6.71}$$

or

$$\frac{\partial u}{\partial y_2} - \frac{\beta_1}{c_1 + c_2} u = -\frac{a_1}{c_1 + c_2} e^{\frac{-\beta_2 y_1}{c_1 + c_2}} e^{\frac{\beta_2 y_2}{c_1 + c_2}} v_{init}(y_2), \tag{6.72}$$

so

$$\frac{\partial}{\partial y_2} u e^{\frac{-\beta_1 y_2}{c_1 + c_2}} = \frac{\partial u}{\partial y_2} e^{\frac{-\beta_1 y_2}{c_1 + c_2}} - \frac{\beta_1}{c_1 + c_2} e^{\frac{-\beta_1 y_2}{c_1 + c_2}} u = -\frac{a_1}{c_1 + c_2} e^{\frac{-\beta_2 y_1}{c_1 + c_2}} e^{\frac{(\beta_2 - \beta_1) y_2}{c_1 + c_2}} v_{init}(y_2). \tag{6.73}$$

This gives

$$\left[ue^{\frac{-\beta_1 y_2}{c_1+c_2}}\right]_{u(y_1,y_2=y_1)}^{u(y_1,y_2)} = -\frac{a_1}{c_1+c_2}e^{\frac{-\beta_2 y_1}{c_1+c_2}}\int_{y_2=y_1}^{y_2} e^{\frac{(\beta_2-\beta_1)s}{c_1+c_2}}v_{init}(s)\mathrm{d}s, \tag{6.74}$$

i.e.

$$u(y_1,y_2)e^{\frac{-\beta_1 y_2}{c_1+c_2}} - u(y_1,y_2=y_1)e^{\frac{-\beta_1 y_1}{c_1+c_2}} = -\frac{a_1}{c_1+c_2}e^{\frac{-\beta_2 y_1}{c_1+c_2}}\int_{y_2=y_1}^{y_2} e^{\frac{(\beta_2-\beta_1)s}{c_1+c_2}}v_{init}(s)\mathrm{d}s, \tag{6.75}$$

or

$$\begin{aligned} u(y_1,y_2) &= u(y_1,y_2=y_1)e^{\frac{-\beta_1 y_1}{c_1+c_2}}e^{\frac{\beta_1 y_2}{c_1+c_2}} \\ &\quad -\frac{a_1}{c_1+c_2}e^{\frac{\beta_1 y_2}{c_1+c_2}}e^{\frac{-\beta_2 y_1}{c_1+c_2}}\int_{y_2=y_1}^{y_2} e^{\frac{(\beta_2-\beta_1)s}{c_1+c_2}}v_{init}(s)\mathrm{d}s. \end{aligned} \tag{6.76}$$

In our original variables,

$$u(x,t) = u_{init}(x+c_1t)e^{-\beta_1 t} + \frac{a_1}{c_1+c_2}e^{\frac{\beta_1(x-c_2t)}{c_1+c_2}}e^{\frac{-\beta_2(x+c_1t)}{c_1+c_2}}\int_{x-c_2t}^{x+c_1t} e^{\frac{(\beta_2-\beta_1)s}{c_1+c_2}}v_{init}(s)\mathrm{d}s, \tag{6.77}$$

so,

$$u(x,t) = u_{init}(x+c_1t)e^{-\beta_1 t} + \frac{a_1}{c_1+c_2}e^{\frac{\beta_1(x-c_2t)-\beta_2(x+c_1t)}{c_1+c_2}}\int_{x-c_2t}^{x+c_1t} e^{\frac{(\beta_2-\beta_1)s}{c_1+c_2}}v_{init}(s)\mathrm{d}s. \tag{6.78}$$

In an infinite range we may derive a dispersion relation, by putting $u = u_0e^{i(kx-\omega t)}$, $v = v_0e^{i(kx-\omega t)}$, in a similar fashion to the last section. We get

$$(\omega + c_1k - i\beta_1)(\omega - c_2k + i\beta_2) = 0. \tag{6.79}$$

From this we conclude that the infinite system, regardless of the coupling, supports two decaying waves travelling in opposite directions. Given our restrictions on c_1, c_2, β_1 and β_2, when the system is uncoupled, we may talk in terms of a u-wave travelling to the left and a v-wave travelling to the right, but this does not apply when $a_1 \neq 0$.

Figures 6.8 to 6.10 show the results of plotting (6.78) for three different values of a_1. We see that, when $a_1 = 0$ and the waves are uncoupled, the u-wave simply travels to the left and decays steadily. However, when $|a_1|$ is

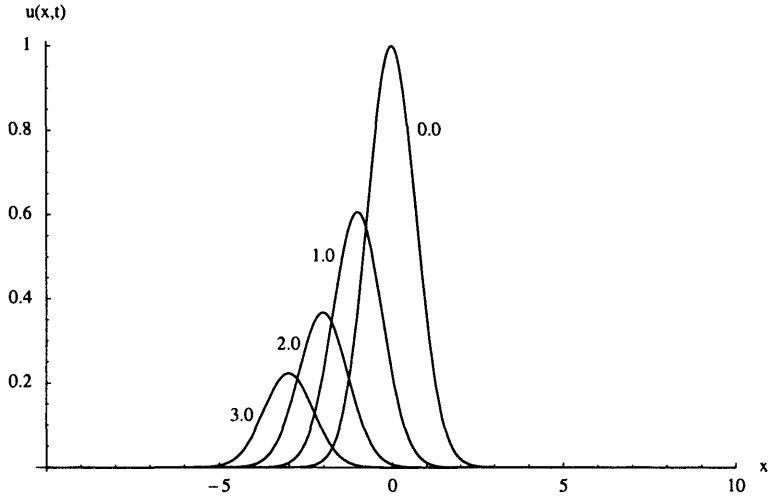

Figure 6.8: Evolution of (6.78) when $a_1 = 0$. t is as marked on the curves. $c_1 = 1$, $c_2 = 1$, $\beta_1 = 0.5$, $\beta_2 = 1$, $u_{init}(x) = v_{init}(x) = e^{-x^2}$.

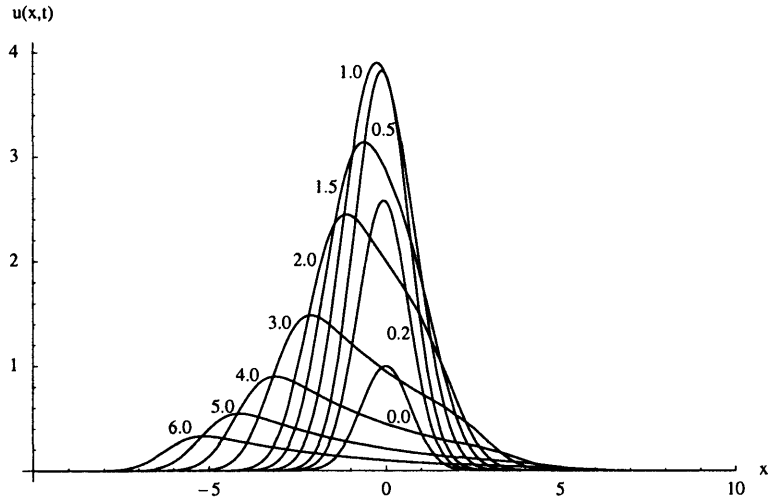

Figure 6.9: Evolution of (6.78) when $a_1 = 10$. t is as marked on the curves. $c_1 = 1$, $c_2 = 1$, $\beta_1 = 0.5$, $\beta_2 = 1$, $u_{init}(x) = v_{init}(x) = e^{-x^2}$.

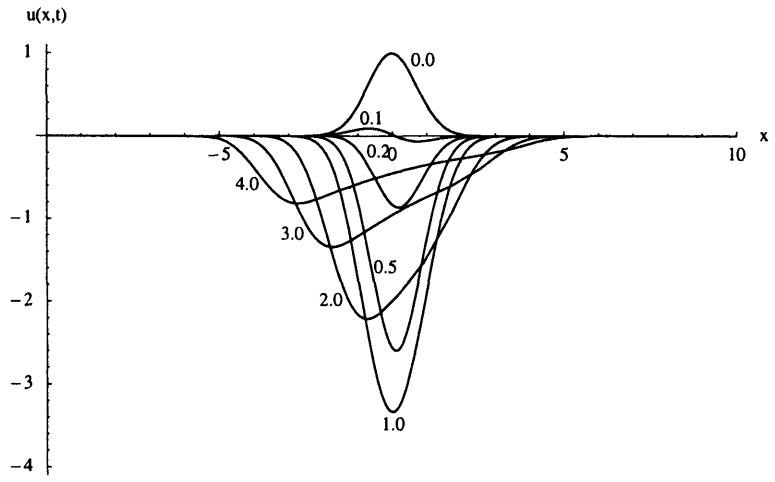

Figure 6.10: Evolution of (6.78) when $a_1 = -10$. t is as marked on the curves. $c_1 = 1$, $c_2 = 1$, $\beta_1 = 0.5$, $\beta_2 = 1$, $u_{init}(x) = v_{init}(x) = e^{-x^2}$.

large and either positive or negative, we see substantial transients before the leftward movement and decay set in.

Next, we consider the finite-range formulation of the problem. We impose reflection-type boundary conditions on (6.68) as follows

$$\begin{aligned} \sigma_1 u + v &= 0 \quad \text{at} \quad x = -L, \\ u + \sigma_2 v &= 0 \quad \text{at} \quad x = 0, \end{aligned} \tag{6.80}$$

for some real positive $\sigma_{1,2}$. We now solve our system, with boundary conditions. We have

$$v = A_2 e^{-i\omega t} e^{\frac{-\beta_2 + i\omega}{c_2} x}. \tag{6.81}$$

u is of the form

$$u = B_1 e^{-i\omega t} e^{\frac{\beta_1 - i\omega}{c_1} x} + B_2 e^{-i\omega t} e^{\frac{-\beta_2 + i\omega}{c_2} x}. \tag{6.82}$$

Substituting this into (6.68) gives

$$-i\omega B_1 e^{s_1 x} - i\omega B_2 e^{s_2 x} - c_1 B_1 s_1 e^{s_1 x} - c_1 B_2 s_2 e^{s_2 x} + \beta_1 B_1 e^{s_1 x} + \beta_2 B_2 e^{s_2 x} = a_1 A_2 e^{s_2 x}, \tag{6.83}$$

where $s_1 = \frac{\beta_1 - i\omega}{c_1}$ and $s_2 = \frac{-\beta_2 + i\omega}{c_2}$. The terms varying like $e^{s_1 x}$ are, of course,

solved identically, but from those which vary like $e^{s_2 x}$ we obtain

$$A_2 = \frac{1}{a_1}\left(\beta_1 - i\omega - c_1 s_2\right) B_2 = \frac{c_1}{a_1}\left(s_1 - s_2\right) B_2. \tag{6.84}$$

After dividing through by $e^{-i\omega t}$, equation (6.80) is, at $x = -L$,

$$\sigma_1 B_1 e^{-s_1 L} + \sigma_1 B_2 e^{-s_2 L} + B_2 \frac{c_1}{a_1}\left(s_1 - s_2\right) e^{-s_2 L} = 0 \tag{6.85}$$

and at $x = 0$,

$$B_1 + B_2 + \sigma_2 \frac{c_1}{a_1}\left(s_1 - s_2\right) B_2 = 0, \tag{6.86}$$

which combine to give

$$-\sigma_1 e^{-s_1 L} - \sigma_1 \sigma_2 \frac{c_1}{a_1}\left(s_1 - s_2\right) e^{-s_1 L} + \sigma_1 e^{-s_2 L} + \frac{c_1}{a_1}\left(s_1 - s_2\right) e^{-s_2 L} = 0, \tag{6.87}$$

so

$$\sigma_1 e^{(s_1 - s_2)L} + \frac{c_1}{a_1}\left(s_1 - s_2\right) e^{(s_1 - s_2)L} = \sigma_1 + \sigma_1 \sigma_2 \frac{c_1}{a_1}\left(s_1 - s_2\right). \tag{6.88}$$

Putting $z = (s_1 - s_2)L$ we obtain

$$\left(z + \frac{\sigma_1 a_1 L}{c_1}\right) e^z = \sigma_1 \left(\sigma_2 z + \frac{a_1 L}{c_1}\right). \tag{6.89}$$

If we put $u = \bar{u}(x)e^{-i\omega t}$, $v = \bar{v}(x)e^{-i\omega t}$ and set $A_2 = 1$, we obtain

$$\begin{aligned} \bar{u} &= \left(-\sigma_2 - \tfrac{a_1}{c_1 z}\right) e^{s_1 x} + \tfrac{a_1}{c_1 z} e^{s_2 x} \\ \bar{v} &= e^{s_2 x} \end{aligned} \tag{6.90}$$

We plot solutions to (6.89) in Figure 6.11, for the parameters $\beta_1 = 0.5$, $\beta_2 = 1$, $c_1 = 1$, $c_2 = 1$, $\sigma_1 = 0.4$, $\sigma_2 = 0.2$, $L = 1$ and several values of a_1. We immediately see that there can be one unstable mode, with a purely imaginary value of ω. The variation of this with a_1 is shown in Figure 6.12. We can find the limits for large positive and negative a_1 as follows: when $a_1 \ll 0$, in order that solutions do not grow exponentially with a_1, we must have that the term multiplied by e^z on the l.h.s. of (6.89) tends to zero exponentially fast. Thus it must be the case that, as $z + \frac{\sigma_1 a_1 L}{c_1} \to 0$,

$$z \to \frac{-\sigma_1 a_1 L}{c_1}, \tag{6.91}$$

or,

$$\omega \to \frac{-ic_2\sigma_1}{c_1+c_2}a_1 + \frac{-i\beta_1 c_2 - i\beta_2 c_1}{c_1+c_2}. \tag{6.92}$$

When $a_1 \gg 0$, the exponential part of (6.89) will tend to zero exponentially fast and so the r.h.s. of the equation must do the same. Thus,

$$z \to \frac{-a_1 L}{\sigma_2 c_1}, \tag{6.93}$$

or,

$$\omega \to \frac{-ic_2}{\sigma_2\left(c_1+c_2\right)}a_1 + \frac{-i\beta_1 c_2 - i\beta_2 c_1}{c_1+c_2}. \tag{6.94}$$

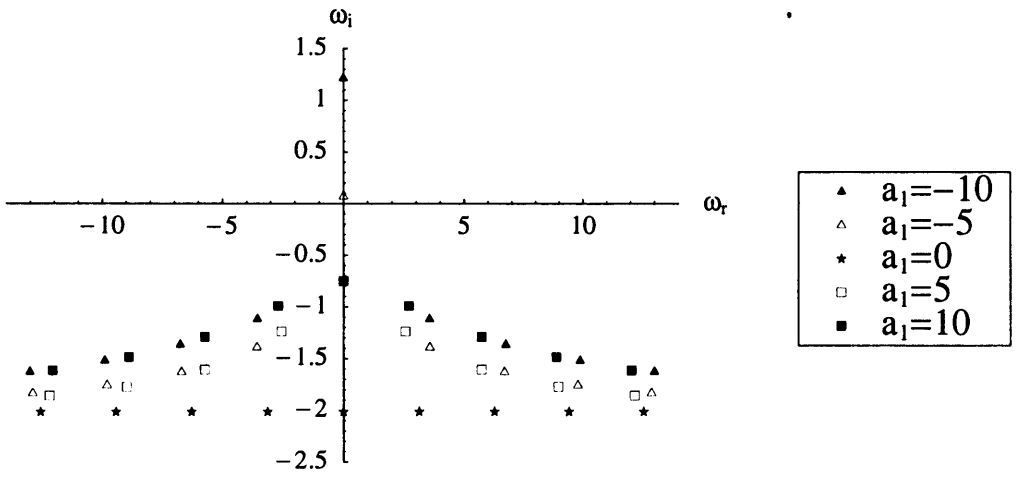

Figure 6.11: Solutions to our two-wave system exhibiting instability due to transients. $\beta_1 = 0.5$, $\beta_2 = 1$, $c_1 = 1$, $c_2 = 1$, $\sigma_1 = 0.4$, $\sigma_2 = 0.2$ and $L = 1$.

These two asymptotes are also shown on Figure 6.12. The point at which all the asymptotes meet, regardless of the values of the reflection coefficients, $\frac{-i\beta_1 c_2 - i\beta_2 c_1}{c_1+c_2}$, is interesting as it is, itself, a solution to the system. However, it is the $z = 0$ solution, for which no eigenfunction exists.

In order to ascertain that the instability shown in Figure 6.12 is not due to 'energy' being fed in through the ends of the system, we consider an 'energy'

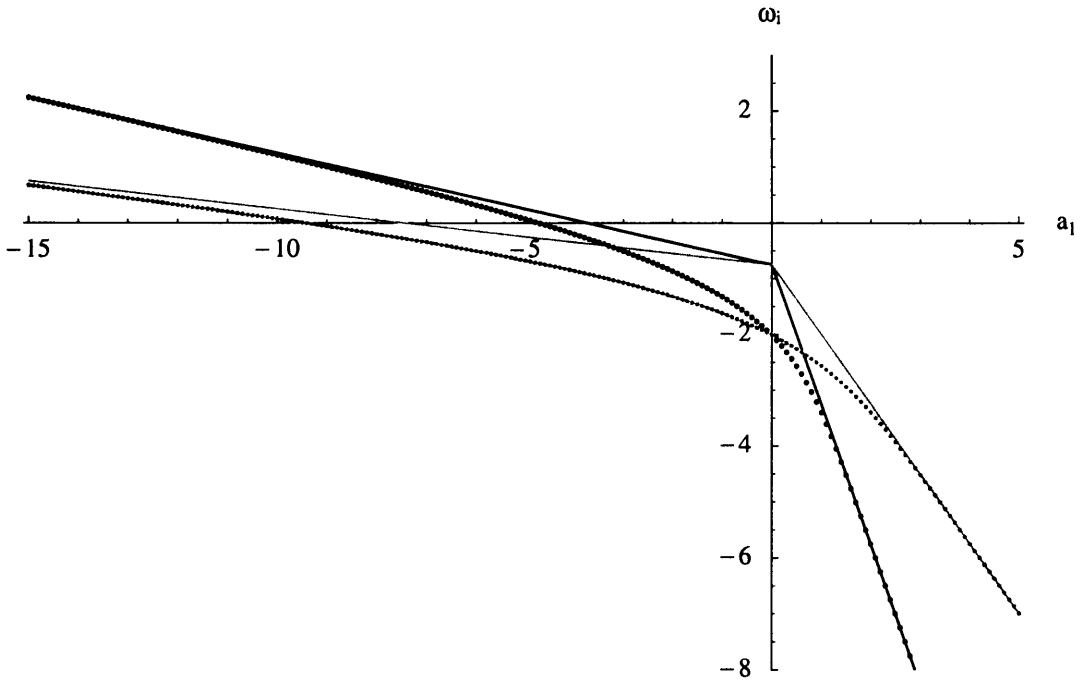

Figure 6.12: The purely-imaginary ω which solves (6.89), plotted as a function of a_1. For the black points, $\sigma_1 = 0.4$ and $\sigma_2 = 0.2$ and for the grey set, $\sigma_1 = 0.2$ and $\sigma_2 = 0.4$. $\beta_1 = 0.5$, $\beta_2 = 1$, $c_1 = 1$, $c_2 = 1$ and $L = 1$ for both. Asymptotes, from (6.92) and (6.94), are also shown.

integral. We multiply the first equation of (6.68) by u and the second by v, add and integrate to obtain

$$\begin{aligned} \frac{\partial}{\partial t}\int_{-L}^{0}\tfrac{1}{2}\left(u^2+v^2\right)\mathrm{d}x &= -\int_{-L}^{0}\left(\beta_1 u^2+\beta_2 v^2\right)\mathrm{d}x \\ &\quad +a_1\int_{-L}^{0}uv\ \mathrm{d}x+\tfrac{1}{2}\Big[c_1u^2-c_2v^2\Big]_{-L}^{0}. \end{aligned} \tag{6.95}$$

Using our end conditions, we have

$$\Big[c_1u^2-c_2v^2\Big]_{-L}^{0}=-v^2\left(0,t\right)\left(c_2-c_1\sigma_2^2\right)-u^2\left(-L,t\right)\left(c_1-c_2\sigma_1^2\right) \tag{6.96}$$

so

$$\begin{aligned} \frac{\partial}{\partial t}\int_{-L}^{0}\tfrac{1}{2}\left(u^2+v^2\right)\mathrm{d}x &= -\int_{-L}^{0}\left(\beta_1 u^2+\beta_2 v^2\right)dx+a\int_{-L}^{0}uv\ \mathrm{d}x \\ &\quad -\tfrac{1}{2}v^2\left(0,t\right)\left(c_2-c_1\sigma_2^2\right)-\tfrac{1}{2}u^2\left(-L,t\right)\left(c_1-c_2\sigma_1^2\right). \end{aligned} \tag{6.97}$$

The first term on the r.h.s. shows that the quantities β_1 and β_2, which cause solutions to decay, tend to stabilise the system, provided u and v are real-valued. Note that we could have considered complex conjugates of solutions throughout and, by addition of these, have obtained real-valued solutions. The last two terms similarly increase the overall stability provided $c_1 > c_2\sigma_1^2$ and $c_2 > c_1\sigma_2^2$. This has been the case in all the numerical results so far. We are left with the term $a_1\int_{-L}^{0}uv\ \mathrm{d}x$. The condition that this be positive for the energy of solutions to grow with time can, therefore, be interpreted as a non-normality condition on u and v over our interval.

Qualitatively, we see that this system creates an unstable global mode from two waves, both of which decay in their direction of propagation. We may explain this by considering the effect of reflecting the v-wave at the $x=0$ end. The v-wave is simply a right-going wave which decays in space. We consider this to have amplitude $O(1)$. When it reaches $x=0$, it is reflected into a left-going signal which is comprised of two waves, propagating in different

directions. From (6.90), we see that each wave will have amplitude $O(a_1)$, in order to give a resultant $O(1)$ disturbance to match the 'incoming' v-wave. The more rapid decay of one of these waves than the other is sufficient to match at the $x = -L$ end and create a global mode.

6.5 The three-wave system revisited

We now briefly revisit the three-wave system from the previous section in order to compare it with the two-wave model. We make our end conditions

$$\begin{aligned} u &= \sigma_1 w \quad \text{at} \quad x = 0, \\ v &= \sigma_2 w \quad \text{at} \quad x = 0, \\ w + \sigma_3 u + \sigma_4 v &= 0 \quad \text{at} \quad x = -L, \end{aligned} \tag{6.98}$$

noting that, although the x-range has changed, we still have two conditions at the right-hand end and one at the left-hand end. We have

$$\bar{w} = C_3 e^{\frac{i\omega - \beta_3}{c_3} x} \tag{6.99}$$

and

$$\bar{v} = B_2 e^{\frac{\beta_2 - i\omega}{c_2} x} + B_3 e^{\frac{i\omega - \beta_3}{c_3} x}, \tag{6.100}$$

so

$$\bar{u} = A_1 e^{\frac{\beta_1 - i\omega}{c_1} x} + A_2 e^{\frac{\beta_2 - i\omega}{c_2} x} + A_3 e^{\frac{i\omega - \beta_3}{c_3} x}, \tag{6.101}$$

for some A_1, A_2, A_3, B_1, B_2 and C_1. As usual, $u = \bar{u}e^{-i\omega t}$, $v = \bar{v}e^{-i\omega t}$ and $w = \bar{w}e^{-i\omega t}$. Substituting these into (6.1) and comparing terms with the same x-variation, we have

$$\begin{aligned} B_2 &= \tfrac{c_1}{a_1}(s_1 - s_2) A_2, \\ B_3 &= \tfrac{c_1}{a_1}(s_1 - s_3) A_3, \\ C_3 &= \tfrac{c_2}{a_2}(s_2 - s_3) B_3 = \tfrac{c_1 c_2}{a_1 a_2}(s_1 - s_3)(s_2 - s_3) A_3, \end{aligned} \tag{6.102}$$

where $s_1 = \frac{\beta_1 - i\omega}{c_1}$, $s_2 = \frac{\beta_2 - i\omega}{c_2}$ and $s_3 = \frac{i\omega - \beta_3}{c_3}$. End conditions give

$$\begin{aligned} A_1 + A_2 + A_3 &= \sigma_1 C_3, \\ B_2 + B_3 &= \sigma_2 C_3, \\ C_3 e^{-\frac{i\omega-\beta_3}{c_3}L} + \sigma_3 A_1 e^{-\frac{\beta_1-i\omega}{c_1}L} + \sigma_3 A_2 e^{-\frac{\beta_2-i\omega}{c_2}L} & \\ +\sigma_3 A_3 e^{-\frac{i\omega-\beta_3}{c_3}L} + \sigma_4 B_2 e^{-\frac{\beta_2-i\omega}{c_2}L} + \sigma_4 B_3 e^{-\frac{i\omega-\beta_3}{c_3}L} &= 0, \end{aligned} \tag{6.103}$$

or

$$\begin{pmatrix} 1 & 1 & 1 - \sigma_1 \frac{c_1 c_2}{a_1 a_2}(s_1 - s_3)(s_2 - s_3) \\ 0 & \frac{c_1}{a_1}(s_1 - s_2) & \frac{c_1}{a_1}(s_2 - s_3) \\ & & -\sigma_2 \frac{c_1 c_2}{a_1 a_2}(s_1 - s_3)(s_2 - s_3) \\ \sigma_3 e^{-s_1 L} & \sigma_3 e^{-s_2 L} & \sigma_3 e^{-s_3 L} + \sigma_4 \frac{c_1}{a_1}(s_2 - s_3) e^{-s_3 L} \\ & +\sigma_4 \frac{c_1}{a_1}(s_1 - s_2) e^{-s_2 L} & + \frac{c_1 c_2}{a_1 a_2}(s_1 - s_3)(s_2 - s_3) e^{-s_3 L} \end{pmatrix}$$

$$\times \begin{pmatrix} A_1 & A_2 & A_3 \end{pmatrix}^T = 0. \tag{6.104}$$

This system has solutions when

$$\begin{vmatrix} 1 & 1 & 1 - \sigma_1 S_{13} S_{23} \\ 0 & S_{12} & S_{23} - \sigma_2 S_{13} S_{23} \\ \sigma_3 e^{-s_1 L} & (\sigma_3 + \sigma_4 S_{12}) e^{-s_2 L} & (\sigma_3 + \sigma_4 S_{23} + S_{13} S_{23}) e^{-s_3 L} \end{vmatrix} = 0, \tag{6.105}$$

i.e.

$$\begin{aligned} S_{12}(\sigma_3 + \sigma_4 S_{13} + S_{13} S_{23}) e^{-s_3 L} - S_{13}(1 - \sigma_2 S_{23})(\sigma_3 + \sigma_4 S_{12}) e^{-s_2 L} & \\ +\sigma_3 e^{-s_1 L}(S_{13}(1 - \sigma_2 S_{23}) - S_{12}(1 - \sigma_1 S_{13} S_{23})) &= 0, \end{aligned} \tag{6.106}$$

where $S_{12} = \frac{c_1}{a_1}(s_1 - s_2)$, $S_{13} = \frac{c_1}{a_1}(s_1 - s_3)$ and $S_{23} = \frac{c_2}{a_2}(s_2 - s_3)$.

Further simplification of this does not seem to be particularly beneficial and so we plot the solutions. In order to make comparisons with our two-wave system, we consider only a_1 to change. We make this the parameter (c.f. the

parameter a_1 in the two-wave problem) which becomes large, while keeping a_2 fixed. The results of this are shown in Figure 6.13.

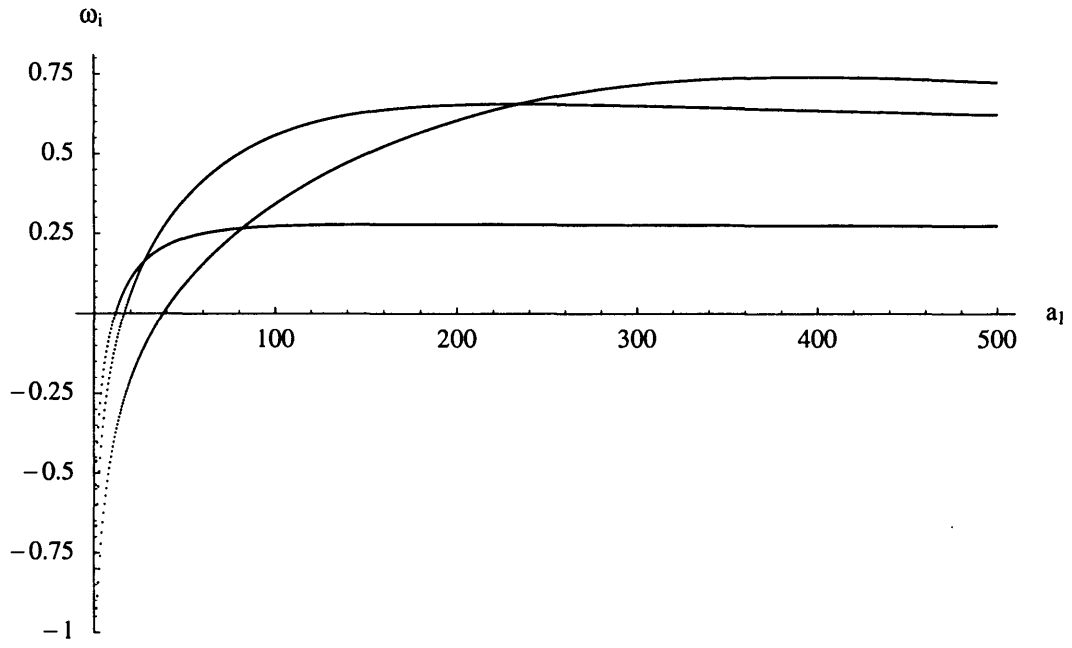

Figure 6.13: The imaginary part of the roots of (6.106) as a function of the coupling parameter a_1. Only three roots are shown, although there appear to be infinitely many. $a_2 = 1$, $\sigma_1 = \sigma_2 = \sigma_3 = \sigma_4 = 0.5$, $\beta_1 = \beta_3 = 0.5$, $\beta_2 = 0.8$, $c_1 = c_3 = 0.5$, $c_2 = 1$ and $L = 1$.

Looking at Figure 6.13, we see that we may have unstable modes for a_1 sufficiently large, similarly to the two-wave case. However, it is also clear that there is more than one unstable mode and that each mode does not have $\omega_i \to \infty$ as $a_1 \to \infty$, although it does appear that the maximum value of ω_i generally increases as more modes are shown. Note that for these modes, $w_r \neq 0$.

6.6 Summary

Two stability-type differential systems have been considered, both of which have the property of being stable for spatially-homogeneous problems. They also have the property of supporting strong transients; in the first example this was through near-resonance of decaying waves and in the second example it was through non-orthogonality of the eigenfunctions of the wave operator. It has been shown that both of these systems can be made globally unstable by confinement to a short finite range, although the eigenvalue distributions are entirely different in the two cases.

For the first system, asymptotics have been used to show the variation of the eigenvalue distribution as two waves approach resonance. For the second system, the limit of the coupling parameter having large modulus has been considered.

Clearly, more work is needed to establish how relevant these results are to, for example, fluid flow dynamics. One general observation is that, even when the dispersion relation of the equivalent homogeneous (e.g. parallel-flow) system predicts only decaying disturbances, the stability of the nonhomogeneous system is not assured.

Chapter 7

A modified Benjamin-Ono equation

7.1 Introduction

The Benjamin-Ono equation,

$$u_t = cu_x + auu_x + \alpha \frac{\partial^2}{\partial x^2} \int_{-\infty}^{\infty} \frac{u(x')}{x' - x} \mathrm{d}x', \tag{7.1}$$

is an equation used in the stability analysis of deep stratified fluids (see [3], [4], [45]) as well in other areas, such as the study of solar magnetic fields (see [57]). In a deep-fluid set-up, the solution of appropriate equations in a fluid layer of finite thickness drives a solution in a region of bulk fluid which is governed by Laplace's equation. This leads to a stability problem featuring a Cauchy integral term of the form shown in (7.1); see [45] for a full derivation.

In this chapter, we will consider a slightly generalised version of this equation, adding a dissipative term and a linear growth rate term. The idea behind adding these terms is to enable investigation of the consequences of having a space-varying linear growth rate term, as was done in Chapter 2. We begin, however, by briefly recalling the soliton solutions that (7.1) admits. The solitons demonstrate a key feature of the integral term: solutions to equa-

tions featuring such a term may have algebraically-decaying tails, unlike the exponentially-decaying tails that we normally associate with purely-differential equations.

The content of this chapter is focused around two issues concerning the solution of our modified Benjamin-Ono equation. The first issue relates to the use of the Briggs-Bers criterion (see Section 1.3) for problems of this type. The power of this criterion has ensured that its use is widespread in stability problems. However, it relies on the idea that the dominant contribution to the large-time asymptotics comes from a saddle point of the dispersion relation. This is not necessarily the case for problems with a Cauchy integral, which leads to a branch cut in the wavenumber plane. That this branch cut may be the most important contributor is demonstrated in Section 7.3.

The second issue covered in this chapter concerns the effect of the algebraically-decaying tails mentioned above on our ability to compute solutions, in this case to a spatially-inhomogeneous problem, numerically. The results of a number of computations are considered which illustrate the difficulty of making the numerical system long enough to fully represent this algebraic decay while remaining numerically stable.

7.2 Formulation

The addition of a dissipative term and a linear growth rate term to (7.1) leads to the following equation:

$$u_t = cu_x + \nu u_{xx} + \beta u + auu_x + \alpha \frac{\partial^2}{\partial x^2} \int_{-\infty}^{\infty} \frac{u(x')}{x' - x} \mathrm{d}x'. \tag{7.2}$$

This equation has, in general, no known analytic solution. As mentioned above, for the case $\nu = \beta = 0$, i.e. the usual Benjamin-Ono equation, soliton solutions exist - see Section 7.2.1 for a discussion of these. Otherwise, any attempt to study this equation clearly must centre around the numerical computation of

solutions, especially those of the Fourier transform of the equation.

Such computations can only be done at a finite number of points and so we should consider discrete, rather than continuous, Fourier transforms of solutions. (See Appendix A.4.1 for more information on discrete Fourier transforms.) The need to use discrete Fourier transforms applies both to computation of eigenvalue solutions, which we present here, and to full computations of an initial-value problem, which were attempted during research but we do not report here. The reason for this is that the initial-value solutions fall victim to the same problems as those we discuss here for eigenvalue problems.

7.2.1 Soliton solutions to the Benjamin-Ono equation

We recall the case with $\nu = \beta = 0$, the usual Benjamin-Ono equation, and show that it has solutions in the form of solitons. Given (7.1 again),

$$u_t = cu_x + auu_x + \alpha \frac{\partial^2}{\partial x^2} \int_{-\infty}^{\infty} \frac{u(x')}{x' - x} \mathrm{d}x',$$

we have solutions of the form

$$u(x,t) = \frac{A_1}{1 + \left(\frac{x + \left(c + \frac{aA_1}{4}\right)t}{\frac{4\alpha\pi}{aA_1}} \right)^2}, \tag{7.3}$$

for any A_1; see Appendix A.4.2 for a derivation. It is clear that, for t fixed and x large, the decay of this will be proportional to x^{-2}. We should thus expect solutions to the related problem (7.2) to demonstrate algebraic, rather than exponential, decay as $x \to \pm\infty$.

7.3 Stability analysis using the dispersion relation

As discussed in Section 7.1, the ultimate aim of this chapter is to study a spatially-nonhomogeneous version of (7.2). Before doing this, however, we

consider the homogeneous version. We do this in two ways. Firstly, we study a stability problem based on the dispersion relation, i.e. assuming travelling-wave disturbances and analysing saddle points of the frequency distribution as a function of complex wavenumber. However, as is usual for solutions derived from consideration of the dispersion relation or, equivalently, Briggs-Bers analysis, this only allows for exponential contributions to the large-time behaviour of disturbances. We show that this is not the correct picture by choosing a set of parameters which predict convective instability by this method and then showing that we have absolute instability when the full stability problem is studied and the branch cuts in the complex wavenumber plane are taken into account. To obtain a dispersion relation for our system, we consider the t dependence to be of the form $e^{-i\omega t}$ and the x dependence to be like e^{ikx}, as is usual for such problems. Focusing only on linear disturbances, we insist for now that $a = 0$. Equation (7.1) becomes

$$-i\omega = cik - \nu k^2 + \beta + \alpha i\pi k|k|. \tag{7.4}$$

Appendix A.4.3 contains details of the derivation of the last term. However, it is worth noting here that the symbol $|k|$ does not, in this case, represent the usual complex modulus of k. Looking at the derivation in Appendix A.4.3, we see that the symbol $|k|$ is used to mean only 'a function of k equal to k on the non-negative real axis and equal to $-k$ on the negative real axis'. Nothing is said about its value elsewhere in the complex k-plane. Recall now that the derivation of the Briggs-Bers (saddle point) criterion in Chapter 1 relies on using contour deformation to determine the stability of systems. Such deformation is, of course, only possible across regions of the complex plane where the function under consideration is analytic. Thus we require a continuation of our '$|k|$ on the real k-axis' function into the complex plane. By the uniqueness of analytic continuations we must choose our complex $|k|$ function to be equal to k on a region of the plane including the entire non-negative real axis but

no part of the negative real axis and equal to $-k$ elsewhere. Henceforth, this is what we will take $|k|$ to mean.

We analyse (7.4) in the usual way: the two roots for k may be separated into the upper- and lower half-planes of the complex k-plane by making ω_i large. Then, as ω_i is reduced to zero, we can find a combination of parameters for which the branches $k(\omega)$ just touch, at a pinch point, implying that upstream, and downstream, influences are indistinguishable. If this occurs for $\omega_i > 0$, it indicates absolute instability.

However, there is a clear problem that the factor $|k|$, even with the definition described above, is not everywhere analytic. We avoid this by taking the two regions of analyticity described above to be separated by the imaginary k-axis and insisting that $k_r > 0$, thus choosing precisely the region with $|k| = k$. Hence

$$(\alpha i\pi - \nu)\, k^2 + cik + (\beta + i\omega) = 0. \tag{7.5}$$

The discriminant for this quadratic equation will tell us when the pinch point is reached:

$$-c^2 - 4\,(\alpha i\pi - \nu)\,(\beta + i\omega) = 0, \tag{7.6}$$

or

$$\omega = \frac{c^2\,(\alpha\pi - i\nu)}{4\,(\alpha^2\pi^2 + \nu^2)} + i\beta. \tag{7.7}$$

For absolute instability to be observed, this pinch point must be reached for a value of ω with $\omega_i > 0$. Thus $\omega_i = 0$ is a distinguishing case - when this is true

$$\beta = \frac{\nu c^2}{4\,(\alpha^2\pi^2 + \nu^2)}. \tag{7.8}$$

It is clear (consider (7.6)) that decreasing β makes the system more stable. This method thus predicts stability, or convective instability, when

$$\beta < \frac{\nu c^2}{4\,(\alpha^2\pi^2 + \nu^2)}. \tag{7.9}$$

Note that, when $c = -0.7$, $\nu = 1$ and $\alpha = 1$, as will be used in the examples and diagrams in this chapter, the critical value of β is 0.01127. We will use

$\beta = 0.011$ as a 'sub-critical' β. When ω is such that the discriminant is zero, we have

$$k = \frac{-ic}{2(\alpha i\pi - \nu)}. \tag{7.10}$$

This gives

$$k_r = \frac{-c\alpha\pi}{2(\alpha^2\pi^2 + \nu^2)}. \tag{7.11}$$

We must ensure that this remains positive in order to justify the assumption that $|k| = k$. This is the case for the set of parameters suggested above.

However, as mentioned above, the dispersion relation calculation does not give us the full picture of stability. We now use the method of steepest descents to show that the system will, in fact, be absolutely unstable for any positive value of β.

7.4 The method of steepest descents

To understand the large-t asymptotic behaviour of our system, we use the method of steepest descents (see e.g. [5]). In the half-plane with $k_r > 0$, i.e. with $|k| = k$, we define

$$\lambda(k) = \beta + cik - \nu k^2 + \alpha\pi ik^2 \tag{7.12}$$

and the full solution to (7.2) with $a = 0$ is given by

$$\begin{aligned} u_1(x,t) &= \tfrac{1}{2\pi}\int_0^\infty e^{-\eta_0 k^2} e^{ikx} e^{\lambda(k)t}\mathrm{d}k \\ &= \tfrac{e^{\beta t}}{2\pi}\int_0^\infty e^{-\eta_0 k^2} e^{ikx} e^{\left(cik - \nu k^2 + \alpha\pi ik^2\right)t}\mathrm{d}k. \end{aligned} \tag{7.13}$$

We have taken the initial condition to be a Gaussian hump like $e^{-\eta_0 k^2}$ in Fourier space and so of similar form in physical space. In the half-plane with $k_r < 0$, i.e. with $|k| = -k$, we put

$$\lambda(k) = \beta + cik - \nu k^2 - \alpha\pi ik^2, \tag{7.14}$$

so

$$u_2(x,t) = \frac{e^{\beta t}}{2\pi} \int_{-\infty}^{0} e^{-\eta_0 k^2} e^{ikx} e^{\left(cik - \nu k^2 - \alpha\pi i k^2\right)t} \mathrm{d}k, \tag{7.15}$$

where, clearly, the full solution is $u(x,t) = u_1(x,t) + u_2(x,t)$. We wish to evaluate these integrals following lines of constant $\lambda_i(k)$, i.e. lines of steepest descent in $\lambda_r(k)$. To this end, we plot $\lambda_r(k) - \beta$ for the two cases of $|k| = k$ and $|k| = -k$, Figures 7.1 and 7.2.

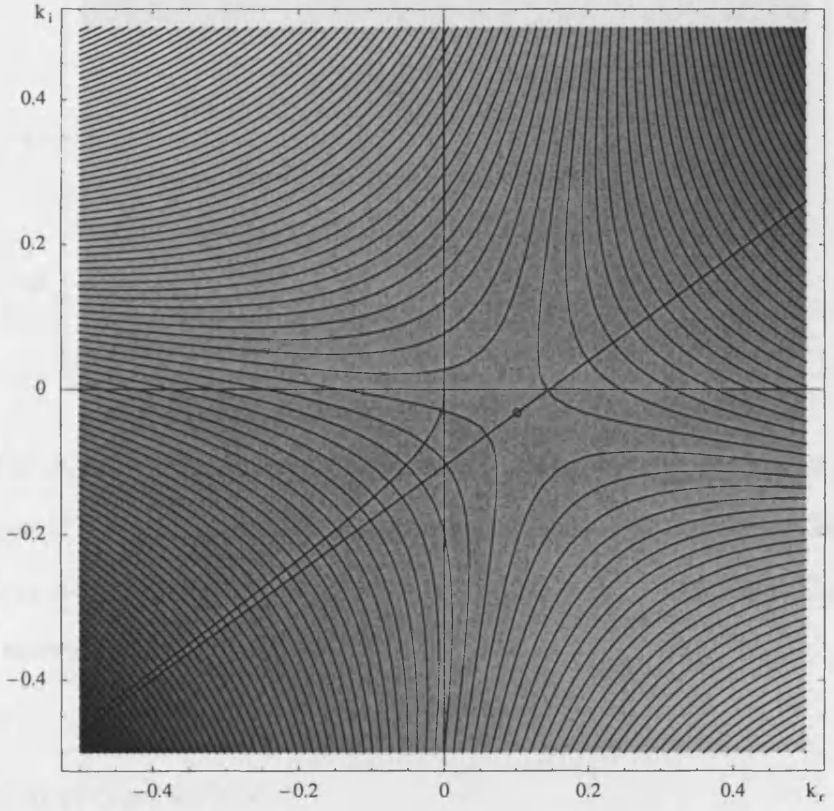

Figure 7.1: $\lambda_r - \beta$ as a function of complex k, when $|k|$ is taken to be equal to k. Areas of $\lambda_r - \beta$ large are light and areas of $\lambda_r - \beta$ small are dark. Our parameters are chosen to be $c = -0.7$, $\nu = 1$, $\alpha = 1$, $\beta = 0.011$. The saddle point is shown by a small circle.

We find that, in each case, there is a saddle point. The lines of steepest descent through the origin, as well as those through the saddle point, are shown in each

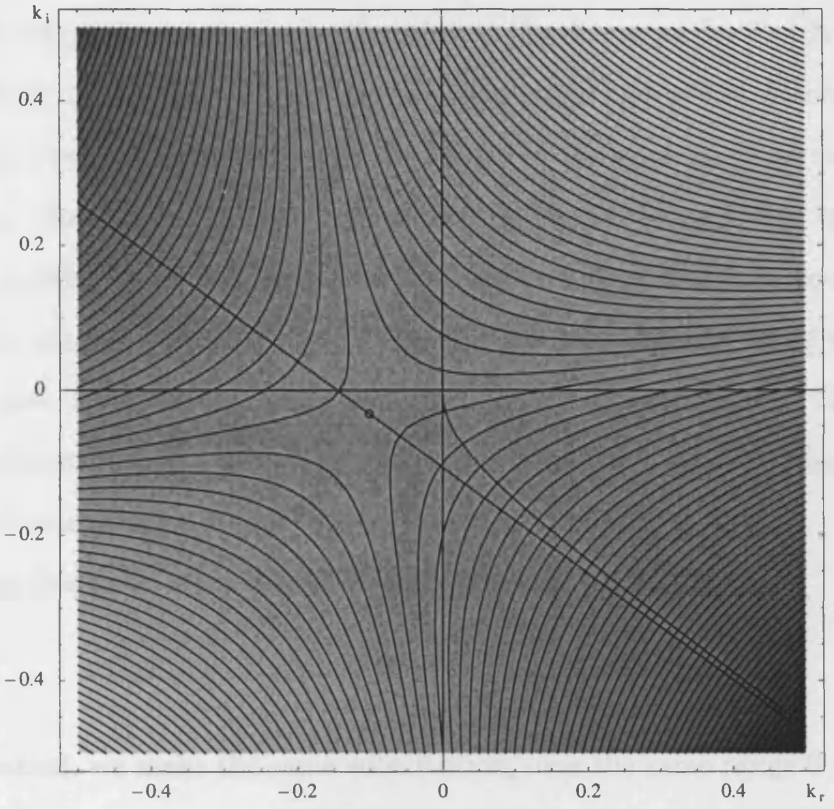

Figure 7.2: $\lambda_r - \beta$ as a function of complex k, when $|k|$ is taken to be equal to $-k$. Areas of $\lambda_r - \beta$ large are light and areas of $\lambda_r - \beta$ small are dark. Our parameters are chosen to be $c = -0.7$, $\nu = 1$, $\alpha = 1$, $\beta = 0.011$. The saddle point is shown by a small circle.

case.

In the first case, we have

$$k_{saddle} = \frac{-c\alpha\pi}{2\left(\alpha^2\pi^2 + \nu^2\right)} + i\frac{\nu c}{2\left(\alpha^2\pi^2 + \nu^2\right)} = 0.101159 - 0.0321999i, \quad (7.16)$$

as in (7.10). At this point, $\lambda - \beta = -0.01127 - 0.0354056i$. In the second case, we have

$$k_{saddle} = \frac{c\alpha\pi}{2\left(\alpha^2\pi^2 + \nu^2\right)} + i\frac{\nu c}{2\left(\alpha^2\pi^2 + \nu^2\right)} = -0.101159 - 0.0321999i. \quad (7.17)$$

Here, $\lambda - \beta = -0.01127 + 0.0354056i$. However, in each case, $\lambda(0) - \beta = 0$ so the origin provides a larger real part of λ than either saddle point and

we expect the origin to make the dominant contribution. We thus consider only a small path near the origin. Looking at the diagrams, we clearly cannot define $|k|$ in a consistent way such that both paths of steepest descent from the origin are also consistent with the values of $|k|$ we must have along the real axis. However, as we are only considering paths close to the origin, it suffices to deform the contours for a short distance such that they go straight down the imaginary axis. This can only be done for a suitably short path as, in each case, further down the imaginary axis λ_r starts to increase. However, we can always choose a path length, ϵ, sufficiently small and still capture the dominant contribution to our integral, i.e. that from the origin.

In the first case, we make the substitution $k = -is$ to get

$$u_1(x,t) = -i\frac{e^{\beta t}}{2\pi}\int_0^{\epsilon} e^{\eta_0 s^2+\nu s^2 t}e^{sx+cst-\alpha\pi i s^2 t}\mathrm{d}s. \tag{7.18}$$

In the second, we make the same substitution, over the same range $0 < s < \epsilon$, to get

$$u_2(x,t) = -i\frac{e^{\beta t}}{2\pi}\int_{\epsilon}^{0} e^{\eta_0 s^2+\nu s^2 t}e^{sx+cst+\alpha\pi i s^2 t}\mathrm{d}s. \tag{7.19}$$

Changing the order of the limits gives

$$u_2(x,t) = i\frac{e^{\beta t}}{2\pi}\int_0^{\epsilon} e^{\eta_0 s^2+\nu s^2 t}e^{sx+cst+\alpha\pi i s^2 t}\mathrm{d}s. \tag{7.20}$$

We have

$$\begin{aligned} u(x,t) = u_1(x,t) + u_2(x,t) &= i\tfrac{e^{\beta t}}{2\pi}\textstyle\int_0^{\epsilon} e^{\eta_0 s^2+\nu s^2 t+sx+cst}\left(e^{\alpha\pi i s^2 t} - e^{-\alpha\pi i s^2 t}\right)\mathrm{d}s \\ &= -2\tfrac{e^{\beta t}}{2\pi}\textstyle\int_0^{\epsilon} e^{\eta_0 s^2+\nu s^2 t+sx+cst}\sin(\alpha\pi s^2 t)\mathrm{d}s. \end{aligned} \tag{7.21}$$

Everything under the integration is real, so we write $\sin\theta = \mathrm{Im}(e^{i\theta})$,

$$\begin{aligned} u(x,t) &= -2\tfrac{e^{\beta t}}{2\pi}\int_0^\epsilon e^{\eta_0 s^2+\nu s^2 t+sx+cst}\mathrm{Im}(e^{i\alpha\pi s^2 t})\mathrm{d}s \\ &= -2\tfrac{e^{\beta t}}{2\pi}\mathrm{Im}\int_0^\epsilon e^{\eta_0 s^2+\nu s^2 t+sx+cst+i\alpha\pi s^2 t}\mathrm{d}s. \end{aligned} \tag{7.22}$$

We put $s = p/t$ to get

$$u(x,t) = -\frac{2}{t}\frac{e^{\beta t}}{2\pi}\mathrm{Im}\int_0^{\epsilon t} e^{\eta_0\frac{p^2}{t^2}+\nu\frac{p^2}{t}+x\frac{p}{t}+cp+i\alpha\pi\frac{p^2}{t}}\mathrm{d}p \tag{7.23}$$

and we have $e^{i\alpha\pi\frac{p^2}{t}} \approx 1+\frac{i\alpha\pi p^2}{t}$, so

$$u(x,t) \approx -\frac{2}{t}\frac{e^{\beta t}}{2\pi}\int_0^{\epsilon t} e^{\eta_0\frac{p^2}{t^2}+\nu\frac{p^2}{t}+x\frac{p}{t}+cp}\alpha\pi\frac{p^2}{t}\mathrm{d}p. \tag{7.24}$$

For large t, e^{cp} dominates, so

$$u(x,t) \approx -\frac{e^{\beta t}}{2\pi}\frac{2\alpha\pi}{t^2}\int_0^{\epsilon t} e^{cp}p^2\mathrm{d}p, \tag{7.25}$$

or

$$u(x,t) \approx e^{\beta t}\frac{2\alpha}{c^3t^2}. \tag{7.26}$$

It is important to note that, in our examples, β is very small but positive. Thus we will initially see algebraic decay like t^{-2}. However, the exponential term will always eventually become dominant and so growth will be seen. Thus, our homogeneous system is absolutely unstable.

We now consider the evolution with time of the peak of our, initially Gaussian, disturbance wavepacket. To do so, we repeat our steepest descent analysis in a moving frame, considering x as a function of t. In general, we could consider $x(t) = x_0 + Ut$ and look for U and x_0 but, when t is large, it seems plausible that the shift by x_0 has little significance. Thus, we put

$$x(t) = Ut. \tag{7.27}$$

Substituting this into (7.13) and (7.15), we immediately see that we change our $\lambda(k)$s, effectively replacing c by $c+U$. We must now check how this affects

the steepest descent path. Changing the c to $c+U$ in our $\lambda(k)$s changes the value of λ_r by $-Uk_i$ in each case. Thus, if $U > 0$, it becomes possible that the path of integration, which extends a short distance down the imaginary axis, is no longer a path of descent. To see whether this is the case, we put $c_U = c + U$. Our new λ, λ_U, has real part given by

$$\lambda_{U,r}(k) = \beta - c_U k_i + \nu k_i^2 \mp 2\alpha\pi k_i k_r - \nu k_r^2, \tag{7.28}$$

where the upper sign is for the case $|k| = k$ and lower sign is for the case $|k| = -k$. Along the axis $k_r = 0$, the last two terms disappear and it is clear that our paths remain paths of descent, provided $c_U < 0$. However, when $c_U = 0$, i.e. $c+U = 0$, the path down the imaginary axis is no longer a descent path. We wish to study this case further.

Consider a path along the real axis, from 0 to ∞, in the first case, i.e. the case $|k| = k$. Along this path, $\lambda_{U,r}(k) = -\nu k_r^2$. Thus it is a path of descent. The steepest descent curve, in fact, is a straight line not parallel to either axis; the origin is the saddle point in this case. In the second case, the same path is also a path of descent. However, so is the path from 0 to $-\infty$. We choose the latter as we wish to find the integral from $-\infty$ to ∞. Therefore, we have

$$\begin{aligned} u_1(Ut,t) &= \tfrac{e^{\beta t}}{2\pi}\int_0^\infty e^{-\eta_0 k^2} e^{\left(c_U ik - \nu k^2 + \alpha\pi ik^2\right)t}\mathrm{d}k, \\ u_2(Ut,t) &= -\tfrac{e^{\beta t}}{2\pi}\int_\infty^0 e^{-\eta_0 k^2} e^{\left(-c_U ik - \nu k^2 - \alpha\pi ik^2\right)t}\mathrm{d}k \\ &= \tfrac{e^{\beta t}}{2\pi}\int_0^\infty e^{-\eta_0 k^2} e^{\left(-c_U ik - \nu k^2 - \alpha\pi ik^2\right)t}\mathrm{d}k. \end{aligned} \tag{7.29}$$

We add these and put $c_U = 0$ so

$$\begin{aligned} u(Ut,t) &= \tfrac{e^{\beta t}}{2\pi}\int_0^\infty e^{-(\eta_0+\nu t)k^2}\left(e^{\alpha\pi ik^2 t} + e^{-\alpha\pi ik^2 t}\right)\mathrm{d}k \\ &= \tfrac{e^{\beta t}}{\pi}\int_0^\infty e^{-(\eta_0+\nu t)k^2}\cos\left(\alpha\pi k^2 t\right)\mathrm{d}k. \end{aligned} \tag{7.30}$$

Now we put $k = p/\sqrt{t}$ and

$$u(Ut,t) = \frac{e^{\beta t}}{\pi\sqrt{t}} \int_0^\infty e^{-\eta_0 \frac{p^2}{t} - \nu p^2} \cos\left(\alpha \pi p^2\right) \mathrm{d}p, \tag{7.31}$$

We neglect the first term under the integral as it is small for large t. We are left with

$$\begin{aligned} u(Ut,t) &= \frac{e^{\beta t}}{\pi\sqrt{t}} \int_0^\infty e^{-\nu p^2} \cos\left(\alpha \pi p^2\right) \mathrm{d}p \\ &= \frac{e^{\beta t}}{\sqrt{\pi t}} \sqrt{\frac{1+\sqrt{1+\frac{\alpha^2\pi^2}{\nu^2}}}{8\nu\sqrt{1+\frac{\alpha^2\pi^2}{\nu^2}}}}. \end{aligned} \tag{7.32}$$

If it is not true that $c + U = 0$, we may keep the original path down the imaginary k-axis. The result is the same as for the $U = 0$ case, except with c replaced by c_U. As mentioned above, we will encounter a problem when $c_U = 0$ and must use the result above, (7.32). This grows faster than for any nonzero c_U and we conclude that the top of the pulse moves such that $c + U = 0$, i.e. $U = -c$ and grows like $e^{\beta t} t^{-\frac{1}{2}}$.

7.5 The inhomogeneous problem

We now consider an inhomogeneous system, in order to demonstrate the difficulties of eigenvalue calculation for such an equation. We illustrate this by considering linear disturbances ($a = 0$ in (7.2)) with β a function of x as shown in Figure 7.3.

This introduces a new length parameter, L, equal to the length between the points where β attains a value halfway between its maximum and minimum. It also introduces a parameter β_0, which is the maximum value of β. The minimum value of β is taken to be -3, with which we ensure very rapid damping of u in the corresponding regions, as follows from (7.26). The ends are chosen to be slightly rounded, with hyperbolic tangent profiles rather than immediate jumps. The reason for this is that fitting Fourier series to this set of points

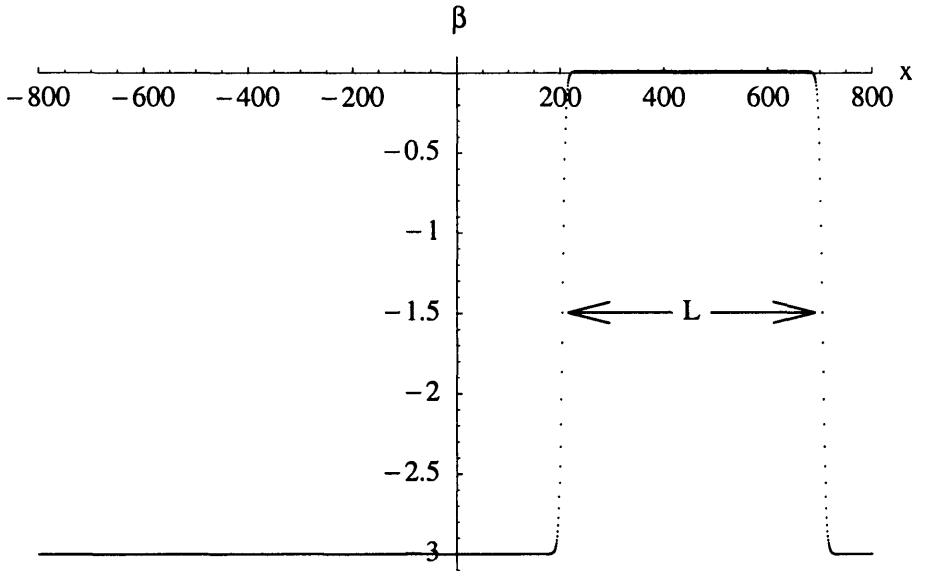

Figure 7.3: $\beta(x)$. Note that the function is given as a set of points. This is because numerical evaluation of solutions necessarily only happens at a finite number of points. The maximum value of $\beta(x)$, β_0, is slightly larger than 0, to act as a source of instability in the system. Here it equals 0.011.

gives a reasonably smooth shape around the jumps, i.e. the Gibbs phenomenon is small there.

Note that, as shown in Figure 7.3, the x-range for which $\beta(x) \approx \beta_0$ extends fairly close to the right-hand end of the domain. In order to prevent the right-hand edge of this range moving beyond the end of the domain, we will move the left-hand edge as L is varied. This has the advantage of keeping the distance between the initial condition and the right-hand end fixed: with $c < 0$ we expect the majority of the signal, initially, to travel towards this end.

Details of how the eigenvalue computation is done can be found in Appendix A.4.4.

Figure 7.4 shows the results of the eigenvalue computation. A system with a 'short' inhomogeneity ($L = 20$, Figure 7.4(a)) seems to produce an eigenvalue spectrum which resembles the continuous spectrum of the outer problem, along with some purely-decaying modes on the real axis. Increasing the length of the inhomogeneity ($L = 100$, Figure 7.4(b)), which potentially could lead to instability through feedback, appears to make some of the spectrum approach that for the problem with parameters equal to those in the high-β section. This may suggest instability if β_0 was positive, which is equivalent to a shift of Figure 7.4 in the real λ direction.

However, when the resolution of the problem is increased in Figure 7.4(c), we see modes moving back towards the real axis and the disappearance of the two small kinks in the spectrum that were present in Figure 7.4(b). The two calculations should represent the same problem physically, but clearly to get an 'accurate' answer for the eigenvalue problem would require the limit for increasing resolution to be known. The figure demonstrates that this is simply not possible computationally. The difference between the 641×641 (b) and the 1153×1153 (c) eigenvalue problems suggests that an enormous eigenvalue problem would have to be solved to get a reliable estimate of the

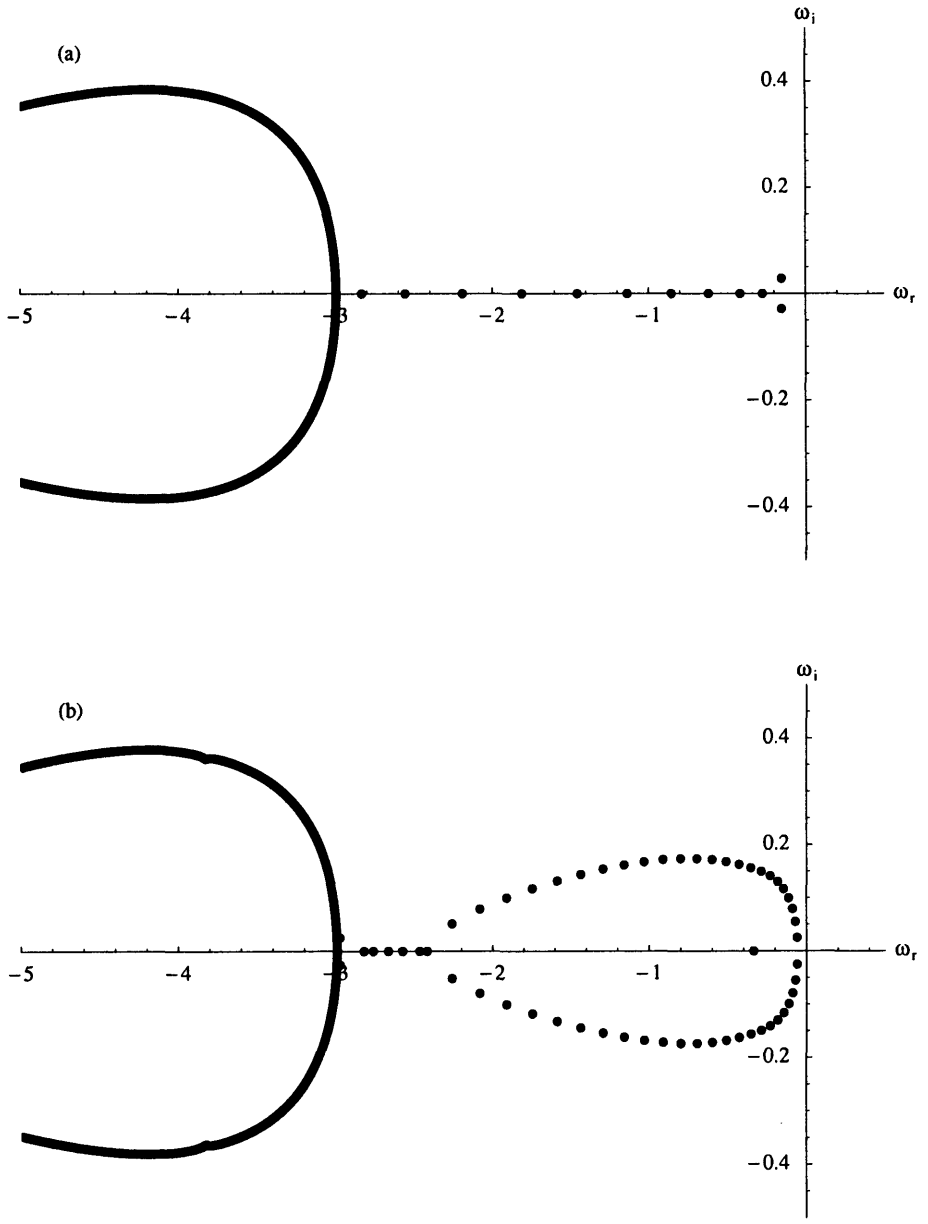
(a)
ω_i
0.4
0.2
ω_r
−5
−4
−3
−2
−1
−0.2
−0.4
(b)
ω_i
0.4
0.2
ω_r
−5
−4
−3
−2
−1
−0.2
−0.4

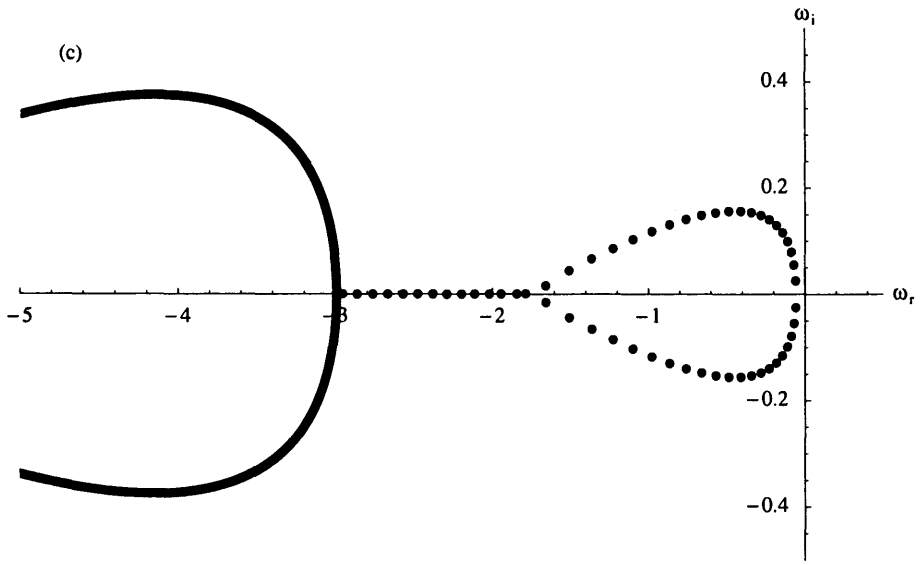

Figure 7.4: Three sets of eigenvalue solutions for our system. In each case, $\nu = 1, c = -0.7$, $\alpha = 0.1$ and $\beta_0 = 0$. In (a), we take the domain of system to be 1000 units long with $L = 20$, computed using 641 points and therefore 641 Fourier modes. We see that most of the modes lie on the continuous spectrum of the homogeneous problem with $\beta = -3$ and a few lie on, or close to, the real axis. In (b) the system has $L = 100$. We see that some modes appear to have moved away from the axis into the complex plane, towards the continuous spectrum of the $\beta = 0$ homogeneous problem. In (c) we again have $L = 100$ but this time with a 'grid refinement' to 1153 Fourier modes.

limiting result. Also, the ∞-norm condition numbers of the matrices used in (a), (b) and (c) were, respectively, 167, 1008 and 2799. This is consistent with the idea, mentioned in Section 1.5, that eigenvalue problems are more difficult to solve accurately for larger matrices.

Many calculations have been done to try to find limits of, for example, long systems, where eigenvalues can be computed for larger L values. However, problems are inevitably encountered, either with the size of the matrices required, or with their condition numbers growing hugely, to the point where the results are 'unstable' with respect to small perturbations of the system.

We suggest that the reason for these problems is the algebraic decay of signals due to the Cauchy integral term. This can influence the system over a huge range in x, unlike the exponential terms which decay rapidly for suitably chosen, i.e. 'sub-critical', β. This means that, to get an accurate result, the system would have to be so large as to make it infeasible computationally. We conclude that eigenvalue problems of this type are not a good method to study such systems.

Finally, it is worth commenting that a number of computations of initial-value problems for this set-up were attempted. In order to determine whether, for example, feedback could be observed between the ends of the $\beta \approx \beta_0$ section, such computations needed to run for a reasonable amount of time. After a fairly short time, however, it was observed that significant disturbances were reaching the ends of the computational domain, leading to potentially unreliable results. For this reason we do not present any such results here.

7.6 Summary

A Benjamin-Ono equation, with a dissipation term and a linear growth rate term added, has been studied in this chapter. Firstly, the soliton solutions

of the 'unmodified' Benjamin-Ono equation were considered; these demonstrate that solutions to equations featuring a Cauchy integral term can decay algebraically at infinity. Next, it was shown that naïve application of the Briggs-Bers (saddle-point) criterion to such problems can lead to incorrect determination of their stability. The dispersion relation contains a term which is not analytic in the wavenumber and the branch cut associated with this non-analyticity makes a more significant contribution to the large-time behaviour than the saddle point.

At the end of the chapter, some consideration was given to the computation of eigenvalues of the system with the linear growth rate term made nonhomogeneous in space. It was argued that the algebraic decay of solutions requires a domain so large as to make accurate numerical computations infeasible.

Chapter 8

Conclusions

The aim in this thesis has been to analyse the stability of a number of spatially-nonhomogeneous systems. There is no general theory for such systems and so we have concentrated on a number of fairly diverse example problems. It is hoped that the work presented here may be useful in the future development of any such general theory.

The use of the Briggs-Bers criterion for the study of the signalling problem is well established for spatially-homogeneous systems. In Chapter 2, a similar criterion was used for a spatially-periodic system, based on the linearised Ginzburg-Landau equation, by means of Floquet's theorem. This relied on continuation from a well-understood homogeneous case. The addition of periodicity was shown, generally, to make the system less stable. However, it was also shown that regions of local absolute instability were not necessarily sufficient to create an unstable global mode.

In Chapter 3, some of the ideas developed in Chapter 2 were used in the context of a fluid-dynamical problem. A geometry was chosen which allowed for an analytic base flow and a linear stability analysis was performed. Continuation from a homogeneous case to a spatially-periodic case was again used to study the signalling problem, by means of Floquet's theorem. The periodicity

of the system was shown to create an infinite set of evenly-spaced wavenumber curves. A three-wave resonance, with one 'wave' being the wall shape, was then shown to force a convectively-unstable homogeneous system into an absolutely-unstable régime for periodic wall variations of any height.

In Chapter 4, examples of systems with spatial nonhomogeneity confined to a finite range were presented. In these, it was necessary to distinguish upstream- from downstream-travelling branches so that no disturbance could come from infinity. A discrete spectrum of modes was sought and, in the case of sinusoidal wall variations, this spectrum was unstable in every case apart from that of a half-period channel expansion. In the case of discrete jumps in wall shape, both contractions and expansions were found to cause global instability although, for expansions, only when the length was sufficiently large. The systems possessed no region of local absolute instability, the observed global instability being due to a feedback mechanism.

Another locally convectively unstable system supporting unstable global modes was considered in Chapter 5. For a straight channel with two fluids separated by a solid wall containing a finite-length aperture, instability was observed for sufficiently long apertures. The idea of feedback between the ends of the aperture section was used to derive an approximation for the instability spectrum in the large-length limit. It was shown that, unlike systems with no feedback such as the linearised Ginzburg-Landau equation, this system remains globally unstable in the infinite-range limit, despite being, at worst, locally convectively unstable everywhere.

Having shown that a locally convectively unstable system permitting feedback can be globally unstable for a nonhomogeneous geometry, in Chapter 6 we considered two example systems which would be stable on an infinite range but which are globally unstable when confined to a finite range. Both systems supported strong transients. The first system comprised three coupled linear kine-

matic wave equations and the transients were due to near-resonance of waves. The second system had two coupled linear kinematic wave equations; here the non-normality of the wave operator was responsible for transient growth.

In the final chapter of research, Chapter 7, a modified Benjamin-Ono equation was considered as a stability model. We recalled that such equations may have solutions which decay algebraically at infinity in space. We then showed that care must be taken when applying the Briggs-Bers criterion to such equations: saddle points may not make the dominant contribution to the large-time asymptotics. Finally, we commented that the algebraic decay of solutions can make numerical results, both of eigenvalue problems and initial-value problems, very difficult to compute accurately.

8.1 Suggestions for further work

In Chapter 2, we observed that, as the magnitude of the periodic linear growth rate (ϵ) increased, the system was seen to move from convective to absolute instability as the two wavenumber curves met in the complex plane. Further increasing ϵ caused the curves to move apart again and it was mentioned that it is not immediately clear whether this corresponds to the system returning to a convectively unstable state or not. This is because we had relied on continuation from the homogeneous case to distinguish upstream- and downstream-travelling waves and this is impossible after the curves have touched. It would therefore be interesting to try to establish a technique for determining the stability of the large-ϵ cases. Looking at Figure 2.7, it would appear that the simple idea of increasing ω_i (decreasing b_0) until the curves move into opposite half-k-planes would be unsuccessful: the system may always pass through an absolutely unstable range before this happens.

The stability problems in Chapters 3, 4 and 5 were all derived by consider-

ing the linear stability of an inviscid two-fluid thin-layer flow. An interesting extension to this work would therefore be to attempt to include the effect of viscosity in the base flow. It is well known that adding viscosity to a fluid model may make it more stable or more unstable and so it is not immediately obvious whether this would restrict the observed instabilities or not. A consequence of adding viscosity is that it may not be possible to find an analytic form for the base flow: it would need to be computed. Computing the base flow would also create an opportunity to remove other restrictions such as the thin-layer approximation.

It is also worth noting that this thesis has been focused only on the linear stability of systems. The consideration of related nonlinear stability problems would also be an interesting extension.

In Chapter 6, the equations used were chosen because they provide a stability-like model through a set of equations which can exhibit transient growth. As was remarked in the chapter, it would be interesting to see whether equations exhibiting similar properties, i.e. instability due to transient growth and feedback, could be derived from a purely fluid-dynamical problem. It is also worth noting that both sets of equations used in the chapter were coupled; it would be interesting to search for problems with coupling only through boundary conditions which demonstrate the instability-through-feedback phenomena.

Appendix A

Derivations and notes

A.1 Notes on the proof of Floquet's theorem

A.1.1 Justification that C in (2.10) is constant

Using all notation as in Chapter 2, we have

$$\Phi(x)C(x) = \Phi(x+\theta), \tag{A.1}$$

where we have now assumed that C may vary with x. Using dashes to represent derivatives w.r.t. x, we have

$$\begin{aligned} \Phi'(x)C(x) + \Phi(x)C'(x) &= \Phi'(x+\theta) \\ &= A(x+\theta)\Phi(x+\theta) \\ &= A(x)\Phi(x+\theta) \\ &= A(x)\Phi(x)C(x), \end{aligned} \tag{A.2}$$

This means

$$\begin{aligned} \Phi(x)C'(x) &= \left(A(x)\Phi(x) - \Phi'(x)\right)C(x) \\ &= 0, \end{aligned} \tag{A.3}$$

and, by the linear independence of the solutions of which $\Phi(x)$ is comprised, $\Phi(x)$ is nonsingular and we conclude that $C'(x) = 0$, so $C(x)$ is a constant, C.

A.1.2 The existence of matrix logarithms for nonsingular matrices

Given a nonsingular square matrix C, we wish to show that there exists a matrix M, say, such that

$$C = e^M. \tag{A.4}$$

As C is nonsingular, it is diagonalisable. If Q is a matrix with the eigenvectors of C as its columns, then

$$C = QDQ^{-1}, \tag{A.5}$$

with D a diagonal matrix with diagonal elements $D_{(11)}$, $D_{(22)} \ldots D_{(nn)}$, say, none of which may be zero by the nonsingularity of C. Consider now a diagonal matrix E which has elements $\log D_{(11)}$, $\log D_{(22)} \ldots \log D_{(nn)}$ along its diagonal. Then

$$\begin{aligned} e^{QEQ^{-1}} &= I + QEQ^{-1} + \frac{QEQ^{-1}QEQ^{-1}}{2!} + \frac{QEQ^{-1}QEQ^{-1}QEQ^{-1}}{3!} + \ldots \\ &= I + QEQ^{-1} + \frac{QE^2Q^{-1}}{2!} + \frac{QE^3Q^{-1}}{3!} + \ldots \\ &= Q\left(I + E + \frac{E^2}{2!} + \frac{E^3}{3!} + \ldots\right)Q^{-1}, \end{aligned} \tag{A.6}$$

and, considering the terms in brackets element-by-element, it is clear that they equal D. Thus we have

$$C = e^{QEQ^{-1}}, \tag{A.7}$$

as required.

A.2 Notes for Chapter 3

A.2.1 The thin-layer approximation

The inviscid, incompressible, 2D Navier-Stokes equations (incompressible Euler equations) for a single fluid are

$$\frac{\partial u}{\partial t} + u\frac{\partial u}{\partial x} + v\frac{\partial u}{\partial y} = -\frac{1}{\rho}\frac{\partial p}{\partial x} + \frac{F_x}{\rho}, \tag{A.8}$$

$$\frac{\partial v}{\partial t} + u\frac{\partial v}{\partial x} + v\frac{\partial v}{\partial y} = -\frac{1}{\rho}\frac{\partial p}{\partial y} + \frac{F_y}{\rho}, \tag{A.9}$$

$$\frac{\partial u}{\partial x} + \frac{\partial v}{\partial y} = 0, \tag{A.10}$$

where u and v are the components of fluid velocity in the x and y directions respectively, p is pressure, ρ the (constant) fluid density and F_x and F_y are the x- and y-components of body forces acting on the fluid. Here, the only body force of interest is gravity, which is irrotational and can thus be represented by a potential. We combine this potential with pressure to form the modified pressure, which the symbol p will represent from now on.

We now appeal to a simple scaling argument to derive thin-layer equations (3.1) - (3.3). Let L be a characteristic length for variations of solutions to (A.8) - (A.10) in the x-direction and δ be such a length in the y-direction. We take our fluid to occupy a region which is small in y-extent, i.e. is thin. Thus $\delta \ll L$. Let U be a characteristic scale for u and V a characteristic scale for v. From (A.10) we have

$$V \approx \frac{\delta U}{L}. \tag{A.11}$$

If P is chosen as a scale for pressure, then we have a choice in how to relate this to other scalings: from (A.8), or from (A.9). Equating the pressure term in (A.8) with the second and third terms gives

$$P \approx \rho U^2, \tag{A.12}$$

(note that since ρ is constant, there is no need for it to have a separate 'scale'), whereas equating the pressure term in (A.9) with the second and third terms would give

$$P \approx \frac{\rho U^2 \delta^2}{L^2}. \tag{A.13}$$

The second scaling makes pressure far smaller than the first and negligible in (A.8). However, the other terms in (A.8) are larger than those in (A.9) by a factor of $\frac{\delta}{L}$, so to assume that pressure is negligible in (A.8) would constitute an unreasonable restriction on pressure variation. We thus choose the first scaling, from (A.12), as the scaling for pressure.

With this choice, we obtain from (A.8) a scaling T for t equal to

$$T \approx \frac{L}{U}. \tag{A.14}$$

(Note that we have a choice of equation to determine this also and choose (A.8) for the same reason.) This and (A.11) make all terms in (A.9) negligibly small, except the pressure term, while (A.8) and (A.10) retain all terms, (except the explicit body force term). This gives (3.1) - (3.3).

A.2.2 Linearisation of the governing equations

Differentiating (3.6) w.r.t. x and substituting from (3.7), we obtain

$$\rho_1 \frac{\partial u_1}{\partial t} + \rho_1 u_1 \frac{\partial u_1}{\partial x} - \rho_2 \frac{\partial u_2}{\partial t} - \rho_2 u_2 \frac{\partial u_2}{\partial x} = -g_\rho \frac{\partial f}{\partial x} + \gamma \frac{\partial^3 f}{\partial x^3}. \tag{A.15}$$

Substituting from (3.16) and keeping terms of order δ, we get

$$i\omega\rho_2 U_2 - \rho_2(U_2 u'_{20} + u_{20} U'_2) - i\omega\rho_1 U_1 + \rho_1(u_{10} U'_1 + u'_{10} U_1) = -g_\rho F' + \gamma F'''. \tag{A.16}$$

We linearise (3.10) and (3.11) to obtain

$$\frac{1}{h_1}\left(i\omega F - u'_{10} F - u_{10} F' - U_1 h'_1\right) = U'_1 \tag{A.17}$$

and

$$\frac{1}{h_2}\left(-i\omega F + u'_{20}F + u_{20}F' - U_2 h'_2\right) = U'_2, \tag{A.18}$$

which may be used in (A.16) to remove derivatives of $U_{1,2}$ on the l.h.s. and obtain (3.17).

A.2.3 The dispersion relation

Substituting (3.19) into (3.17) and remembering that, for a straight channel, $h_1(x) = h_{1\infty}$, $h'_1(x) = 0$, $h_2(x) = h_{2\infty}$, $h'_2(x) = 0$, $u_{10}(x) = u_{1\infty}$, $u'_{10}(x) = 0$, $u_{20}(x) = u_{2\infty}$, $u'_{20}(x) = 0$, we get

$$\begin{aligned}
\tfrac{1}{h_{1\infty}}\left(i\omega - iku_{1\infty}\right)F &= ikU_1, \\
-\tfrac{1}{h_{2\infty}}\left(i\omega - iku_{2\infty}\right)F &= ikU_2, \\
i\omega\rho_2 U_2 - \rho_2 u_{2\infty}\left(\tfrac{-i\omega}{h_{2\infty}} + \tfrac{u_{2\infty}ik}{h_{2\infty}}\right)F & \\
-i\omega\rho_1 U_1 + \rho_1 u_{1\infty}\left(\tfrac{-i\omega}{h_{1\infty}} + \tfrac{u_{1\infty}ik}{h_{1\infty}}\right)F &= -g_\rho ikF - \gamma ik^3 F.
\end{aligned} \tag{A.19}$$

We put the first two of these equations into the third and eliminate F, obtaining

$$\begin{aligned}
-\tfrac{\rho_2\omega}{h_{2\infty}k}(\omega - ku_{2\infty}) - \tfrac{\rho_2 u_{2\infty}}{h_{2\infty}}(\omega - ku_{2\infty}) & \\
-\tfrac{\rho_1\omega}{h_{1\infty}k}(\omega - ku_{1\infty}) - \tfrac{\rho_1 u_{1\infty}}{h_{1\infty}}(\omega - ku_{1\infty}) &= -g_\rho k - \gamma k^3,
\end{aligned} \tag{A.20}$$

which is equivalent to (3.20).

A.2.4 The form of $A(x)$

In order to simplify the following manipulation, we make the definition

$$K = \frac{\rho_1 u_{1\infty}^2}{\rho_2 u_{2\infty}^2}, \tag{A.21}$$

so,

$$h_2(x) = \frac{h_{2\infty}}{\sqrt{1+K\left(\frac{h_{1\infty}^2}{h_1^2(x)}-1\right)}},$$

$$u_{20}(x) = \frac{u_{2\infty}h_{2\infty}}{h_2(x)} = u_{2\infty}\sqrt{1+\frac{\rho_1 u_{2\infty}^2}{\rho_2 u_{2\infty}^2}\left(\frac{h_{1\infty}^2}{h_1^2(x)}-1\right)} = u_{2\infty}\sqrt{1+K\left(\frac{h_{1\infty}^2}{h_1^2(x)}-1\right)}. \tag{A.22}$$

Thus

$$h_2'(x) = \frac{h_{2\infty}Kh_{1\infty}^2h_1'(x)}{\left(1+K\left(\frac{h_{1\infty}^2}{h_1^2(x)}-1\right)\right)^{3/2}h_1^3(x)},$$

$$u_{10}'(x) = \frac{-u_{1\infty}h_{1\infty}h_1'(x)}{h_1^2(x)}, \tag{A.23}$$

$$u_{20}'(x) = \frac{-u_{2\infty}h_{2\infty}h_2'(x)}{h_2^2(x)} = \frac{-u_{2\infty}Kh_{1\infty}^2h_1'(x)}{h_1^3(x)\sqrt{1+K\left(\frac{h_{1\infty}^2}{h_1^2(x)}-1\right)}}.$$

We put $h_1(x) = h_{1\infty} + \epsilon\sin(x)$ (equation 3.22) into $A(x)$ (equation 3.18) to get

$$A_{(11)}(x) = \frac{-\epsilon\cos(x)}{h_{1\infty}+\epsilon\sin(x)}, \tag{A.24}$$

$$A_{(13)}(x) = \frac{\epsilon h_{1\infty}u_{1\infty}\cos(x)}{(h_{1\infty}+\epsilon\sin(x))^3} + \frac{i\omega}{(h_{1\infty}+\epsilon\sin(x))}, \tag{A.25}$$

$$A_{(14)}(x) = \frac{-h_{1\infty}u_{1\infty}}{(h_{1\infty}+\epsilon\sin(x))^2}, \tag{A.26}$$

$$A_{(22)}(x) = \frac{-\epsilon h_{1\infty}^2K\cos(x)}{(h_{1\infty}+\epsilon\sin(x))^3\left(1+K\left(\frac{h_{1\infty}^2}{(h_{1\infty}+\epsilon\sin(x))^2}-1\right)\right)}, \tag{A.27}$$

$$A_{(23)}(x) = -\frac{\epsilon h_{1\infty}^2u_{2\infty}K\cos(x)}{h_{2\infty}(h_{1\infty}+\epsilon\sin(x))^3} - \frac{i\omega}{h_{2\infty}}\sqrt{1+K\left(\frac{h_{1\infty}^2}{(h_{1\infty}+\epsilon\sin(x))^2}-1\right)}, \tag{A.28}$$

$$A_{(24)}(x) = \frac{u_{2\infty}}{h_{2\infty}}\left(1+K\left(\frac{h_{1\infty}^2}{(h_{1\infty}+\epsilon\sin(x))^2}-1\right)\right), \tag{A.29}$$

$$A_{(34)}(x) = 1, \tag{A.30}$$

$$A_{(45)}(x) = 1, \tag{A.31}$$

$$A_{(51)}(x) = \frac{\rho_1}{\gamma}\left(-i\omega - \frac{2\epsilon h_{1\infty}u_{1\infty}\cos(x)}{(h_{1\infty}+\epsilon\sin(x))^2}\right), \tag{A.32}$$

$$A_{(52)}(x) = \frac{\rho_2}{\gamma}\left(i\omega + \frac{2\epsilon h_{1\infty}^2 K u_{2\infty}\cos(x)}{(h_{1\infty}+\epsilon\sin(x))^3\sqrt{1+K\left(\frac{h_{1\infty}^2}{(h_{1\infty}+\epsilon\sin(x))^2}-1\right)}}\right), \tag{A.33}$$

$$\begin{aligned} A_{(53)}(x) &= \frac{\rho_1 u_{1\infty} h_{1\infty}}{\gamma}\left(\frac{\epsilon h_{1\infty} u_{1\infty}\cos(x)}{(h_{1\infty}+\epsilon\sin(x))^4} + \frac{i\omega}{(h_{1\infty}+\epsilon\sin(x))^2}\right) + \\ &\quad \frac{\rho_2 u_{2\infty}\sqrt{1+K\left(\frac{h_{1\infty}^2}{(h_{1\infty}+\epsilon\sin(x))^2}-1\right)}}{\gamma}\times \\ &\quad \left(\frac{\epsilon h_{1\infty}^2 K u_{2\infty}\cos(x)}{h_{2\infty}(h_{1\infty}+\epsilon\sin(x))^3} + \frac{i\omega}{h_{2\infty}}\sqrt{1+K\left(\frac{h_{1\infty}^2}{(h_{1\infty}+\epsilon\sin(x))^2}-1\right)}\right), \end{aligned} \tag{A.34}$$

$$\begin{aligned} A_{(54)}(x) &= \frac{g_\rho}{\gamma} - \frac{h_{1\infty}^2 u_{1\infty}^2 \rho_1}{\gamma(h_{1\infty}+\epsilon\sin(x))^3} \\ &\quad -\frac{\rho_2 u_{2\infty}^2}{\gamma h_{2\infty}}\left(1+K\left(\frac{h_{1\infty}^2}{(h_{1\infty}+\epsilon\sin(x))^2}-1\right)\right)^{3/2}, \end{aligned} \tag{A.35}$$

with all other components of A equal to 0.

A.2.5 The form of $A^{(0)}$, $A^{(1+)}$ and $A^{(1-)}$

Approximating each of the above elements in the form $A_{(xy)} = A_{(xy)}^{(0)} + \epsilon A_{(xy)}^{(1)} + O(\epsilon^2)$, we get:

$$A_{(11)}(x) = 0 + \epsilon\frac{-\cos(x)}{h_{1\infty}} + O(\epsilon^2), \tag{A.36}$$

$$A_{(13)}(x) = \frac{i\omega}{h_{1\infty}} + \epsilon\left(\frac{u_{1\infty}\cos(x) - i\omega\sin(x)}{h_{1\infty}^2}\right) + O(\epsilon^2), \tag{A.37}$$

$$A_{(14)}(x) = \frac{-u_{1\infty}}{h_{1\infty}} + \epsilon\frac{2u_{1\infty}\sin(x)}{h_{1\infty}^2} + O(\epsilon^2), \tag{A.38}$$

$$A_{(22)}(x) = 0 + \epsilon\frac{-K\cos(x)}{h_{1\infty}} + O(\epsilon^2), \tag{A.39}$$

$$A_{(23)}(x) = \frac{-i\omega}{h_{2\infty}} + \epsilon\left(\frac{-u_{2\infty}K\cos(x) + i\omega K\sin(x)}{h_{1\infty}h_{2\infty}}\right) + O(\epsilon^2), \tag{A.40}$$

$$A_{(24)}(x) = \frac{u_{2\infty}}{h_{2\infty}} + \epsilon\frac{-2u_{2\infty}K\sin(x)}{h_{1\infty}h_{2\infty}} + O(\epsilon^2), \tag{A.41}$$

$$A_{(34)}(x) = 1, \tag{A.42}$$

$$A_{(45)}(x) = 1, \tag{A.43}$$

$$A_{(51)}(x) = \frac{-i\omega\rho_1}{\gamma} + \epsilon\frac{-2\rho_1 u_{1\infty}\cos(x)}{\gamma h_{1\infty}} + O(\epsilon^2), \tag{A.44}$$

$$A_{(52)}(x) = \frac{i\omega\rho_2}{\gamma} + \epsilon\frac{2\rho_2 u_{2\infty} K\cos(x)}{\gamma h_{1\infty}} + O(\epsilon^2), \tag{A.45}$$

$$\begin{aligned} A_{(53)}(x) \;=\; & \tfrac{i\omega\rho_1 u_{1\infty}}{\gamma h_{1\infty}} + \tfrac{i\omega\rho_2 u_{2\infty}}{\gamma h_{2\infty}} + \\ & \epsilon\left(\tfrac{\rho_1 u_{1\infty}^2\cos(x) - 2i\omega\rho_1 u_{1\infty}\sin(x)}{\gamma h_{1\infty}^2} + \tfrac{\rho_2 u_{2\infty}^2 K\cos(x) - 2i\omega\rho_2 u_{2\infty} K\sin(x)}{\gamma h_{1\infty} h_{2\infty}}\right) \\ & + O(\epsilon^2), \end{aligned} \tag{A.46}$$

$$A_{(54)}(x) \;=\; \tfrac{g_\rho}{\gamma} - \tfrac{u_{1\infty}^2\rho_1}{\gamma h_{1\infty}} - \tfrac{u_{2\infty}^2\rho_2}{\gamma h_{2\infty}} + \epsilon\left(\tfrac{3u_{1\infty}^2\rho_1\sin(x)}{\gamma h_{1\infty}^2} + \tfrac{3u_{2\infty}^2\rho_2 K\sin(x)}{\gamma h_{1\infty} h_{2\infty}}\right) + O(\epsilon^2), \tag{A.47}$$

We now alter the expansion of A slightly, so that $A = A^{(0)} + \epsilon A^{(1+)}e^{ix} + \epsilon A^{(1-)}e^{-ix} + O(\epsilon^2)$ and

$$A^{(0)} = \begin{pmatrix} 0 & 0 & \frac{i\omega}{h_{1\infty}} & \frac{-u_{1\infty}}{h_{1\infty}} & 0 \\ 0 & 0 & \frac{-i\omega}{h_{2\infty}} & \frac{u_{2\infty}}{h_{2\infty}} & 0 \\ 0 & 0 & 0 & 1 & 0 \\ 0 & 0 & 0 & 0 & 1 \\ \frac{-i\omega\rho_1}{\gamma} & \frac{i\omega\rho_2}{\gamma} & \frac{i\omega\rho_1 u_{1\infty}}{\gamma h_{1\infty}} + \frac{i\omega\rho_2 u_{2\infty}}{\gamma h_{2\infty}} & \frac{g_\rho}{\gamma} - \frac{\rho_1 u_{1\infty}^2}{\gamma h_{1\infty}} - \frac{\rho_2 u_{2\infty}^2}{\gamma h_{2\infty}} & 0 \end{pmatrix}, \tag{A.48}$$

$$A^{(1+)} = \begin{pmatrix} \frac{-1}{2h_{1\infty}} & 0 & \frac{u_{1\infty}-\omega}{2h_{1\infty}^2} & \frac{-iu_{1\infty}}{h_{1\infty}^2} & 0 \\ 0 & \frac{-K}{2h_{1\infty}} & \frac{-u_{2\infty}K+\omega K}{2h_{2\infty}h_{1\infty}} & \frac{iu_{2\infty}K}{h_{1\infty}h_{2\infty}} & 0 \\ 0 & 0 & 0 & 0 & 0 \\ 0 & 0 & 0 & 0 & 0 \\ \frac{-\rho_1 u_{1\infty}}{\gamma h_{1\infty}} & \frac{\rho_2 u_{2\infty}K}{\gamma h_{1\infty}} & \frac{\rho_1 u_{1\infty}^2 - 2\omega\rho_1 u_{1\infty}}{2\gamma h_{1\infty}^2} + \frac{\rho_2 u_{2\infty}^2 K - 2\omega\rho_2 u_{2\infty}K}{2\gamma h_{1\infty}h_{2\infty}} & \frac{-3i\rho_1 u_{1\infty}^2}{2\gamma h_{1\infty}^2} + \frac{-3i\rho_2 u_{2\infty}^2 K}{2\gamma h_{1\infty}h_{2\infty}} & 0 \end{pmatrix}, \tag{A.49}$$

$$A^{(1-)} = \begin{pmatrix} \frac{-1}{2h_{1\infty}} & 0 & \frac{u_{1\infty}+\omega}{2h_{1\infty}^2} & \frac{iu_{1\infty}}{h_{1\infty}^2} & 0 \\ 0 & \frac{-K}{2h_{1\infty}} & \frac{-u_{2\infty}K-\omega K}{2h_{2\infty}h_{1\infty}} & \frac{-iu_{2\infty}K}{h_{1\infty}h_{2\infty}} & 0 \\ 0 & 0 & 0 & 0 & 0 \\ 0 & 0 & 0 & 0 & 0 \\ \frac{-\rho_1 u_{1\infty}}{\gamma h_{1\infty}} & \frac{\rho_2 u_{2\infty}K}{\gamma h_{1\infty}} & \frac{\rho_1 u_{1\infty}^2 + 2\omega\rho_1 u_{1\infty}}{2\gamma h_{1\infty}^2} + \frac{\rho_2 u_{2\infty}^2 K + 2\omega\rho_2 u_{2\infty}K}{2\gamma h_{1\infty}h_{2\infty}} & \frac{3i\rho_1 u_{1\infty}^2}{2\gamma h_{1\infty}^2} + \frac{3i\rho_2 u_{2\infty}^2 K}{2\gamma h_{1\infty}h_{2\infty}} & 0 \end{pmatrix}, \tag{A.50}$$

A.2.6 Some differential equation theory

By linearity, we may write solutions to equations such as (3.34) as linear combinations of solutions to equations such as

$$\frac{\partial \mathbf{u}}{\partial x}(x) - A\mathbf{u}(x) = \mathbf{Q}e^{\lambda x}, \tag{A.51}$$

where $\mathbf{u}(x)$ is a vector of length n and A is an $n \times n$ matrix. $\mathbf{Q}$ is a constant vector. We assume throughout that A has n distinct eigenvalues. If λ is not an eigenvalue of A then solutions to (A.51) look like

$$\mathbf{u}(x) = -(A - \lambda I_n)^{-1}\mathbf{Q}e^{\lambda x} + \sum_j \mathbf{q}_j e^{ik_j x}, \tag{A.52}$$

where the ik_js are the eigenvalues of A and the $\mathbf{q}_j$s are the corresponding eigenvectors. The invertibility of $(A - \lambda I_n)$ is guaranteed by the fact that its determinant is equal to $(ik_1 - \lambda)(ik_2 - \lambda)\ldots(ik_n - \lambda)$, which cannot be zero.

If λ is an eigenvalue of A, ik_m say, then as A has n distinct eigenvalues, its eigenvectors are linearly independent and thus form a spanning set. So we may write

$$\mathbf{Q} = a_1\mathbf{q}_1 + a_2\mathbf{q}_2 + \ldots + a_n\mathbf{q}_n, \tag{A.53}$$

with the a_js unique, provided that the $\mathbf{q}_j$ have already been fixed. The solution to (A.51) is then

$$\begin{aligned}\mathbf{u}(x) \;=\; & \Big(-\tfrac{a_1}{ik_1-ik_m}\mathbf{q}_1 - \tfrac{a_2}{ik_2-ik_m}\mathbf{q}_2 - \ldots - \tfrac{a_{m-1}}{ik_{m-1}-ik_m}\mathbf{q}_{m-1} - \\ & \frac{a_{m+1}}{ik_{m+1}-ik_m}\mathbf{q}_{m+1} - \ldots - \frac{a_n}{ik_n-ik_m}\mathbf{q}_n + a_m x\mathbf{q}_m\Big)e^{ik_m x} \\ & + \sum_j l_j\mathbf{q}_j e^{ik_j x},\end{aligned} \tag{A.54}$$

for some $l_j \in \mathbb{R}$.

This solution can be derived by assuming a solution of the form $\mathbf{u}(x) = \mathbf{v}_0 e^{ik_m x} + \mathbf{v}_1 x e^{ik_m x}$, equating coefficients of $xe^{ik_m x}$ and $e^{ik_m x}$ and using the fact

that A is diagonalisable. This gives the part of the solution corresponding to $\mathbf{v}_1 x e^{ik_m x}$ and effectively eliminates the term $a_m \mathbf{q}_m$ from $\mathbf{Q}$. $\mathbf{v}_0$ can then be obtained by reversing the diagonalisation of A.

An important consequence of this, which is useful in the main text, is the fact that the condition for an equation like (A.51) to have no solution which varies like $xe^{ik_m x}$ is equivalent to saying that the expansion of $\mathbf{Q}$ in (A.53) has $a_m = 0$, where $\lambda = ik_m$. This follows from the uniqueness of the expansion.

A.2.7 The form of $A^{(\omega)}$

When we expand $A(x)$ in the form given by (3.46), the forms of $A^{(0)}$, $A^{(1+)}$ and $A^{(1-)}$ all remain the same as in Appendix A.2.5, but with ω replaced by ω_0. $A^{(\omega)}$ essentially just contains the terms in $A^{(0)}$ proportional to ω with ω brought out as a factor. Its form is therefore

$$A^{(\omega)} = \begin{pmatrix} 0 & 0 & \frac{i}{h_{1\infty}} & 0 & 0 \\ 0 & 0 & \frac{-i}{h_{2\infty}} & 0 & 0 \\ 0 & 0 & 0 & 0 & 0 \\ 0 & 0 & 0 & 0 & 0 \\ \frac{-i\rho_1}{\gamma} & \frac{i\rho_2}{\gamma} & \frac{i\rho_1 u_{1\infty}}{\gamma h_{1\infty}} + \frac{i\rho_2 u_{2\infty}}{\gamma h_{2\infty}} & 0 & 0 \end{pmatrix}. \tag{A.55}$$

A.3 Notes for Chapter 4

A.3.1 The fourth-order system

In order to derive $A_4(x)$, the matrix describing the fourth-order system, we begin by substituting (4.1) into (A.15) to get, after rearrangement

$$\begin{aligned}
&-\left(\rho_2 f_{h,2}^2(x,t)\left(u_1(x,t)\tfrac{\partial f_{h,1}}{\partial t}(x,t)+f_{h,1}(x,t)\tfrac{\partial u_1}{\partial t}(x,t)\right)\right)\\
&+\rho_2(h_{1\infty}u_{1\infty}+h_{2\infty}u_{2\infty}-f_{h,1}(x,t)u_1(x,t))^2 f'_{h,2}(x,t)\\
&+\rho_2 f_{h,2}(x,t)\left(h_{1\infty}u_{1\infty}+h_{2\infty}u_{2\infty}-f_{h,1}(x,t)u_1(x,t)\right)\times\\
&\left(-\tfrac{\partial f_{h,2}}{\partial t}(x,t)+u_1(x,t)f'_{h,1}(x,t)+f_{h,1}(x,t)u'_1(x,t)\right)\\
&+f_{h,2}^3(x,t)\left(\rho_1\tfrac{\partial u_1}{\partial t}(x,t)+g_\rho f'(x,t)+\rho_1 u_1(x,t)u'_1(x,t)-\gamma f'''(x,t)\right)=0,
\end{aligned} \tag{A.56}$$

where the temporary substitutions $f_{h,1}=f(x,t)+h_1(x)$ and $f_{h,2}=f(x,t)-h_2(x)$ have been made and primes denote derivatives w.r.t. x. We linearise this, using the same substitutions as (3.16). Equation (A.17) remains the same as before and is again used to remove derivatives of $U_1(x)$. This gives

$$\begin{aligned}
&h_2^3\rho_1 u_{10}\left(u_{10}F'+U_1h'_1\right)+h_1^3\rho_2\left(h_2U_1u_{10}+u_{10}^2F'-2U_1u_{10}h'_2\right)\\
&+h_1^2\rho_2\left(ih_2^2U_1\omega+h_2U_1u_{10}h'_1-2\left(h_{1\infty}u_{1\infty}+h_{2\infty}u_{2\infty}\right)\left(u_{10}F'-U_1h'_2\right)\right)\\
&+F\left(-\left(h_1^3\rho_2u_{10}^2\right)+h_2^3\rho_1u_{10}\left(u_{10}-i\omega\right)\right)\\
&+F\left(h_1^2\rho_2\left(u_{10}\left(h_{1\infty}u_{1\infty}+h_{2\infty}u_{2\infty}\right)+h_2u_{10}\left(u_{10}+2i\omega\right)-u_{10}^2\left(h'_1+2h'_2\right)\right)\right)\\
&+Fh_1\left(h_2^2u_{10}\left(3\rho_1u_{10}+i\rho_2\omega\right)+h_2\rho_2\left(-2i\left(h_{1\infty}u_{1\infty}+h_{2\infty}u_{2\infty}\right)\omega+u_{10}^2h'_1\right)\right)\\
&+Fh_1\left(+\rho_2u_{10}\left(h_{1\infty}u_{1\infty}+h_{2\infty}u_{2\infty}\right)\left(h'_1+2h'_2\right)\right)\\
&+h_1\left(\rho_2(h_{1\infty}u_{1\infty}+h_{2\infty}u_{2\infty})^2F'+h_2^3\left(i\rho_1U_1\left(iu_{10}+\omega\right)-g_\rho F'+\gamma F'''\right)\right)=0
\end{aligned} \tag{A.57}$$

for the other equation. This means that the matrix $A_4(x)=$

$$\begin{pmatrix}
\frac{-h'_1}{h_1} & \frac{i\omega-u'_{10}}{h_1} & \frac{-u_{10}}{h_1} & 0\\
0 & 0 & 1 & 0\\
0 & 0 & 0 & 1\\
A_{4,(41)}(x) & A_{4,(42)}(x) & A_{4,(43)}(x) & 0
\end{pmatrix}, \tag{A.58}$$

where

$$A_{4,(41)}(x) = \frac{-\left(h_2^3 u_{10}\rho_1 h_1'\right)+h_1^2\rho_2\left(-i\omega h_2^2-h_2 u_{10}h_1'-2(h_{1\infty}u_{1\infty}+h_{20}u_{2\infty})h_2'\right)}{\gamma h_1 h_2^3}+ \tag{A.59}$$

$$\frac{h_1 h_2^3\rho_1\left(-i\omega+u_{10}'\right)+h_1^3\rho_2\left(2u_{10}h_2'-h_2u_{10}'\right)}{\gamma h_1 h_2^3},$$

$$A_{4,(42)}(x) = \frac{h_1h_2\rho_2\left(2i\omega(h_{1\infty}u_{1\infty}+h_{20}u_{2\infty})-u_{10}^2h_1'+h_1u_{10}\left(-2i\omega-u_{10}'\right)\right)+ih_2^3u_{10}\rho_1\left(\omega+iu_{10}'\right)}{\gamma h_1h_2^3}+$$

$$\frac{h_1(h_1u_{10}-h_{1\infty}u_{1\infty}-h_{20}u_{2\infty})\rho_2\left(u_{10}\left(h_1'+2h_2'\right)+h_1u_{10}'\right)+h_1h_2^2u_{10}\left(-i\omega\rho_2-3\rho_1u_{10}'\right)}{\gamma h_1h_2^3}, \tag{A.60}$$

$$A_{4,(43)}(x) = \frac{g}{\gamma}-\frac{u_{10}^2\rho_1}{\gamma h_1}-\frac{(-(h_1u_{10})+h_{1\infty}u_{1\infty}+h_{20}u_{2\infty})^2\rho_2}{\gamma h_2^3}. \tag{A.61}$$

A.3.2 Asymptotics of flow past rectangular steps

Considering Figure 4.6, in section $\langle 1\rangle$ we have

$$\mathbf{u}_{4,\langle 1\rangle} = l_{nu}(L)\mathbf{q}_{nu}e^{ik_{nu}x}+l_u(L)\mathbf{q}_ue^{ik_ux}, \tag{A.62}$$

where we use the subscript nu to refer to quantities associated with the near-neutral upstream-travelling wave, the subscript u to refer to those associated with the other upstream-travelling wave, nd for the near-neutral downstream-travelling wave and d for the other downstream-travelling wave. $l_{nu}(L)$ etc. are functions of L, rather than values at $x = L$. We insist that $l_{nu}(L) = 1$ at $O(1)$. In section $\langle 2\rangle$, we have

$$\mathbf{u}_{4,\langle 2\rangle} = a_1(L)\mathbf{q}_1e^{ik_1x}+a_2(L)\mathbf{q}_2e^{ik_2x}+a_3(L)\mathbf{q}_3e^{ik_3x}+a_4(L)\mathbf{q}_4e^{ik_4x} \tag{A.63}$$

and we do not need to distinguish the waves which travel upstream from those which travel downstream. In section $\langle 3\rangle$, we have

$$\mathbf{u}_{4,\langle 3\rangle} = m_{nd}(L)\mathbf{q}_{nd}e^{ik_{nd}x}+m_d(L)\mathbf{q}_de^{ik_dx}. \tag{A.64}$$

At $x = 0$, we get

$$l_{nu}(L)B_{jump}\mathbf{q}_{nu} + l_u(L)B_{jump}\mathbf{q}_u = a_1(L)\mathbf{q}_1 + a_2(L)\mathbf{q}_2 + a_3(L)\mathbf{q}_3 + a_4(L)\mathbf{q}_4. \tag{A.65}$$

We write

$$B_{jump}\mathbf{q}_{nu} = a_{1nu}(L)\mathbf{q}_1 + a_{2nu}(L)\mathbf{q}_2 + a_{3nu}(L)\mathbf{q}_3 + a_{4nu}(L)\mathbf{q}_4 \tag{A.66}$$

and

$$B_{jump}\mathbf{q}_u = a_{1u}(L)\mathbf{q}_1 + a_{2u}(L)\mathbf{q}_2 + a_{3u}(L)\mathbf{q}_3 + a_{4u}(L)\mathbf{q}_4, \tag{A.67}$$

so that $a_1 = l_{nu}a_{1nu} + l_u a_{1u}$ etc. At $x = L$, we get

$$\begin{aligned} &a_1(L)\mathbf{q}_1 e^{ik_1 L} + a_2(L)\mathbf{q}_2 e^{ik_2 L} \\ &+a_3(L)\mathbf{q}_3 e^{ik_3 L} + a_4(L)\mathbf{q}_4 e^{ik_4 L} \end{aligned} = m_{nd}(L)B_{jump}\mathbf{q}_{nd}e^{ik_{nd}L} + m_d(L)B_{jump}\mathbf{q}_d e^{ik_d L}, \tag{A.68}$$

so we set

$$B_{jump}\mathbf{q}_{nd} = a_{1nd}(L)\mathbf{q}_1 + a_{2nd}(L)\mathbf{q}_2 + a_{3nd}(L)\mathbf{q}_3 + a_{4nd}(L)\mathbf{q}_4 \tag{A.69}$$

and

$$B_{jump}\mathbf{q}_d = a_{1d}(L)\mathbf{q}_1 + a_{2d}(L)\mathbf{q}_2 + a_{3d}(L)\mathbf{q}_3 + a_{4d}(L)\mathbf{q}_4. \tag{A.70}$$

(A.68) is now

$$\begin{aligned} \begin{pmatrix} \mathbf{q}_1 & \mathbf{q}_2 & \mathbf{q}_3 & \mathbf{q}_4 \end{pmatrix} \begin{pmatrix} a_1 e^{ik_1 L} \\ a_2 e^{ik_2 L} \\ a_3 e^{ik_3 L} \\ a_4 e^{ik_4 L} \end{pmatrix} &= m_{nd}e^{ik_{nd}L} \begin{pmatrix} \mathbf{q}_1 & \mathbf{q}_2 & \mathbf{q}_3 & \mathbf{q}_4 \end{pmatrix} \begin{pmatrix} a_{1nd} \\ a_{2nd} \\ a_{3nd} \\ a_{4nd} \end{pmatrix} \\ &\quad + m_d e^{ik_d L} \begin{pmatrix} \mathbf{q}_1 & \mathbf{q}_2 & \mathbf{q}_3 & \mathbf{q}_4 \end{pmatrix} \begin{pmatrix} a_{1d} \\ a_{2d} \\ a_{3d} \\ a_{4d} \end{pmatrix}, \end{aligned} \tag{A.71}$$

giving

$$l_{nu}\begin{pmatrix} a_{1nu}e^{ik_1L} \\ a_{2nu}e^{ik_2L} \\ a_{3nu}e^{ik_3L} \\ a_{4nu}e^{ik_4L} \end{pmatrix} + l_u \begin{pmatrix} a_{1u}e^{ik_1L} \\ a_{2u}e^{ik_2L} \\ a_{3u}e^{ik_3L} \\ a_{4u}e^{ik_4L} \end{pmatrix} = m_{nd}e^{ik_{nd}L}\begin{pmatrix} a_{1nd} \\ a_{2nd} \\ a_{3nd} \\ a_{4nd} \end{pmatrix} + m_d e^{ik_dL}\begin{pmatrix} a_{1d} \\ a_{2d} \\ a_{3d} \\ a_{4d} \end{pmatrix}. \tag{A.72}$$

Choosing $-$'s to refer to quantities in sections $\langle 1 \rangle$ and $\langle 3 \rangle$ and $+$'s to refer to quantities in section $\langle 2 \rangle$, we have

$$\mathbf{q}_{nu} = \begin{pmatrix} \omega - k_{nu}u_1^- \\ k_{nu}h_1^- \\ ik_{nu}^2 h_1^- \\ -k_{nu}^3 h_1^- \end{pmatrix} \tag{A.73}$$

and

$$\mathbf{q}_1 = \begin{pmatrix} \omega - k_1 u_1^+ \\ k_1 h_1^+ \\ ik_1^2 h_1^+ \\ -k_1^3 h_1^+ \end{pmatrix}, \quad \mathbf{q}_2 = \begin{pmatrix} \omega - k_2 u_1^+ \\ k_2 h_1^+ \\ ik_2^2 h_1^+ \\ -k_2^3 h_1^+ \end{pmatrix},$$

$$\mathbf{q}_3 = \begin{pmatrix} \omega - k_3 u_1^+ \\ k_3 h_1^+ \\ ik_3^2 h_1^+ \\ -k_3^3 h_1^+ \end{pmatrix}, \quad \mathbf{q}_4 = \begin{pmatrix} \omega - k_4 u_1^+ \\ k_4 h_1^+ \\ ik_4^2 h_1^+ \\ -k_4^3 h_1^+ \end{pmatrix}. \tag{A.74}$$

B_{jump} is given by (equations (4.14) to (4.16) again)

$$\begin{pmatrix} \frac{h_1^-}{h_1^+} & \frac{u_1^- - u_1^+}{h_1^+} & 0 & 0 \\ 0 & 1 & 0 & 0 \\ 0 & 0 & 1 & 0 \\ B_{jump,(41)} & B_{jump,(42)} & 0 & 1 \end{pmatrix},$$

where

$$B_{jump,(41)} = \frac{1}{\gamma}\left(\frac{u_2^+\rho_2 h_1^-}{h_2^+} + \frac{\rho_1 u_1^+ h_1^-}{h_1^+} - \frac{u_2^-\rho_2 h_1^-}{h_2^-} - \rho_1 u_1^-\right)$$

and

$$\begin{aligned} B_{jump,(42)} &= \frac{1}{\gamma}\left(\frac{\rho_2 u_2^+(u_1^+ - u_2^+)}{h_2^+} - \frac{\rho_2 u_2^-(u_1^- - u_2^-)}{h_2^-} + \right. \\ &\quad \left.\left(u_1^- - u_1^+\right)\left(\frac{u_2^+\rho_2}{h_2^+} + \frac{u_1^+\rho_1}{h_1^+}\right)\right), \end{aligned}$$

so

$$\begin{pmatrix} a_{1nu} \\ a_{2nu} \\ a_{3nu} \\ a_{4nu} \end{pmatrix} = \begin{pmatrix} \omega - k_1 u_1^+ & \omega - k_2 u_1^+ & \omega - k_3 u_1^+ & \omega - k_4 u_1^+ \\ k_1 h_1^+ & k_2 h_1^+ & k_3 h_1^+ & k_4 h_1^+ \\ ik_1^2 h_1^+ & ik_2^2 h_1^+ & ik_3^2 h_1^+ & ik_4^2 h_1^+ \\ -k_1^3 h_1^+ & -k_2^3 h_1^+ & -k_3^3 h_1^+ & -k_4^3 h_1^+ \end{pmatrix}^{-1} \tag{A.75}$$

$$\times B_{jump} \begin{pmatrix} \omega - k_{nu} u_1^- \\ k_{nu} h_1^- \\ ik_{nu}^2 h_1^- \\ -k_{nu}^3 h_1^- \end{pmatrix}.$$

Similarly,

$$\begin{pmatrix} a_{1u} \\ a_{2u} \\ a_{3u} \\ a_{4u} \end{pmatrix} = \begin{pmatrix} \omega - k_1 u_1^+ & \omega - k_2 u_1^+ & \omega - k_3 u_1^+ & \omega - k_4 u_1^+ \\ k_1 h_1^+ & k_2 h_1^+ & k_3 h_1^+ & k_4 h_1^+ \\ ik_1^2 h_1^+ & ik_2^2 h_1^+ & ik_3^2 h_1^+ & ik_4^2 h_1^+ \\ -k_1^3 h_1^+ & -k_2^3 h_1^+ & -k_3^3 h_1^+ & -k_4^3 h_1^+ \end{pmatrix}^{-1} \tag{A.76}$$

$$\times B_{jump} \begin{pmatrix} \omega - k_u u_1^- \\ k_u h_1^- \\ ik_u^2 h_1^- \\ -k_u^3 h_1^- \end{pmatrix},$$

$$\begin{pmatrix} a_{1nd} \\ a_{2nd} \\ a_{3nd} \\ a_{4nd} \end{pmatrix} = \begin{pmatrix} \omega - k_1 u_1^+ & \omega - k_2 u_1^+ & \omega - k_3 u_1^+ & \omega - k_4 u_1^+ \\ k_1 h_1^+ & k_2 h_1^+ & k_3 h_1^+ & k_4 h_1^+ \\ i k_1^2 h_1^+ & i k_2^2 h_1^+ & i k_3^2 h_1^+ & i k_4^2 h_1^+ \\ -k_1^3 h_1^+ & -k_2^3 h_1^+ & -k_3^3 h_1^+ & -k_4^3 h_1^+ \end{pmatrix}^{-1} \times B_{jump} \begin{pmatrix} \omega - k_{nd} u_1^- \\ k_{nd} h_1^- \\ i k_{nd}^2 h_1^- \\ -k_{nd}^3 h_1^- \end{pmatrix}, \tag{A.77}$$

$$\begin{pmatrix} a_{1d} \\ a_{2d} \\ a_{3d} \\ a_{4d} \end{pmatrix} = \begin{pmatrix} \omega - k_1 u_1^+ & \omega - k_2 u_1^+ & \omega - k_3 u_1^+ & \omega - k_4 u_1^+ \\ k_1 h_1^+ & k_2 h_1^+ & k_3 h_1^+ & k_4 h_1^+ \\ i k_1^2 h_1^+ & i k_2^2 h_1^+ & i k_3^2 h_1^+ & i k_4^2 h_1^+ \\ -k_1^3 h_1^+ & -k_2^3 h_1^+ & -k_3^3 h_1^+ & -k_4^3 h_1^+ \end{pmatrix}^{-1} \times B_{jump} \begin{pmatrix} \omega - k_d u_1^- \\ k_d h_1^- \\ i k_d^2 h_1^- \\ -k_d^3 h_1^- \end{pmatrix}. \tag{A.78}$$

We put

$$\begin{aligned} l_{nu} &= 1 + l_{nu,1} L + \ldots, \\ l_u &= l_{u,0} + l_{u,1} L + \ldots, \\ m_{nd} &= m_{nd,0} + m_{nd,1} L + \ldots, \\ m_d &= m_{d,0} + m_{d,1} L + \ldots. \end{aligned} \tag{A.79}$$

At leading order we have $\omega = \omega_0$, $k_{nu} = k_{nd} = k_0$, $k_u = k_{u0}$ and $k_d = k_{d0}$.

(A.72) simplifies considerably, giving

$$\begin{aligned} l_{nu,0}\begin{pmatrix} \omega_0 - k_0 u_1^- \\ k_0 h_1^- \\ ik_0^2 h_1^- \\ -k_0^3 h_1^- \end{pmatrix} & = m_{nd,0}\begin{pmatrix} \omega_0 - k_0 u_1^- \\ k_0 h_1^- \\ ik_0^2 h_1^- \\ -k_0^3 h_1^- \end{pmatrix} \\ +l_{u,0}\begin{pmatrix} \omega_0 - k_{u0} u_1^- \\ k_{u0} h_1^- \\ ik_{u0}^2 h_1^- \\ -k_{u0}^3 h_1^- \end{pmatrix} & \quad +m_{d,0}\begin{pmatrix} \omega_0 - k_{d0} u_1^- \\ k_{d0} h_1^- \\ ik_{d0}^2 h_1^- \\ -k_{d0}^3 h_1^- \end{pmatrix}. \end{aligned} \tag{A.80}$$

Trivially, $m_{nd,0} = 1$, $l_{u,0} = 0$ and $m_{d,0} = 0$. We put

$$M = \begin{pmatrix} \omega - k_1 u_1^+ & \omega - k_2 u_1^+ & \omega - k_3 u_1^+ & \omega - k_4 u_1^+ \\ k_1 h_1^+ & k_2 h_1^+ & k_3 h_1^+ & k_4 h_1^+ \\ ik_1^2 h_1^+ & ik_2^2 h_1^+ & ik_3^2 h_1^+ & ik_4^2 h_1^+ \\ -k_1^3 h_1^+ & -k_2^3 h_1^+ & -k_3^3 h_1^+ & -k_4^3 h_1^+ \end{pmatrix} \tag{A.81}$$

and

$$\begin{aligned} \omega &= \omega_0 + \omega_2 L^2, \\ k_1 &= k_{1,0} + k_{1,2} L^2, \\ k_2 &= k_{2,0} + k_{2,2} L^2, \\ k_3 &= k_{3,0} + k_{3,2} L^2, \\ k_4 &= k_{4,0} + k_{4,2} L^2, \end{aligned} \tag{A.82}$$

ignoring all higher-order terms. Also,

$$\begin{aligned} k_{nu} &= k_0 + k_{nu,1} L, \\ k_u &= k_{u,0} + k_{u,2} L^2, \\ k_{nd} &= k_0 + k_{nd,1} L, \\ k_d &= k_{d,0} + k_{d,2} L^2, \end{aligned} \tag{A.83}$$

giving

$$\mathbf{q}_{nu} = \begin{pmatrix} \omega_0 - k_0 u_1^- \\ k_0 h_1^- \\ ik_0^2 h_1^- \\ -k_0^3 h_1^- \end{pmatrix} + L \begin{pmatrix} -k_{nu,1} u_1^- \\ k_{nu,1} h_1^- \\ 2ik_0 k_{nu,1} h_1^- \\ -3k_0^2 k_{nu,1} h_1^- \end{pmatrix} + L^2 \begin{pmatrix} \omega_2 \\ 0 \\ ik_{nu,1}^2 h_1^- \\ -3k_0 k_{nu,1}^2 h_1^- \end{pmatrix}, \quad \text{(A.84)}$$

$$\mathbf{q}_u = \begin{pmatrix} \omega_0 - k_{u,0} u_1^- \\ k_{u,0} h_1^- \\ ik_{u,0}^2 h_1^- \\ -k_{u,0}^3 h_1^- \end{pmatrix} + L^2 \begin{pmatrix} \omega_2 - k_{u,2} u_1^- \\ k_{u,2} h_1^- \\ 2ik_{u,0} k_{u,1} h_1^- \\ -3k_{u,0}^2 k_{u,1} h_1^- \end{pmatrix}, \quad \text{(A.85)}$$

$$\mathbf{q}_{nd} = \begin{pmatrix} \omega_0 - k_0 u_1^- \\ k_0 h_1^- \\ ik_0^2 h_1^- \\ -k_0^3 h_1^- \end{pmatrix} + L \begin{pmatrix} -k_{nd,1} u_1^- \\ k_{nd,1} h_1^- \\ 2ik_0 k_{nd,1} h_1^- \\ -3k_0^2 k_{nd,1} h_1^- \end{pmatrix} + L^2 \begin{pmatrix} \omega_2 \\ 0 \\ ik_{nd,1}^2 h_1^- \\ -3k_0 k_{nd,1}^2 h_1^- \end{pmatrix}, \quad \text{(A.86)}$$

$$\mathbf{q}_d = \begin{pmatrix} \omega_0 - k_{d,0} u_1^- \\ k_{d,0} h_1^- \\ ik_{d,0}^2 h_1^- \\ -k_{d,0}^3 h_1^- \end{pmatrix} + L^2 \begin{pmatrix} \omega_2 - k_{d,2} u_1^- \\ k_{d,2} h_1^- \\ 2ik_{d,0} k_{d,1} h_1^- \\ -3k_{d,0}^2 k_{d,1} h_1^- \end{pmatrix}. \quad \text{(A.87)}$$

We define E to be a diagonal matrix with $e^{ik_1 L}$, $e^{ik_2 L}$, $e^{ik_3 L}$ and $e^{ik_4 L}$ as its diagonal elements and let E_1, E_2,... be defined by $E = I_4 + LE_1 + L^2 E_2 + \ldots$. At $O(1)$, (A.72) reads

$$M_0^{-1} B_{jump} \mathbf{q}_0 + l_{u,0} M_0^{-1} B_{jump} \mathbf{q}_{u,0} - m_{nd,0} M_0^{-1} B_{jump} \mathbf{q}_0 - m_{d,0} M_0^{-1} B_{jump} \mathbf{q}_{d,0} = 0 \quad \text{(A.88)}$$

with $l_{u,0} = 0$, $m_{nd,0} = 1$ and $m_{d,0} = 0$ as before. M_0 is the leading-order term

in the expansion of M (as a series in L). At $O(L)$, (A.72) is

$$\begin{aligned} l_{nu,0}E_1M_0^{-1}B_{jump}\mathbf{q}_0 + l_{nu,0}M_0^{-1}B_{jump}\mathbf{q}_{nu,1} + l_{nu,1}M_0^{-1}B_{jump}\mathbf{q}_0 \\ +l_{u,0}E_1M_0^{-1}B_{jump}\mathbf{q}_{u,0} + l_{u,1}M_0^{-1}B_{jump}\mathbf{q}_{u,0} - m_{nd,0}ik_0M_0^{-1}B_{jump}\mathbf{q}_0 \\ -m_{nd,0}M_0^{-1}B_{jump}\mathbf{q}_{nd,1} - m_{nd,1}M_0^{-1}B_{jump}\mathbf{q}_0 \\ -m_{d,0}ik_{d,0}M_0^{-1}B_{jump}\mathbf{q}_{d,0} - m_{d,1}M_0^{-1}B_{jump}\mathbf{q}_{d,0} &= 0, \end{aligned} \tag{A.89}$$

so

$$\begin{aligned} (E_1 + I_4(l_{nu,1} - ik_0 - m_{nd,1}))M_0^{-1}B_{jump}\mathbf{q}_0 + M_0^{-1}B_{jump}\mathbf{q}_{nu,1} \\ +l_{u,1}M_0^{-1}B_{jump}\mathbf{q}_{u,0} - M_0^{-1}B_{jump}\mathbf{q}_{nd,1} - m_{d,1}M_0^{-1}B_{jump}\mathbf{q}_{d,0} &= 0. \end{aligned} \tag{A.90}$$

At $O(L^2)$, the equation reads

$$\begin{aligned} (l_{nu,2} + l_{nu,1}E_1 + l_{nu,0}E_2)M_0^{-1}B_{jump}\mathbf{q}_0 \\ +(l_{nu,1} + l_{nu,0}E_1)M_0^{-1}B_{jump}\mathbf{q}_{nu,1} \\ +l_{nu,0}M_0^{-1}B_{jump}\mathbf{q}_{nu,2} + l_{nu,0}M_2^{-1}B_{jump}\mathbf{q}_0 \\ +(l_{u,2} + l_{u,1}E_1 + l_{u,0}E_2)M_0^{-1}B_{jump}\mathbf{q}_{u,0} \\ +l_{u,0}M_0^{-1}B_{jump}\mathbf{q}_{u,2} + l_{u,0}M_2^{-1}B_{jump}\mathbf{q}_{u,0} \\ -(m_{nd,2} + m_{nd,1}ik_0 + m_{nd,0}(-\tfrac{1}{2}k_0^2 + ik_{nd,1}))M_0^{-1}B_{jump}\mathbf{q}_0 \\ -(m_{nd,1} + m_{nd,0}ik_0)M_0^{-1}B_{jump}\mathbf{q}_{nd,1} \\ -m_{nd,0}M_0^{-1}B_{jump}\mathbf{q}_{nd,2} - m_{nd,0}M_2^{-1}B_{jump}\mathbf{q}_0 \\ -(m_{d,2} + m_{d,1}ik_{d,0} + m_{d,0}(-\tfrac{1}{2}k_{d,0}^2))M_0^{-1}B_{jump}\mathbf{q}_{d,0} \\ -m_{d,0}M_0^{-1}B_{jump}\mathbf{q}_{d,2} - m_{d,0}M_2^{-1}B_{jump}\mathbf{q}_{d,0} &= 0. \end{aligned} \tag{A.91}$$

Simplifying, using the $O(1)$ result, gives

$$\begin{aligned} (l_{nu,2} + l_{nu,1}E_1 + E_2)C\mathbf{q}_0 + (l_{nu,1} + E_1)C\mathbf{q}_{nu,1} + C\mathbf{q}_{nu,2} + (l_{u,2} \\ +l_{u,1}E_1)C\mathbf{q}_{u,0} - (m_{nd,2} + m_{nd,1}ik_0 - \tfrac{1}{2}k_0^2 + ik_{nd,1})C\mathbf{q}_0 \\ -(m_{nd,1} + ik_0)C\mathbf{q}_{nd,1} - C\mathbf{q}_{nd,2} - (m_{d,2} + m_{d,1}ik_0)C\mathbf{q}_{d,0} &= 0, \end{aligned} \tag{A.92}$$

where $C_{jump} = M_0^{-1}B_{jump}$ has no dependence on L. We now consider the dependence of k on ω. Substituting (A.83) into the straight-channel dispersion

relation (3.20 again):

$$\frac{\rho_1}{h_1}(\omega - ku_1)^2 + \frac{\rho_2}{h_2}(\omega - ku_2)^2 = gk^2 + \gamma k^4,$$

gives, for k_u, at $O(L^2)$

$$\begin{aligned} k_{u,2} &= \omega_2 \left(\rho_1 h_2^-(\omega_0 - u_1^- k_{u,0}) + \rho_2 h_1^-(\omega_0 - u_2^- k_{u,0})\right) / \\ &\quad \left(\rho_1 u_1^- h_2^-(\omega_0 - u_1^- k_{u,0}) + \rho_2 u_2^- h_1^-(\omega_0 - u_2^- k_{u,0})\right. \\ &\quad \left. + h_1^- h_2^- g k_{u,0} + 2h_1^- h_2^- \gamma k_{u,0}^3\right) \end{aligned} \tag{A.93}$$

and similarly

$$\begin{aligned} k_{d,2} &= \omega_2 \left(\rho_1 h_2^-(\omega_0 - u_1^- k_{d,0}) + \rho_2 h_1^-(\omega_0 - u_2^- k_{d,0})\right) / \\ &\quad \left(\rho_1 u_1^- h_2^-(\omega_0 - u_1^- k_{d,0}) + \rho_2 u_2^- h_1^-(\omega_0 - u_2^- k_{d,0})\right. \\ &\quad \left. + h_1^- h_2^- g k_{d,0} + 2h_1^- h_2^- \gamma k_{d,0}^3\right). \end{aligned} \tag{A.94}$$

At $O(L)$, for k_{nu}, we get

$$\begin{aligned} & k_{nu,1}\left[k_0 \rho_1 h_2^-(u_1^-)^2 + k_0 \rho_2 h_1^-(u_2^-)^2\right. \\ & \left. -\rho_1 u_1^+ \omega_0 h_2^- - \rho_2 u_2^+ \omega_0 h_1^- - g k_0 h_1^- h_2^- - 2\gamma k_0^3 h_1^- h_2^-\right] = 0, \end{aligned} \tag{A.95}$$

with the term in square brackets equalling zero. At $O(L^2)$ we get

$$\begin{aligned} k_{nu,1} &= \pm\sqrt{\omega_2}\sqrt{\frac{2h_2^-\rho_1(\omega_0 - u_1^- k_0) + 2h_1^-\rho_2(\omega_0 - u_2^- k_0)}{g h_1^- h_2^- + 6\gamma h_1^- h_2^- - h_2^-\rho_1(u_1^-)^2 - h_1^-\rho_2(u_2^-)^2}} \\ &= \sqrt{\omega_2} k_{nu,1,\omega}, \end{aligned} \tag{A.96}$$

say, where the sign can be chosen by the large root sign and

$$k_{nd,1} = -k_{nu,1}. \tag{A.97}$$

This means that

$$\mathbf{q}_{nd,1} = -\mathbf{q}_{nu,1} \tag{A.98}$$

and

$$\mathbf{q}_{nd,2} = \mathbf{q}_{nu,2}. \tag{A.99}$$

(A.90) is now

$$\begin{aligned} & (E_1 + I_4(l_{nu,1} - ik_0 - m_{nd,1}))C_{jump}\mathbf{q}_0 \\ & + 2C_{jump}\mathbf{q}_{nu,1} + l_{u,1}C_{jump}\mathbf{q}_{u,0} - m_{d,1}C_{jump}\mathbf{q}_{d,0} = 0. \end{aligned} \tag{A.100}$$

Putting

$$\mathbf{q}_{nu,1} = \sqrt{\omega_2}\mathbf{q}_{nu,1,\omega}, \tag{A.101}$$

say, and $\Psi_{n,1} = l_{nu,1} - ik_0 - m_{nd,1}$ we get

$$(E_1 + \Psi_{n,1}I_4)C_{jump}\mathbf{q}_0 + 2\sqrt{\omega_2}C_{jump}\mathbf{q}_{nu,1,\omega} + l_{u,1}C_{jump}\mathbf{q}_{u,0} - m_{d,1}C_{jump}\mathbf{q}_{d,0} = 0, \tag{A.102}$$

or

$$m_{d,1}\mathbf{q}_{d,0} - l_{u,1}\mathbf{q}_{u,0} - 2\sqrt{\omega_2}\mathbf{q}_{nu,1,\omega} - \Psi_{n,1}\mathbf{q}_0 = C_{jump}^{-1}E_1C_{jump}\mathbf{q}_0. \tag{A.103}$$

Thus,

$$\begin{pmatrix} m_{d,1} \\ -l_{u,1} \\ -2\sqrt{\omega_2} \\ -\Psi_{n,1} \end{pmatrix} = (\mathbf{q}_{d,0}\ \mathbf{q}_{u,0}\ \mathbf{q}_{nu,1,\omega}\ \mathbf{q}_0)^{-1}C_{jump}^{-1}E_1C_{jump}\mathbf{q}_0. \tag{A.104}$$

A.4 Notes for Chapter 7

A.4.1 The discrete Fourier transform

The well-known continuous Fourier transform of a function $u(x)$, and its inverse, can be written as

$$\hat{u}(k) = \int_{-\infty}^{\infty} u(x)e^{-2\pi ikx}\mathrm{d}x, \qquad u(x) = \int_{-\infty}^{\infty} \hat{u}(k)e^{2\pi ikx}\mathrm{d}k, \tag{A.105}$$

as well as in several other ways involving multiplying different factors in the exponent and overall equations (see e.g. [8]). To represent the Fourier transform at a finite number of points, we encounter two problems: k values are separated by finite amounts, and there are maximal and minimal k values that can be represented.

To get around the first of these, we must treat the function u as periodic. This means that its transform will be a series of equispaced delta functions,

the wavenumbers, k, of which are multiples of that corresponding to the period of u. We represent each delta function by the value of its integral.

To deal with the second problem, we apply the same principle the other way round. By taking the function u to be a string of delta functions, represented by the values of their integrals, the transform will be periodic and so can be represented by a finite range of k-values. Thus, both u and $\hat{u}$ are represented by periodic strings of delta functions.

So far, this all lies within the continuous theory (strictly, the continuous theory in the limit). However, we now change our variables so that x and k can be represented by integers, essentially making our transform into a Fourier series. For example

$$x = x_0 + X\Delta x, \tag{A.106}$$

for integer X between 0 and $N-1$. We have as our discrete Fourier transform

$$\hat{u}(K) = \sum_{X=0}^{N-1} u(X)e^{-2\pi iXK/N}, \tag{A.107}$$

for integer K. It is important to note that the quantity K/N is our analogue of wavenumber. Thus, the lowest positive wavenumber is $\frac{1}{N}cycles/(sampling\ length)$, the lowest nonzero wavenumber which can be represented by a sample of N points separated by $(sampling\ length)$.

From sampling theory, we have that the highest wavenumber which can be thus represented is $\frac{1}{2}cycles/(sampling\ length)$, corresponding to one wavelength for every 2 samples. This corresponds to $K = N/2$. We may thus view the remaining K values as being negative wavenumbers from $-\frac{N/2-1}{N}$ to $-\frac{1}{N}$, due to the periodicity in K. Note that these are non-dimensional, by virtue of X begin non-dimensional in (A.106).

Equivalently, we may change the limits of our summation. By changing the value of x_0 by $N\Delta x/2$ we can shift the X values by 'half a wavelength'

and (A.107) is then equal to

$$\begin{aligned}\sum_{X=-N/2}^{N/2-1} u(X)e^{-2\pi i(X+N/2)K/N} &= e^{-\pi iK}\sum_{X=-N/2}^{N/2-1} u(X)e^{-2\pi iXK/N} \\ &= (-1)^K \sum_{X=-N/2}^{N/2-1} u(X)e^{-2\pi iXK/N}.\end{aligned} \tag{A.108}$$

We note that we could equally have chosen these as our original range of values for X. This is an important point: whereas a continuous Fourier transform is normally taken to have a single answer, a discrete Fourier transform may have a phase shift for each K value. This is due to it being unclear what the 'best' place to start the summation is. Counting from $-N/2$ to $N/2-1$ seems most like the continuous case, but from 0 to $N-1$, as in (A.107), is more convenient computationally. The phase shift for each K may then mean that the discrete transform is not 'smooth', in the sense that it does not approach a continuous function as N is increased.

We have, from before, that $K = 1$ corresponds to a single wavelength in $N\Delta x$. This gives it a wavenumber of

$$\frac{1}{N\Delta x}. \tag{A.109}$$

Other wavenumbers are multiples of this. Thus

$$k = K\frac{1}{N\Delta x} \tag{A.110}$$

gives us a physical scale for k.

An inverse for (A.107) is

$$u(X) = \frac{1}{N}\sum_{K=0}^{N-1} \hat{u}(K)e^{2\pi iXK/N}. \tag{A.111}$$

That this works follows from the fact that

$$\sum_{X=0}^{N-1} e^{-2\pi iXK/N}e^{2\pi iXK'/N} = \begin{cases} N & K = K' \\ 0 & K \neq K'. \end{cases} \tag{A.112}$$

This inverse has the same problems with the choice of range for K as the forward transform has for the choice of range for X.

Returning to the idea of the discrete transform as an approximation to a continuous function, we consider the derivative theorem. That the Fourier transform of $u_x = \frac{\partial u}{\partial x}$ can be written as

$$\widehat{u'}(K) = 2\pi i k_c \sum_{X=0}^{N-1} u(X) e^{-2\pi i X K/N} \tag{A.113}$$

follows from the derivative theorem for a continuous Fourier transform, with variables then changed into their discrete counterparts. We must, however, be a little careful in choosing the values of k_c to use, where the symbol k_c has been used to emphasize the fact that it is not necessarily the k in (A.110). If we wish the k_c values to be approximately symmetric about 0, we must still ensure that $k_c = 0$ coincides with $K = 0$. Thus, we define k_c as

$$k_c = \begin{cases} K\frac{1}{N\Delta x} & 0 \le K \le N/2 - 1 \\ \\ (K-N)\frac{1}{N\Delta x} & N/2 \le K \le N-1, \end{cases} \tag{A.114}$$

with a 'discontinuity' at $K = N/2$.

A.4.2 Benjamin-Ono soliton solutions

We have (equation (7.1) again)

$$u_t = cu_x + auu_x + \alpha \frac{\partial^2}{\partial x^2} \int_{-\infty}^{\infty} \frac{u(x')}{x' - x} \mathrm{d}x'.$$

We look for a solution of the form $f(x - vt) = f(z)$. Thus

$$\begin{aligned} -vf_z &= cf_z + aff_z + \alpha \tfrac{\partial^2}{\partial x^2} \textstyle\int_{-\infty}^{\infty} \frac{f}{x'-x} \mathrm{d}x', \\ &= cf_z + aff_z + \alpha \tfrac{\partial^2}{\partial z^2} \textstyle\int_{-\infty}^{\infty} \frac{f(z')}{z'-z} \mathrm{d}z'. \end{aligned} \tag{A.115}$$

If f is of the form

$$\frac{A_1}{1 + \left(\frac{z}{L}\right)^2}, \tag{A.116}$$

then the integral is

$$\begin{aligned}\int_{-\infty}^{\infty}\frac{f(z')}{z'-z}dz' &= A_1\int_{-\infty}^{\infty}\frac{\mathrm{d}z'}{\left(1+\left(\frac{z'}{L}\right)^2\right)(z'-z)} \\ &= A_1\int_{-\infty}^{\infty}\frac{\mathrm{d}\frac{z'}{L}}{\left(1+\left(\frac{z'}{L}\right)^2\right)\left(\frac{z'}{L}-\frac{z}{L}\right)}.\end{aligned} \tag{A.117}$$

Partial fractions gives the integral as

$$\left[\frac{-2\left(\frac{z}{L}\right)\tan^{-1}\left(\frac{z'}{L}\right)+2\log\left(\frac{z'}{L}-\frac{z}{L}\right)-\log\left(1+\left(\frac{z'}{L}\right)^2\right)}{2+2\left(\frac{z}{L}\right)^2}\right]_{-\infty}^{\infty}=\frac{-\pi\frac{z}{L}}{1+\left(\frac{z}{L}\right)^2}. \tag{A.118}$$

Now,

$$f'(z)=-\frac{2A_1z}{L^2\left(1+\left(\frac{z}{L}\right)^2\right)^2} \tag{A.119}$$

and we have

$$\left(v+c+a\frac{A_1}{1+\left(\frac{z}{L}\right)^2}\right)\frac{2A_1z}{L^2\left(1+\left(\frac{z}{L}\right)^2\right)^2}=-\alpha\frac{\partial^2}{\partial x^2}\left(\frac{\pi\frac{z}{L}}{1+\left(\frac{z}{L}\right)^2}\right), \tag{A.120}$$

or

$$\begin{aligned}\left(v+c+a\frac{A_1}{1+\left(\frac{x-vt}{L}\right)^2}\right)\frac{2A_1(x-vt)}{L^2\left(1+\left(\frac{x-vt}{L}\right)^2\right)^2} &= -\alpha\frac{\partial^2}{\partial x^2}\left(\frac{\pi\frac{x-vt}{L}}{1+\left(\frac{x-vt}{L}\right)^2}\right) \\ &= -A_1\alpha\pi\frac{2L\left(-3L^2+(x-vt)^2\right)(x-vt)}{\left(L^2+(x-vt)^2\right)^3},\end{aligned} \tag{A.121}$$

or

$$\frac{\left((v+c)\left(1+\left(\frac{x-vt}{L}\right)^2\right)+aA_1\right)L^2}{L^2+(x-vt)^2}\times\frac{2A_1(x-vt)L^2}{\left(L^2+(x-vt)^2\right)^2}=-2LA_1\alpha\pi\frac{\left(-3L^2+(x-vt)^2\right)(x-vt)}{\left(L^2+(x-vt)^2\right)^3}, \tag{A.122}$$

$$\begin{aligned}&\left((v+c)\left(1+\left(\frac{x-vt}{L}\right)^2\right)+aA_1\right) \\ &\qquad\times(x-vt)L^3 = -\alpha\pi\left(-3L^2+(x-vt)^2\right)(x-vt),\end{aligned} \tag{A.123}$$

$$\begin{aligned}&\left(\frac{v+c}{L^2}\left(L^2+(x-vt)^2\right)+aA_1\right) \\ &\qquad\times(x-vt)L^3 = -\alpha\pi\left(-3L^2+(x-vt)^2\right)(x-vt),\end{aligned} \tag{A.124}$$

$$\left(\frac{v+c}{L^2}\left(L^2+(x-vt)^2\right)+aA_1\right)L^3=-\alpha\pi\left(-3L^2+(x-vt)^2\right). \quad \text{(A.125)}$$

Comparing the constant quantities, we obtain

$$(v+c+aA_1)\,L=3\alpha\pi \quad \text{(A.126)}$$

and comparing the coefficients of $(x-vt)^2$,

$$(v+c)\,L=-\alpha\pi, \quad \text{(A.127)}$$

so

$$4(v+c)+aA_1=0, \quad \text{(A.128)}$$

or

$$v=-c-\frac{aA_1}{4} \quad \text{(A.129)}$$

and

$$L=\frac{4\alpha\pi}{aA_1}. \quad \text{(A.130)}$$

This provides the full solution as given in (7.3).

A.4.3 The Fourier transform of the Cauchy integral term

For completeness, we briefly derive the transform of the last term on the right of (7.2). We have

$$\frac{\partial^2}{\partial x^2}\int_{-\infty}^{\infty}\frac{u(x')}{x'-x}\mathrm{d}x'=-u_{xx}*\frac{1}{x}, \quad \text{(A.131)}$$

taking the derivatives inside the integral and using $*$ to represent the convolution of two functions. From the convolution theorem it just remains to calculate the Fourier transform of $\frac{1}{x}$. Due to the infinite discontinuity at the origin, we write

$$\widehat{\left(\frac{1}{x}\right)}=\lim_{\epsilon\to 0}\left(\int_{-\infty}^{-\epsilon}\frac{e^{-ikx}}{x}\mathrm{d}x+\int_{\epsilon}^{\infty}\frac{e^{-ikx}}{x}\mathrm{d}x\right), \quad \text{(A.132)}$$

where, again, the symbol 'hat' is taken to mean 'the Fourier transform of'. Consider now the often-used path for integration in the upper half-plane consisting of the segment $(-R,\epsilon)$, R large, along the negative real axis, a semicircle

of radius ϵ past the origin, the segment (ϵ, R) of the positive real axis and a semicircle of radius R back to the start. Along this path, the integral of our function is given by

$$\int_{-R}^{-\epsilon} \frac{e^{-ikx}}{x} \mathrm{d}x + \int_{\pi}^{0} ie^{-ik\epsilon e^{i\theta}} \mathrm{d}\theta + \int_{\epsilon}^{R} \frac{e^{-ikx}}{x} \mathrm{d}x + \int_{0}^{\pi} ie^{-ikRe^{i\theta}} \mathrm{d}\theta. \qquad \text{(A.133)}$$

This is equal to zero by virtue of the path enclosing no poles. As $R \to \infty$, the fourth integral vanishes and as $\epsilon \to 0$, the second is equal to $i\pi$ for $k > 0$ and $-i\pi$ for $k < 0$. So

$$\lim_{\epsilon \to 0} \left(\int_{-\infty}^{-\epsilon} \frac{e^{-ikx}}{x} \mathrm{d}x + \int_{\epsilon}^{\infty} \frac{e^{-ikx}}{x} \mathrm{d}x \right) + i\pi \mathrm{sgn}(k) = 0 \qquad \text{(A.134)}$$

and we have

$$\widehat{\left(\frac{1}{x}\right)} = -i\pi \mathrm{sgn}(k), \qquad \text{(A.135)}$$

with the transform of the entire last term being $i\pi k|k|$. Our transformed equation is

$$\hat{u}_t = ikc\hat{u} - k^2\nu\hat{u} + \beta\hat{u} + au * (ik\hat{u}) + \alpha i\pi k|k|, \qquad \text{(A.136)}$$

where, again, $*$ is convolution.

A.4.4 The Benjamin-Ono eigenvalue problem

We now consider the linear problem in Fourier space and take the time dependence to be of the form $e^{\lambda t}$. By considering $\hat{u}$ and k to take discrete values, we arrive at an eigenvalue problem for λ. We consider N wavenumbers and the same number of $\hat{u}$ values, where N is odd in our examples, for symmetry about $k = 0$. The k values are taken to be the same as those discussed above,

in Appendix A.4.1. Thus

$$\hat{u} = \begin{pmatrix} \hat{u}_{-(N-1)/2} \\ \vdots \\ \hat{u}_{-1} \\ \hat{u}_0 \\ \hat{u}_1 \\ \vdots \\ \hat{u}_{(N-1)/2} \end{pmatrix}, \qquad k = \begin{pmatrix} k_{-(N-1)/2} \\ \vdots \\ k_{-1} \\ k_0 \\ k_1 \\ \vdots \\ k_{(N-1)/2} \end{pmatrix} = \begin{pmatrix} -\frac{(N-1)/2}{N\Delta x} \\ \vdots \\ -\frac{1}{N\Delta x} \\ 0 \\ \frac{1}{N\Delta x} \\ \vdots \\ \frac{(N-1)/2}{N\Delta x} \end{pmatrix}. \tag{A.137}$$

Our equation then becomes

$$\lambda \hat{u}_m = \left(2\pi i c k_m - 4\pi^2 \nu k_m^2 + 4\pi^3 i \alpha k_m |k_m|\right) \hat{u}_m + (\hat{\beta} * \hat{u})_m, \tag{A.138}$$

where $\hat{\beta}$ is the Fourier transform of β. The only question which remains is how to do the convolution. We approximate the solution as

$$(\hat{\beta} * \hat{u})_m = \sum_{n=-(N-1)/2}^{(N-1)/2} \hat{\beta}_n \hat{u}_{m-n}, \tag{A.139}$$

We now put $n_{min} = -(N-1)/2$ and $n_{max} = (N-1)/2$. Then, if we put $\Omega_n = 2\pi i c k_n - 4\pi^2 \nu k_n^2 + 4\pi^3 i \alpha k_n |k_n|$, we can define

$$D_\Omega = \begin{pmatrix} \Omega_{n_{min}} & 0 & \dots & \dots & \dots & 0 \\ 0 & \ddots & \ddots & \ddots & \dots & \vdots \\ \vdots & \ddots & \Omega_0 & 0 & \ddots & \vdots \\ \vdots & \ddots & 0 & \Omega_1 & \ddots & \vdots \\ \vdots & \dots & \ddots & \ddots & \ddots & 0 \\ 0 & \dots & \dots & \dots & 0 & \Omega_{n_{max}} \end{pmatrix} \tag{A.140}$$

and

$$M_\beta = \begin{pmatrix} \hat{\beta}_0 & \dots & \hat{\beta}_{n_{min}} & \hat{\beta}_{n_{max}} & \dots & \hat{\beta}_1 \\ \vdots & \ddots & \vdots & \vdots & \ddots & \vdots \\ \hat{\beta}_{n_{max}} & \dots & \hat{\beta}_0 & \hat{\beta}_{-1} & \dots & \hat{\beta}_{n_{min}} \\ \hat{\beta}_{n_{min}} & \dots & \hat{\beta}_1 & \ddots & \ddots & \hat{\beta}_{n_{max}} \\ \vdots & \ddots & \vdots & \ddots & \ddots & \vdots \\ \hat{\beta}_{-1} & \dots & \hat{\beta}_{n_{max}} & \hat{\beta}_{n_{min}} & \dots & \hat{\beta}_0 \end{pmatrix}, \tag{A.141}$$

where the third row and column lie in the middle of the matrices. This leads us to the full matrix form of the eigenvalue problem

$$\lambda \hat{u} = (D_\Omega + M_\beta)\, \hat{u}. \tag{A.142}$$

Bibliography

[1] D. E. Ashpis, E. Reshotko, The vibrating ribbon problem - revisited, *J. Fluid Mech.* 213:531-47 (1990)

[2] G. K. Batchelor & A. E. Gill, Analysis of the stability of axisymmetric jets, *J. Fluid Mech.* 14:529-51 (1962)

[3] T. B. Benjamin, Internal waves of finite amplitude and permanent form, *J. Fluid Mech.* 25:241-70 (1966)

[4] T. B. Benjamin, Internal waves of permanent form in fluids of great depth, *J. Fluid Mech.* 29:559-92 (1967)

[5] C. M. Bender & S. A. Orszag, *Advanced mathematical methods for scientists and engineers*, New York: McGraw-Hill (1978)

[6] A. Bers, Linear waves and instabilities, in *Physique des plasmas* ed C. DeWitt & J. Peyraud 117-215 (1975)

[7] A. Bers, Space-Time Evolution of Plasma Instabilities - Absolute and Convective, *Handbook of Plasma Physics*, North-Holland Publishing Company (1983)

[8] R. N. Bracewell, *The Fourier transform and its applications*, Third edition, McGraw-Hill (2000)

[9] K. S. Breuer & T. Kuraishi, Transient growth in two- and three-dimensional boundary layers *Phys. Fluids* 6(6):1983-93 (1994)

[10] L. Brevdo & T. J. Bridges, Absolute and convective instabilities of spatially periodic flows, *Phil. Trans. R. Soc. Lond.* 354:1027-1064 (1996)

[11] R. J. Briggs, *Electron-stream interaction with plasmas*, M.I.T. Press (1964)

[12] J.-M. Chomaz, Absolute and convective instabilities in nonlinear systems, *Phys. Rev. Lett.* 69:1931-4 (1992)

[13] J.-M. Chomaz, Global instabilities in spatially developing flows, *Ann. Rev. Fluid Mech.* 37:357-392 (2005)

[14] J.-M. Chomaz & A. Couairon, Against the wind, *Phys. Fluids* 11:2977-2983 (1999)

[15] , J.-M. Chomaz, P. Huerre & L. G. Redekopp, Bifurcations to local and global modes in spatially-developing flows, *Phys. Rev. Lett.* 60:25-28 (1988)

[16] J.-M. Chomaz, P. Huerre & L. G. Redekopp, A Frequency Selection Criterion in Spatially Developing Flows, *Studies in Applied Mathematics* 89:119-144 (1991)

[17] J. B. Conway, *A Course in Functional Analysis*, Second edition, Springer-Verlag (1990)

[18] C. Cossu & J.-M. Chomaz, Global measures of local convective instabilities, *Phys. Rev. Lett.* 78(23):4387-90 (1997)

[19] A. Couairon & J.-M. Chomaz, Global instabilities in fully nonlinear systems, *Phys. Rev. Lett.* 77:4015-8 (1996)

[20] A. D. D. Craik, *Wave interactions and fluid flows*, C.U.P. (1985)

[21] D. G. Crighton & M. Gaster, Stability of slowly diverging jet flow, *J. Fluid Mech.* 77:397-413 (1976)

[22] Y. Ding & R. Magnusson, Resonant leaky-mode spectral-band engineering and device applications, *Optics Express* 12(23) 5661-74 (2004)

[23] P. G. Drazin & W. H. Reid, *Hydrodynamic Stability*, Second edition, C.U.P. (2004)

[24] W. S. Edwards, L. S. Tuckerman, R. A. Friesner, D. C. Sorensen, Krylov methods for the incompressible Navier-Stokes equations, *J. Comp. Phys.* 110:82-102 (1998)

[25] A. S. Fokas & D. T. Papageorgiou, Absolute and Convective Instability for Evolution PDEs on the Half-Line, *Studies in Applied Mathematics* 114:95-114 (2005)

[26] D. A. Hammond & L. G. Redekopp, Global dynamics of symmetric and asymmetric wakes, *J. Fluid Mech.* 331:231-60 (1997)

[27] K. Hasselmann, A criterion for nonlinear wave stability, *J. Fluid Mech.* 30:737-9 (1967)

[28] T. H. Havelock, The Propagation of Groups of Waves in Dispersive Media, with Application to Waves on Water produced by a Travelling Disturbance, *Proc. Roy. Soc. A* 549:398-430 (1908)

[29] W. Heisenberg, Über Stabilität und Turbulenz von Flussigkeitsströmen, *Ann. Phys. Lpz.* 74:577-627 (1924). Translated as 'On stability and turbulence of fluid flows', *Tech. Memor. Nat. Adv. Comm. Aero. Wash.* 1291 (1951)

[30] H. von Helmholtz, Überdiscontinuirliche Flüssigkeitsbewegungen, *Monats. Königl. Preuss. Akad. Wiss. Berlin* 23:215-28 (1868). Translated into English by F. Guthrie as 'On discontinuous movements in fluids' *Phil. Mag.* (4) 36:337-46 (1868)

[31] M. S. Howe, Edge, cavity and aperture tones at very low Mach numbers, *J. Fluid Mech.* 300:61-84 (1997)

[32] H. Hristova, S. Roch, P. J. Schmid & L. S. Tuckerman, Transient growth in Taylor-Couette flow, *Phys. Fluids* 14(10):3475-3484 (2002)

[33] P. Huerre, Open shear flow instabilities, in *Perspectives in fluid dynamics*, ed. G. K. Batchelor, H. K. Moffatt, M. G. Worster (2000)

[34] P. Huerre & P. A. Monkewitz, Absolute and convective instabilities in free shear layers, *J. Fluid Mech.* 159:151-68 (1985)

[35] P. Huerre & P. A. Monkewitz, Local and Global Instabilities in Spatially Developing Flows, *Annu. Rev. Fluid Mech.* 22:473-537 (1990)

[36] Lord Kelvin, Hydrokinetic solutions and observations, *Phil. Mag.* (4) 42:362-77 (1871)

[37] I. Kim & A. J. Pearlstein, Stability of flow past a sphere, *J. Fluid Mech.*, 211:73-94 (1990)

[38] W. Koch, Local instability characteristics and frequency determination of self-excited wake flows, *J. Sound Vib.* 99:53-83 (1985)

[39] M. Lessen & P. J. Singh, The stability of axisymmetric free shear layers, *J. Fluid Mech.*, 60(3):433 (1973)

[40] L. M. Mack, A numerical study of the temporal eigenvalue spectrum of the Blasius boundary layer, *J. Fluid Mech.* 73:497-520 (1976)

[41] L. F. McGoldrick, Resonant interactions among capillary-gravity waves, *J. Fluid Mech.* 21:305-332 (1965)

[42] P. Monkewitz, P. Huerre & J.-M. Chomaz, Global linear stability analysis of weakly non-parallel shear flows, *J. Fluid Mech.* 251:1-20 (1993)

[43] P. M. Morse & H. Feshbach: *Methods of Theoretical Physics*, McGraw-Hill (1953)

[44] A. H. Nayfeh (Ed), *Introduction to Perturbation Techniques*, Wiley (1993)

[45] H. Ono, Algebraic solitary waves in stratified fluids, *J. Phys. Soc. Japan* 39:1082-91 (1975)

[46] W. M'F. Orr, The stability or instability of the steady motions of a perfect liquid and of a viscous liquid, *Proc. Roy. Irish Acad.* 27:9-68 (1907)

[47] P. L. O'Sullivan & K. S. Breuer, Transient growth in circular pipe flow. I. Linear disturbances, *Phys. Fluids* 6(11):3643-51 (1994)

[48] O. M. Phillips, On the dynamics of unsteady gravity waves of finite amplitude. Part 1. The elementary interactions, *J. Fluid Mech.* 9:193-217 (1960)

[49] R. T. Pierrehumbert, Local and global baroclinic instability of zonally varying flow, *J. Atmos. Sci.* 41:2141-62 (1984)

[50] R. T. Pierrehumbert, Spatially amplifying modes of the Charney baroclinic instability problem, *J. Fluid Mech.* 170:293-317 (1986)

[51] W. H. Press, S. A. Teukolsky, W. T. Vetterling & B. P. Flannery, *Numerical Recipes in C++*, Second Edition, C. U. P. (2002)

[52] Lord Rayleigh, On the instability of jets, *Proc. Lon. Math. Soc.* 10:4-13 (1879)

[53] Lord Rayleigh, On the stability, or instability, of certain fluid motions, *Proc. Lon. Math. Soc.* 11:57-70 (1879)

[54] S. C. Reddy & L. N. Trefethen, Pseudospectra of the convection-diffusion operator, *SIAM J. Appl. Math.* 54(6):1634-49 (1994)

[55] O. Reynolds, An experimental investigation of the circumstances which determine whether the motion of water shall be direct or sinuous, and of the law of resistance in parallel channels, *Phil. Trans. Roy. Soc.* 174:935-82 (1883)

[56] G. F. Roach, *Green's Functions*, Second Edition, C. U. P. (1982)

[57] B. Roberts & A. Mangeney, Solitons in solar magnetic flux tubes, *Mon. Not. R. Astr. Soc* 198:7-11 (1982)

[58] H. Schlichting, Zur Entstehung der Turbulenz bei der Plattenströmung, *Nachr. Ges. Wiss. Göttingen, Math.-phys. Kl.* 181-208 (1933)

[59] P. J. Schmid & D. S. Henningson, *Stability and transition in shear flows*, New York:Springer-Verlag (2001)

[60] G. B. Schubauer & H. K. Skramstad, Laminar boundary layer oscillations and transition on a flat plate, *J. Res. Nat. Bur. Stand.* 38:251-92 (1947)

[61] A. Sommerfeld, Ein Beitrag zur hydrodynamischen Erklaerung der turbulenten Fluessigkeitsbewegungen, *Proceedings 4th International Congress of Mathematicians, Rome* Vol III 116-24 (1908)

[62] P. A. Sturrock, Kinematics of growing waves, *Phys. Rev.* 112:1488-1503 (1958)

[63] M. D. Thomas, The nonlinear stability of flows over compliant walls, *J. Fluid Mech.* 239:657-70 (1992)

[64] S. N. Timoshin & J. M. Linkins, Transient feedback and global instability in non-homogeneous systems, *Phil. Trans. Roy. Soc. A* 363:1235-1245 (2005)

[65] S. N. Timoshin & F. T. Smith, personal communication

[66] S. M. Tobias, M. R. E. Proctor & E. Knobloch, Convective and absolute instabilities of fluid flows in finite geometry, *Physica D* 113:4-72 (1998)

[67] W. Tollmien, Über die Entstehung der Turbulenz, *Nachr. Ges. Wiss. Göttingen, Math.-phys. Kl.* 21-44 (1929). Translated as 'The production of turbulence', *Tech. Memor. Nat. Adv. Comm. Aero. Wash.* 609 (1931)

[68] A. E. Trefethen, L. N. Trefethen & P. J. Schmid, Spectra and pseudospectra for pipe Poiseuille flow, *Comput. Methods Appl. Mech. Engrg.* 1926:413-420 (1999)

[69] L. N. Trefethen, Pseudospectra of linear operators, *SIAM rev.* 39(3):383-406 (1997)

[70] L. N. Trefethen, A. E. Trefethen, S. C. Reddy, T. A. Driscoll, Hydrodynamic stability without eigenvalues, *Science* 261:578-84 (1993)

[71] L. S. Tuckerman, F. Bertagnolio, O. Daube, P. Le Quéré, D. Barkley, Stokes preconditioning for the inverse Arnoldi method, in *Continuation Methods for Fluid Dynamics Notes on Numerical Fluid Mechanics*, ed. D. Henry, A. Bergeon (2000)

[72] Ferdinand Verhulst, *Nonlinear Differential Equations and Dynamical Systems*, Springer-Verlag (1990)